OPTIMAL DESIGN AND EVALUATION OF SOLAR BIFACIAL PV-WIND-BATTERY-SPLIT GENSET HYBRID POWER SYSTEM

by

IBUKUN DAMILOLA FAJUKE

Doctoral thesis submitted in fulfilment of the requirements for the degree of

Doctor of Engineering in Electrical Engineering

In the faculty of Engineering and the Built Environment

at the Cape Peninsula University of Technology

Supervisor: **Prof. Raji Atanda**

Bellville Campus

Date submitted: November, 2022

DECLARATION

I, Ibukun Damilola Fajuke declare that the contents of this dissertation represent my own unaided work, and that the dissertation has not previously been submitted for academic examination towards any qualification. Furthermore, it represents my own opinions and not necessarily those of the Cape Peninsula University of Technology.

09/11/2022

…… …….

Date Signature

ABSTRACT

A Hybrid Power System (HPS) is a power generation system consisting of renewable and non-renewable means of energy generation, and an energy storage scheme. It is considered as a more suitable alternative energy generation for sustainable development in off-grid and grid-connected applications. However, the optimal design of the components making up the HPS is very essential in reducing not only the total cost and environmental effects of the system, but to also improve its reliability**.** Most of the existing solution methods were found to be time-consuming, unable to handle a large number of control variables and suffer from slow convergence speed; leading to system designs with low-quality optimal solutions. Thus, there is need to develop an HPS model with a fast run time and high speed of convergence, that is reliable and cost-effective. This work, therefore, aims to design an optimal off-grid hybrid solar bifacial PV-wind-battery-split Genset power system model using Giza Pyramids Construction (GPC) Algorithm as an optimization technique.

Individual component of the proposed HPS is modeled in Simulink using their respective mathematical equations. In order to increase the share of renewable energy in the optimal system design, a bifacial PV, which has the ability to generate more additional energy compared to the conventional monofacial PV was used as the solar generator component. The performance of the bifacial PV module is evaluated by determining the most appropriate orientation state capable of producing more additional energy. A multi-objective optimization solution method was employed to find the optimal design of the proposed HPS using the GPC algorithm. The proposed approach was applied to study four case studies including (split genset only, wind/battery/split genset, bifacial PV/battery/split genset and Bifacial PV/wind/battery/split genset) to meet the load requirement of a remote community located in northern part of Nigeria using real time meteorological data of the area. The performance evaluation of the GPC algorithm was done by comparing its solution with those obtained using Firefly Algorithm (FA) and Whale Optimization Algorithm (WOA) techniques respectively using Life Cycle Cost (LCC) and Total Environmental Pollution (TEP) as performance metrics. To further illustrate the performance of the GPC algorithm, a comprehensive comparison based on numerical analysis is carried among the reported optimization algorithms.

Simulation results showed that the optimal design of the proposed HPS consisting of Bifacial PV/wind/battery/split genset is the most practical energy solution to meet the energy requirement of the studied area, as all the three algorithms predicted the lowest values of LCC and TEP for the optimal configuration as compared to using the split genset only with LCC and TEP values of $1,830,752.40 and 3,241,987.00 kg respectively. The LCC and TEP obtained using the proposed algorithm, WOA and FA techniques are $803,599.09 and 1,265,933.58 kg, $799,243.58 and 1,188,139.91 kg and $836,135.65 and 1,469,829.44 kg respectively; which corresponds to 56.10 % and 60.95 %, 56.34 % and 63.35 % and 54.32

% and 54.66 % reduction as compared to the split genset only configuration. The results also showed that GPC algorithm converges faster than the two other optimization algorithm and has a simulation run time of 9.78 minutes as compared to 10.59 and 12.28 minutes recorded for both WOA and FA techniques respectively. Moreover, the results of numerical analysis carried out on the fitness score of the objective function over 20 runs showed that the GPC algorithm has a standard deviation and efficiency of 1.0096 and 96.28 % as compared to 3.4915 and 87.09; and 07142 and 97.36 estimated for both WOA and FA techniques respectively.

Generally, the results demonstrate the robustness and efficient performance of the GPC algorithm as compared to WOA and FA techniques in solving optimal design problem of HPS. The significant reduction in the values of LCC and TEP of the proposed approach is expected to enhance wider acceptability of HPS consisting of both renewable and non-renewable energy sources among policy makers, decision makers, government agencies and power system engineers for sustainable development and a safer environment.

Keywords

Giza Pyramids Constructions, Hybrid Power System, Bifacial PV, Split Genset, Renewable Energy, Battery Energy System, Optimization, Simulation

Acknowledgements

I would like to express my gratitude to the following.

- Firstly, I would like to express my sincere gratitude to my supervisor, Prof. A.K. Raji for his continuous support and guidance during the entire period of the program. His dedication, valuable contributions and constructive criticism are some of the yardsticks responsible for improving my research and bringing out the best in me. Thank you for all the trust and opportunities given to me, which enable me to explore and participate in multiple conferences and gain valuable experience in working with experts and researchers in other projects. I consider it a great privilege to have carried out this study under your supervision.
- Heartfelt thanks also go to my academic mentor, Prof. G.A Adepoju for his positive contributions and words of encouragement towards the success of this study.
- I would also like to appreciate the CPUT library management and staff for granting me access to necessary information required to carry out this study, the Center for power system and Distributed Engineering, and the Department of Electrical and Computer Engineering as a whole for providing me with the necessary resources required to carry out my research.
- I would also like to show my appreciation to my fellow researchers and friends at the university, Engr. Ogunniyi Emmanuel and Engr. Showers for their support, motivation and excellent comments and suggestion.
- Special thanks to my family and friends who have in one way or the other contributed to the success of this study, your words of encouragement and support helped me to carry on with my study during difficult times.
- I am absolutely grateful from the bottom of my heart to my wife, Fajuke Tolulope who has continuously inspired me and honestly made it possible for me to see this study to the finish line. In addition to that, I would love to appreciate my little boys, Fajuke Bright and Fajuke Wisdom for their understanding and cooperation throughout the period of my study.
- Most importantly, I would like to appreciate the Almighty God for giving me the grace to complete this study. Although there were times of ups and downs, I return all praises to him for giving me strength and good health to complete my program.

DEDICATION

Dedicated to almighty God; and to the memories of my late mother and grandfather.

TABLE OF CONTENTS

List of figures

List of tables

Appendix A

GLOSSARY

Abbreviations

ABC:	Artificial Bee Colony
AC:	Alternating Current
ACO:	Ant Colony Optimization
ACS:	Annual Cost of System
AI:	Artificial Intelligence
AVR:	Automatic Voltage Regulator
BBO:	Biography Based Optimization
BES:	Battery Energy Storage
BESS:	Battery Energy Storage System
BF:	Bacterial Foraging
BSO:	Brain Storm Optimization
CSA:	Cuckoo Search Algorithm
CSP:	Concentrated Solar Power
DC:	Direct Current
DE:	Differential Evolution
DFIG:	Double-Fed Induction Generator
DG:	Diesel Generator
DOD:	Depth of Discharge
DP:	Dynamic Programming
EENS:	Expected Energy Not Served
EP:	Evolution Programming
EP:	Evolution Programming
EPRI:	Electric Power Research Institute
EST:	Energy Storage Technology
FA:	Firefly Algorithm
FCWT:	Full Converter Wind Turbine

FF:	Fossil Fuel
FPO:	Flower Pollination Optimization
GA:	Genetic Algorithm
GPC:	Giza Pyramids Construction
GWO:	Grey Wolf Optimizer
HAWT:	Horizontal Axis Wind Turbine
HNN:	Hopfield Neural Network
HOGA:	Hybrid Optimization by Genetic Algorithm
HOGA:	Hybrid Optimization by Genetic Algorithm
HOMER:	Hybrid Optimization of Multiple Energy Resources
HOMER:	Hybrid Optimization Model for Electric Renewable
HPS:	Hybrid Power System
HSA:	Harmony Search Algorithm
HSAT:	Horizontal Single-axis Tracking
KCL:	Kirchhoff's Current Law
LCC:	Life Cycle Cost
LCOE:	Levelized Cost of Electricity
LOLP:	Loss of Load Probability
LP:	Linear Programming
LPSP:	Loss of Power Supply Probability
MBO:	Mine Blast Optimization
MFO:	Moth Flame Optimization
NASA:	National Aeronautic and Space Administration
NPC:	Net Present Cost
NREL:	National Renewable Energy Laboratory
NSGA-II:	Non-dominated Sorting Genetic Algorithm
PERC:	Passive Emitter and Rear Cell
PMSG:	Permanent Magnet Synchronous Generator
PO:	Political Optimizer

PS:	Pattern Search
PSO:	Particle Swarm Optimization
PV:	Photovoltaic
RE:	Renewable Energy
RERL:	Renewable Energy Research Laboratory
SA:	Simulated Annealing
SAPS:	Small Autonomous Power System
SBBO:	Satin Bower Bird Optimization
SCIG:	Squirrel-Cage Induction Generator
SHRES:	Standalone Hybrid Renewable Energy System
SOC:	State of Charge
TEP:	Total Environmental Pollution
TRNSYS:	Transient Energy System Simulation Program
TRNSYS:	Transient Energy System Simulation Program
TS:	Tabu Search
TSP:	Traveling Salesman Problem
WOA:	Whale Optimization Algorithm
WRIG:	Wound Rotor Induction Generator
WRSG:	Wound Rotor Synchronous Generator
WT:	Wind Turbine
WTG:	Wind Turbine Generator

Mathematical Notations

f_f	Frictional force due to stone block movement
μ_f	Co-efficient of frictional force
θ	Ramp angle
g	Acceleration due to gravity
m	Mass of stone block
z	Acceleration of the stone block
u_0	Initial velocity of the stone block
D_s	Displacement of the stone block

‘γ’,	Fixed light absorption coefficient
L	Varying light intensity
L_0	Initial light intensity of the firefly
β_0	Attractiveness of a firefly
X_{rand}	Random whale
C_c	Initial capital cost
OM_c	Operation and maintenance cost
R_c	Replacement cost
$F_{c(dg)}$	Fuel cost
G_{dir},	Direct irradiance
G_{diff}	Diffuse irradiance
G_{alb},	Irradiance due albedo
G_{beam}	Reflected (beam) irradiance
F_v	View factor
A_i	Anisotropy index
R_b	Geometric factor
γ_c	Albedo coefficient
I_{ph}	Current generated due to the irradiance
I_0	Diode reverse saturation current
V_T	Thermal voltage
i_f	Ideality factor
R_s	Series resistance
R_{sh}	Shunt resistance
I_{ph-f}	Front side photocurrent
I_{ph-b}	Back side photocurrent
N_s	Number of cells connected in series
μ_{bif}	Heat conductivity of bifacial module
α_{bif}	Reflectance coefficient of bifacial module
η_{bif}	Module efficiency
T_{bif}	Module temperature
T_{amb}	Ambient temperature
c_a,	Constant acceleration
E_k	Kinetic energy
v_u	Upstream wind velocity

v_d	Downstream wind velocity
C_p	Turbine power coefficient
v_s	Blade tip speed ratio
λ_p	Blade pitch angle
V_o	Output voltage
K_m	Torque constant
ω_m	Motor speed
I_a,	Armature current
R_a	Armature resistance
L_{aa}	Armature inductance
B_m	Frictional force of generator
N_T	Number of wind turbines
S_f	Safety factor
P_c	Compression ratio
k_1	Amplification factor
R_d	Speed droop
ω_{ref}	Engine speed
m_B	Fuel consumption rate

LIST OF PUBLICATIONS

A. Published articles

1. **Fajuke, I.D.**, Raji, A. and Adepoju, G. A (2021). Optimal Sitting and Sizing of Static Synchronous Compensator on Longitudinal Transmission System for Power Loss Reduction Using Firefly Algorithm. *Proc. Of the International Conference on Electrical, Computer and Energy Technologies (ICECET) 9-10 Dec., 2021. Cape Town, South Africa*. 1-6.
2. **Fajuke, I.D** and Raji, A.K. Firefly Algorithm-Based Optimization of the Additional Energy Yield of Bifacial PV Modules. *Energies* **2022**, *15*, 2651. https://doi.org/10.3390/en15072651

B. Articles accepted for publications

1. **Fajuke, I.D.** and Raji A.K. (2022) Optimal tuning of Proportional Integral Derivative Controller for speed control of Direct Current motor using Equilibrium Optimizer. *Indonesian Journal of Electrical Engineering and Computer Science*

C. Articles submitted for publication

1. **Fajuke, I.D** and Raji, A.K. (2022). A Review on Application of Intelligent Solution Techniques to Power System Optimization Problems. *AIMS energy*
2. **Fajuke, I.D** and Raji, A.K. (2022). Modeling the rear side irradiance of bifacial PV modules-A review. *Journal of Engineering Science and Technology review*
3. **Fajuke, I.D.** and Raji, A.K. (2022). Optimal design of Hybrid PV/Wind/Battery/Diesel generator power system using Constriction Co-efficient Particle Swarm Optimization (CC-PSO). *Journal of Energy in Southern Africa.*
4. **Fajuke, I.D.** and Raji, A.K. (2022). The influence of additional energy of bifacial PV module on the optimal design of hybrid renewable energy system. *Environmental Innovations and Societal Transitions.*
5. **Fajuke, I.D.** and Raji, A.K. (2022). Application of Giza Pyramid Construction (GPC) and Corona Virus Optimization (CVO) algorithms to optimal design of solar bifacial PV/wind/battery/split genset hybrid power system. *Elsevier: Scientific African*

CHAPTER ONE
INTRODUCTION

1.1 Background of the study

In the last two centuries, the availability of Fossil Fuel (FF) has played a significant role in the development of modern civilization. Fossil fuels were majorly used as the source of energy generation, and the amount of energy availability of any nation is a direct indication of its development (Babatunde et al., 2020). However, the rise in primary energy consumption, which is as a result of the continuous increase in population growth and industrial revolution both in developed and developing countries, may lead to an unsustainable situation in the near future owing to the limited availability of FF (Tito et al., 2013). From the early 1970s oil crisis to the present, the gradual depletion of traditional energy sources and the concerns of global warming contribute to the need for alternative energy generation sources (Nair et al., 2017; Pan et al., 2009; Zhou et al., 2010). A viable alternative has pointed in the direction of Renewable Energy (RE) sources (Zhou et al., 2010).

Renewable energy as defined by Adebanji et al., (2017) is any energy generated from RE sources (solar, wind, hydro and biomass) that can reproduce itself through natural or biological process. Solar Photovoltaic (PV) module and wind turbines are the most prominent RE technologies, both of which produce zero pollution and have a source that is free and abundance in nature (Koutroulis et al., 2006). Solar PV technology in particular, has become a promising option to global energy production with more than 650 GWp of accumulated installed capacity as of 2020. The most recent of this technology is the solar bifacial PV module. These types of modules are designed to collect sunlight using both the front and back sides for energy production. Since their inception, studies have shown that these modules have a higher energy output potential when compared to their monofacial PV counterparts (Janssen et al., 2015).

Nair et al., (2017) and Nehrir et al., (2011) stated that the main drawbacks of each of these RE technologies are the unpredictable nature of their sources, as well as their dependence on irregular weather and climatic conditions. Consequently, they are unable to match the load requirements as at when required. It should also be noted that over-reliance on a single technology generally results in over-sizing of the system, thereby increasing the investment cost (Hassan et al., 2016). However, considering the complementary nature of their sources, most of the drawbacks can be addressed by overcoming the weakness of one by the strength of the other (Nair et al., 2017). Combining these two types of RE technologies with a back-up, such as diesel generator and energy storage systems or fuel cells will help create an economically viable system capable of improving the power supply reliability (Yuan et al., 2018).

A system which brings together diverse electrical energy generation sources, storage and consumption technologies in a single system, and subsequently improves the overall benefits as compared to a system depending on one single energy source is referred to as Hybrid Power System (HPS) (Babatunde et al., 2020). Formerly, this type of system was designed as a combination of conventional, non-renewable energy generation such as diesel generator and Battery Energy Storage System (BESS). However, the recent deployment of RE technologies has widened their definition to include systems whose energy generation is mainly based on RE source Therefore, a more suitable definition of HPS is the integration of several types of energy generation equipment such as traditional electrical energy generators, energy storage system and RE technologies (Atia & Yamada, 2016; Pan et al., 2009).

The integration of HPS continue to grow in capacity from small, standalone system of a few kilowatt, typically designed for low voltage DC and AC applications to larger megawatt systems expanding to medium voltage grid-connected systems (Zhou et al., 2010). However, the most important feature of the HPS design is to efficiently generate energy at any point in time by optimally utilizing the available RE sources and storing the excess energy for later use as demanded (Babatunde et al., 2020). Nevertheless, as more energy sources and system components are incorporated into the system design; the proper selection of the HPS components and sizes, optimal allocation of the energy resources, battery life cycle as well as the optimal operation control strategy becomes imperative in achieving the overall efficiency of the system (Sawle et al., 2016a).

The optimal operation of HPS requires the optimization of its performance, taking into consideration its technical and economic constraints. Optimization of HPS looks into the process of selecting the best components and its sizing with appropriate operation strategy to provide efficient, reliable and cost effective alternative energy for use in both urban and isolated areas (Babatunde et al., 2020; Tito et al., 2013). This optimization complexity arises for several reasons such as the high number of variables involved in system design, conflicting objective such as cost, reliability, environmental pollution, supply/demand management, grid limitations, among others. Also, the non-linearity, non-convexities and mixed type variables often limits the possibility of using conventional and commercially available optimization software and techniques to properly address this problem (Sawle et al., 2016a; Zhou et al., 2010).

In the past few years, researchers are harnessing intelligence techniques most especially the heuristic and meta-heuristics algorithms such as (Genetic Algorithm (GA), Simulated Annealing (SA), Particle Swarm Optimization (PSO) and many others) for the optimal design of HPS such that there is an overall improvement on system cost, environmental effects and reliability. These techniques have shown their

capability in terms of simulation run time, convergence speed and accuracy in solving various optimization problems. (Babatunde et al., 2020; Bandaru & Deb, 2016).

In this study, Giza Pyramids Construction (GPC), a novel meta-heuristic optimization technique was used to find the optimal design of a stand-alone HPS comprising of solar bifacial PV, wind turbines, split diesel generator set and BESS. The objectives considered in the optimization are minimization of the system life cycle cost and total environmental pollution; the reliability of the HPS design was measured using the loss of power supply probability which was included as constraints during the optimization process. The choice of GPC optimization algorithm is due to its ability to handle high-dimensional problems, converge at shorter run time and produce efficient solutions in solving many optimization problems (Harifi, Mohammadzadeh, et al., 2020). In order to demonstrate the robustness of the GPC, The result obtained using the GPC algorithm were compared with those obtained using Firefly Algorithm (FA) and Whale Optimization Algorithm (WOA). The proposed HPS design model can be used as a temporary or long-term solution for electrification of rural areas, critical infrastructure, educational institutions and many other areas where the need for economically viable, environmentally friendly and reliable power solution is required.

1.2 Problem statement

Renewable energy technologies are becoming more popular due to the recent breakthroughs in the deployment of the technology (Zhou et al., 2010). The combination of different types of RE technologies coupled with energy storage units such as batteries and diesel generator as back-up; provide a stand-alone energy system which serves as a realistic alternative to traditional power system generation. This type of system is usually referred to as HPS (Babatunde et al., 2020).

Existing studies have shown a significant development in the design, analysis and implementation of HPS. The sizing of each RE technology is mostly important in the consideration of the investment cost, operation and maintenance costs and the reliability of supply of the energy demanded (Vishakha et al., 2020). In many of the HPS design available in literatures, the traditional monofacial PV module was used; even though they are cheaper as compared to the proposed bifacial PV modules in this study, they are only able to generate energy using the front side only despite occupying the same land size area. Besides, bifacial PV modules have the potential to compensate for the extra cost and have longer life span as compared to their monofacial counterparts (Pelaez, Deline, Greenberg, et al., 2019). In addition, split diesel generator set was used as opposed to a large-sized diesel generator used in many HPS system design available literature. The split diesel generator set is expected to further reduce the environmental pollution and dump energy in the system (Ogunjuyigbe et al., 2016).

Moreover, the optimal and economical sizing of the entire system can be done via several optimization techniques such as the commercially available optimization approach, conventional and intelligence-based optimization techniques (Babatunde et al., 2020; Zhou et al., 2010). Although, the problem of cost optimization and reliability of HPS containing a large combination of components has been addressed by various researchers; in most cases, conventional optimization and commercially available optimization methods were used, resulting in higher calculation inefficiency, high run time, slow convergence and computational burden (Sawle et al., 2016a). Computational drawbacks of existing numerical methods in the context of optimization problems have thus compelled researchers to repose their trust in computational intelligence-based techniques (Babatunde et al., 2020). While, speed is seen to have improved to a certain extent using intelligent methods, the possibility of trapping into local optimum is still present due to the high number of control variables in the design of HPS (Sawle et al., 2016a).

In this study, a recent computational intelligence-based technique Giza Pyramids Constriction (GPC) was applied to optimize an off-grid solar bifacial PV-wind-battery-split generator set system. The choice of GPC is due to its ability to handle large number of control variables which is peculiar to most HPS design and subsequently attaining global optimal solution in less run time and fast convergence speed when compared with other intelligence-based optimization techniques (Harifi, Mohammadzadeh, et al., 2020).

1.3. Research Questions

This study provides adequate answers to the following research questions.

1. What are the techno-economic benefits and environment effect of two or more RE source such as solar and wind in the optimal design of HPS?
2. What is the influence of the additional energy yield of a bifacial solar PV on the optimal design of the HPS?
3. What is the effect of using a GPC optimization algorithm in the optimal design of the proposed HPS in terms of run time, convergence speed and quality of the solution?
4. What effects do other meta-heuristics optimization techniques have on the optimal design of HPS based on the minimization of an encoded objective function, convergence speed and run time, system cost and total environmental pollution as compared to the use of GPC algorithm?

1.4 Research aim and objectives

This section describes the main aim of the study as well as stepwise objectives used in achieving the aim of the research.

1.4.1 Aim

The aim of this study is to develop an optimal design and to evaluate the performance of a solar bifacial PV-wind-battery-split genset hybrid power system

1.4.2 Objectives

The specific objectives of this research are to;

i. conduct the feasibility study of the proposed site for integration of the solar bifacial PV-wind-battery-split genset hybrid power system and analyze the available renewable energy sources taking into consideration the solar radiation, wind speed and load demand pattern.
ii. carry out the mathematical modeling of the various components of the proposed HPS such as solar bifacial PV, wing turbine generator, split generator set, energy storage system and converter in SIMULINK environment.
iii. formulate a cost-efficient and environmentally friendly off-grid solar bifacial PV-wind-battery-split genset hybrid power system model and optimize it using Giza Pyramids Constriction (GPC) optimization algorithm.
iv. implement objective (iii) in MATLAB/SIMULINK using total life cycle cost of system and total environmental pollution as performance metrics.
v. evaluate the performance of the developed model in (iii) by comparing its results with that of other intelligent-based optimization algorithms namely Whale Optimization Algorithm (WOA) and Firefly Algorithm (FA).

1.5 Significance of the research

Hybrid Power System (HPS) has become an important research area due to the continuous increase in global energy demand and the need for safer environment. It is therefore important to harness the potential of two or more RE sources and energy storage system in the design of HPS, with a back-up such as diesel generator for the electrification of isolated locations, extremely remote areas, critical facilities such as military base and hospitals, among others. However, the optimal design of the components making up the HPS is a very complex task as it involves the proper combination of large number of components. Hence, there is need to design a HPS model that is not only capable appropriate component selections, but also reliable, cost-effective and able to meet the load demand of proposed location while maintaining system integrity. Optimal design of an off-grid hybrid solar PV-wind-battery power system with split diesel generator set as back-up will not only help in reducing the life cycle cost of the system as well as total environmental pollution, it will also improve system reliability and ensure uninterrupted supply of power.

1.6 Scope of the study

The scope of the study is to design of an off-grid Hybrid Power System (HPS) comprising solar bifacial PV system, wind turbine (WT) generator, energy storage system and split diesel generator set. Other RE sources such as biomass, hydro, among others were not considered in this study.

1.7 Hypothesis

The hypothesis is based on the reviewed investigations on HPS system configuration types, as well as design methods and techniques applied in the referenced papers to solve the problem of optimal design of HPS consisting of solar and wind energies, diesel generators and energy storage system. Most of the reviewed papers investigated the optimal design of the conventional monofacial solar PV and a single generator set in their system configuration. The introduction of solar bifacial PV to replace the conventional monofacial PV is a new concept in the design of the HPS. It is hypothesized that the additional energy yield produced from the rear side of the bifacial PV will help lower the total cost of the system and cost of energy. Similarly, the use of a split generator set in system configuration of the HPS is another new concept which is expected to help improve system reliability and reduce carbon emission for safer environment. Most of the literatures reviewed on HPS employed a large single generator in the design of the HPS.

In terms of design methodologies, many of the reviewed papers investigated applied several methods to solve the design optimization problem of HPS, each optimization method has its own advantages and disadvantages according to the quality of the solution, accuracy, reliability, run time and convergence speed. Most existing studies make use of the commercially available optimization software such as Hybrid Optimization of Multiple Energy Resources (HOMER), Hybrid Optimization by Genetic Algorithm (HOGA) and many others. In some literatures, the conventional optimization methods such as Linear Programming (LP), graphical construction technique, among others were also used in the optimal design of the HPS. However, the use of commercially available and conventional optimization software were found to be time consuming, suffer from slow convergence speed and are liable to get trapped in local optimal solutions. This is mainly due to the high number of design variables involved in the optimization problem.

In the last decade, meta-heuristic algorithms such as Genetic Algorithm (GA), Particle Swarm Optimization (PSO), Tabu Search (TS) and many others have also been applied in the optimal design of HPS. A noticeable feature common to these optimization algorithm when compared to conventional techniques is in the speed of convergence and reduction in run time. However, their inability to efficiently handle the high number of variables involved in system design has led to discrepancies in the quality of their solutions. Hence, for the purpose of this study, a novel intelligent algorithm namely Giza Pyramids Constriction

(GPC) optimization technique was used to develop a model for the optimal design of HPS. The developed model using GPC was aimed at producing optimal solutions in terms of total life cycle cost and total environmental pollution of the system, and improved system reliability in less run time and fast convergence speed.

1.8 Thesis Layout

The background of the study, awareness of the problem, research questions, aim and objectives, significance of the study, scope of the study, hypothesis and layout of the thesis are all discussed in Chapter One. A review of the literature studies similar to this research is presented in Chapter two. It discusses the various renewable energy sources and technologies along with their current status and potential. A brief discussion of hybrid power system types, mode of connections and the various components of the proposed system are also described in this chapter. Moreover, the various methodologies used in the optimal design of hybrid power system consisting of renewable energy sources are also briefly summarized. In addition, the proposed optimization techniques are also presented towards the end of this chapter. The mathematical modeling of the various components used in the design of the proposed HPS are presented in chapter three. The energy flow algorithm and flowchart of the system design is also presented in this chapter. Chapter Four covers the developed optimization problem, as well as the implementation procedure of the proposed optimization algorithms. Simulation results and discussion are covered in Chapter Five of this study; while Chapter Six summarizes the conclusions drawn from this study, contributions to knowledge, and recommended future work based on the result of this study.

CHAPTER TWO
LITERATURE REVIEW

2.1 Status quo of conventional energy generation

Generally, energy is regarded as one of the basic need for human existence, as it is required in almost every phase of our daily lives. Over the years, the majority of the energy required across the globe are generated using traditional methods such as fossil fuels and coal (IRENA, 2013). In a recent report by REN21, (2012), 81 % of the total global energy are generated using fossil fuels. Some well developed countries have also generated their energy using nuclear sources, about 2.8 % of the global energy generation are generated using nuclear power, while hydropower contributes about 3.4 % to the energy generation mix. Despite the huge amount of energy generation, more than a billion of the world population are still living without sustainable energy supply. As such, the demand for energy will continue to grow as the years pass by, and further attempt to close the supply-demand energy gap across the globe using traditional energy generation sources will lead to their complete depletion (Larsson, 2009). The projected availability of conventional energy generation sources is depicted in Figure 2.1.

As shown in figure 2.1, oil, which is the major byproduct of fossil fuel is expected to have been exhausted before the end of 21st century. (HTE, 2012). Hence, as a result of the current global fear over complete depletion of fossil fuelled power generation sources, their negative environmental impacts and the anticipated increase in the price of fossil fuel; the need for alternative energy generating options becomes imperative (Nehrir et al., 2011). The use of diesel and gas powered generators has been the major option for mini-grid electrification purpose both in rural and urban areas. However, factors such as high maintenance and lifecycle cost due to their daily fuel consumption, high carbon emissions, fluctuating price and limited availability of diesel fuel have all contributed to a push for a more promising option which is economically viable, as well as guarantees sustainability and reliability (Babatunde et al., 2020). As such, the attention of world leaders, policy makers and researchers have been drown towards the use of renewable resources as a viable alternative for energy generation (Ellabban et al., 2014).

2.2 Renewable energy resources

Renewable Energy (RE) resources is projected to play a significant role in meeting the future energy demand in both developed and developing nations in the world (Edenhofer et al., 2011). As the need to curb the adverse environmental effect of energy generation using non-renewable energy sources continue to intensify, the development and utilization of renewable sources must be given a high priority. RE resources are naturally occurring resources that are unlimitedly available in our environment. Typical examples of RE resources include hydro, wind, solar, tidal waves, geothermal, biomass and biogas (Alrikabi, 2014a).

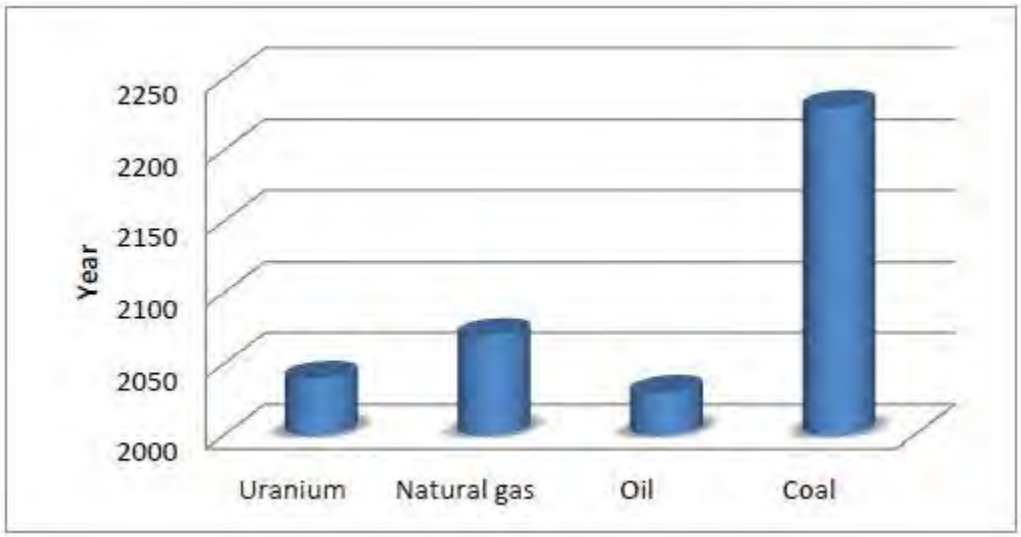

Figure 2.1: Projected availability of conventional energy sources (HTE, 2012)

The source of most RE resources originated from the sun; the only exceptions are tidal and geothermal resources. Every form of RE resources have the ability to generate electrical energy, mechanical energy, thermal energy, as well as produce fuels that can be utilized as multiple energy needs (Edenhofer et al., 2011)

RE resources has always been around us for a long period of time, and has been used to generate energy in many parts of the world. For example, energy generation using hydro has been in existence for a long time; however, it is only suitable for locations with a large volume of constant water flow and therefore limiting its usage. On the other hand, solar and wind resources have more presence in almost every part of the world than hydro; and could be explored to meet the present and future energy demand across the globe (Frp et al., 2021). It has been projected that the share of energy generation in the world using solar and wind resources by the year 2050, would amount to 452 billion kWh and 1,839 billion kWh respectively as depicted in Figure 2.2. (IEO, 2013). Theoretically, RE resources have the potential to generate the present and future global energy demand; however, the main task is how to maximize this potential in the delivery of various energy services in an economical and environmentally friendly manner (Larsson, 2009). A brief description of some common RE resources are subsequently presented.

2.2.1 Biomass

Biomass is a form of RE resource that can be found in food and fibre production, forest products, as well as waste and residue management. It is majorly used in developing counties in a low efficient form such as wood, straws, dung and other manures that are used in cooking, lighting and space heating (Alrikabi, 2014b; Edenhofer et al., 2011). This form of biomass has been reported to be environmentally unfriendly due to the release of carbon dioxide in the atmosphere which is harmful to health and living conditions of its users. In recent times, biomass has been used in high efficiency form such as liquid biofuels, biodiesels and methane to generate heat, electricity and transportation of fuels. It also exists in solid form such as chips, pellets, used woods and many others. Generally, energy production using biomass can be unsustainable as it causes serious social and environmental concern; However, its huge potential in most developing nations cannot be overemphasized; and it is projected that the global biomass harvest should achieve a 150 EJ/yr of bioenergy by the middle of the current century (Edenhofer et al., 2011).

2.2.2 Hydropower

Hydropower is a RE resource that has been in use for over 2000 years, it uses the energy of a flowing water to generate electrical energy. They are mostly used to generate centralized electricity, but can also be used as mini and micro hydro to provide electricity in remote and islanded areas. Some of the main advantage

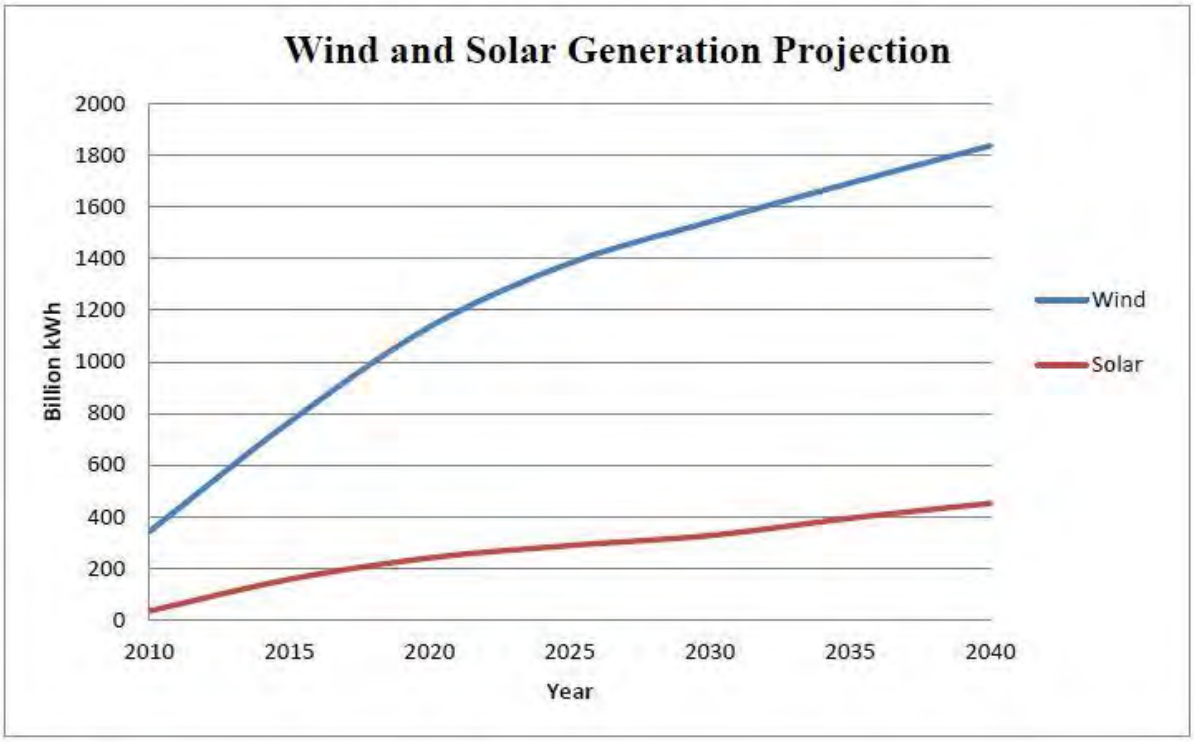

Figure 2.2: Projected share of solar and wind energy generation (IEO, 2013)

of energy generating using hydro resource include its non-exhaustible and non-polluting nature, as well as its low operational costs. However, setting up a hydro power plant is capital intensive and have negative impacts on ecological lives (Holt & Pengelly, 2008). Presently, hydropower resource has the potential to generate 3,721 GW of electrical power globally. However, the potential of this resource has not been fully explored despite its wide acceptance in electricity generation (Fullerton et al., 2008). Africa has the most undeveloped capacity with only about 8 % of hydro potential being currently utilized. In Europe, the use of hydropower resource is more pronounced with about 53 % of the total global capacity installed across the continent. Despite the huge technical potential of the resource in Asia and Latin America, their development is still at the infancy stage. Globally, it is projected that the generation capacity of hydro resource could rise as much as 4.05 TWh by 2050 (Edenhofer et al., 2011).

2.2.3 Geothermal

This type of RE resource are made from thermal energy beneath the earth surface, and are usually found in both rock and trapped steam or liquid water. It is considered a family of the RE resources because the tapped heat in the active reservoir is constantly restored via the process of natural heat production, conduction and convection. (Alrikabi, 2014)The process of extracting the geothermal fluids is a reversible one, thereby making it possible for the fluids to be replenished via natural revitalization and by re-injecting the cold fluids back to the reservoir. They find wide applications in the generation of electrical energy using thermal power plants. They are also used for domestic and agriculture purposes, where the need for heat and combined heat and power are required. Energy generation using geothermal resource are environmentally friendly and have little or zero impact on climate change. It has been reported that the amount of electrical energy that can be generated using geothermal resources is in the range of 118 EJ to 146 EJ per year at a depth of 3000 meters to 318 EJ to 1,109 EJ per year at a depth of 10,000 meters (Edenhofer et al., 2011).

2.2.4 Ocean energy

Ocean energy is regarded as one of the RE resource with the potential to meet the present human energy demanded across the globe (Holt & Pengelly, 2008). The energy is harvested by harnessing the chemical and heat potential of the water in the ocean. It exists in six different forms namely wave energy, tidal range tidal currents, ocean currents, ocean thermal energy conversion and salinity gradients, which is also referred to as osmotic power (Edenhofer et al., 2011). Some of the many advantages of this type of energy resource is their ability to lower carbon emission and low environmental impact. Even though the development of various technologies used in converting the resource to energy is very slow, it is understood that they have low investment cost which could impact the cost of electricity generated using their sources (Holt & Pengelly, 2008). The projected potential of ocean energy resource across the globe is estimated to be 77,731

TWh per year. Efforts are being made to implement certain government policies that will accelerate the potential deployment of their technology in many parts of the world (Edenhofer et al., 2011).

2.2.5 Solar energy

Solar RE resource is obtained through the sun's radiation reaching the earth. The rotation of the earth around the sun in an elliptical manner results in variation of extraterrestrial radiation. The amount of this extraterrestrial radiation reaching the earth varies from one location to another, and it is determined by several factors such as climatic condition, time of the day and the amount of water vapor present in the atmosphere (Edenhofer et al., 2011; Holt & Pengelly, 2008). In order to maximize the solar radiation reaching the earth surface at a specific location, it is important to analyze the characteristics of solar radiation before implementation. The amount of solar radiation received on a square meter of the earth surface is referred to as solar insolation. The solar insolation outside the earth's atmosphere is estimated at 1.37 kW/m2, while the solar insolation within the atmosphere is assumed to be 1.0 kW/m2 (Edenhofer et al., 2011; Fullerton et al., 2008). In a report by (IRENA, 2013), the amount of radiation obtained from the sun is more than enough to meet the entire energy needs in the world. The projected energy generation using the sun stands at 49,837 EJ per year (Edenhofer et al., 2011).

Solar resource has been used extensively in various applications such as solar water heaters, solar dryers, solar cookers, solar thermal refrigerators, water pumping system, solar powered receivers, telecommunications repeater stations and electricity generation both in urban and rural locations. Some of the merits of using this resource for energy generation include its non-polluting and inexhaustible nature. The major drawback is the intermittent nature due to varying climatic conditions (Holt & Pengelly, 2008).

2.2.6 Wind energy

Majority of the RE resources available are byproducts of the sun; one of such is the wind resource. Wind is simply defined as the movement of air in space, this movement is usually caused by the displacement resulting from the heating of some parts of the earth by the sun. Wind is one of the oldest RE resource available, it was firstly used about 5000 years ago to sails ship in the Nile River; other early application areas include crushing of grains, pumping of water and charging of batteries for used as source of power(Fullerton et al., 2008; Holt & Pengelly, 2008). However, due to the discovery of fossil fuels which was found to be quite economical and more reliable as at then, the interest in the resource suddenly cooled off. It was reintroduced into the power generation discussion because of the oil crisis in 1970. Since its re-introduction, wind resource has been used as grid-connected electricity production and remote electrifications in many parts of the world (Larsson, 2009; Martins et al., 2019).

Various government funded programs on research and development have been highlighted to improve the technologies used in harnessing the energy from the wind. In 2021, global wind capacity increased from 500,000 MW in 2016 to 1,100,000 MW globally; while the projected amount of energy that can be harvested from wind resource stands at 125,000 TWh per year, which is far above the global energy demanded as at 2021 (Edenhofer et al., 2011). The main advantage of generating energy using wind resource is the guarantee of a healthy environment due to reduction in the level of harmful gases into the atmosphere. In a report by International Energy Agency (IEA), the yearly reduction in environmental pollution is expected to rise from 863 million tons in 2020 to 1447 million tons by the year 2030 at the current rate of utilizing the resource (Alrikabi, 2014).

2.3 Renewable energy technologies

The need to transit from traditional fossil fuel based sources of energy generation to RE resources form requires the development of appropriate technologies. Renewable Energy Technologies (RET) are technologies used in the conversion of available RE resources into useful energy. For example, photovoltaic (PV) modules are required to convert the energy of the sun for use as electricity for both residential and commercial purposes. It should be noted that the competitiveness of RE resources depend on the availability and cost of conversion technologies (IRENA, 2013). Various RET have been developed over the years, some of them include cooking stoves, hydrothermal reservoirs, enhanced geothermal systems, hydropower turbines, tidal energy turbines, wind turbines, solar collector, concentrated solar plate and PV modules (Edenhofer et al., 2011). The two most deployed RET across the globe are wind turbines and PV modules; and are both considered in this study. A detailed description of these two technologies are subsequently presented.

2.3.1 Wind turbine technology

Wind turbines are one of the most deployed RET across the globe, and are very effective in converting the kinetic energy from the wind into useful mechanical power. If the mechanical power is used directly for pumping of water and crushing of grains, it is referred to as windmill; however, if the mechanical power is converted into electrical power, it is referred to as wind turbine generator with rated capacity ranging from less than 100kW, but can be built into a large wind farm rated at 5MW or more (IRENA, 2016; Yaramasu et al., 2015). Power is generated in the turbine when the kinetic energy of the wind exceeds the minimum value (cut-in speed). The higher the wind speed, the higher the power generated by the turbine; a point is reached when the turbine stops generating power due to the presence of control mechanisms, this point is known as cut-off speed. The power output of the turbine depends mainly on the wind speed, wind direction, air density, wind turbine dimensions, and wind turbine aerodynamics (Olabi et al., 2021). The power output of the wind turbine for various wind speed is presented in Table 2.1.

Table 2.1: Power output for various wind speed

Wind Speed	Power Output of Wind Turbine
Below cut-in speed	$P_o = 0$; where P_o is the power output of the turbine
Between cut-in speed and rated speed	$P_o = P_{Mac}$; where P_{Mac} is max. extractable power from the wind turbine
Between rated and cut-out speed	$P_o = P_{rated}$; where P_{rated} is the rated output of the wind plant
Above cut-out speed	$P_o = 0$

Source: (Olabi et al., 2021)

Some of the basic components of a wind turbine are tower, rotor, turbine blades, nacelle, and the turbine rotor control structure, which is also known as yawing mechanism as shown in Figure 2.3. The main components of the turbine is the tower as it provides the necessary support to the gear box and the electric generator which are located in the nacelle. The driven train connecting the aerodynamic rotor with electrical output terminals is also an essential components of the wind turbine (TeacherGeek.com, 2006). Traditionally, there are three major types of Wind Turbine Generators (WTGs) that may be considered for various wind turbine system. They include Direct Current (DC), Alternating Current (AC) synchronous, and Alternating Current (AC) asynchronous generators. Theoretically, each of the generators may be run at a fixed or variable speed. However, due to the fluctuation in wind power output, it is desirable to run the WTG at variable speed, which lowers physical stress on the turbine blades and drive train and enhances system aerodynamic efficiency and torque transient behaviors (Cao et al., 2012; Reinemann & Heinzen, 2014).

Another important component is the yawing mechanism, it is basically used to direct the turbine rotor towards the direction of wind flow in order to maximize the kinetic energy from the wind. The kinetic energy of the wind speed produces a torque which is converted into electrical power via the gear box and the electrical generator. Some of the obvious characteristics of a modern wind turbines include (Cao et al., 2012; Kim et al., 2010).;

i. dependability
ii. noise and pollution free
iii. economically viable
iv. competitive in business terms

Generally, there are two generations of wind turbines that are commercially available; the first generation wind turbines are the vertical axis wind turbine which include the Darrieus and Savonius wind turbines. The second generation of wind turbines are the horizontal axis wind turbine; the Swift Wind turbine falls under this category (Olabi et al., 2021; L. Wang et al., 2009). A brief discussion of the two existing generations of wind turbines are subsequently presented.

2.3.1.1 Vertical axis wind turbines

The two most common types of vertical axis wind turbines are the Darrieus and Savonius. This type of turbine does not make use of the yawning mechanism when generating electricity. This property can be attributed to the construction of the blades in such a way that it is able to capture the direction of wind speed in any direction. The Darrieus wind turbines use the airfoil concept to turn its blades along a vertical axis, thus allowing for an infinite rotation speed (Olabi et al., 2021).

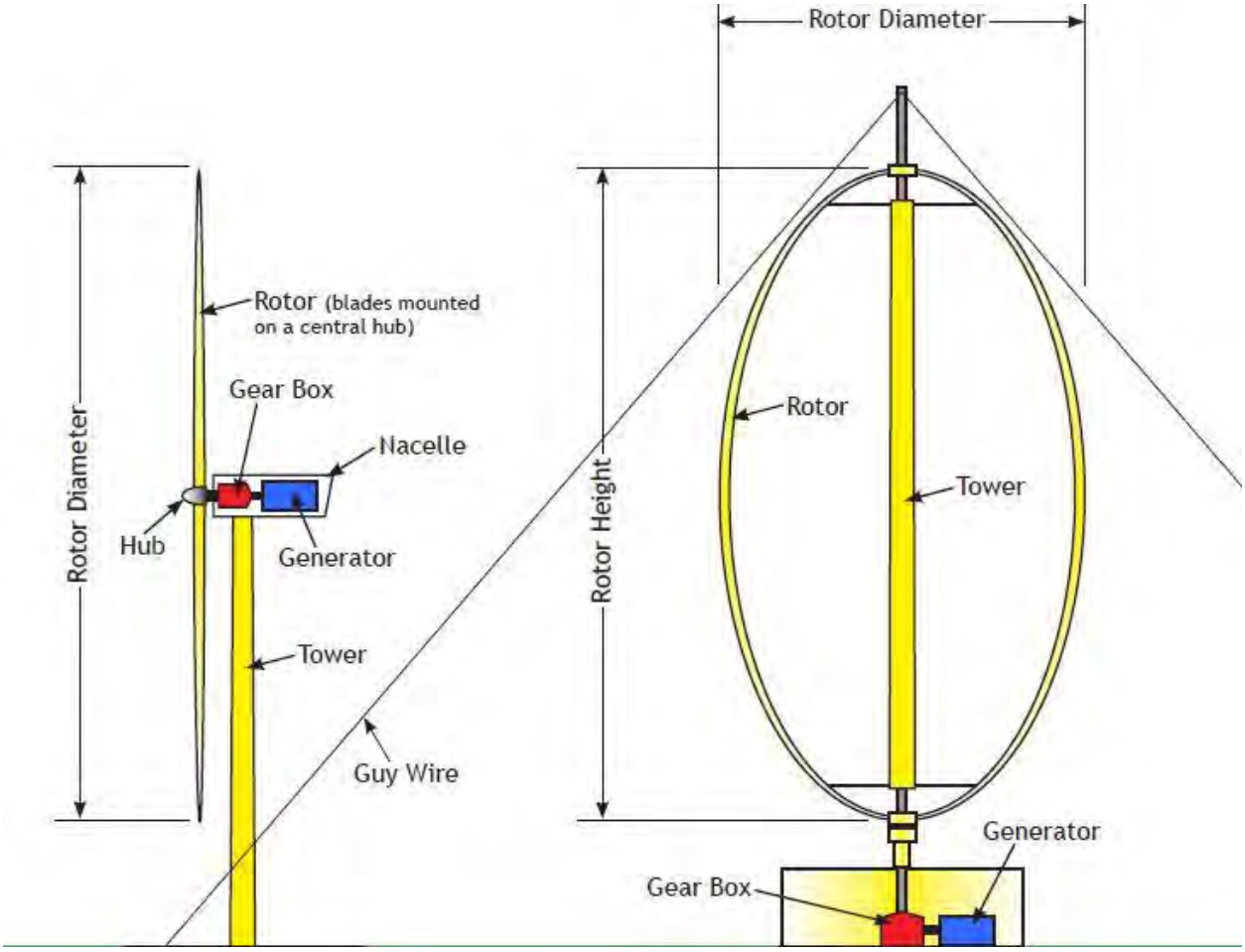

Figure 2.3: Basic Components of Different Wind Turbine Types (TeacherGeek.com, 2006)

Noise and structural instability are two major demerits associated with this type of turbine, but their low maintenance cost and minimal environmental impacts makes them suitable for residential and commercial purposes. A more recent design of the Darrieus wind turbine, shown in Figure 2.4 showed that they have a more helical shape which is necessary to improve structural stability, reduce wear and tear, as well as noise pollution (Chandrashekhar et al., 2019).

Unlike the Darrieus wind turbines, the design of Savonius wind turbines are less complicated. The main concept behind its operation is the use of drag force produced by the wind speed to turn the rotor; this simply means that speed of rotation is mainly dependent on the maximum speed of the wind. They are mainly used in home projects to power small amount of load. They are small and quiet, which makes it perfect for residential purposes (Tywoniuk and Skorupka, 2018). Many of the vertical axis wind turbines are majorly used for onshore purposes such as small-scale electricity generation, pumping of water, grinding of grains, among others (crystals12, 2012). Generally, it has been reported that vertical axis turbines technology are fast becoming popular and various designs continue to emerge for any type of area where sufficient amount of wind resource is experienced. And as the need for cleaner energy continue to be a top priority, vertical axis wind turbines will continue to dominate the market for residential and commercial purposes either through purchase or by self-operated designs (IRENA, 2016).

2.3.1.2 Horizontal axis wind turbines

The Horizontal Axis Wind Turbine (HAWT) is the most common wind turbine technology used in various applications. The most popular ones for electricity generation are the horizontal axis turbines with three blades. In addition to being parallel to the ground, the axis of blade rotation is parallel to the wind flow. It consists of the tower structure which holds the nacelle. The nacelle is a compartment where the gearbox and the electrical generator are located (Olabi et al., 2021; L. Wang et al., 2009). They are majorly use in offshore application for electricity generation, but can also be operated on a small scale design to supply electricity to remote location with sufficient wind speed. Small scale horizontal axis wind turbines, such as swift wind turbine uses a tail vane to direct the nacelle and rotor towards the direction of the wind. However, when they are implemented on a large scale, the nacelle and rotor are directed in and out of the wind direction with the help of a yawning mechanism, pitch control or a stall (X. Yang & Bai, 2010). A wider classification of the horizontal axis wind turbines showing their various application is presented in Table 2.2.

The tower of horizontal axis wind turbine are usually built to be very tall because of the need to capture high speed wind currents, which is the most important factor for power production. Another factor that

Figure 2.4: Typical Vertical Axis Wind Turbine (WED, 2015)

Table 2.2: Various types of horizontal axis wind turbines

HAWT Types	Features	Applications
Swift	Smaller turbine blades, easy to set up and less noisy.	They can be used majorly to generate electrical energy in cities and urban areas.
Eclectic	Turbine blades have the ability to generate power at low wind speed and low weight.	They can also be used to generate electrical in urban areas by tying it to building structures
Fortis Montana	Zero noise during operation	They are majorly used to generate electricity for domestic purposes due to their reduced size
Scirocco	Equipped with two-rotor turbine blade for efficient operation and can generate power at low speed.	They are used by utilities to provide cheap and reliable electrical energy
Tulipo	Can generate power at low wind speed and are also less noisy.	They are also used by utilities to generate large amount of electrical energy at low speed areas.

Source: (X. Yang & Bai, 2010)

determines the power produced by a horizontal axis wind turbine is the size of the cross-sectional area. This is the main reason why the rotor of the turbine is usually large. Horizontal axis wind turbines have been reported to have low cut-in-speed and relatively higher power co-efficient, and are therefore more stable and more suitable for electricity generation as compared to their vertical axis counterparts (crystals12, 2012). Moreover, the rotor of horizontal axis wind turbine is flexible as it can be operated either in the upwind or downwind of the tower. Another important feature of this type of turbine is the absence of pitch regulation, as the generator is located at ground level. The main problem associated with this type of turbine is their dependence on an external mechanism to start the rotor (Olabi et al., 2021).

Although, the most common type of horizontal axis wind turbines is the triple-bladed type, they also exist as a single-bladed, twin-bladed and multi-bladed types. The tip speed ratio of a horizontal axis wind turbine depends solely on the number of blades; several studies have shown that horizontal axis wind turbine with two or three blades have high tip speed ratio and is therefore considered in this study (Tywoniuk and Skorupka, 2018). It should be noted that horizontal axis wind turbines with more than 20 blades are only appropriate for pumping of water and cannot be used for the production of electrical energy because of the high degree of aerodynamic losses (Cao et al., 2012; Kim et al., 2010). An array of triple-bladed horizontal axis wind turbine plant is depicted in Figure 2.5.

2.3.2 Photovoltaic technology

Solar cells are made of semiconductors, which have weakly bonded electrons occupying a band of energy called the valence band. A semiconductor is described as silicon combined with phosphorous to make negative type silicon and boron to make positive type silicon, which can be combined to produce an electric field. A typical silicon cell is composed of a thin wafer consisting of an ultra-thin layer of phosphorus-doped (N-type) silicon on top of a thicker layer of boron-doped (P-type) silicon (Gray, 2011). An electrical field is created near the top surface of the cell where these two materials are in contact, called the P-N junction. When an energy beyond the band gap energy is applied to a valence electron, the bonds are broken and the electron is liberated to a new energy band called the conduction band where it is able to conduct electricity as depicted in Figure 2.6 (Oliveti et al., 2014). In simple terms, a solar cell is a P-N junction that absorbs light in form of radiation from the sun and releases electrons and holes, thus creating a voltage in the cell. An assembly of a number of solar cells in a single framework to generate direct current electricity using the energy from the sun is referred to as Photovoltaic (PV) module (Gray, 2011; Oliveti et al., 2014).

A single solar cell can only generate a minimum amount of electrical power; in order to generate more power, a number of cells are interconnected together to form modules. When more electrical power is to be generated, the modules can also be connected to form an array of different sizes (Eteiba et al., 2013).

Figure 2.5: A three-bladed horizontal axis wind turbine plant (EE, 2021)

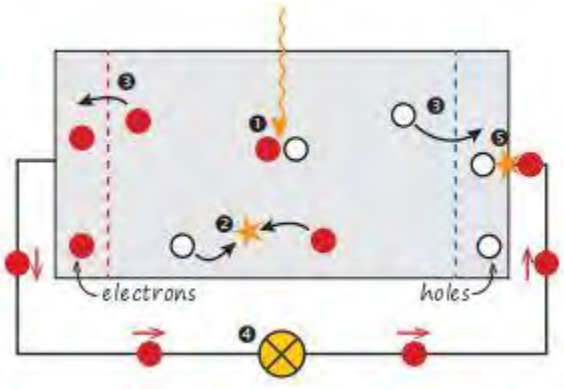

Figure 2.6: A simple model of the solar cell (Oliveti et al., 2014)

A single PV module is made of 33 to 36 silicon cells which are connected in string to a terminal box for interconnection purpose. The assembled cells are encapsulated between a transparent window and a reflective backing to shield them from weather and accidental damage; the edge of the PV module is sealed against moisture ingress and protected using a metal frame. A clamp is usually attached to the module to act as a supporting structure during installation (Balaraju & Chengaiah, 2020). A pictorial representation of a solar PV cell, module and array is as shown in Figure 2.7.

Solar cells are made majorly from three types of semiconductor materials; the first generation of solar PV cell is the crystalline silicon and at the moment, it is the main technology used commercially with more than 95 % share of global PV technology market (Bright, 2008). It has been produced in various forms, including single-crystalline, multi-crystalline, and amorphous. The second generation is polycrystalline thin films, with different grades of copper indium diselenide (CIS), cadmium telluride (CdTe), and thin-film silicon. Lastly, the single crystalline thin-film, which focuses majorly on cells made using gallium arsenide has also been used in producing solar cells (B.Eteiba et al., 2013; Bright, 2008). There are many other types of semiconductor materials that are also undergoing intense research in the production of solar cells in order to improve their efficiency, and reduce cost of PV technologies (Okere & Tariq Iqbal, 2021). Some of the many advantages of the PV technology in the production of electricity as given by Oliveti et al., (2014) are as follows.

i. It is clean and non-polluting
ii. They do not cause noise pollution as compared to wind turbines
iii. They require very little maintenance
iv. They require no fuel costs as they are abundant and free in nature
v. They have long life span.

Solar PV technology has been used extensively for various applications. Other than the obvious usage for electricity production for both residential and commercial purposes, they are also very useful in powering space vehicles such as satellites and telescopes; recently, they have also been used as a source of power to electric vehicles in many developed countries. As the global usage of PV technology continue to rise, it is only wise to improve on its current technology to meet the global demand. Improvements in PV technology will not only improve the efficiency, it will also help in reducing the cost, which in turn will further improve the cost of energy supplied using PV systems. Several emerging PV technologies which have the potential to displace the dominant single-faced silicon crystalline PV modules have been developed. A brief description of the various emerging PV technologies are subsequently presented.

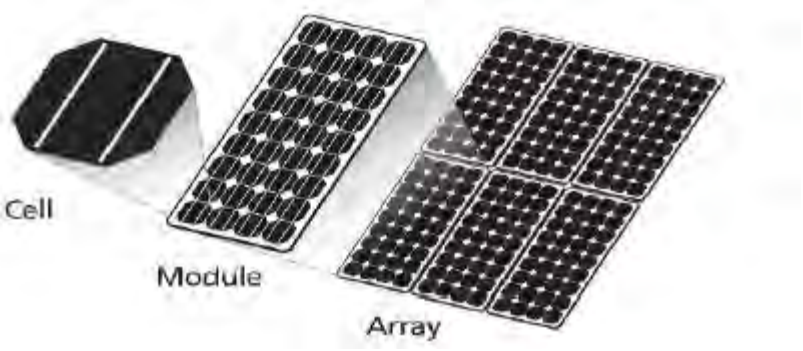

Figure 2.7: Pictorial representation of PV cell, module and array (Balaraju & Chengaiah, 2020)

2.3.2.1 Passive Emitter and Rear Cell (PERC) PV technology

Okere & Tariq Iqbal, (2021) reported that the PERC modules are gradually being introduced into the PV market due to its improved efficiency as compared to the traditional Aluminum Back Surface Field (AL-BSF) multi-crystalline solar PV modules. The improved efficiency of the PERC modules is mainly attributed to the reduction in the recombination process and reflectivity of the back side of the module.

The design of the PERC module consist of a dielectric layer; a combination of aluminum oxide and silicon nitride which separates the screen-printed aluminum layer and the silicon surface. This setup enables the PERC modules to absorb more radiation and subsequently produce more electricity as compared to the traditional crystalline silicon modules. Moreover, the loss of energy experience in traditional PV module design is not peculiar to PERC modules due to the design layout (Deng et al., 2015). The presence of the dielectric layer makes it possible for the PERC modules to absorb more light using its back side, and prevents the aluminum surface from interacting with the silicon surface. As a result, it reduces the back side recombination and improve its reflectivity, which leads to increased efficiency and improved performance regardless of the intensity of the radiation. It has been reported that PERC modules have the ability to produce a bifacial gain of up to 8 % (Okere & Tariq Iqbal, 2021).

2.3.2.2 Half-cell PV technology

The modules of half-cell PV technology consists of solar cell that are much more than the traditional PV technology. Generally, the modules consists of 120 to 144 half cells as compared to the 66 and 72 half cells used in the design of the conventional modules. The main reason for the increased in the number of solar cells is to improve the performance and life span of the technology. Some of the advantages of using a half-cell solar modules include reduced resistive losses since the current in a cell depends majorly on the cell area (Okere & Tariq Iqbal, 2021). Moreover, it also offer an improved electrical energy production due to the presence of two half cells which are capable of producing more energy than a single full cell; a 3 % energy gain has been reported for half-cell modules in literatures. Half-cell module also helps eliminate the issues related with hot spot; in addition to that, it offer better utilization of the land size area, responds faster to the effect of shadow due to the flexible interconnections of the cells and it offer enormous economic advantages (Mesquita et al., 2019; Okere & Tariq Iqbal, 2021).

2.3.2.3 Hetero-junction with thin layer (HIT) PV technology

Another important emerging PV technology is the Herero-junction with thin Layer (HIT) PV technology; basically, HIT PV is a hybrid of crystalline and non-crystalline silicon solar cell in a single module. Thus HIT technology combines the high efficiency and high stability of crystalline silicon with the minimal temperature and low cost of non-crystalline silicon in a single module. The resulting combination has been

reported to produce 27 % efficiency which is presently the highest of all PV modules commercially available (Mesquita et al., 2019; Okere & Tariq Iqbal, 2021).

2.3.2.4 Bifacial PV Technology

Bifacial PV module is a promising technology which allows solar cells to absorb light from the front and rear side simultaneously as shown in Figure 2.8a. Despite the increase in cost resulting from modifying the solar cell and module structure, bifacial solar modules produce more power compared to their mono-facial counterparts (Mesquita et al., 2019). Bifacial solar cell's front design is usually the same as the conventional mono-facial solar cell. However, the rear side structure varies, the main difference is observed in the surface rear contact. In a conventional mono-facial solar cell, an aluminum rear contact covers the entire backside of the module. However, in bifacial solar cells, a finger grid is used to allow the light onto the backside of the surface of the cell (Sun et al., 2018). A typical bifacial solar cell and module showing the front and rear side is depicted in Figure 2.8b.

Recently, bifacial PV module has gained much attention in the PV industry as it accounts for about 20 % of the total market share, however, the usage of bifacial cells continues to rise. As at 2021, bifacial cells account for about 28 % of the total global cells used in production of PV technologies. This fact further establish the huge improvement made in the modification of existing solar cells to increase energy production (Mesquita et al., 2019; Okere & Tariq Iqbal, 2021). As reported by Fajuke & Raji, (2022), the additional power output from a bifacial PV module could be as high as 45 % depending on various factors such as mounting surface, mounting angle and mounting orientation. The most important of these factors is the albedo of the mounting surface as it determines the amount of the energy gain using bifacial PV modules. In simple terms, the albedo of a mounting surface is defined as the ratio of the reflected light to the direct incident radiation of the sun (Okere & Tariq Iqbal, 2021). The albedo values of some popular mounting surface is presented in Table 2.3.

Bifacial PV modules and systems have a strong potential to surpass mono-facial ones as there are many conditions where the total amount of incident light on both sides could lead to higher energy generation than the conventional mono-facial module installed with an optimum tilt angle (Graefenhain et al., 2017; Russell et al., 2017). Hence, it is of great interest to researchers, utility companies and decision makers to understand this technology; and how much more power output is to be expected out of it with respect to economic implications (Arifin et al., 2021).

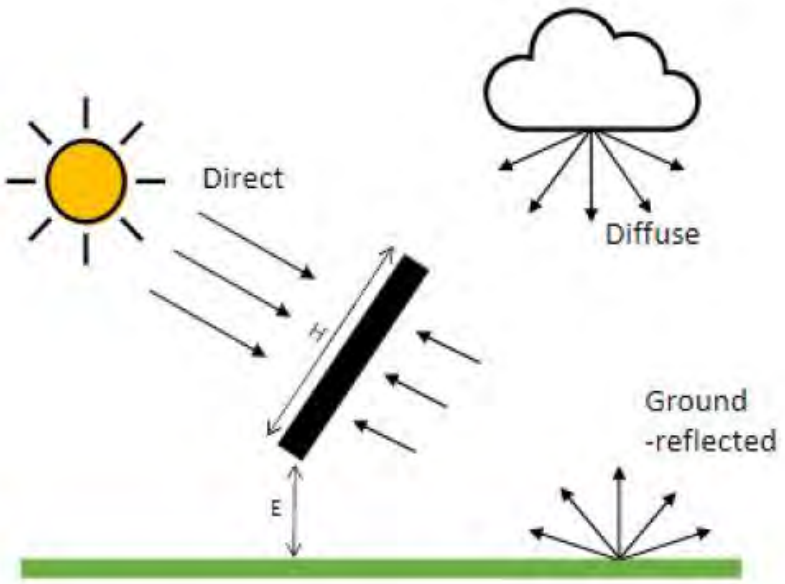

Figure 2.8a: Basic operation principle of bifacial PV module (Oliveti et al., 2014)

Figure 2.8b: Typical bifacial PV cell and module (Mesquita et al., 2019)

Table 2.3: Sample albedo co-efficient value of selected surfaces

SURFACE TYPE	ALBEDO CO-EFFICIENT (%)
Ocean ice	(50-70)
New concrete with white portland cement,	(70-80)
New concrete (traditional),	(40-55)
Aged concrete	(20-30)
Desert sand	40
Fresh snow	(80-90)
White acrylic paint	80
galvanized steel	24
Soil (Dark/Wet)	5
Soil (Light/Grey)	40
Green grass	25
Bare soil	17
white paper sheet	(60-70)
polished aluminum	(65-75)
Mirror	(72-85)
Water,	(3-100)

Source: (Sun et al., 2018)

2.4 Hybrid power system

In general terms, a hybrid system is defined as a combination of two or more systems with different characteristics, inputs and dynamics that uses the strengths of one sub-system to overcome the weakness of the other in order to improve its own overall efficiency (Heemels et al., 2011). The concept of hybrid system in power system refers to a combination of two or more power generating systems (renewable or non-renewable) in a single system to provide electrical energy to a specified location; this resulting combination is popularly known as Hybrid Power System (HPS) (Lassalle et al., 2022). The major goal of hybridization of energy systems is to compensate for the numerous downside exhibited by one system with the merits of the other. Typical HPS includes a conventional generator powered by either gas, or diesel, for example, and a RE generator which could include solar PV, wind turbine, small-hydro and energy storage system such as battery unit if required, as shown in Figure 2.9 (A. Raji & Kahn, 2012; Sawle et al., 2016a).

HPS consisting of solar PV, wind turbine and small-hydro systems have been found to be cost-effective on a lifetime basis for providing power to the many remote areas where the cost for large scale expansion of electrical grids is difficult, and critical facilities where an economical, uninterrupted and reliable supply of electrical energy is required (A. K. Raji & Luta, 2019; Sengupta et al., 2012). HPS consisting of clean energy sources such as solar and wind as main energy sources are environmentally friendly and can be easily maintained. The main components of the HPS proposed in this study consists of solar bifacial (PV) generator, wind turbine generator, battery bank and split diesel generator set (genset) as back-up.

There are majorly two categories of HPS as reviewed in various literatures; the first category of HPS is based on system operation while the second category describes the basic connection of the system (Ammari et al., 2021). A brief description of the two categories are presented in the following sub-sections.

2.4.1 Hybrid power system operation

Hybrid power system can either be operated as a grid-connected or standalone system. A grid-connected HPS is described as a self-contained power system that is connected to the power grid, which functions as a storage unit with an infinite capacity, eliminating the need for a battery storage (Abaye, 2018; Syafaruddin & Zinger, 2020). The main purpose of a grid-connected system is to meet local load demand, with surplus energy being sent into the grid. On the other hand, a standalone HPS is a self-sustaining power system which is designed to operate independently. This type of system are suitable for remote electrification and critical facilities where grid extension is not feasible. (Ibrahim et al., 2011; Shi et al., 2017). For better performance of a standalone HPS, individual solar PV or wind turbine combination require an energy storage system to store any excess energy during peak period of the RE generators, and a diesel generator set as backup. The resulting configuration will help enhance the efficiency of the system for

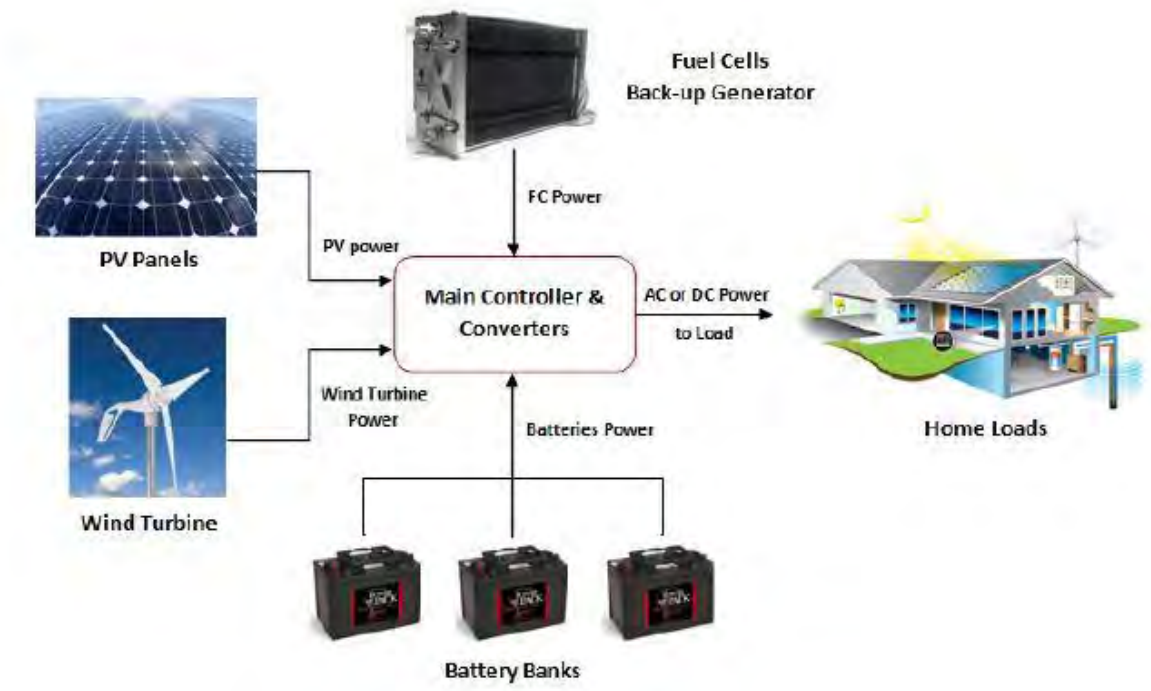

Figure 2.9: Typical hybrid power system configuration (Babatunde et al., 2020)

improved operation, better reliability and reduction in life cycle cost of the system (Bourennani et al., 2015).

2.4.2 Hybrid power system connections

There are three typical ways in which the components of HPS can be connected, and they include Direct Current (DC), Alternating Current (AC) and DC-AC coupled connections. The three connections are named based on the type of bus-bar connecting the various energy generating sources of the system to the load (Babatunde et al., 2020; Nehrir et al., 2011). The various categories of HPS connections are subsequently discussed.

2.4.2.1 DC coupled hybrid power system connection

The DC coupled HPS connection is also referred to as a series HPS configuration, this type of connection has all the components of the system including the energy storage unit and electrical energy generating devices are connected to a DC bus. All the devices output are converted into DC and then connected to the main DC bus. The DC bus is then connected to a DC or an AC load via DC/AC inverter depending on the need of the final consumer as shown in Figure 2.10 (Babatunde et al., 2020; del Moral & Egido, 2012). The DC coupled HPS are simple, easy to implement and produce stable energy output. However, the main shortcoming of this connection type is its low overall efficiency and limited overall DC/AC inverter capacity (del Moral & Egido, 2012; Tahir & Khaliq, 2018).

2.4.2.2 AC coupled hybrid power system connection

The AC coupled HPS is also referred to as parallel HPS configuration. In AC coupled HPS connection, all system components including the energy storage and electrical energy generating devices are connected to an AC bus (Babatunde et al., 2020). Each device output is directly inverted to AC voltage via the DC/AC inverter and then connected to the AC bus as shown in Figure 2.11. The AC coupled HPS has a better performance when compared to DC coupled HPS in terms of overall system efficiency. In this type of configuration, each generator can supply the load independently from other generators (Babatunde et al., 2020; Nehrir et al., 2011). The main advantage of this connection is their ability to manage smaller power, improved overall system efficiency and better overall system stability. Their main drawback is its complicated control system, which is required to maintain optimum synchronization among system components (del Moral & Egido, 2012).

2.4.2.3 DC-AC coupled hybrid power system connection

The DC-AC coupled HPS connection utilizes both AC and DC bus bar it is also known as alternative parallel configuration. In a DC-AC couples HPS connection, all electrical energy generating components which supply AC such as the wind turbine generator and diesel generator are connected to an AC bus and

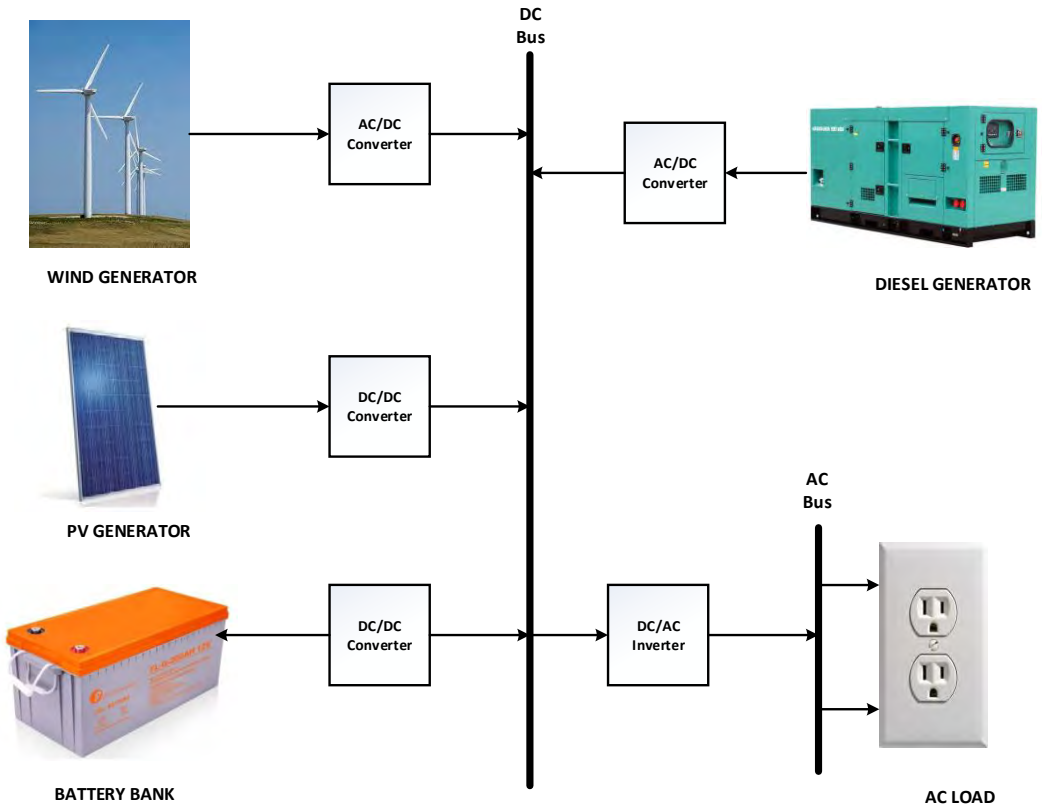

Figure 2.10: DC-coupled HPS connection (Babatunde et al., 2020)

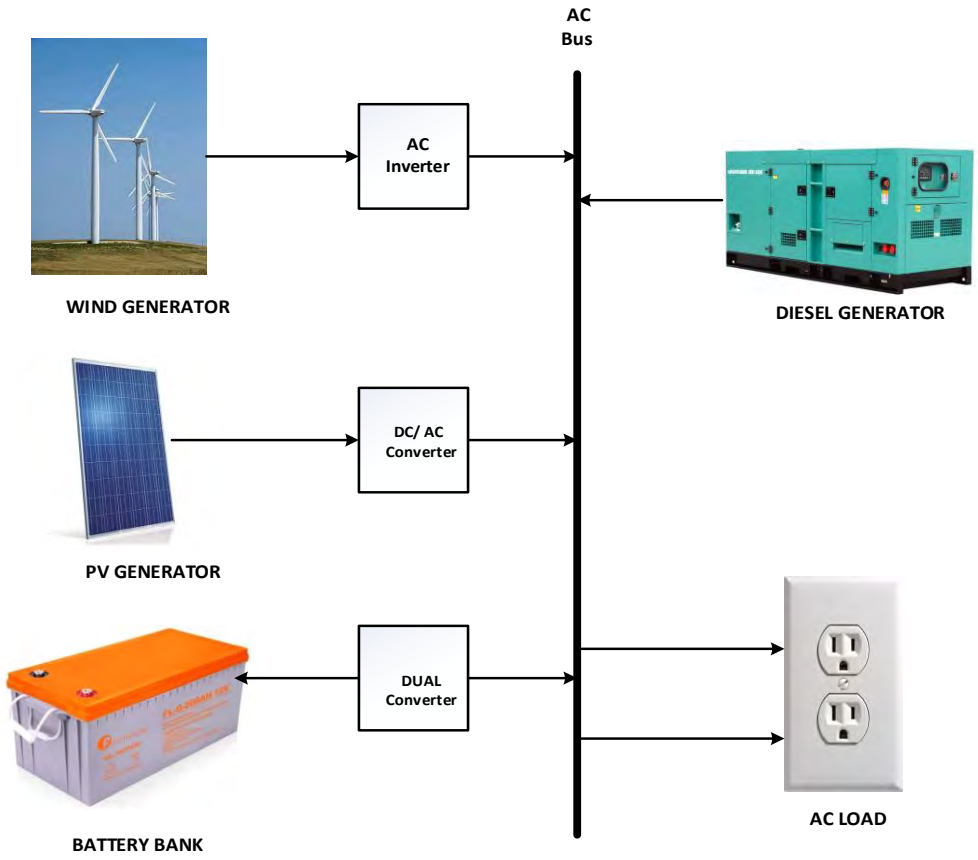

Figure 2.11: AC-coupled HPS connection (Babatunde et al., 2020)

DC components such as solar PV generator and energy storage system are connected to a DC bus as shown in Figure 2.12. Both AC/DC converter and DC/AC inverter are used between the two buses, which depend entirely on the design and system requirements (Nehrir et al., 2011). The main advantage of this type of connection is its minimal conversion losses due to the direct connection of AC and DC loads to their respective buses. Moreover, this type of connections offers higher efficiency and lower system cost. However, control and energy management is much more complex when compared to both DC and AC coupled connections (del Moral & Egido, 2012; Tahir & Khaliq, 2018).

2.4.3 Hybrid power system control schemes

The main purpose of the control scheme in HPS configuration is to monitor, regulate and control the endless interaction among the various energy sources and the consumer load. Failure to provide the necessary control scheme will have negative effect on the overall efficiency of the system. An effective control scheme will not only improve the reliability of the HPS, it will also help in reducing the cost implication of the entire HPS configuration (Nehrir et al., 2011). The control scheme in a HPS are classified into three main categories namely the centralized control scheme, distributed control scheme and hybrid control scheme. For each category, each of the energy generating sources is equipped with a localized controller to regulate its optimal operation and then connected to a central bus (Babatunde et al., 2020). A brief description of the individual category is presented in the following sub-sections.

2.4.3.1 Centralized control scheme

The centralized control scheme is arranged in such a way that each of the energy generating components are equipped with a local controller which are interconnected to a master controller. The master controller controls the activities of all other controllers in this scheme; it collects all the information received by the local controller from the various energy generating components and uses it to make accurate decisions for efficient operation of the system (Babatunde et al., 2020). In other words, the master controllers monitors and control the interaction among the various energy generating components in the system. The centralized control scheme has been reported to be very efficient and reliable, however, it involves a lot of mathematical computation and the failure of one of the sub-controller may lead to complete breakdown in the scheme (Babatunde et al., 2020; Nehrir et al., 2011).

2.4.3.2 Distributed control scheme

As compared to the centralized control scheme, the arrangement of in a distributed control scheme does not involve the utilization of a master controller (Nehrir et al., 2011). Energy coordination is done via the interaction among the various sub-controller of the energy generating components. Even though distribution control scheme have been reported to have minimal computational complexity and does not suffer from

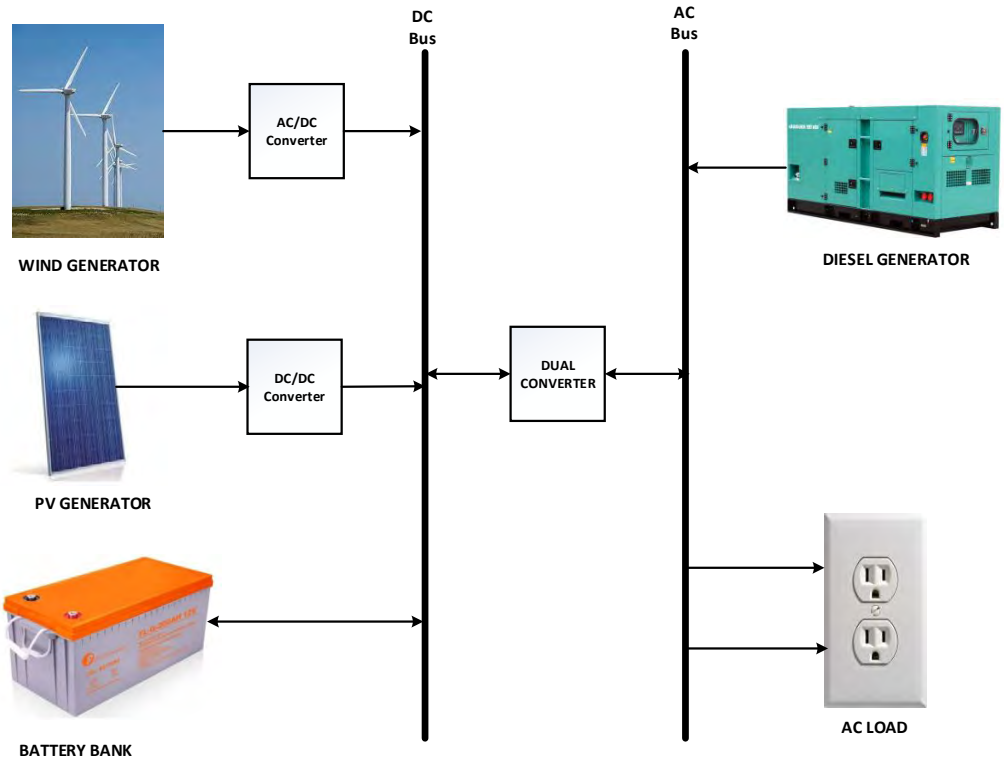

Figure 2.12: AC-DC coupled HPS connection (Babatunde et al., 2020)

issues related with single point failure, the complexity that arises via interaction of the sub-controllers may result to instability of the HPS.

2.4.3.3 Hybrid control scheme

The hybrid control scheme is a combination of the centralized and distributed control schemes. Energy generating components with similar characteristics within the HPS configuration are connected to a single sub-controller; the output of each sub-controllers are subsequently connected to a master controller resulting to an arrangement similar to the distributed control scheme (Babatunde et al., 2020; Nehrir et al., 2011). The master controllers are then made to communicate within themselves to make informed decisions on the control, regulation and monitoring of the various energy generating sources of the HPS. This type of control scheme is reported to be the most efficient of the three HPS control schemes currently available. It is reliable, effective and has minima computational complexity (Babatunde et al., 2020).

2.5 Description of the major components of the proposed HPS

The description of the major power generating components of the proposed HPS is presented in this section; power generating components are responsible for the energy conversion process taking place in the system. These components include solar bifacial PV system, wind turbine generators, energy storage system, split generator set and power converters. The primary source of energy are the solar and wind energy components, the storage system and the split generator set are included in the configuration as a back-up. The appropriate sizing of these components is significant to the efficient and reliable operation of the HPS. A detailed description of each of the components used in this study is subsequently presented.

2.5.1 Bifacial PV component

The basic operation principle of generating energy using bifacial PV module is quite similar to energy generation using traditional mono-facial PV modules which has been described in sub-section 2.3.2 of this study. However, a bifacial PV module can produce more energy using its front and back side due to the presence of the back electrode which is absent in mono-facial modules (Fajuke & Raji, 2022; Okere & Tariq Iqbal, 2021). Generally, many of the commercially available bifacial PV modules are made using mono-crystalline silicon materials. As research continue to intensify towards improved PV technology, hetero-junction with intrinsic thin layers, Passivated Emitter and Rear Cell Technology (PERC), Passivated Emitter and Rear Totally diffused (PERT) and Passivated Emitter and Rear Locally diffused (PERL) have all been used in the design of recent bifacial PV module in order to improve its efficiency (Mesquita et al., 2019; Okere & Tariq Iqbal, 2021).

A typical bifacial PV module has a glass covering on both the front and back side which protects the solar cell in the module from corrosion and early degradation. Generally, the power rating of PV panel depends

on the number of cells and the size of the module (Kopecek & Libal, 2021). A bifacial PV module is equipped with solar cells at both the front and rear side, thus increasing its power rating. The interconnection of the bifacial PV modules forms an array which is capable of generating more power at a constant voltage. Interconnecting these array of modules to generate electrical power subsequently results in what is known as a bifacial PV system (Wang et al., 2015). The performance of bifacial PV system depends on the spatial distribution of the incident irradiance on the back side of the module, which is strongly affected by several conditions such as albedo of the ground surface, module elevation, azimuth, tilt angle, size of the system, and the distance between module rows (Russell et al., 2017; Solarworld, 2015). The diverse effects of these conditions on the additional energy of a bifacial PV system are as follow.

1. **Albedo**

The albedo, otherwise known as the ground reflectance, is one of the most important conditions that decide the extra energy gain of bifacial PV modules. It is a property of a non-luminous surface that describes the capacity to reflect part of the solar radiation received. Mathematically, it is expressed as the ratio between the reflected radiation and the incident radiation on a surface. Increasing the albedo of the surface of the PV plant increases the amount of the reflected radiation on the back side of the module and subsequently, the system's overall performance (Russell et al., 2017).

2. **Mounting Elevation**

Unlike mono-facial PV systems, performance of bifacial systems design depends on the height of the modules above the ground. The module height (elevation) is simply defined as the distance between the bottom of the lowest part of the module and the installation surface. The module height is of great importance to the extra energy yield of the bifacial module. A bifacial module installed close to the surface will be affected by self-shadowing (Wang et al., 2015). However, an increase in the height of the modules over the ground leads to an increase in the clearance of the ground and subsequently leads to an increase in the backside irradiance. It is also of great importance to be aware of the fact that due to higher wind loads, high module mounting structures are also more expensive and mechanically more challenging. Therefore, determining the optimal height of the modules is also a compromise between finding the height in which the modules are far enough from its own shadow (Fajuke & Raji, 2022; Moehlecke et al., 2014).

Moreover, it is worth noting that for surfaces with high values of albedos, bifacial gain increases with the height. However, the trend has a saturating effect; this occurrence is due to the fact that for certain heights the self-shadowing on backside irradiance is diminished and increasing the height does not increase the performance (Solarworld, 2015; Wang et al., 2015).

3. Bifaciality of the module

Another important condition is the bifaciality of the module. In addition to the front side power, a new important parameter is added to the bifacial modules. The transparent and active back sides of bifacial PV modules enable an extra energy yield, also known as the "energy gain". Mathematically, the bifaciality, B of the module is expressed as the ratio of the back side power (P_{mpp}) to the power generated from the light captured from the front side at Standard Test Conditions (STC) (Ganilha, 2017).

4. Azimuth

In order to fully understand the concept of azimuth angle, it is important to understand the ideal of module orientation. Optimal orientation of bifacial modules is an important condition to be considered in the design of bifacial PV systems. When analyzing the orientation of the modules two orientations state must be confined (Ganilha, 2017). The first orientation state is the vertical east-west-facing bifacial modules and the second is horizontal north-south-facing bifacial modules. It has been reported that vertical east-west-facing modules suffers less from self-shading and can produce more power than horizontal south-north-facing modules (Fajuke & Raji, 2022) Hence, the vertical east-west module orientation is majorly considered for simulation purpose in this study.

5. Size of the System

Since PV systems are hardly installed singularly or involving one-row modules and they are rather installed in a field with neighboring modules and several module rows, simulations and experiments with stand-alone modules or single module rows are insufficient to enable an accurate prediction of the extra energy yield of a bifacial module PV system. It has been stated that the higher the number of modules, the bigger the impact on the bifacial gain and hence the system's overall performance (Razongles et al., 2016). However, it is also expected that with a higher number of adjacent modules, a saturation point in which bifacial gain is no longer negatively affected is achieved. This means, that up to a certain number of modules self-shading does not increase further. Therefore, when considering the design of a bifacial PV system, it is very important to consider the size of the system during simulations (Pelaez, Deline, Greenberg, et al., 2019; Razongles et al., 2016).

6. Tilt Angle

This describes the mounting angle of the module, This parameter varies from site to site, but generally, 3 to 12 degrees more than the mono-facial tilt angle have been reported to be quite effective. It should be noted that an increase in the tilting angle will slightly decrease the temperature of the mounting surface. Moreover, the optimal tilt angle also depends on many other factors such as the size of the system, location of the plant and the time of the year (Fajuke & Raji, 2022; Salloom et al., 2018).

7. **Pitch**

This is known as the distance separating each module in a bifacial PV system setup. In the design of bifacial PV systems, beside considering allowable amount of module front side shading by other modules, also the blocking of the ground-reflected irradiance by the shadowing produced by neighboring module rows has to be taken into consideration. Hence, finding the optimum distance between two modules makes it possible to reach a compromise between minimizing the shading losses from both front and rear sides of a module as well as maximizing the number of rows installed for a finite available land surface (Ganilha, 2017)

Generally, PV systems including mono-facial and bifacial PV systems are installed in different orientations. The most popular installation option for both commercial mono-facial and bifacial PV systems is the fixed-tilt orientation. In this configuration, PV arrays are tilted at a fixed angle and are installed with their front sides facing the equator (south facing for north hemisphere sites and north facing for south hemisphere sites) (Solarworld, 2015). The tilt angle is usually chosen to maximize the annual energy yield of the system. However, many others installation option have been researched to maximize the energy production of bifacial PV systems (Pelaez et al., 2019; Salloom et al., 2018). The three main configurations of a bifacial PV system are subsequently presented

2.5.1.1 Vertical bifacial PV systems

Although the main advantage of bifacial PV system design is the additional energy yield, there are also applications that are impossible to carry out with the use of mono-facial modules. Vertical mounting bifacial PV systems, typically in an east-west orientation, is one of the most considered installation option for bifacial PV modules. Vertical bifacial PV systems present particular benefits such as no sticking snow in snow-rich regions and minimized soiling and sand deposition for desert locations (Louw & Rix, 2019; Pelaez et al., 2019). Moreover, this type of installation avoids the maximum power generation peak at noon and instead contributes to a more consistent energy production throughout the day. Thus, improving the alignment between electricity production and demand. However, vertically installed bifacial PV systems suffer from very pronounced shading and therefore, the energy yield will heavily depend on the specific lay-out of the PV system (Pelaez et al., 2019)

2.5.1.2 Horizontal floating bifacial PV systems

The main reason for floating PV is attributed to the large size of land required for ground-mounted PV systems; in many areas of the world land is scarce or there simply is not enough usable land to supply renewable energy locally (M. Alam et al., 2021). A clear advantage is the potentially large scale of projects; as long as the original function of the water surface is not compromised, large patches of water are potentially available for bifacial PV installation. Another advantage is the additional cooling effect thanks to the temperature inertia of the water mass. Besides from those advantages, bifacial modules add an extra

and significant advantage which is the bifacial gain (Deline et al., 2017). In general, water is regarded as a material that has a very low albedo of below 10 % and as such, the bifacial gain of the installed bifacial PV system is not fully utilized. The albedo of the mounting surface is a very important factor when considering the additional energy yield of bifacial PV systems (Pelaez et al., 2019).

2.5.1.3 Horizontal single-axis tracked bifacial systems

During the last few years, Horizontal Single-axis Tracking (HSAT) has become a very important technology in regions close to the equator with the goal of maximizing the energy yield as well as to reduce the electricity generation costs. And even though bifacial systems in combination with tracking have thought to be incompatible, recently studies reveal that the combination of tracking with bifacial modules makes very much sense and lead to very high-power generations. Another demerit of this type of installation method is the huge cost of building a tracker (Kopecek & Libal, 2021; Pelaez et al., 2019).

2.5.2 Wind turbine component

The continuous growth in wind turbine technology has led to an increase in wind power generation into the energy generation mix. Wind turbine generators are designed to capture the kinetic energy present in wind and convert it to electrical energy. The power output of a wind turbine generator depends majorly on the interaction between the wind turbine rotor and the wind; however, the mean power output is determined by the mean wind speed (Sateesh Kumar et al., 2020). Horizontal Axis Wind Turbine (HAWT) is the most dominant wind turbine technology used in various wind power plant for commercial purposes and are usually rated between 500 kW to 5 MW (Chaar et al., 2011). Wind energy as reported by Reinemann and Heinzen, (2014) is critical to the development of a low-carbon, environmentally friendly economy. The energy from the wind was originally used in the late 19th century to create electricity, but did not gain momentum because of the dominance of steam turbine power generation in those days (Cao et al., 2012; Kim et al., 2010).

The HAWT consists majorly of a blade and hub rotor assembly which are used to extract power from the wind, a gear train which is used to step up the kinetic energy of the wind from low values available at the rotor shaft to higher values required to drive the generator; and an induction generator which converts the mechanical power into useful electrical power (Davis et al., 2021). An induction machine is used as a generating unit in the wind turbine generator because of their asynchronous nature which is capable of coping with the varying wind speeds in the atmosphere, lowering physical stress on the turbine blades and drive train and enhances the system aerodynamic efficiency and torque transient behaviors (Sateesh Kumar et al., 2020).

Based on the energy conversion process in wind turbine technology, wind turbine generators are categorized into four major types; The fixed speed wind turbine generators which uses the squirrel-cage induction machines, variable speed wind turbine generator which uses the wound rotor induction machine, Double-Fed Induction Generator (DFIG) wind turbine which also uses the wound rotor induction machine and the full converter wind turbine generator which uses both induction machine and permanent magnet (Cao et al., 2012; Reinemann & Heinzen, 2014; WESL, 2016). A brief description of the different categories of wind turbine generators are presented in the following sub-sections.

2.5.2.1 Fixed-speed wind turbine generator

The first generation of wind turbines were designed to operate at fixed speed, such that the kinetic energy of the wind have zero effect on the speed of the turbine blades. As a result, they are not equipped with blade-pitching capability; however, the main parameters that influences the speed of the turbine blades are the gear ratio and generator design. Many of the fixed speed wind turbines employ a squirrel-cage induction generator (SCIG) which converts the mechanical energy of the generator to electrical energy (Bhaskar & Jimoh, 2016). Although, fixed speed wind turbine generator have been reported to be relatively robust and reliable, the resulting power output captured from the wind is very low and requires an external reactive power compensation for efficient operation. A typical fixed speed wind turbine generator is made of turbine rotor and blade assembly, shaft and gearbox, the SCIG, as well as the control system as shown in Figure 2.13a. They are mostly used in domestic applications due to their relatively low cost (Bhaskar & Jimoh, 2016; M. Singh & Santoso, 2012).

2.5.2.2 Variable-speed wind turbine generator

Unlike the fixed-speed wind turbines generators, the variable speed wind turbine generator can be operated over a wide range of wind speed and can extract the maximum power output from the wind regardless of the wind speed range. This type of turbine have the ability to generate power, even at higher wind speeds due to the presence of a variable resistor, that controls the range of the wind speeds which has been reported to vary between zero to ten percent above synchronous speed (Bhaskar & Jimoh, 2016). The electromechanical conversion of the variable-speed turbine generator is provided by a Wound Rotor Induction Generator (WRIG). The soft starting method in in the configuration of the variable-speed wind turbine generator helps to minimize the input current and thus eliminate the need for reactive power compensation. However, the turbine has its own inherent limitations such as limited usage of speed range, poor control of active and reactive power and power losses due to hear in the rotor circuit (M. Singh & Santoso, 2012). The setup of a typical variable-speed wind turbine generator is as shown in Figure 2.13b.

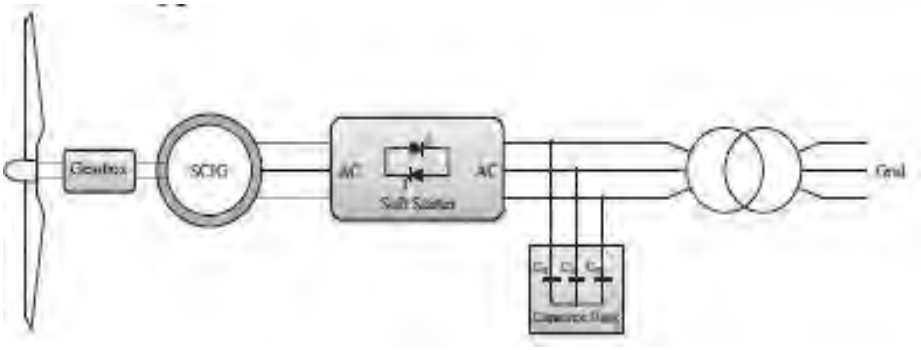

Figure 2.13a: Fixed-speed wind turbine generator (Bhaskar & Jimoh, 2016)

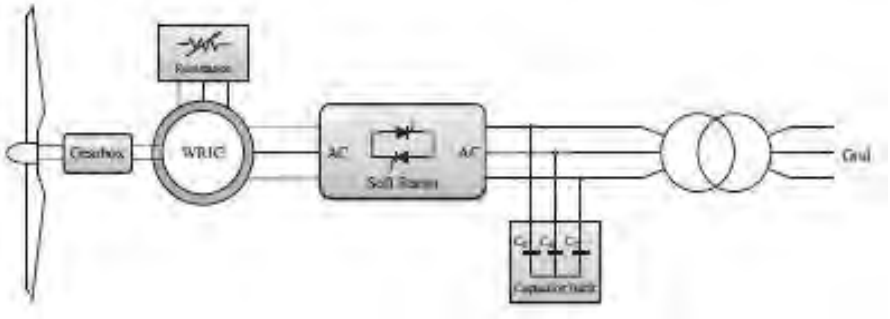

Figure 2.13a: Variable-speed wind turbine generator (Bhaskar & Jimoh, 2016)

2.5.2.3 Double-Fed Induction Generator (DFIG) wind turbines

The construction of a Double-Fed Induction Generator (DFIG) wind turbine is akin to that of the variable-speed wind turbine generator, the only difference is the inclusion of the partial scale power converter which is connected between the rotor, through the stator and the main grid. This arrangement helps to extract and regulate the maximum mechanical power from the wind resource (Bhaskar & Jimoh, 2016; M. Singh & Santoso, 2012). It is essentially made up of turbine blades and hub assembly which are linked to the generator shaft via a gearbox and a partial scale converter as depicted in Figure 2.14a. The main function of the gearbox is to increase the angular speed and communicate with the induction generator during the electromechanical conversion process (WESL, 2016). It should be noted that the power converter in a DFIG wind turbine only regulate the power in the rotor circuit; therefore, its rating does not necessarily have to correspond to the rated output of the generator (Aliprantis & Lafayette, 2014).

Reactive power compensation in DFIG wind turbines is provided by flux-vector control of the rotor currents, which also helps in maximizing the extractable wind power and reduce mechanical stress on the turbine blades. Similar to the variable-speed wind turbine, the electromechanical conversion is performed by a wound-rotor induction generator (Bhaskar & Jimoh, 2016). The real and reactive power are controlled by controlling the current passing through the rotor circuit using a control system which is capable of extracting the maximum possible power from the wind and control the power output of the generator. The vector control, which is also known as field-oriented control approach has been reported to be the most reliable control method (Babu & Divya, 2017; M. Singh & Santoso, 2012).

Some of the advantages of the DFIG turbines are their cost-effectiveness and provision of a simple blade-pitching capability, which provides independent control of active and reactive power. The DFIG turbines have also been reported to offer some advantages over emerging wind turbine technologies such as the full converter wind turbine; the full-converter turbine generator makes use of a full AC-DC-AC power converter for the stator, thus implying that the rating of the converter has to match the entire power output of the generator, which subsequently increases the cost when compared to the DFIG turbines (Bhaskar & Jimoh, 2016; M. Singh & Santoso, 2012). Therefore, in this study, the DFIG turbine is considered for simulation purposes.

2.5.2.4 Full converter wind turbine generator

The full converter wind turbine (FCWT) generators are recent wind turbine technologies, which have been deployed in many parts of the world. Some of the contributing factors behind the increasing deployment of this type of turbine include the absence rotor windings and slip rings which minimizes excitation losses and size of the generating unit and frequent maintenance. They are constructed with a full scale power converter

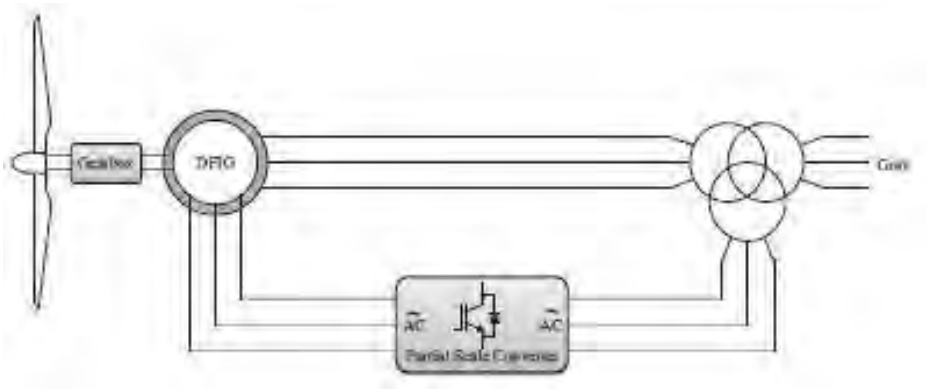

Figure 2.14a: Double-Fed Induction Generator (DFIG) wind turbines (Bhaskar & Jimoh, 2016)

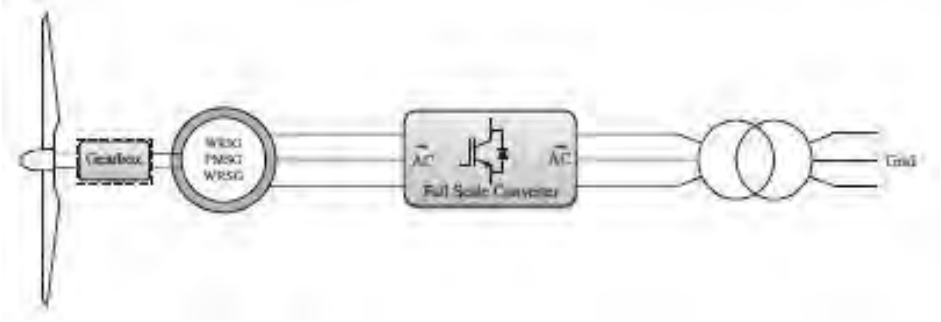

Figure 2.14b: Full converter wind turbine generator (Bhaskar & Jimoh, 2016)

which is capable of handling the power flowing through the rotor and the generator (Aliprantis & Lafayette, 2014). Hence, the only path for power flow from the turbine generator to the grid is through the full scale converter system. The electromechanical conversion in FCWT can be provided by any of wound rotor synchronous generator (WRSG), WRIG and Permanent Magnet Synchronous Generator (PMSG) as depicted in Figure 2.14b (Bhaskar & Jimoh, 2016).

The main strengths of the FCWT over other turbines are improved fault response, high capability in extracting the maximum power from the wind and constant supply of reactive power compensation to the grid. However, they have also been reported to uneconomical due to the cost implication of the power converter. Many of the FCWT are used in offshore wind power plants (M. Singh & Santoso, 2012).

2.5.3 Split diesel generator set

A Diesel Generator (DG) as described by Mobarra et al., (2022) is referred to as a diesel engine combined with an electrical generator (an alternator) to generate electrical energy. It essentially consists of diesel engine, governor, excitation and a synchronous generator as depicted in Figure 2.15. The basic operation principle of a DG set is based on two important components, the diesel engine and the generator, usually a synchronous generator which is mostly used for many industry standard DG set. The diesel engine a prime mover with constant speed and an output frequency of 50 Hz or 60 Hz (Benhamed et al., 2016). There are various categories of diesel engines; generally, they are categorized in accordance with the number of strokes, method of cooling, intake of air, number of cylinders, arrangement of cylinder and the rotational speed (Knudsen, 2017). A brief description of each category is presented as follow.

1. *Classification according to the number of strokes*: The two main types of diesel engine under this category are the four strokes and two strokes engines.
2. *Classification according to the cooling way:* Water-cooled and air-cooled engines fall under this category. However, water cool engines finds wide application.
3. *Classification according to the air admission way:* The non-supercharging (naturally aspirated) and supercharging engines the main family of this category.
4. *Classification according to the cylinder number:* The members of this category include horizontal bar, parallel bars and multi-cylinder diesel engines.
5. *Classification according to the cylinder arrangement: there are in- line type:* V type, horizontal type and opposite type diesel engines fall under this category.
6. *Classification according to the rotation speed:* The rotating speed of a diesel engine can be at low speed, medium speed or at high speed. Low speed engines fall between 150 to 450 rpm, Medium

.

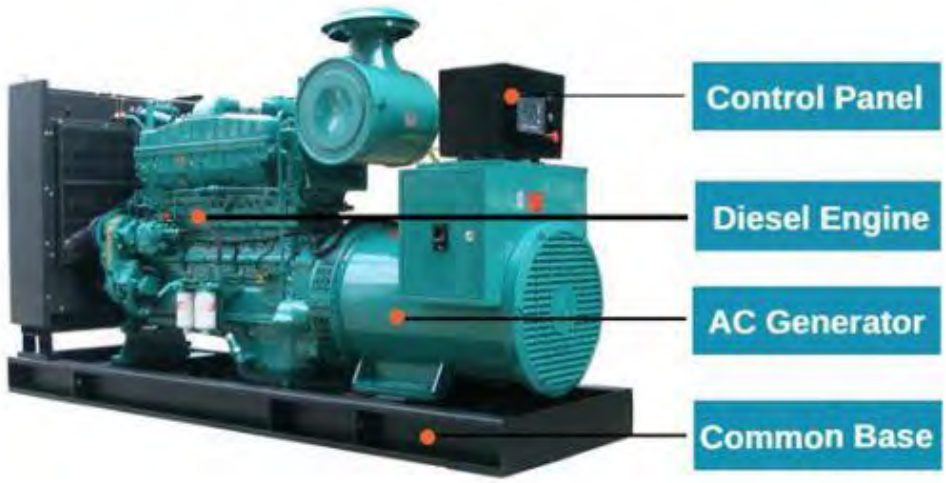

Figure 2.15: A typical structure of a DG set (SP, 2017)

speed engines ranges from 600 to 1200 rpm and finally, high speed engines are between 1500 to 1800 rpm for medium and small size machines.

The most common type of prime mover in a DG set is a four stroke cycle engine. The upward or downward movement of the piston, which is connected to the crankshaft inside the engine cylinder converts the linear motion into rotational movement required to generate the needed mechanical energy by the alternator (NRC - E111 - Chapter 9, 2011). As the rotor rotate around the field excitation windings in the synchronous generator, it becomes an electromagnet which is capable of inducing an alternating voltage in the stator windings. The induced voltage subsequently leads to the production of electrical output of the DG set. An efficiency of up to 90 % has been reported for most synchronous generator (Mobarra et al., 2022).

An Automatic Voltage Regulator (AVR) is usually installed to regulate the generated output voltage. For synchronous generators the frequency of the generated voltage is usually relative to the angular velocity of the engine crankshaft. Nevertheless, an Automatic Controller (AC) unit is usually required for advanced controls such as active and reactive regulation and automatic mains failure response (Theubou et al., 2012). Some of the many advantages of using a DG set include low installation cost, short delivery periods and installation period, high efficiency, increased efficient plant performance at varying loads, suitable for different type of fuels such as low sulphur heavy stock and heavy fuel oil in case of large capacities, minimum cooling water requirements and short start up time (Knudsen, 2017).

Diesel generator set has been used extensively in various applications such as communicate base system to ensure a stable and reliable power supply. It has also been used in many homes and industries as a standby power supply during the period of blackouts and can also be used as portable power source for mobile work scene. Moreover, it has been used as a back-up, non-renewable source in many HPS configurations to augment the intermittent nature of RE sources. In such case, it is usually used as back-up energy source when the power supplied from the main energy generating source is unable to meet the load demand. (Girma, 2013).

In its application to various HPS configuration, a single large sized DG unit is majorly used; however, the power obtained from a single large sized generator will amount to waste of the resource if it is not efficiently utilized or not completely used up by the load, which is the case for many HPS configurations. Therefore, operating multiple units of diesel generators might be more practical in this type of system configuration to serve the load demand during different periods (Ayodele et al., 2017). The schematic diagram illustrating the setup of a single large sized generator and a split genset supplying a load are depicted in Figure 2.16a and 2.16b respectively.

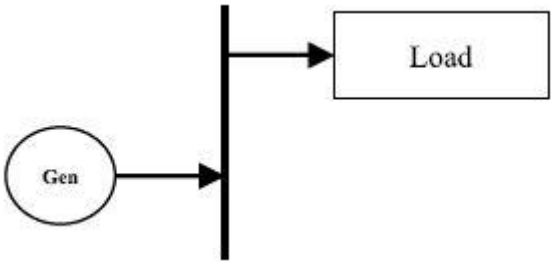

Figure 2.16a: Block diagram of large-sized single DG system (Ayodele et al., 2017)

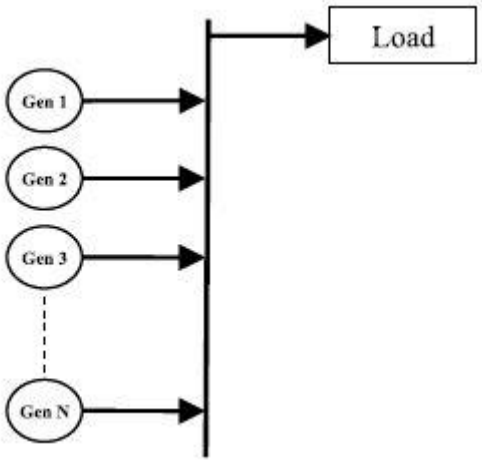

Figure 2.16b: Block diagram of split genset system (Ayodele et al., 2017)

During the operation of a single large sized generator, it produces maximum power independent of the load demand. As a result, fuel is used at the rate of power production, with a corresponding rise in the amount of dangerous gas emissions, which can be both economically and environmentally unfriendly in the operation of the proposed HPS; thereby contradicting one of the main goals of the HPS design, (Ayodele et al., 2017; Theubou et al., 2012). Based on these economic and environmental issues, the HPS model designed in this study uses a small sized split diesel generator set rather than the usual single large sized diesel generator used in many HPS configurations. The introduction of a split diesel generator set in the optimal design of HPS has been reported to lower the life cycle cost of the system, net fuel consumption and hazardous gas emission, subsequently leading to a more stable, reliable and efficient system (Ayodele et al., 2017).

2.5.4 Energy storage technology

Energy Storage Technology (EST) plays a significant role in the reliable operation of HPS consisting of intermittent RE sources such as solar and wind. An energy storage technology is simply defined as a scheme that can take in energy in a charging process and retain this energy for some finite time and later release the stored energy in a discharging process when required (Behabtu et al., 2020). Energy storage scheme is one of the most important components when considering the design of HPS. They store the excess energy produced by either of the two RE sources during their peak period and made available to the load as at when required; and in doing so, helps prevent energy wastage and subsequently, a reduction in cost of electrical energy (S. Ali & Jang, 2020). Some of the major advantages of EST include increased penetration of RE resources, enhanced flexible operation of mini and micro grids, increased reliability and improved overall efficiency of power system behavior (Aneke & Wang, 2016).

Energy storage technologies have been classified in various categories, the first of which is based on their area of applications and requirement and the second is based on the form of energy (Achkari & Fadar, 2018; Kiehbadroudinezhad et al., 2022). Since the focus of this study is solely on the design of an energy system, the second category is of more priority than the other. The three main classes of EST under this category are mechanical, electromechanical and electrical energy storage technologies, among the three classes of EST available, electromechanical storage scheme has received the highest attention for many power system applications (AL Shaqsi et al., 2020; Aneke & Wang, 2016). A broad view of the various members of each of the EST categories are presented in Table 2.4.

Some of the EST involve the conversion of energy from one form to another while others don't. Generally, many practical EST involve the conversion of energy from one form to the other which subsequently leads

Table 2.4: Broad view of various energy storage technologies

Energy Storage Technologies		
Mechanical	***Electromechanical***	***Electrical***
Pump Hydro (PHS)	Secondary Batteries (lead Acid, nickel cadmium, sodium sulphur, lithium ion)	Double Layer Capacitor (DLC)
Compressed air (CAES)	Flow Batteries (Redox/Hybrid flow)	Superconducting Magnetic Coil (SMES)
Flywheel (FES)	Hydrogen (Electrolyzer and Fuel Cell)	Sensible Heat Storage (Molten salt)

Source: (Kiehbadroudinezhad et al., 2022)

to energy loss (H. Chen et al., 2009). Hence, different schemes have different efficiencies; the two fundamental characteristics of energy storage schemes as stated in the work of Behabtu et al., (2020) are;

i. The power rating of the scheme: This is also known as the discharge capacity and it is referred to as the maximum amount of power that can be drawn from the scheme during discharge when configured properly.
ii. The Energy rating of the scheme: This is also known as the storage capacity and it is referred to as the amount of energy that can be stored in the scheme. It is usually specified in kWh or Ah, but both have the same inference.

A brief description of some popular EST highlighting their principle of operations, areas of applications, as well as the merits and demerits are presented in the following sub-sections.

2.5.4.1 Flywheel

The design of a flywheel storage technology consists of a central shaft, which holds the rotating part and a flywheel together. Energy is store in a flywheel via the acceleration of the rotor at high speeds, this maintaining the energy in the device in form of kinetic energy. The stored energy is discharged through a reversal process of the storing the energy such that the motor now act as a generator (Aneke & Wang, 2016). During the discharge process, the rotor gradually reduces its rotating speed until it eventually come to a halt. The amount of energy stored in a flywheel device depends majorly on the rotation speed of the rotor; hence it is usually desirable to design the device with high rotor speed. In recent years, eighty to ninety percent efficiency have been reported for flywheel technology due to the recent advances in energy storage technologies (Kiehbadroudinezhad et al., 2022).

Some of the many advantages of using this type of storage technology include fast dynamic response, long lifespan, minimal maintenance cost and environmentally friendly. However, they are very costly when compared to battery storage device and also suffer energy losses when they are placed on standby. Owing to their many advantages, flywheel technology are majorly used in application where there is need for power quality enhancement such as Uninterruptable Power Supply (UPS), they are also used to power electric vehicle and reduce frequency variation in power system applications (Achkari & Fadar, 2018; Aneke & Wang, 2016).

2.5.4.2 Super-capacitor energy storage

As the name implies, a super-capacitor is made of two parallel capacitor plates of opposing charge, which are separated by a dielectric insulator. The dielectric insulator is usually made of a thin film polymers, while carbon nanotube are used as electrodes. The interaction between the two opposing charges induces an electric field where energy can be stored. The amount of energy stored in a super-capacitor is a function of

the voltage across the two capacitor plates or the value of capacitance of the two plates; the higher the capacitance, the higher the induced electric field and subsequently, the higher the energy stored in the device (AL Shaqsi et al., 2020; Aneke & Wang, 2016).

The main selling point of a super-capacitor storage device is its fast rate of charge and discharge, others include high long life span, minimal degradation, among others. Nonetheless, their low energy storage density often leads to high investment cost for large scale applications. In addition to that, they are heavy and weigh more than conventional battery storage system. Although, super-capacitor have been reported to have low energy storage density, yet, they have been used extensively in various applications such as hybrid cars, cellular phones, as well as load levelling tasks (Achkari & Fadar, 2018; Aneke & Wang, 2016).

2.5.4.3 Pumped hydro energy storage

The major components of a pumped hydro energy storage scheme are motor/generator, a reversible pump-turbine and two large water reservoirs at higher and lower elevations. Energy is stored in the device through the movement water from the region of lower water elevation to higher water elevation during low load period. The stored energy is then discharged at peak period by using the water in the higher reservoir to drive a hydroelectric generator that generates the required electrical energy. The process continue to repeat itself through the entire life cycle of the device (Achkari & Fadar, 2018).

Pumped hydro energy technology is an efficient scheme in storing excess energy on a large scale basis, with about 65% to 80 % efficiency reported in many studies. Some of the many advantages of the scheme include fast startup time, longer lifespan, ability to store large amount of energy, among others. The main drawback is their overdependence on weather and geological condition, as well as its high investment cost (Aneke & Wang, 2016). In a report by the Electric Power Research Institute (EPRI) in 2010, pumped hydro energy storage are by far the most deployed EST for large scale applications with over 90 GW 90GW of pumped storage implemented in various power plants across the world.

2.5.4.4 Concentrated solar power (CSP) energy storage

The operation of a concentrated solar power (CSP) system is similar to that of PV technology where the energy from the sun is converted into heat. The heat is subsequently moved to the heat exchanger, which heats the molten salt in the hot tank used to produce electrical energy during the discharge process. However, unlike PV technologies, the CSP storage schemes are capable of storing the heat for a short period before they are used to produce the required energy (Aneke & Wang, 2016). During off peak period of the sun, the CSP scheme can be combined with thermal storage so it can continue to generate required energy. CSP storage device are capable of storing energy between 10 kW and 200 MW. An efficiency of 60 % to 70 % has been reported for CSP storage scheme and can rise up to 90 % during heat cycle. The storage and

back-up ability of the CSP scheme are worth mentioning as they contribute to the efficient operation of a power grid; some of which include reduction in energy losses during the discharge process, as well as low initial and maintenance cost (Aneke & Wang, 2016; H. Chen et al., 2009).

2.5.4.5 Hydrogen fuel cells

Hydrogen fuel cell is one of the most important member of the hydrogen energy storage technology (HEST) with less than 20 MW capacity. The assembly of a fuel cell include two electrodes that are separated by an electrolyte, which is decomposed into hydrogen and oxygen (Aneke & Wang, 2016). The hydrogen is passed over the negative electrode while the oxygen is passed over the positive electrode, thus resulting in the formation of hydrogen ions and electrons at the anode. If an external circuit is connected to the setup, electrons begin to move from the anode towards the positive electrode and electrical energy is generated. More electrolyte are produced through the migration of the hydrogen ions from the positive electrode to the negative electrode. The major contributing factor to the energy produced in hydrogen fuel cell include the operating temperature, the type of fuel cell and the catalyst (Achkari & Fadar, 2018; Aneke & Wang, 2016).

Hydrogen fuel cell are very flexible and reliable as they do not cause any type of pollution and have no moving parts. However, they experience high energy losses due to the numerous energy conversion process taking place in the setup. In addition, they have very low efficiency and high investment cost (Achkari & Fadar, 2018).

2.5.4.6 Battery energy storage

Battery energy storage (BES) scheme usually includes an array of different electrochemical technologies. The two main categories of BES technology are primary BES, which are discarded after use and secondary BES, which can be recharged after its usage. Some example of secondary BES device used for energy storage include lead Acid, nickel cadmium, sodium sulphur, lithium ion, to mention but a few. They are considered as the most popular EST for power system applications (Atia & Yamada, 2016; Tito et al., 2013). They are very versatile and can be used for both power and energy applications depending on the specific technology. BES are by far the easiest to scale down for portable applications as can be seen with lithium Ion batteries on virtually all portable electronic gadgets today. However, for large scape applications, lead acid, nickel cadmium and sodium sulphide have been used extensively for various power system applications due to their relative cost (Aneke & Wang, 2016; Behabtu et al., 2020).

The BES scheme, regardless of battery type is essentially made up of an anode, electrolyte, and a cathode, the movement of charge and discharge electrons from the anode to the cathode and vice versa via an electrolyte initiates the charging and discharging of the battery. BES scheme are very easy to produce, maintain and recycle, have high energy density and fast response time. The main drawback is that they are

very expensive, heavy and bulky, have moderate lifespan and minimal environmental concerns (Aneke & Wang, 2016; Siddique et al., 2016). Some of the major applications of BES scheme include electric power grid, hybrid electric vehicles, marine and submarine missions, aerospace operation, portable electronics systems and wireless communication base stations (Abaye, 2018; Achkari & Fadar, 2018). An overview of some common BES technologies that are commonly used in power system applications is as follow.

I. Sodium Sulphur battery

One of the most commercially used BES scheme for storing electrical energy is the Sodium sulphide (NaS). NaS battery consists of sulphur in the molten state at the positive electrode and molten sodium at the negative electrode separated by a solid beta alumina ceramic electrolyte. It discharges through the oxidation of the sodium at the sodium/beta alumina interface, leading to the formation of Na+. The Na+ passes through the electrolyte to combine with the reduced sulphur at the positive electrode, resulting in the formation of a compound known as sodium pentasulphide (Na2S5). The reverse process is used at the charging stage (Aneke & Wang, 2016).

Some of the important features of the NaS battery are high energy density, improved energy efficiency, long lifespan, high storage capacity, fast response time, to mention a few. The major drawbacks of this type of BES scheme are high investment cost, high operational temperature requirement and high operational hazard due to the use of metallic sodium which is combustible if exposed to water. NaS batteries have been used in various applications to provide support for utility distribution grid, integration of wind energy system and integrated grid services. It is economical with low maintenance cost (Chen et al., 2009; Kiehbadroudinezhad et al., 2022).

II. Nickel-Cadmium battery

Another important member of the BES technology is the Nickel-Cadmium (NiCd). Similar to the construction of all members of the BES scheme, it is made of nickel oxyhydroxide at the positive electrode and metallic cadmium at the negative electrode with an aqueous potassium hydroxide as the electrolyte (Behabtu et al., 2020). The battery is discharged through the combination of the nickel oxyhydroxide and water at the positive electrode, resulting in the production of nickel hydroxide and a hydroxide ion, while the chemical reaction taking place at the negative electrode leads to the formation of a cadmium hydroxide. The chemical reaction taking place inside the NiCd battery is a reversible process used in charging and discharging the battery (Aneke & Wang, 2016).

NiCd batteries have faster responses (within milliseconds), longer lifespan, than other batteries and they can be operated over a wide range of temperature. However, they also have inherent weakness such as issues of memory effects, energy loss and significant environmental concerns. Areas of applications include

domestic purposes such as remote control and rechargeable lamps; transportation purpose such as the aircraft and diesel engine starters, and finally, they are also used as secondary energy device for many solar generating systems (Chen et al., 2009; Kiehbadroudinezhad et al., 2022).

III. Lead Acid battery

The lead acid PbO2 battery is the most matured of all types of BES scheme, and has been used extensively for domestic and commercial purposes. It consists essentially of lead-dioxide at the positive electrode, metallic lead at the negative electrode, with tetraoxosulphate (VI) acid as an electrolyte. The charging and discharging process of the battery is a result of the oxidation and reduction taking place at the positive and negative electrode respectively. Most of the PB02 batteries have a rated voltage of 2 V, energy density of about 30 Wh/kg and power density of around 150 W/kg (Aneke & Wang, 2016; Kiehbadroudinezhad et al., 2022).

Even though lead battery have been reported to have very low self-discharge rate, this drawback is overcome by their numerous advantages such as low cost, reliability, maturity level in technology, extended life span, fast response time, high energy efficiency (85 to 90%), as well as low maintenance and investment cost. Although, their commercial usage has been reduced significantly due to the development of more efficient batteries, they still find wide applications as storage device for electric power grids, starting the engine of automobiles, among others (Aneke & Wang, 2016; Behabtu et al., 2020).

IV. Lithium Ion battery

Lithium Ion (Li-ion) battery is an emerging BES technology with the potential to replace most of the existing batteries due to its high efficiency and reliability. The major components of the Lithium ion battery are the positive/negative electrodes and an electrolyte (Aneke & Wang, 2016). Lithium cobalt oxide is placed at the positive electrode, while a carbon material is used as the negative electrode. The electrolyte is made of a thin sheet of micro-perforated plastic, which acts as a divider between the positive and negative electrodes. The entire components is enclosed in an outer case made of metal material (Aneke & Wang, 2016; Kiehbadroudinezhad et al., 2022).

The battery is charged through an external power source by supplying a higher voltage to at the negative electrode, thereby triggering the flow of current in the reverse direction. As a result, lithium ions moves from the positive electrode to the negative electrode as illustrated in Figure 2.17. The reverse process is used to discharge the battery to supply power to an external load as at when required. Lithium-Ion battery has many advantages over other types of secondary BES devices; some of which include high energy density, high cell voltage, low maintenance cost, high efficiency, high life span and many other (Aneke & Wang, 2016). Due to the numerous advantages, lithium battery has become the focal point of many HPS

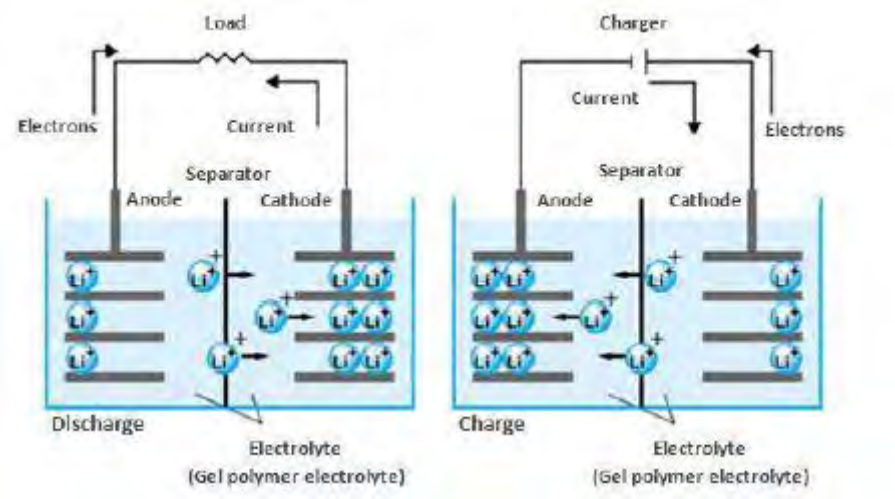

Figure 2.17: Operation mechanism of Li-ion battery (Aneke & Wang, 2016)

consisting of renewable and non-renewable energy sources and is simulated in this study. The only drawback is the high capital cost (Chen et al., 2009; Kiehbadroudinezhad et al., 2022). A comparison of some common secondary BES devices is presented in Table 2.5.

2.5.5 Power converter

The configuration of any HPS consisting of different energy sources usually comprise a power converter; a power converter is used to convert the input power to the required output power using basic switching electronic devices (Bordry & Aguglia, 2015; Roy et al., 2022). Over the years, the conversion of electrical power from one form to another was usually done using electromechanical converters. However, due to the advancement made in the power electronics industry, semiconductor materials were used in the design of power converters. An ideal power converter is able to control power flow between two sources (sending and receiving) with zero losses as illustrated in Figure 2.18. It consists of linear elements such as semiconductor devices and electronic switches which are used in the commutation mode and non-linear elements such as capacitors and transformers which are used as an intermediate energy storage and current/voltage filters (Bordry & Aguglia, 2015).

The current output of the energy generating sources in a HPS differs from one component to the other. In the case of the PV systems, a Direct Current (DC) is usually generated, while in the case of the wind energy system, the current could either be a DC or an Alternating current (AC) depending on the generator type. Moreover, the split DG set and BES scheme produce AC and DC respectively. Power converters are required to convert the AC component of the current to DC and vice-versa depending on the consumer load. Based on the method of conversion, power converters are classified into two categories namely a rectifier and an inverter (Bordry & Aguglia, 2015; Rehman et al., 2020).

The rectifier is used to transform the AC component from the wind energy system and split genset to DC component, while the inverter does the reverse for both PV system and BES scheme. In some HPS configurations, a bi-directional converter has also been used to; a bi-directional converter perform the functions of both the rectifier and the inverter. Power converters have used extensively for various applications such as information processing, telecommunication, transportation, and power utilities (Bordry & Aguglia, 2015; Zinoviev, 2008).

Table 2.5: Characteristics of various battery energy storage technologies

BES Technology	Energy Density (Wh/kg)	Discharge duration	Response time	Efficiency (%)	Lifetime
Lead-acid batteries	30-40	3-4 %	∠¼ cycle	70-92	3-12 years
Nickel-cadmium batteries	40-60	20 %	N/A	70-90	15-20 years
Sodium-sulphur batteries	30-80	30 %	N/A	75-86	5 years
Vanadium redox flow batteries	50-70	40 %	N/A	70-85	10 years
Zinc-bromine flow batteries	40-70	35 %	∠¼ cycle	75	2000 cycles
Lithium Ion Batteries	150-250	5-10 %	∠¼ cycle	99	1200-10000 cycles

Source: (Aneke & Wang, 2016; Kiehbadroudinezhad et al., 2022)

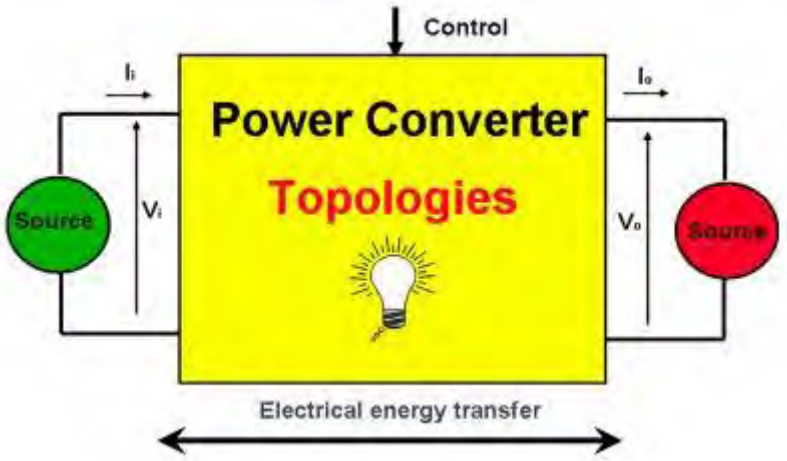

Figure 2.18: Arrangement of a typical power converter (Bordry & Aguglia, 2015)

2.5.6 Charge controller

Battery energy storage (BES) scheme form a large part of the capital investment of many HPS. It is therefore reasonable to preserve the lifespan of the BES scheme used in the configuration of the system in order ensure the life cycle cost of the system is minimal (Marcel et al., 2021). The most common approach used to ensure that the BES remains within the maximum and minimum boundaries of State of Charge (SOC), given in the manufacturer's datasheet is by using a charge controller. A controller is a switch which connects and disconnects the main energy generating sources and the load demand from the battery in accordance with the battery's SOC, Depth of Discharge (DOD) and temperature (Bhikabhai, 2005; Dodo et al., 2020).

Charge regulators are broadly classified into three main categories namely shunt or series regulators, linear or switching regulators and the manual or automatic Regulators. A shunt regulator is one in which the energy source is continually operated at full available power and excess power is dumped in a dummy load. The regulator is installed in parallel with the source and the battery. In wind and hydropower systems they can also act as a load to prevent over speeding of the generator. On the contrary, a series regulator is connected between the charge source and the battery. Some series regulators may switch the source to an alternative system such as water pumping or auxiliary battery bank. A linear regulator continuously adjusts the charge supplied to the battery at any given moment to maintain the optimum voltage (Bhikabhai, 2005).

2.6 Hybrid power system design techniques

The focus of this study is the optimal design of a hybrid power system consisting of Bifacial PV panels, wind turbines, storage system and a split diesel generator for off grid applications. The optimal design of any hybrid power systems consisting of renewable and non-renewable energy sources involves the appropriate combination of the various energy generating components of the system, as well as their optimal energy capacities that satisfy the design objectives (Mohammed et al., 2019). Objectives may take the form of the total cost of the, system, cost of energy, environmental concerns, reliability, among others. The main aim of HPS design is to achieve a balance between components sizing, cost and reliability of the system (Kharrich et al., 2021).

Various techniques have been applied in many studies for the design of HPS, the use of Conventional techniques such as graphical construction technique, iterative technique and probabilistic approach are well documented (Kalantari et al., 2018). Moreover, commercially available, HPS simulation software such as Hybrid Optimization Model for Electric Renewables (HOMER), Hybrid Optimization by Genetic Algorithms (HOGA), Hybrid Power System Simulation (HYBRID2), and many others have also been used in the design of HPS (Babatunde et al., 2020). In the last decade, artificial intelligence techniques such as Particle Swarm Optimization (PSO), Genetic Algorithm (GA), Tabu Search (TS), Artificial Bee Colony

(ABC), among others have also been applied to find the optimal design of HPS for various configurations and applications (Babatunde et al., 2020; Vishakha et al., 2020). Each of these techniques has their inherent merits and demerits when applied to the optimal design of HPS A brief overview of these techniques are subsequently presented.

2.6.1 Conventional optimization techniques

The conventional or classical approaches are otherwise known as deterministic or analytical approach optimization methods. Examples are Dynamic Programming (DP), Linear Programming (LP), Quadratic Programming (QP), iterative approach, graphical construction technique and many others. Many of these conventional techniques are employed most especially when the search space is non-linear. They have been applied to solve the optimal design problem of HPS in many research studies, but the obtained results are sub-optimal. (Sawle et al., 2016a; Tito et al., 2013; Vishakha et al., 2020). However, despite the scholarly advancements that have been made in classical approaches in terms of run time and mathematical computations, yet classical approach presents some limitations in its implementation. The identified limitations among others include (Babatunde et al., 2020; Sawle et al., 2016a);

i. Poor convergence.
ii. Inability to handle non-continuous function
iii. The solution is highly computationally expensive.
iv. Finding only a single optimized solution in a single simulation run and the treatments of operational constraints are somehow tedious.

Most deterministic optimization methods are viewed as local search methods because they are known for producing the same set of solutions even if the algorithm starts under the same initial conditions (Babatunde et al., 2020; Bandaru & Deb, 2016). Some common classical approach that have been implemented in the design of HPS are briefly discussed in the following sub-sections.

2.6.1.1 Graphical construction method

The graphical construction method is implemented using a set of graphs plotted using the variables of the system components. The plot is then review to check for points of intersections, which is subsequently used to determine the most feasible solution to the design problem (Abaye, 2018; Zhou et al., 2010).

2.6.1.2 Probabilistic approach

Just as the name implies, the probabilistic approach is majorly based on prediction of a feasible solution using statistical tools. The variables in the tools are made of randomly collected data over a period of time, the collected data are processed into a statistical tool which is used to predict the most feasible solution of the HPS design problem (Abaye, 2018; Kalantari et al., 2018).

2.6.1.3 Iterative approach

Iterative approach involves the application of a stepwise mathematical or computational process aimed at achieving a solution closer to the approximated value of a problem. At each iteration, a solution is obtained which is used in the estimation of subsequent solutions (Kalantari et al., 2018). The process continue to repeat itself until it terminates when an appropriate solution has been attained. Iterative approach is classified into three main categories viz hill climbing, dynamic programming and linear programming. Hill climbing is considered a local search iterative procedure, which begins with a pre-defined solution to a problem; and then try to obtain an approximate solution by altering one of the component of the solution at each iteration (Nabipour-Afrouzi et al., 2018).

The most feasible solutions in a dynamic programming are obtained by breaking down a complex problem into various categories and obtaining a solution to each category; each smaller solutions then recombines as the most feasible solution. Finally, the solutions in linear programming are obtained using by modeling the system using a set of linear equations and running a simulation to obtain the most feasible solution (Kalantari et al., 2018; Nabipour-Afrouzi et al., 2018; Zhou et al., 2010).

2.6.2 Commercial optimization software tools

Simulation programs are the most common tools for gauging the performance of hybrid power systems. By using computer simulation, it is feasible to find an optimal configuration by comparing the performance and energy production cost of various system configurations (Mira et al., 2017). Several software tools are commercially available for designing HPS. The most popular among these software tools are Hybrid Optimization Model for Electric Renewables (HOMER), Hybrid Power System Simulation Model (HYBRID2), Hybrid Optimization by Genetic Algorithms (HOGA) and Transient Energy System Simulation Program (TRNSYS) (Babatunde et al., 2020).

The main drawbacks of these software is their high simulation time, complex user interface and slow convergence speed (Hassan et al., 2016). HOMER has been extensively used in many research studies involving HPS design because the user interface is less complex and offers the flexibility of optimizing the system based on economic and environmental analysis. However, the simulation process is time consuming, just as is the case for many of the commercially available optimization software (Babatunde et al., 2020; Sawle et al., 2016a). A brief overview of some commonly used software tools in the design of HPS are subsequently presented.

2.6.2.1 Hybrid Optimization Model for Electric Renewable (HOMER)

This was developed by National Renewable Energy Laboratory (NREL), USA. It is the most widely used optimization software for most HPS configurations. The software can simulate a wide variety of mini and

micro power system configurations. The simulation is carried out in an hour interval, during which all of the parameters (load demand, the power output of the generating components, as well as the power output of the system) remain constant (Babatunde et al., 2020).

Two types of dispatch strategies are available in HOMER software. The first type is the load following strategy, where the conventional generator set is used to supply the exact amount of power required by the load whenever there is deficiency in the power supplied by the RE generators. The second type of strategy is known as the cycle charging strategy. In the cycle charging strategy, the generator set is usually optional; and if it is included in the design is made to run at full power and any excess power is used to charge the storage system (Sawle et al., 2016). The type of dispatch strategy employed depends on the type of components used in the system configuration. A system with both storage system and diesel generator set used as back up to the renewable generator, the software automatically selects the appropriate dispatch strategy for optimum system configuration. (Энергии & Sleptsov, 2017).

Three basic tasks can be performed using HOMER software via simulation, optimization, and sensitivity analysis. Simulation is used to evaluate the performance of the system with respect to a particular configuration. It describes the operational relationship among the different energy generating sources and select determine the appropriate operating strategy for the exact system configuration. At the simulation stage, the technical and economic viability of the system can be determined (Sawle et al., 2016). The economic viability is measured using a metric known as the Net Present Cost. This single value includes all costs and revenues that occur within the project lifetime, with future cash flows discounted to the present (Babatunde et al., 2020). Sensitivity analysis evaluated the impact of future varying component cost on the system, while optimization determines the most appropriate system configuration taking into consideration several variables such as number of the generating components, cost of the components and the capacity of energy generated (Sawle et al., 2016; Zhou et al., 2010).

Hybrid Optimization Model for Electric Renewables software has been used extensively in numerous studies for the design of HPS consisting of several RE generators and for validation purposes and results have been quite promising (Kiehbadroudinezhad et al., 2022). Although, simulations can take a long time, depending on the number of variables used; its operation is simple and straightforward. The main advantage using the software is due to its easy user interface and its ability to obtain the most suitable system configuration capable of serving the load at lowest life cycle cost. However, the core disadvantages of the simulation approach is that it is mainly an economical model and the algorithms and calculations are not visible or accessible, thus making it difficult to implement design constraints (Alam & Mehar, 2021; Энергии & Sleptsov, 2017).

2.6.2.2 Hybrid Power System Simulation Model (HYBRID2)

The software was developed by the Renewable Energy Research Laboratory (RERL) at the University of Massachusetts. The hybrid systems may include three types of electrical loads, multiple wind turbines of different types, photovoltaic generators, multiple diesel generators, battery storage, and four types of power converters (Sawle et al., 2016). Other components, such as, fuel cells or electrolyzers, can also be modeled using the software. It has been reported that the simulation process using HYBRID2 can be very precise, as it can define time intervals from ten minutes to one hour. In addition to that, the software has been found to have high possibilities of selecting the most appropriate control strategies for system configuration. Nevertheless, its inability to optimize the system makes it difficult to evaluate the economic viability the generated system configuration (Babatunde et al., 2020; Энергии & Sleptsov, 2017). The developers of the software suggest the optimization of the system design using HOMER software before improving the design using HYBRID2. However, unlike HOMER, HYBRID2 can only simulate one configuration at a time (Энергии & Sleptsov, 2017).

2.6.2.3 Hybrid Optimization by Genetic Algorithm (HOGA)

Hybrid Optimization by Genetic Algorithm (HOGA) is another popular member of the HPS simulation software tools. The program was developed by José L. Bernal-Agustín and Rodolfo Dufo-López of the Electric Engineering Department of the University of Zaragoza in Spain. The optimization process in the software is done using genetic algorithm, and can be the design problem can be formulated as single-objective or multi-objective problem (Alam & Mehar, 2021; Энергии & Sleptsov, 2017). Components of the HPS such as photovoltaic generator, battery energy storage scheme, wind turbines, hydraulic turbine, AC generator, fuel cells, electrolyzer, hydrogen tank, rectifier, and inverter can be selected for system configuration. The HOGA software permits the addition of either AC or DC load, as well as hydrogen loads. Similar to both HOMER and HYBRID2, the simulation is carried out using 1-hour intervals, during which all of the parameters remained constant. However, the economic viability and control strategies in HOGA are optimized using Genetic Algorithm. (Babatunde et al., 2020; Sawle et al., 2016).

2.6.2.4 Transient Energy System Simulation Program (TRNSYS)

The energy system simulation software was developed as a result of the collaboration between University of Wisconsin and the University of Colorado, USA in 1975. The program codes were written using FORTRAN, and it was primarily developed to simulate thermal system. However, as the years progressed, the software was improved upon to become a hybrid system simulator, including photovoltaic, thermal solar and other system components (Энергии & Sleptsov, 2017). The standard TRNSYS library includes many of the components commonly found in thermal and electrical renewable energy systems. The simulation is carried out with great precision, allowing the viewing of graphics with great detail and

precision. However, it does not permit the optimization of the HPS configuration (Sawle et al., 2016). A comparison of some popular optimization software tools that are commercially available is presented in Table 2.6.

2.6.3 Artificial Intelligence (AI) optimization techniques

The use of machine learning to efficiently perform different tasks, in a way that goes beyond human reasoning is described using the term "Artificial Intelligence" (AI). This type of optimization technique, also know stochastic approach has been used over the years to solve various engineering optimization problems. (A. Alam & Mehar, 2021; Nabipour-Afrouzi et al., 2018). AI techniques are classified as heuristic or meta-heuristic optimization technique; heuristics techniques are able to obtain the optimal solution in a realistic amount of time, but they are easily trapped in local optimal solution. On the other hand, meta-heuristic techniques have inbuilt characteristics, that can be used to attain a balance between randomization and local search to obtain global optimal solution in minimal amount of time, thus making them suitable for varieties of optimization problems (Babatunde et al., 2020; Bouaouda & Sayouti, 2022).

They have been applied to solve many optimization problems where quality and efficient solution are required. Unlike the conventional optimization techniques, AI techniques are able to handle the complex, non-linear, multi-dimensional, mixed variables, discontinuous and conflicting objectives common to most optimization problems with minimal fuss. With AI techniques, optimal solution can be obtained using a set of predefined rules centered on the inspiration behind the development of a particular optimization technique (Elmanakhly et al., 2021). Examples include GA, PSO, ABC, TS, Cuckoo Search Algorithm (CSA), Bacterial Foraging (BF), Whale Optimization Algorithm (WOA), Pattern Search (PS), Evolution Programming (EP), Firefly Algorithm (FA), Differential Evolution (DE), Harmony Search Algorithm (HSA), Ant Colony Optimization (ACO), Hopfield Neural Network (HNN), Political Optimizer (PO), to mention but a few (Bandaru & Deb, 2016; Bouaouda & Sayouti, 2022).

Many studies on optimal design of HPS have reported that these techniques are capable of producing efficient, reliable and quality solutions. In some studies, a combination of two AI techniques known as hybrid optimization technique has also been explored for the optimal design of HPS in order to improve the quality of the solution obtained. Some of the reported advantages of using AI as an optimization technique are listed as follow. (Bandaru & Deb, 2016; Harifi et al., 2020; Sawle et al., 2016).

i. Faster convergence rate.
ii. Ease of implementation
iii. Ability to attain global solution within shortest time possible.
iv. Efficient capabilities for handling complex system.

Table 2.6: Comparison of some common commercial simulation software tools

Simulation Software	Merits	Demerits
HOMER	i. The interface is user friendly ii. Good presentation of results	i. Inability to import time series data ii. Non-adjustable design constraints
HOGA	i. Ability to implement more than one design objective. ii. It permits the addition of high number of design variables	i. Does not permit the evaluation of sensitivity analysis ii. Does not allow the selection of higher load profile range
HYBRID2	i. It allows the addition of many electrical loads ii. It utilizes a comprehensive dispatch strategy	i. The simulation run time is too long ii. It can only simulate one system configuration at a time
RETscreen	i. It has the widest database for renewable energy resources ii. It is designed with an inbuilt Microsoft excel.	i. Inability to import time series data ii. Limitation in the number of input data for system configuration
TRNSYS	i. It has a flexible user interface ii. The simulation results are precise and well presented	i. It has a limited number of components that can be simulated ii. Does not allow the optimization of system configuration

Source: (Babatunde et al., 2020; Sawle et al., 2016)

However, the most common drawback peculiar to majority of the AI techniques is the time taken to achieve convergence and level of complexity (Bouaouda & Sayouti, 2022). Table 2.7 highlights the merits and demerits of some common member of AI techniques that have been applied in the optimal design of HPS; while an overview of the three AI techniques considered for the optimal design of the proposed HPS model in this study are subsequently presented.

2.6.3.1 Firefly algorithm

Firefly Algorithm (FA) is one of the most popular nature inspired optimization algorithm, which has been applied to many complex optimization problems. The algorithm, which is inspired by the flashing activities among a group of fireflies was developed by Yang and Deb in the year 2008. A firefly is commonly known as a winged beetle with the capability to produce flashing light during the night (Yang, 2014). The flashing light is produced at the bottom abdomen through a chemical process known as bioluminescence. The flashing light is an important trait of fireflies as it is used to draw the attention of neighboring fireflies and to alert them of any impending danger (Johari et al., 2013; Wang & Chu, 2019).

Firefly Algorithm belongs to the family of swarm intelligence optimization techniques that emulate the basic features of living things such bats, birds, bees and others. Other members of the family include PSO, ABC and CSA, to mention but a few (Ali et al., 2014). FA has been reported in many studies as a very efficient optimization algorithm, and it is capable of outperforming other swarm intelligence based techniques, as well as evolutionary algorithms based on its performances using various benchmarks in different optimization problems which include digital image compression, feature selection, engineering design problems, and many others (Altherwi, 2020; Sulaiman et al., 2012). It was established that the algorithm is robust enough to handle high dimension, non-linear, multimodal design problems with minimal fuss. It was also reported that the algorithm can outperform other swarm intelligence based optimization techniques in terms of optimal solution and simulation run time (Yang & He, 2013).

The algorithm is modeled based on the global interaction among the fireflies using individual flashing light, which varies from one firefly to the other. A firefly with a brighter flashing light will attract another firefly with less bright flashing light. Hence, the attractiveness of a firefly is a function of the flashing light, which is responsible for the sub-division among the fireflies (Yang & He, 2013). The algorithm uses this feature to search for global and local optimal solution simultaneously. New solutions are generated via random walk and attraction of the fireflies; that is, in the absence of any other fireflies with a brighter flashing light relative to the brightest firefly in the sub-divisions, the brightest firefly will move randomly (Qi et al., 2017; Yang & He, 2013).

Table 2.7: Comparison of common AI techniques

Artificial Intelligence Techniques	Strengths	Weaknesses
Genetic Algorithm (GA)	It is capable of providing multiple optimal solutions It requires minimal details to process optimal solutions.	It can be time consuming due to the many mathematical computation required It suffers from issues of slow convergence rate
Particle Swarm optimization (PSO)	It is easy to implement due to the limited number of control parameters It is computationally efficient	It is easily trapped in location solutions It has slow convergence rate
Artificial Bee Colony (ABC)	It is easy to implement for optimization purposes It has efficient exploration capability	It is unable to handle multi-dimensional problems due to poor exploitation ability
Harmony Search Algorithm (HSA)	It has high efficiency in searching global solutions. It has considerable simulation run time	It exhibits issues of premature convergence It can become unstable during the optimization process
Biography Based Optimization (BBO)	It has reasonable simulation run time It Can be easily modified to suit all types of optimization problems.	The conventional BBO is unable to handle complex problems due to poor exploitation ability It is also difficult to identify the global solutions from each generation
Mine Blast Optimization (MBO)	It can generate quality optimal solution if the control parameters are properly adjusted	It involves a lot of mathematical computation It has too many control parameters

Table 2.7 contd.

Brain Storm Optimization (BSO)	It is easy to implement and can be very effective in generating quality solutions It is very flexible	Unsuitable for multi-objective optimization problems. Issues of slow convergence in the presence of many optimization variables
Grey Wolf Optimizer (GWO)	It has the ability to generate optimal solution in lesser time. It is very easy to implement and realize.	It has a very slow convergence It generates sub-optimal solutions.
Moth Flame Optimization (MFO)	It has very few control parameters It is very easy to implement	It has low convergence speed It is easily trapped in sub-optimal solutions.
Flower Pollination Optimization (FPO)	It has high efficiency due to its ability to search for optimal solution in larger search space medium.	It is difficult to obtain quality solutions when used to solve multi-objective optimization problems It suffers from premature convergence

Source: (Jarraya & Bouri, 2012; Z. Wang et al., 2021)

In a bid to simplify the operation of the algorithm, three basic rules were specified by the developer and are listed as follow (Yang, 2014).

i. All fireflies in the swarm are unisex in nature; that is, irrespective of their sex, each firefly in the swarm will attract the other.
ii. The level of attraction of an individual firefly depends solely on the brightness level of its flashing light and the distance separating it from another firefly. However, two fireflies of the same flashing light intensity will experience random walk.
iii. Finally, the brightness of each firefly in the swarm is evaluated using the formulated objective function.

Firefly Algorithm can be used solve optimization problems with there is need to maximize or minimize a specified objective function. For maximization of an objective function, the brightness of individual firefly is computed directly using the formulated objective function. On the contrary, for minimization of an objective function, the brightness is estimated using an inverted value of the formulated objective function. In its application to any optimization problem, an initial population of fireflies is distributed randomly in the search space, whose dimension represents the number of variables to be optimized (Yang & He, 2013).

Moreover, the initial position of individual firefly represents a possible solution to the optimization problem. A fitness value is attached to each of the firefly positioned in the search space by evaluating the formulated objective function. The intensity of the flashing light of each firefly is relative to its fitness value; hence, a bright firefly will be attracted towards a brighter firefly. In other words, a brighter firefly will exhibit a higher degree of attraction and subsequently, the faster the velocity of attraction (Yang, 2009; Yang & He, 2013).

However, the attractiveness between two fireflies depends solely on the distance separating them. In each iterative step, the algorithm evaluates the brightness and attractiveness of each firefly using the formulated objective function and positions of all the fireflies are adjusted until the best possible position is achieved. The firefly located at the best possible position represents the optimal solution to the optimization problem (Ali et al., 2014; Johari et al., 2013). The two most important parameters used in developing the FA optimization technique are highlighted as follow.

1) Attractiveness

The attractiveness, β of a firefly is measured using the degree of its brightness. In simple terms, the attractiveness of a firefly is a function of its brightness, which is usually determined using the value of the

objective function, $f(x)$. Consider a firefly i, located at position p on the search space, the brightness b of such firefly is related to the objective function using expression (2.1) (Yang & He, 2013)

$$b \ \alpha \ f(x) \tag{2.1}$$

Expression (2.1) is only valid for optimization problems where the objective function has to be maximized. In case of minimization of the objective function considered in this study, the brightness of a firefly is given using expression (2.2) (Yang & He, 2013).

$$b \ \alpha \ \frac{1}{f(x)} \tag{2.2}$$

Nonetheless, attractiveness is a relative parameter as it depends on the perception of other fireflies. Therefore, it is a function of the distance r_{ij} between firefly i, located at p_i and firefly, j located at p_j. Another factor which affects the attractiveness of a firefly in given search space medium is the light intensity, which decreases with an increasing distance from its source and rate of light absorption in a given search medium (Yang & He, 2013).

Consider a given medium with a fixed light absorption coefficient 'γ', the light intensity L is a function of the distance, r separating any two fireflies and it is expressed using equation (2.3) (Yang & He, 2013).

$$L = L_0 e^{-\gamma r} \tag{2.3}$$

Where L_0 represents the initial light intensity of the firefly.

Since the light intensity of a firefly is a function of its attractiveness, which varies with its distance, the attractiveness of a firefly is thus expressed using equation (2.4) as follow (Yang & He, 2013).

$$\beta = \beta_0 e^{-\gamma r} \tag{2.4}$$

where β_0 is a parameter that denotes the attractiveness of a firefly at its starting position ($r = 0$).

The distance r between any two fireflies at different positions in the search medium as given by Yang & He, (2013) is expressed using equation (2.5).

$$r_{ij} = \left| p_i - p_j \right| = \sqrt{\sum_{k=1}^{d} \left(p_{i,k} - p_{j,k} \right)^2} \tag{2.5}$$

where $p_{i,k}$ denotes the k_{th} component of the spatial coordinate between the positions of the two fireflies and d represents the total number of distance covered. Assuming $d = 2$, substituting the value of d in equation (2.5), the distance between any two fireflies is simplified as given in equation (2.6) (Yang & He, 2013).

$$r_{ij} = \sqrt{\left(p_{i,1} - p_{j,1} \right)^2 + \left(p_{i,2} - p_{j,2} \right)^2} \tag{2.6}$$

1) Movement of fireflies

Once a firefly i with a lesser light intensity and located at position pi, identifies another firefly j with a brighter light intensity and located at position, p_j, it is attracted to firefly j and tries to move towards it. The mathematical expression describing this movement as given by Yang (2014) is presented using equation (2.7).

$$p_i = p_i + \beta_0 e^{-\gamma_{ij}^2}\left(p_j - p_i\right) + \sigma\varepsilon \qquad 2.7$$

The second term of equation (2.7) is used to describe the attractiveness of a firefly relative to the perception of an adjacent firefly, while the third term is used to express the random movement of a firefly in the absence of any brighter firefly. Where σ represents the randomization parameter and represents a vector of random number which are generated using Gaussian method and are uniformly distributed over the search medium (Farahani et al., 2011). The flowchart of FA is as shown in Figure 2.19.

2.6.3.2 Whale optimization algorithm (WOA)

The algorithm was developed in 2016 by Mirjalili. It was employed to solve 29 mathematical optimization problems and was found to have strong potential in searching both local and global solutions. It is inspired based on the predatory behavior of humpback whales; this special specie animals are regarded as the biggest mammal in the world (Mirjalili & Lewis, 2016). Some of the many traits of the humpback whales include their intelligence and emotional nature. They have some common cells located in strategic parts of their brain, this cell is similar to the spindle cells human being. The size of these cells in whales are twice that of human being, and it is basically responsible for their strong intelligence quotient. These cells are used to judge, learn, think, experience emotions and interact socially among themselves. These types of animals are usually found alone or in groups, but on many occasions, they usually co-exist in groups (Mirjalili & Lewis, 2016; Pham et al., 2020).

Humpback whales feed on krill and small fish herds, the method used in scouting for their food is the basis behind the development of the algorithm for solving most optimization problems. The search process is divided into two phases namely the exploitation and the exploration phase. At the exploration phase, they exhibit a foraging behavior known as bubble net feeding method when searching for their food (prey) as illustrated in Figure 2.20a (Mirjalili & Lewis, 2016; Diab et al., 2019). The humpback whales exploit their prey close to the surface of the water by creating a distinctive bubbles along a circle or 9'-shaped path as shown in Figure 2.20b. Using this tactics, they form a circle around the target prey who can no longer escape. The whales closest to the target prey are all possible solution to the optimization problem, while a particular whale that attacks the prey first is the optimal solution to the optimization problem (Mirjalili & Lewis, 2016).

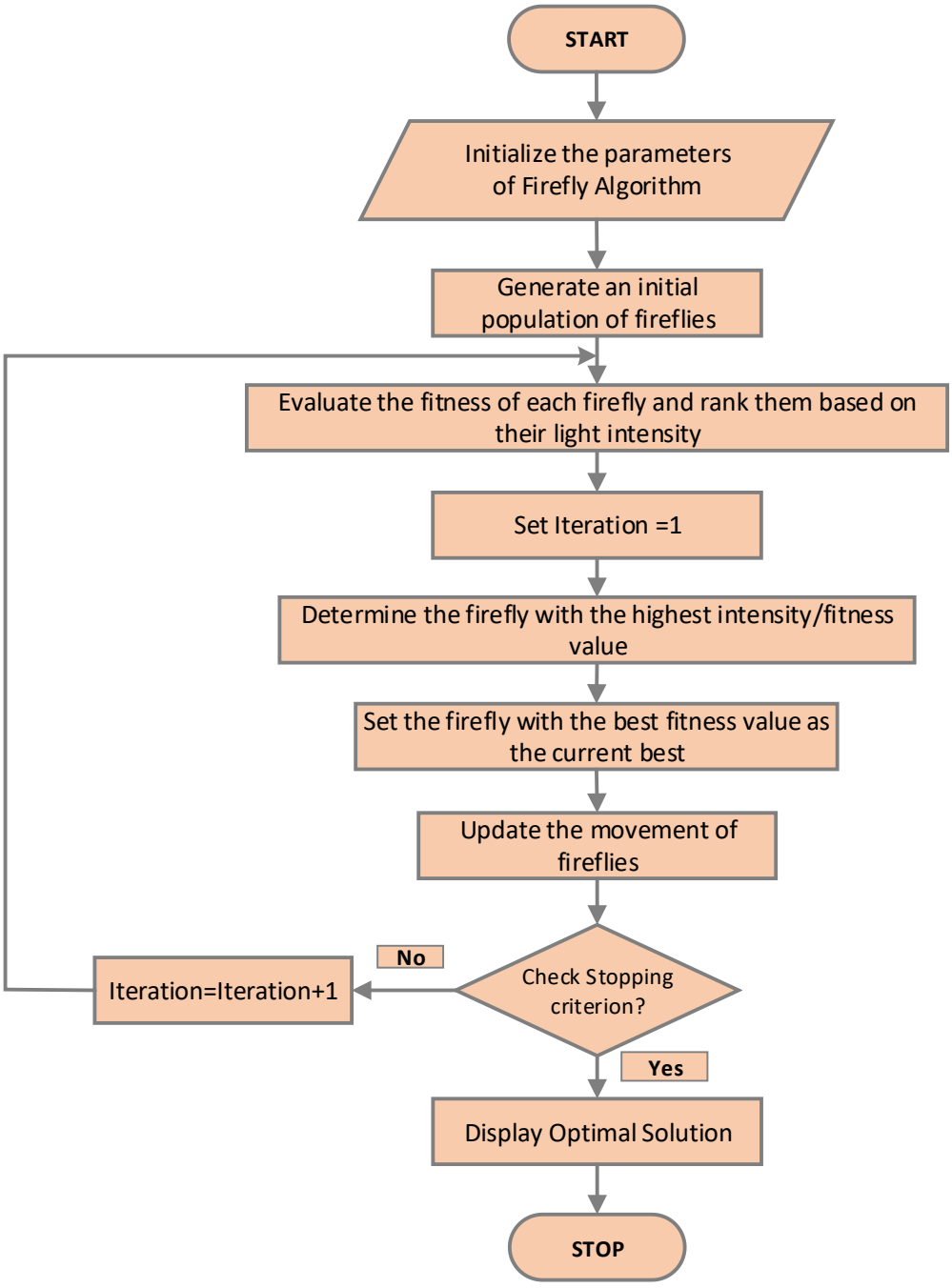

Figure 2.19: Flowchart of firefly algorithm (Kaabeche et al., 2017)

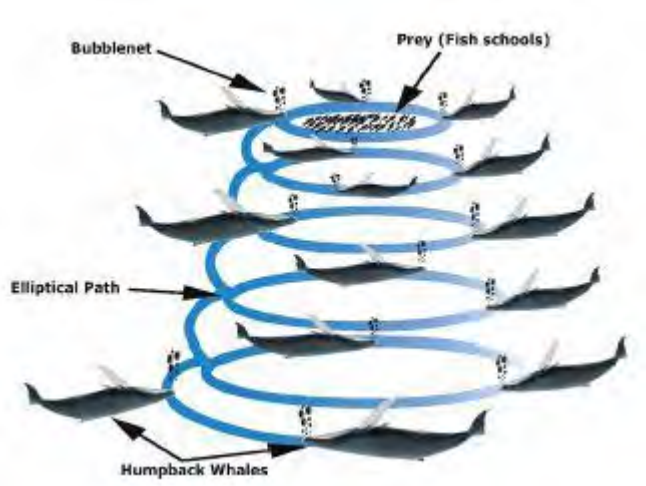

Figure 2.20a: Bubble-net foraging behavior of humpback whales (Mirjalili & Lewis, 2016)

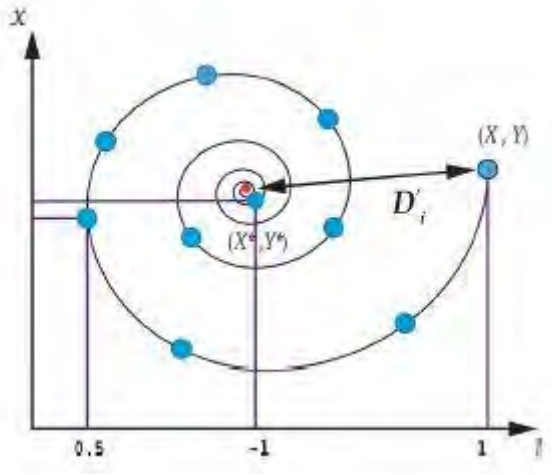

Figure 2.20b: 9-shaped position updating behavior of humpback whales (Mirjalili & Lewis, 2016)

When applied to solve optimization problems, the first thing the algorithm does is to identify the position of the prey as the objective function of the problem. The target prey is then encircled by the number of whales, also known as search agents in the population. The position of this prey is assumed to be the possible best solution as it is close to the optimum (Diab et al., 2019). Therefore, each of the whale in the population will continually adjust its position to match that of the target prey. The whale with the same position as the target prey after the entire search process is chosen as the optimal solution to the optimization problem (Mirjalili & Lewis, 2016; Z. Yang, 2020). Expression (2.8) and (2.9) as given by Mirjalili & Lewis, (2016) are used to mathematically describe the search behavior of the search agents (whales).

$$D = \left|\vec{C}.\vec{X}^{*}(t) - X(t)\right| \tag{2.8}$$

$$X(t+1) = \vec{X}^{*}(t) - \vec{A}.D \tag{2.9}$$

where t represents the present iteration, A and C are coefficient vectors, X^{*} is the position vector of the current best solution obtained so far, X is the position vector of the previous best solution, | | is the absolute value, also known as an element-by-element multiplication. It should be noted that X^{*} should be updated in each iteration to check for better solutions. The vectors A and C according to Mirjalili & Lewis, (2016) are estimated using equations (2.9) and (2.10).

$$A = 2a.s - a \tag{2.9}$$

$$C = 2.s \tag{2.10}$$

The constant a should be linearly reduced from '2' to '0' until maximum iteration is reached; the value should be adjusted for both exploration and exploitation phases, s is a random vector in the range [0, 1]. The position (X, Y) of any search agent is usually updated based on the position of the possible best solution (X^{*}, Y^{*}) in the search space. The position of the whales are updated spirally by initially calculating the distance between the whale located at (X, Y) and the target prey located at (X^{*}, Y^{*}) (Mirjalili & Lewis, 2016). As described earlier, the movement of the whales towards their target prey is usually a helix-shaped movement and it is described using equation (2.11) (Mohammed et al., 2019).

$$X(t+1) = \vec{D}.e^{hl}.\cos(2\pi l) + \vec{X}^{*}(t) \tag{2.11}$$

where $\vec{D} = \left|\vec{X}^{*}(t) - \vec{X}(t)\right|$ is an expression that specifies the distance of the i^{th} whale to the prey (possible best solution), h is a constant used to define the shape of the logarithmic spiral and l is a random number ranging from [-1, 1]. As the search agent swim around their prey by creating a shrinking circle along a spiral-shaped path. This attribute is modeled by assuming that there is a 50 % chance that the whale will

pick either the shrinking encircling mechanism or the spiral model for position updating. This behavior as described by Mirjalili & Lewis, (2016) is modeled mathematically using equation (2.12).

$$\vec{X}(t+1) = \begin{cases} \vec{X}^*(t) - \vec{A}.D \\ \vec{D}.e^{hl}.\cos(2\pi l) + \vec{X}^*(t) \end{cases} \qquad n \le 0.5 \tag{2.12}$$

where n is a random number in the range [0, 1].

The same approach is used during the exploration phase. The position of the prey is searched by varying the vector, A. This search procedure is performed randomly relative to the position of other whales in the population. For this reason, the variation of the vector, A during the exploration phase is usually varied between values greater than 1 or less than -1. This is done to alter the position of the search agent from a reference whale (Mirjalili & Lewis, 2016; H. M. Mohammed et al., 2019). In addition, position updating during the exploration phase is done via a random selection of a search agent as compared to chosen the best search agent during exploitation phase (Mirjalili & Lewis, 2016). The algorithm uses this trait when performing a global search. The mathematical model of this attribute as expressed by Mirjalili & Lewis, (2016) is given in equation (2.13) and (2.14).

$$D = \left|\vec{C}X_{rand} - \vec{X}\right| \tag{2.13}$$

$$\vec{X}(t+1) = X_{rand} - \vec{A}.\vec{D} \tag{2.14}$$

where X_{rand} is a random position or a whale chosen from the entire population size.

The algorithm usually begins with a set of random solutions and at each iteration, the position of each search agent in the population are updated relative to a randomly chosen search agent (whale) which acts as a reference whale or according to the best solution obtained so far. A random search agent is chosen only when $|A| > 1$, while the best solution is selected when $|A| < 1$ for updating the position of the search agents (H. M. Mohammed et al., 2019) Finally, the algorithm is ended when the termination condition is met; usually, when the maximum number of iterations or when convergence is achieved. Although, the algorithm has been reported to suffer from issues of slow convergence which arises due to many random parameters; however, it offers some advantages which makes it suitable for multi-dimensional optimization problem such as the optimal design of HPS (Mirjalili & Lewis, 2016; Diab et al., 2019). Some of the advantages of WOA are listed as follow (Mirjalili & Lewis, 2016; Pham et al., 2020).

i. Its ease of implementation with basic mathematical and logic operations to handle non-linear algebraic equations

i. Its ability to bypass local optimal solution due to the balance provided between exploitation and exploration phases.

The flowchart of the WOA technique is depicted in Figure 2.21.

2.6.3.3 Giza pyramid construction optimization algorithm

The Giza Pyramids Construction (GPC) optimization algorithm is inspired by the ideology and inspiration of ancient times. It was developed by Harifi et al., (2020) in the year 2020. It is considered the first ancient-inspired meta-heuristic optimization algorithm. In the ancient past, there were numerous technological limitations, but various man-made structures that existed in the olden days showed that these technological limitations can be overcome by some sort of optimization procedure that exist at that time.

A careful look at how some of the existing structures and artifacts as at that time, were built despite the lack of sophisticated technologies relative to the advent of new technologies that are in existence right now begs the issue as to how the optimization methods were implemented in the construction of these structures and artifacts (Harifi, et al., 2020; Hawass, 1998).

One of the most significant contribution of such optimization methods is the construction of the three pyramids in Egypt. Several theories have been put forward about the method used in the construction of the pyramids; however, none of these theories are proven or approved. It is a general belief that the stones of these pyramids were removed from mines, shipped and then placed in place, such that ramps were used to mount them at higher levels. This same belief was not shared by the Greeks, as they believe that slaves were exploited in the construction of the pyramids (Rigby, 2016; Harifi *et al.*, 2020).

On the contrary, recent findings suggest that the pyramids were built by skilled workers ranging from fourteen to forty thousand people, and were built for a period of approximately 20 years. The number of blocks used in the largest pyramid stands at two million pieces. An advanced approach to project and construction management was also employed during their construction; a testament to the complexity and logistical requirements of this extraordinary project. The pyramid stands today as an awesome testimony to the skill and sheer determination of the ancient race that built it (Harifi et al., 2020; Hawass, 1998).

As stated earlier, the workers are skillful workers led by an expert agent. This expert agent is a foreman called Pharaoh's special agent. Each of the workers is expected to maintain an initial position and carry stone blocks as directed by the expert agent. In order to make the process a competitive one, a worker who does his work efficiently will receive a sublime rank as a reward. The best rank is related to Pharaoh's special agent. Moreover, energy is lost by each worker during the process of transporting the stones. During

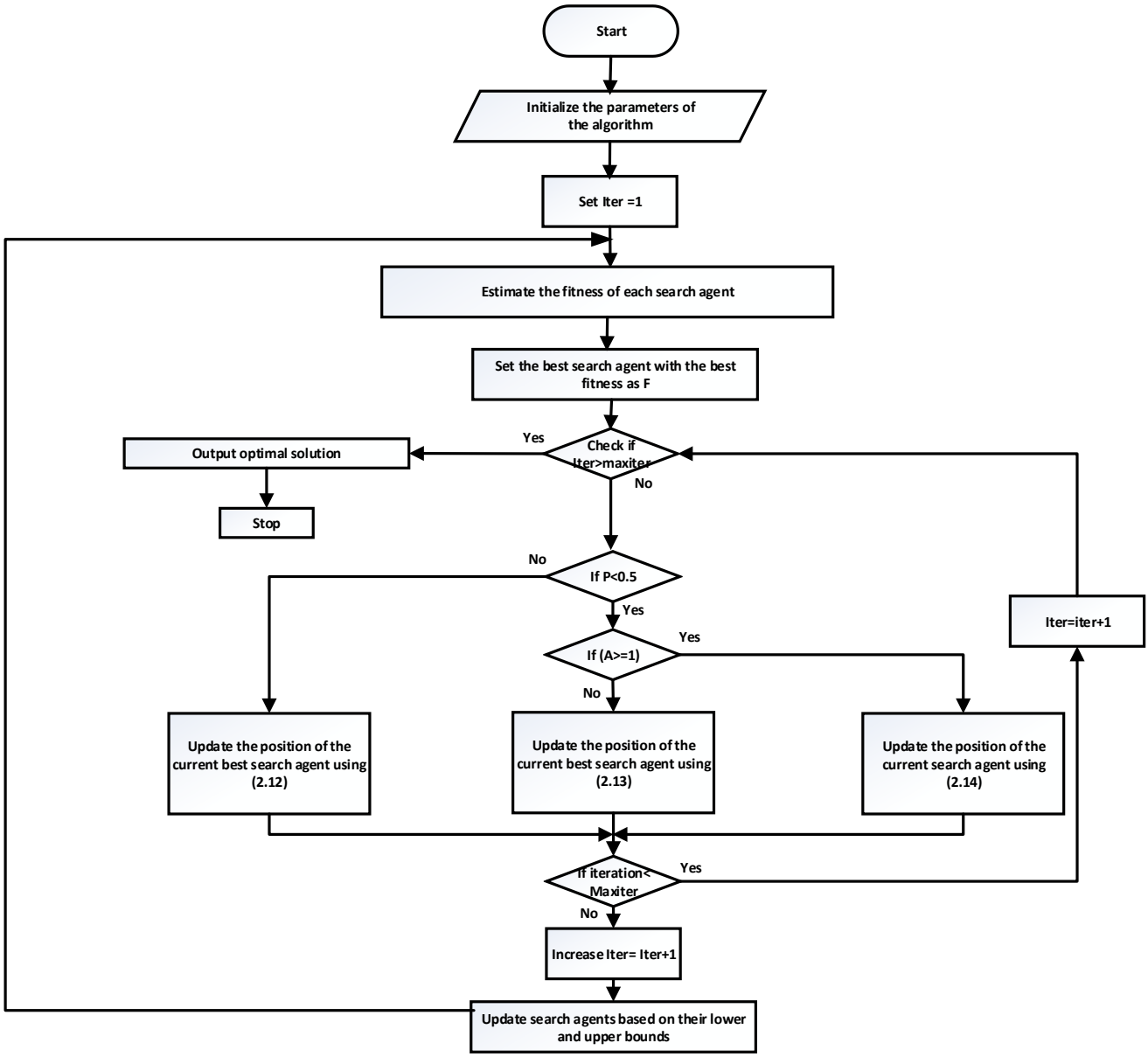

Figure 2.21: Flowchart of Whale Optimization Algorithm (Zaki Diab et al., 2019)

this process, power is lost be each worker and when a worker losses too much power, he is substituted by a new energetic worker. In addition to competing for sublime rank, there is another motivational competition among workers, which is the experience and expertise gained over a period of time (Harifi et al., 2020).

During the pyramid construction process, stone blocks which are scattered by agents such as miners around the construction site are carried by the workers from where they are scattered and moved closer to the pyramid installation site. Ramps are then used to carry the stone blocks an initial location to a final location close to the pyramid. The distance traveled to push the stone from a starting position to the location of the pyramid construction site is determined by the employees' abilities (Harifi et al., 2020).

Therefore, if numerous stone blocks are spread throughout the construction site, workers are required to move the blocks from their original position to the final place near the pyramid using ramps. Each block's starting position and costs are given. The slope of the ramp and its friction affect the displacement of the stone blocks (Dukes et al., 2021). The employees are continuously shifting their position to obtain the optimum position for controlling the movement of the stone blocks. Due to the different characteristics of the work force, it is possible to substitute a worker from a certain group to balance the strength of workers in another group to move the stone blocks. Consequently, some of the workers' positions will thus be replaced by the others. This replacement creates a change in the system which results in power balance in moving the stone blocks (Rigby, 2016; Harifi *et al.*, 2020).

In its application to optimization problems, the following assumptions guide the GPC optimization algorithm in achieving an optimal solution (Harifi et al., 2020).

1. The pyramids were built by using a straight-on ramp.
2. It is also assumed that only one ramp was used throughout the construction process.
3. In the algorithm, the angle the ramp makes with the horizontal surface is less than 15 degree and can be varied. (Archaeologists believe the angle was between 8 and 12 degrees).
4. In its application to an optimization problem, the optimal solutions are derived from the resultant effect of the position of the worker and stone blocks.
5. The effect of frictional force is considered in the displacement of the stone blocks, but negligible for the workers.

During the construction process, which is similar to the optimization process of the algorithm, the displacement of the workers from an initial position to a new position is an important stage in the optimization process. If a worker applies a force to the stone block, it begins to move at an initial velocity,

however, the force of friction forces the stone block to halt after a period of time. As a result, the worker applies additional force to the stone block, causing it to move again at new velocity. In each iteration, the initial velocity is considered a random number, because each time the worker attempts to move the stone block, the applied force depends on the amount of energy consumed by the worker (Harifi et al., 2020).

The fundamental principle of the algorithm is that the workers responsible for the movement of the stone blocks will continue to adjust their movement in order to displace the stone block from its current position. The continuous adjustments of the workers leads to further movement of the stone block towards the installation site and subsequently, new positions are acquired by the stone blocks, which is relative to the movement of the workers encouraging (Harifi et al., 2020; Kharrich et al., 2021; Kumar, 2021). The most suitable position of the worker in moving the stone block closer to its final location is considered the optimal solution to the optimization problem. An important feature of the GPC algorithm is its ability to fully and intelligently utilize the available information of the population size to orient the search and optimization process (Harifi et al., 2021; Kumar, 2021; Nssibi et al., 2021)

The algorithm is modeled mathematically based on the motion of the worker/stone on a ramp, which can be akin to the movement of an object on an inclined plane as depicted in Figure 2.22. The distance traveled by the stone block from an initial position to a new position as described by Harifi et al., (2021) can be estimated using equation (2.15) to (2.19). Equation (2.15) is used to describe the frictional force acting on the stone block during its movement from one position to the other on the ramp. Equation (2.16) is obtained using Newton second law of motion, while equation (2.17) is obtained by substituting equation (2.15) into equation (2.16). The displacement of the stone block from one location to the other on the ramp is derived from equation (2.17) at steady state acceleration and expressed using equation (2.18) (Harifi et al., 2021).

$$f_f = \mu_f mg\cos\theta \tag{2.15}$$

$$-mg\sin\theta - f_f = mz \tag{2.16}$$

$$z = -g\left(\sin\theta + \mu_f \cos\theta\right) \tag{2.17}$$

$$D_s = \frac{u_0^2}{2g\left(\sin\theta + \mu_f \cos\theta\right)} \tag{2.18}$$

where f_f is the frictional force, μ_f is the co-efficient of the frictional force which is usually set between its minimum and maximum values, θ is the angle that the ramp makes with the horizontal axis, g is the

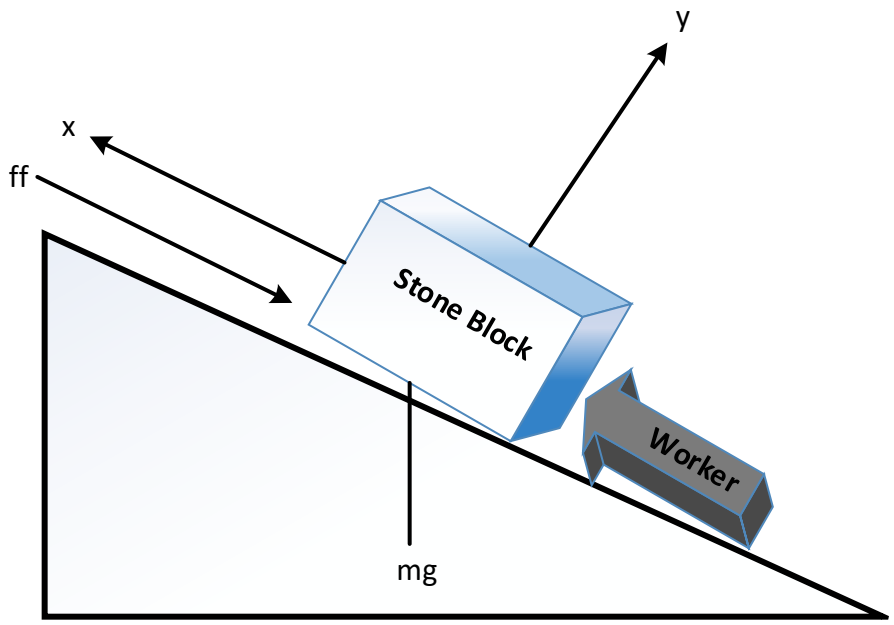

Figure 2.22: Position of the workers and stone block on the ramp (Harifi et al., 2020)

acceleration due to gravity, which is usually set at 9.8, m and z are the mass and acceleration of the stone block respectively, u_0 is the initial velocity of the stone block which is determined randomly in the range of [0,1] and D_s is the displacement value of the stone block.

Since the displacement of the stone block is dependent on the continuous adjustment of the workers, the movement of the workers can be estimated using equation (2.18), albeit in the absence of frictional force, f_f , as friction does not affect the movement of the workers along the ramp. Hence, the displacement of the workers as described by Harifi et al., (2020) and Nssibi et al., (2021) is expressed using equation (2.19).

$$D_w = \frac{u_0^2}{2g\sin\theta} \tag{2.19}$$

New position of the workers, as well as the stone block along the ramp can be determined once the displacement of the stone block in equation (2.18) and the movement of the workers given in equation (2.19) are estimated. The new position corresponds to new solution at every iteration step and it is expressed using equation (2.20) (Harifi et al., 2021).

$$P_{new} = \left(P_{old} + D_s\right) \times D_w \varphi_i \tag{2.20}$$

where P_{new} represents the new position, P_{old} represents the current position and φ_i represents a randomization parameter which is generated using Gaussian method.

The final computational stage of the algorithm is the investigation of substituting a tired worker among the group of workers pushing the stone block towards the installation site. This is achieved by applying the principle of uniform crossover operator and is described mathematically by Harifi et al., (2021) using equation (2.21).

$$\zeta_k = \begin{cases} \psi_k & if rand(0,1) \le 0.5 \\ \phi_k; & otherwise \end{cases} \tag{2.21}$$

where ϕ_k represents the primary solutions, ψ_k represents the generated solutions and ζ_k represents the new solutions after substituting tired workers.

The GPC optimization algorithm has been applied to different optimization problems including the optimal design of HPS, and the results have been very encouraging (Harifi et al., 2020; Kharrich et al., 2021; Kumar, 2021). Some of the main strengths of the algorithm over other existing optimization algorithms are as follow.

1. The ability to retain previous information, a feature that is not present in most meta-heuristic algorithm.
2. High speed of convergence, ease of implementation, low number of control parameters and absence of premature convergence.
3. Increase in the balance between exploration and exploitation stage.
4. Ability to handle high dimensional, multi-modal and non-linear functions.
5. Special control parameters are not required.
6. Ability to find the global optimal without even considering initial values.
7. Ability to change from multiplicative to the accumulative mode when finding the global solution (optimum position of the workers).
8. The ability to easily convert from continuous mode to the integer or discrete binary form.
9. The ability to find an optimal solution in a non-linear constrained optimization problem with penalty function.
10. It does not get trapped in local optimum as the members of the population (solution) representing the workers are closer to each other.
11. Increase in the population only leads to a linear increase in the run time as compared to other population based algorithm where an increase in population leads to an exponential increase in their run time.

The main drawback is that it cannot be applied to some combinatorial problems such as Traveling Salesman Problem (TSP) unless it is developed; and just like every other meta-heuristic algorithms, an increase in the population size may result in high run time and the possibility of obtaining sub-optimal solutions. Therefore, the initial population of workers must be carefully chosen when applying the algorithm to various optimization problems (Harifi, Mohammadzadeh, et al., 2020). The algorithm is modelled mathematically as follow. The flowchart of the proposed GPC optimization algorithm is as shown in Figure 2.23.

2.7 Hybrid power system design criteria

The main aim of applying an optimization technique in the design of HPS consisting of renewable and non-renewable energy sources is to address the issues of minimizing or maximizing certain design criteria that are used to evaluate the performance of the system. This criteria are regarded as pointers that assists the designers, policy and decision makers, as well as government agencies to make informed decisions with respect to reliability, feasibility and viability of the system (Lassalle et al., 2022). More than one criteria may be used in evaluating the performance of the system; in such case, the design problem is usually formulated as a multi-objective optimization problem, thereby prompting the need to achieve a balance among the various conflicting criteria used in the design of HPS (Babatunde et al., 2020). Several design

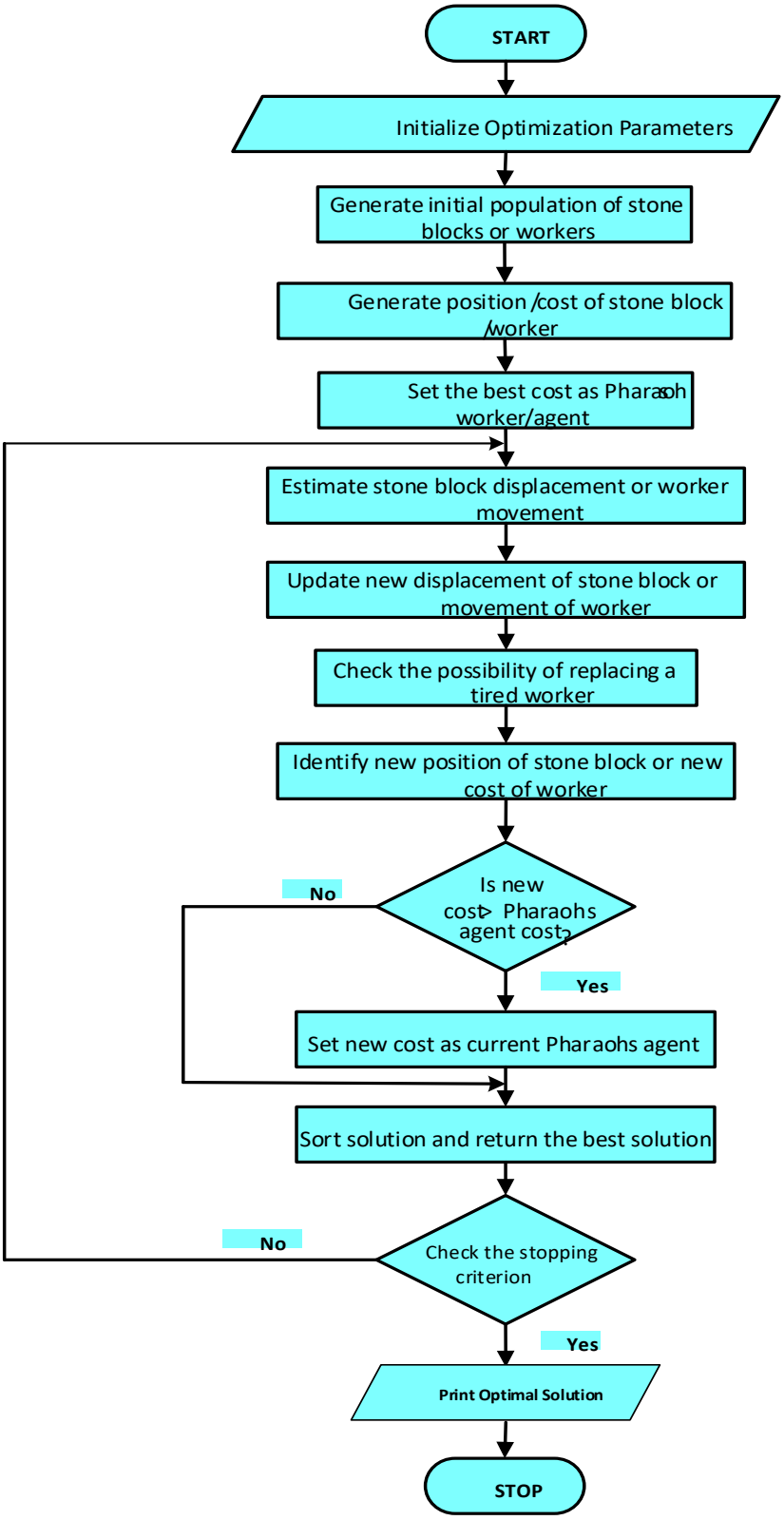

Figure 2.23: Flowchart of the proposed Giza Pyramids Construction (GPC) algorithm (Harifi et al., 2020)

ccriteria have appeared in most literatures to evaluate the performance of HPS, The three main classifications of HPS design criteria are economic, environmental and technical criteria (Kiehbadroudinezhad et al., 2022). A brief discussion on each of these classifications are subsequently presented.

2.7.1 Economic criteria

In order to properly optimize the design of HPS, the economic criteria must be modeled and analyzed appropriately to produce cost-effective solutions. They are considered the most important criteria as they are used to evaluate the financial implication of the HPS. Some of the criteria under this category include Levelized Cost of Electricity (LCOE), Life Cycle Cost (LCC), Net Present Cost (NPC), Annual Cost of System (ACS), to mention but a few (Kiehbadroudinezhad et al., 2022; Palej et al., 2019). A brief description of some popular economic criteria are presented in the following sub-sections.

2.7.1.1 Levelized Cost of Electricity

The Levelized Cost of Electricity (LCOE), which is also referred to as levelized cost of energy is a suitable metric for measuring the overall cost effectiveness of the designed HPS. It is a measure of the average income per unit of energy generated by the HPS to repay the total investment cost on the system during its entire lifecycle (Kiehbadroudinezhad et al., 2022; Sawle et al., 2016). It represents the ratio of the overall cost in terms of initial investment capital, operation and maintenance cost (fixed and variable), discounted negative cash flows, taxes, lifecycle or major replacement costs to the actual quantity of energy delivered by the HPS (Lassalle et al., 2022). It is calculated according to Rehman et al., (2020) using expression (2.22).

$$LCOE = \frac{\sum LifeCycleCost - \sum LifeCycle\,\mathrm{Re}bates}{LifeCycleEnergy} \qquad 2.22$$

The LCOE is considered an important economic criteria because it is able to hybridize both fixed and variable costs as a single tool to measure the performance of the HPS. Nevertheless, the hybridization may lead to ambiguity when analyzing the results (Kiehbadroudinezhad et al., 2022).

2.7.1.2 Annual cost of system

The Annual Cost of System (ACS) is another important economic criteria that has been used to gauge the financial performance of HPS. It essentially comprises of the capital cost, replacement cost and maintenance of the system over the period of one year. The major drawback of the ACS criteria is the need to estimate the discount rate and capital cost for each of the energy generating component separately (Kiehbadroudinezhad et al., 2022). Generally, the ACS of any HPS configuration can be estimated according to Maheshwari & Ramakumar, (2017) using equation (2.23).

$$ACS_{HPS} = C_{acc} + C_{arc} + C_{amc} \quad 2.23$$

where C_{acc}, C_{arc} and C_{amc} account for the annualized capital cost, annualized replacement cost and annual maintenance cost of the system respectively.

It should be noted that the annualized capital cost of each of the energy generating sub-system also takes into account the installation cost.

2.7.1.2 Life Cycle Cost

One of the most important economic criteria that has also been used in evaluating the performance of HPS is the Life Cycle Cost (LCC) of the system. The LCC, which is also referred to as Net Present Cost (NPC) in HOMER software, estimates the total cost of the system throughout the entire lifetime of the project. It takes into account the whole financial implication of the project during its lifecycle. Financial implication may include the initial capital cost of the system, the operation and maintenance cost, the replacement cost and all discounted costs (Kiehbadroudinezhad et al., 2022; Sawle et al., 2016). The main advantage of using this type of economic criteria is that it is able to give a detailed financial representation of the system taking into consideration the total cost incurred over the specified period of operation. However, the information required to accurately estimate the operation and maintenance costs are not readily available in most database and predictive tools (Kiehbadroudinezhad et al., 2022). LCC can be estimated mathematically using expression (2.24) as given by Kharrich et al., (2021).

$$LCC = C_c + OM_c + R_c + F_{c(dg)} \quad 2.24$$

where C_c is the initial capital cost of the system, OM_c is the operation and maintenance cost, R_c is the replacement cost and $F_{c(dg)}$ is the fuel cost of the DG set.

The LCC is one of the objective considered in this study because of the need to give a detailed financial implication of the proposed HPS.

2.7.2 Environmental criteria

Since the main aim of introducing RE sources into the power generation mix is to reduce the emission of harmful gases produced by non-renewable energy source into the atmosphere; environmental criteria is used to investigate the impact of the system on the environment. It is considered as an important design criteria as it helps determine the level of carbon emission and the penetration of the RE sources. The two most common environmental criteria used in many studies involving HPS design is the minimization of carbon oxide and the maximization of RE resources penetration (Arifin et al., 2021; Lassalle et al., 2022).

2.7.3 Technical criteria

Technical design criteria is used to evaluate the performance of the HPS under various operating conditions that are unrelated to both economic and environmental criteria. This criteria helps determine the capacities and operational details of the various sub-system of the HPS. It can be introduced into the design model as either a constraints or in form of control and energy management (Kiehbadroudinezhad et al., 2022). The two major performance criteria that fall under this category are renewable energy fraction and system reliability. System reliability is an important metrics to the design as it is used to gauge the integrity of the system while renewable energy fraction is used to measure the penetration of RE resources (Lassalle et al., 2022). Some common criteria used in measuring the reliability of HPS are Loss of Power Supply Probability (LPSP), Loss of Load Probability (LOLP), Expected Energy Not Served (EENS), among others (Kiehbadroudinezhad et al., 2022). The two most common criteria used in many literatures are briefly discussed in the following sub-sections.

2.7.3.1 Loss of power supply probability

Loss of Power Supply Probability (LPSP) is the probability that an insufficient power supply occur when the system is unable to meet the load demand (A. Alam & Mehar, 2021). It has been used in many studies to evaluate the performance of HPS with respect to its integrity and reliability. LPSP must be monitored as a key constraint in ensuring that power supplied by the system is able to meet the load at all time (Kiehbadroudinezhad et al., 2022). For the purpose of this study, the LPSP was treated as one of the most important constraints in the proposed HPS. It is usually determined once the power capacity of each of the energy generation sources has been modeled. Its mathematical representation as described by Kiehbadroudinezhad et al., (2022) is given in equation (2.25).

$$LPSP = \frac{\sum_{i=1}^{N}\left[P_L(t_i) - P_{HPS}(t_i)\right]}{\sum_{i=1}^{N} P_L(t_i)} \qquad 2.25$$

where N is the number of hours, $P_L(t_i)$represent the power required by the load at a given time step on hour i, $P_{HPS}(t_i)$ represents the power generated from the HPS at given time step on hour i.

2.7.3.2 Loss of Load Probability

Loss of Load is defined as the inability of the HPS to meet the daily peak load demand. This scenario usually occurs whenever the consumer load exceeds the available power generated by the system. The overall probability that there will be a shortage of power (loss of power) is referred to as Loss of Load Probability (LOLP) which is expressed in terms of days per year, hours per day or percentage of time (Esan et al., 2019; Kiehbadroudinezhad et al., 2022) The LOLP as described by Kiehbadroudinezhad et al., (2022) is calculated using equation (2.26).

$$LOLP = \frac{\sum_{t=1}^{n} hours\left(P_{HPS}(t) < P_D(t)\right)}{100} \quad 2.26$$

Where P_{HPS} is the power supplied by the HPS at hour t, $P_D(t)$ is the power required by the load at hour t and n is total number of hours.

2.8 Review of related works

An approach for optimal design, simulation and analysis of hybrid PV/wind system based on discrete optimization technique is presented by (Badejani et al., 2007). The total capacities of the RE sources are computed with respect to the annual power demand. The performance of the system was evaluated under different environmental condition of the PV system and blade angle pitch control of the wind turbine. A single objective optimization problem based on cost function is formulated and solved using the proposed approach. System simulation and energy balance estimated for a period of three years were used to compensate for any error in the design process. Simulation results showed that the proposed approach optimized the cost of the system with significant reduction in the overall cost of the system.

Suryoatmojo *et al.*, (2009) performed an optimal design of an integrated system involving wind-PV-diesel-battery system for isolated island with CO_2 emission evaluation using GA. The proposed system was design for the hybrid power generation in East Nusa Tenggara, Indonesia. Mathematical modeling of the various components of the system was carried out using MATLAB/Simulink and the objective function was minimized using GA. Simulation results showed that the proposed system was able to minimize the total annual cost of the system and reduce carbon emission into the atmosphere.

Wang and Singh, (2009) designed a hybrid power generation system including wind power and solar power on the basis of cost, reliability, and emission criteria using a Modified Particle Swarm Optimization algorithm (MOPSO). A set of tradeoff solutions were obtained using the multi-criteria meta-heuristic method. Moreover, in one of the designs, system uncertainties, such as equipment failures and stochastic generation/load variations were also considered by conducting adequacy evaluation based on probabilistic methods. Numerical simulations were used to illustrate the applicability and validity of the developed MOPSO based optimization procedure, and some sensitivity studies were also carried out. Simulation results showed that the developed model was very effective in the optimum design of the system at low cost and low carbon emission.

Ardakani et al., (2010) designed a grid connected wind/photovoltaic/battery power system for a region in North-west Iran using Particle Swarm Optimization with the aim of reducing the annualized cost of system (ACS) for an operation period of 20 years. The problem was formulated as a single objective optimization

problem taking into consideration the technical, economic and reliability constraints of the system. PSO technique was used to obtain the optimal sizing of the system components that minimizes the annualized cost of the system. Simulation results showed that the hybrid system is the most feasible for the electrification of the region as it gives the best value of ACS over its entire lifespan.

Saif *et al.*, (2010) presented the capacity design problem of a PV-Wind-Diesel-Battery HPS using LP. The model was formulated with the aim of minimizing total cost and carbon emissions. A multi objective optimization approach was employed for this purpose taking into consideration the various constraints of the system design. Model inputs were extracted from real time environmental and technical data. The proposed approach was applied on a case study which entails designing a HPS for a city of 50,000 residents. Simulations results showed an increase in the reliability of the proposed system and a reduction in the amount of carbon emission.

Bansal et al., (2011) presented an artificial intelligence based optimization of a stand-alone hybrid system consisting of solar and wind energy resources. An optimization problem which focuses on the reduction of net present cost of the system was formulated and optimized using Meta Particle Swarm Optimization (MPSO). The system was simulated for a period of 25 years using MATLAB software. Simulation results showed that the global optimal searching ability of the proposed algorithm is significantly improved, as it avoids the possibility of getting trapped in local optimal solution.

Hassanzadehfard, Moghaddas-Tafreshi and Hakimi, (2011) considered the optimal sizing and operation strategy of micro-grid systems consisting of wind turbines, PV arrays, fuel cells, battery banks, reformers and DC/AC converters for a northwestern region of Iran using PSO. The problem was formulated as a nonlinear integer minimization problem which minimizes the sum of the total capital, operational and maintenance and replacement costs of the Distributed Energy Resources (DERs). Additionally, some basic notions of reliability were considered for the proposed micro-grid system and the effect of reliability on the total cost of the system were evaluated. Simulation results showed that the proposed methodology provides excellent convergence and feasible optimum solution for sizing of islanded micro-grid system using PSO.

The technical and economic analysis of a wind/solar hybrid system using HOMER software is presented by Zhang et al., (2011). Individual components of the hybrid system was modeled, simulated and optimized using HOMER software with the aim of finding the optimum economic performance of the system. The optimal results was analyzed for different system configurations. The results of analysis showed that wind speed greatly influence the overall cost of the system.

The optimal design and power management selection of hybrid renewable energy system comprising of solar PV generator, wind turbine, battery storage, fuel cell, electrolyzer, hydrogen tanks and diesel generators using hybrid differential evolution and fuzzy logic technique was presented by Abedi et al., (2012). The uncertainties in solar and wind resources were modeled using Weibull and Beta probability, a multi-objective optimization problem to minimize the overall cost of the system, unmet load and fuel emission under various optimization constraints was developed and optimized using hybrid different evolution-fuzzy technique. Simulation of the hybrid system was done using MATLAB. The results demonstrated the efficacy and capability of the proposed optimization algorithm for hybrid energy system design.

Bilal et al., (2012) proposed a methodology for designing a stand-alone hybrid PV/wind/diesel/battery system for the community of Gandon located in north-west of Senegal; with the aim of minimizing the Levelized Cost of Energy (LCE) and carbon emission using Genetic Algorithm. An assessment of the community was done to determine the weather condition and load profile of the area. Mathematical modeling of the considered components were done using Simulink, while a multi-objective optimization model was developed and written as a script code in MATLAB. Genetic algorithm was applied to determine the optimal system configuration with the least LCOE and carbon emission, and results were presented as an optimal pareto front. Simulation results showed that for the optimal system configuration, an increase in LCOE corresponds to a decrease in carbon emission and vice-versa.

The optimal design of hybrid renewable energy system for electrification of a remote village in Egypt using homer Pro software is presented by Helal et al., (2012). The components of the hybrid system was modeled, simulated and optimized using HOMER software. The optimization process considered every possible system configuration and searches for the system with the least total Net Present Cost as the optimal system design. Simulation results showed that the PV-wind-battery system is the most feasible system configuration as it gives the least NPC.

A hybrid Simulated Annealing (SA) and Tabu Search (TS) method for the solution of a Small Autonomous Power System (SAPS) optimal sizing problem was proposed by Katsigiannis, Georgilakis and Karapidakis, (2012). The objective function was formulated such that the SAPS cost of energy is minimized. Mathematical modeling of the various components of the SAPS such as wind, PV, diesel generator, battery size and converter rating was carried out using MATLAB/Simulink. The performance of the proposed hybrid optimization methodology was studied for a large number of alternative scenarios via sensitivity analysis. The proposed method was successfully applied to Chania region, Greece. The results showed that

the proposed hybrid SA-TS improves the obtained solutions, in terms of quality and convergence as compared to the solutions provided by individual SA or individual TS methods.

Yadav et al., (2012) presented the optimal design of a wind-diesel hybrid power system for the electrification of an isolated region using HOMER. The components of the system were modeled, optimized and simulated using HOMER software, with the objective to minimize the cost of the system and carbon emission. The results of the hybrid system were compared with those obtained using diesel generator only to meet the load demand of the region. Simulation results showed that the proposed hybrid wind-diesel system can be economical and environmentally friendly if properly sized as compared to using the diesel generator only.

Zhang, Barakat and Yassine, (2012) focused on the development of a methodology for sizing and optimization of four hybrid systems (PV/wind/diesel/battery, PV/wind/diesel, PV/diesel/battery and wind/diesel/battery) in the city of Le Havre, France using Direct Search Algorithm (DSA). Collection of hourly environment data such as solar radiation, wind speed and ambient temperature for a period of 5-year was carried out. Mathematical modeling of the various components of the hybrid system was performed using SIMULINK. The developed model was optimized using direct search algorithm and simulated in MATLAB. The results showed that the use of long term data is very helpful when calculating the performance of hybrid systems. The results also showed that the combination of the hybrid PV/wind/diesel with battery system is the most cost effective type of hybrid system.

Moreover, a method for the optimization of power generated from a Hybrid Renewable Energy Systems (HRES) using PSO) to minimize the Levelized Cost of Energy (LCOE) was presented by Amer, Namaane and M'Sirdi, (2013). The problem was defined and objective function was introduced taking into consideration the fitness values sensitivity in particle swarm process. The algorithm structure was built using MATLAB software. Simulation results showed that the proposed PSO algorithm was found to very competitive in terms of energy cost and carbon emission reduction.

Mahmud, (2013) designed a hybrid power generation system consisting of solar PV, wind turbine battery and diesel generator system for a remote island in Bangladesh using HOMER software. Feasibility study of the Island was examined to determine the solar and wind resources, as well as the load consumption of the Island. The various components of the system are modeled and simulated in HOMER with the aim of reducing the cost of fuel and minimize the emission of harmful gases in the environment. Simulation results showed that the PV-diesel-wind-battery configuration is the most feasible for implementation.

Mohamed and Khatib, (2013) presented the optimization of a micro grid that consists of photovoltaic (PV) array, wind turbine, diesel generator and storage battery based on iterative simulation method. The mathematical models for the system components and meteorological variables, such as solar energy, temperature and wind speed, were employed for design purpose and model using MATLAB/Simulink. The approach was applied to Kuala Terengganu, Malaysia. The results were validated by comparing the proposed optimization method with the method in the HOMER software. The results showed that the proposed method provides more accurate results compared with the method used in the HOMER software.

An approach to determine the optimal capacities of the components of a hybrid system consisting of PV system, diesel generator and battery bank based on iterative technique is presented by An et al., (2014). Individual component of the hybrid system is modeled in Simulink, A constrained optimization problem based on the minimization of annual cost of system (ACS) with zero unmet loads was formulated. The number of PV panels, the capacity of the battery and diesel generator are considered as the decision variables in the optimization problem. The hybrid system was simulated using MATLAB to evaluate its performance. Simulation results showed that the proposed approach is able to find the optimal solution to the design problem, albeit a high simulation run time

Unit sizing optimization of hybrid energy system consisting of renewable and non-renewable energy sources using Genetic Algorithm is presented by Arun et al., (2014). An objective function with the aim of minimizing the cost of energy under various system constraints is formulated and solved using the proposed algorithm. HOMER pro software was also used to optimize the same hybrid system and the results are compared to illustrate the performance of the proposed method. Simulation results showed that the proposed approach gives a better COE results with respect to HOMER pro software.

The optimal design of hybrid renewable energy system using differential evolution technique is investigated by Delgado & Dominguez-Navarro, (2014). A multi-objective optimization problem based on the overall cost of the system and the penetration of the renewable sources was formulated and solved using DE. A universal generating function was used at the optimization stage to minimize computational time of the proposed algorithm. The results of simulation are compared with those obtained using Monte Carlo simulation. The results showed that the proposed method generate adequate results in a short period of time as compared to those obtained using Monte Carlo approach.

A methodology for the optimal sizing of hybrid, stand-alone PV-WG system to supply a residential household using GA is presented by Tégani *et al.*, (2014). The method, based on differential flatness approach was applied for optimal sizing design and strategy control of the hybrid stand-alone system. The problem was formulated such that the total system cost for a 20 year round is minimized subject to the

constraint that the load energy requirements are completely covered. Simulation was carried out using MATLAB/Simulink software tool. The results were compared with conventional optimization methods such as dynamic programming and gradient techniques. Simulation results showed that the proposed approach has the aptitude to attain the global optimum with relative computational simplicity.

Clark, Cronje and Wyk, (2015) presented the optimal economic design of a hybrid energy system for a small university using convex optimization approach. Simulation model of a grid connected PV/Wind/diesel hybrid system was implemented using Simulink in Mathworks. An interior point convex solver was then used to design an optimal PV/wind/diesel system with lowest overall cost to determine the viability of the proposed approach. The results were compared with those obtained using existing HOMER software package. Simulation results showed that the solution obtained from the proposed approach agree with that of HOMER software which is based on slow discrete combinatorial optimization.

The optimal design of a hybrid system consisting of wind turbine, photovoltaic generator, diesel generator and battery bank using particle swarm optimization is presented by Mandal et al., (2015) A multi-objective optimization problem based on minimization of Life cycle cost and cost of energy was formulated and optimized using the improve particle swarm optimization. The performance of the proposed approach was illustrated by comparing its results with those obtained using iterative technique used for the same purpose. The results showed that the proposed method produces superior solutions in terms of convergence characteristics and simulation run time with respect to the iterative technique.

Mekhamer et al., (2015) introduced an approach for the optimal sizing of a grid-connected hybrid power generation system using Ant Lion Optimizer and Grey Wolf Optimizer. The problem was formulated as a single objective optimization problem that minimizes the Total Annual Cost of the system considering various equality and non-equality constraints. The proposed algorithm is applied to solve the resulting optimization problem. The performance of the proposed algorithms was demonstrated by comparing their results with those obtained using Cuckoo Search Algorithm and Flow Pollination Algorithm (FPA). All simulation was executed using MATLAB software. Simulation results showed that the proposed ALO and GWO generate a more reliable results as compared to CSA and FPA.

The optimal design of the hybrid power generation system using was obtained by Mekhamer *et al.*, (2015) using Cuckoo Search (CS) and Firefly Algorithm (FA). A feasibility study of the proposed area was conducted for weather condition and load data. Objective functions based on the two optimization techniques proposed were formulated and implemented using MATLAB. The optimization results were compared with that of PSO applied to the same case study. Simulation results showed that the proposed

techniques are better, powerful and are recommended for use in the optimal solution for hybrid power generation systems.

Tan et al., (2015) proposed the design of a micro-grid distributed power consisting of wind turbine, photovoltaic, batter and diesel generator system for the electrification of an islanded area using HOMER pro software. The aim of the design is to minimize the overall costs of the micro-grid. Each components of the system was modeled and optimized in model to verify the feasibility of the micro-grid; the optimization was also done for different battery technology and the results of the various configurations obtained were compared with one another. The results showed that the micro-grid system with Lithium ion battery gives the least overall cost as compared to other system configurations.

A general approach based on multi-objective combinatorial model for optimizing hybrid PV-wind-diesel-battery system configuration using evolutionary algorithm was presented by Wang, Zhang and Zhang, (2015). The problem was modeled as a multi-objective combinatorial model where the four objectives are the minimization of the life-time system cost, life-time emission of CO_2 and SO_2 and maximization of the system output power. The multi-objective evolutionary algorithm based on decomposition approach was employed to obtain a set of Pareto optimal solutions to the problem. Simulations were done using MATLAB/Simulink. Simulation results showed that the developed model provides convenience especially for non-expert users when selecting suitable components in the design of HRES.

Kamjoo *et al.*, (2016) presented the use of Non-dominated Sorting Genetic Algorithm (NSGA-II) for the design of a standalone Hybrid Renewable Energy Systems (HRES) comprising of wind turbine, PV panel and battery bank. The problem was formulated as a multi-objective problem for minimizing system cost and maximizing reliability. A Chance Constrained Programming (CCP) method was used to address the uncertainties in renewable resources such as wind speed and solar irradiance. The proposed method was validated on a case study and the results obtained were compared with the conventional method of incorporating uncertainties using Monte Carlo simulation. The results showed that the proposed method yields conservative results in lower reliability values and better results in high reliability values.

Kushida & Abe, (2016) presented the optimal design of a grid connected hybrid PV-diesel power system for a residential area in Japan using linear programming technique. The annual load curves of the customers was used in addition to the hourly solar irradiation of the area to simulate the proposed hybrid system. An optimization problem based on minimization of system cost is formulated and solved using linear programming technique. Simulation results showed that the hybrid system is capable of supplying multiple customers and subsequently reducing the overall cost of the system. However, the approach was found to be time consuming.

Mallikarjuna et al., (2016) conducted a study on the reliability constrained optimization of an off-grid hybrid system consisting of solar PV, wind turbine and hydro resources using Cuckoo Search Algorithm (CSA). Individual model for wind speed, solar irradiation, water availability and load profile based on semi-Markov function is formulated, the Fast Fourier Transform (FFT) analysis was used to combine each of the energy generation model with the load model. A multi-objective optimization problem with the goal of optimally sizing the components and minimizing the overall cost of the system is formulated and optimized using the proposed technique. All analysis were carried out using MATLAB software and the results of simulation are compared with those obtained using GA and PSO algorithm. Simulation results showed that the proposed approach gives the best results in terms of cost minimization and optimal system combination as compared to GA and PSO techniques.

A genetic algorithm based multi-objective design of a grid independent PV/Wind/Split-Diesel/Battery hybrid energy for the electrification of a residential home in Nigeria is presented by Ogunjuyigbe et al., (2016). Feasibility assessment of the residential home was conducted to determine the hourly load profile, as well as solar and wind resource potential of the area. An optimization model to minimize the Life Cycle Cost, carbon emission and dump energy was developed and optimized using Genetic Algorithm. Five different scenario of the hybrid system was simulated using the proposed algorithm to determine the most feasible configuration that satisfy the set objectives. Simulation results showed that optimal configuration comprising of the PV/Wind/Split-Diesel/Battery is the most feasible scenario when compared to other scenarios in terms of LCC, carbon emission and dump energy. The results also demonstrated the efficiency of using split diesel generator over a single large sized generator.

Okinda *et al.*, (2016) reported on the findings of examining the problems of optimal sizing of a hybrid wind and solar renewable energy power generation system using genetic algorithm. A target site was first identified and meteorological data collected. Components of the system were then mathematically modeled from which an objective function was developed. A parallel multi-deme implementation of genetic algorithm was then used to optimize the system. Multiple scenarios were prepared and simulated to obtain an optimal configuration of the hybrid power system. The results showed that wind and solar have complementary regimes and can thus be hybridized to minimize the LCOE. The result also showed that the least cost configuration didn't necessary maximize on the utilization of the abundant resource.

A multi-objective design of hybrid wind-photovoltaic-storage system using Artificial Bee Colony was proposed by Shayeghi et al., (2016). A multi-objective optimization problem considering annual cost of the overall system and carbon emissions was formulated and solved using ABC algorithm. A fuzzy making method was used to obtain the best solution from the set of pareto-optimal solution obtained. The proposed

method was applied to a remote location in north-western Iran using long meteorological data of the area. Simulation results demonstrate the efficiency of the proposed method in yielding the optimal combination of system components and also ensure maximum economic and environmental profits.

A Teaching Learning based Optimization (TLBO) technique is applied by Deb et al., (2017) to the optimal design of a hybrid power system consisting of PV panels, wind turbine and diesel generator. The problem was formulated as a multi-objective optimization considering the minimization of overall cost of system and carbon emission, and improving reliability. The teaching learning based optimization technique was used to solve the resulting optimization problem. The system was simulated for a period of ten years using MATLAB software. Simulation results showed that the TLBO is capable of producing quality optimal solution. Nevertheless, the approach was found to be time consuming as it involves too many control parameters during the optimization process.

He *et al.*, (2017) presented a hybrid energy system based on the renewable resources in a certain area using HOMER software. The paper implemented economic analysis and also considered the capacity shortage effect of the hybrid system. Mathematical modeling of individual components was carried out based on the available capacity. Simulations were carried out using HOMER software. The results showed that the capacity of the battery changed mostly when the reality of the system declined. The results also showed that the economic performance improved significantly with the Cost of Electricity (COE).

Huang et al., (2017) proposed the optimal design of a stand-alone micro-grid using Mixed Integer Linear Programming (MILP) model to meet the energy demand of an isolated island. The developed optimization model considered the initial investment cost, maintenance and replacement cost, fuel cost, environmental management cost and power shortage penalty cost. The utilization rate of RE sources, single and total loss of power supply probability and dump energy production are considered as constraints in the optimization problem. The resulting optimization problem was solved using the proposed approach. Simulation results demonstrate the ability of the proposed approach in obtaining optimal solution hybrid power system design problems. However, the method was found to be time consuming and computationally exhaustive.

Kaabeche et al., (2017) proposed a PV/wind hybrid optimization method using Firefly Algorithm (FA) under Load Dissatisfaction Rate (LDR) criteria and the Electricity Cost (EC) indicator conditions for power reliability and system cost. The various components of the hybrid system were modeled in Simulink environment; an objective function to minimize the cost of energy considering reliability constraints was formulated and implemented using MATLAB. The developed model was applied to supply the energy required by a group of households located in Bouzareah, Algeria. The effectiveness of the proposed optimization technique was evaluated by comparing its performance with other popular optimization

algorithms such as Accelerated Particle Swarm Optimization (APSO) algorithm, Generalized Evolutionary Walk Algorithm (GEWA) and Bat Algorithm (BA). Simulation results showed that proposed algorithm produces the most promising solution in terms of energy cost when compared with the other optimization algorithm. The results also showed that the hybrid PV/Wind/Battery system is more economically feasible compared to either standalone wind or PV system only.

Another methodology for optimization of Smart Integrated Renewable Energy Systems (SIRES) to minimize ACS and maximize reliability for remote and rural areas using GA was described by Maheshwari and Ramakumar, (2017). A hypothetical rural area with a population of 700 was considered and basic energy requirements for this area were estimated. Availability of resources and weather conditions were analyzed. System components, ACS and system reliability were modeled. A flowchart for implementation of GA was developed and the optimal number of system components and minimum ACS for target reliability was obtained. The results showed that the proposed approach was able to reduce Greenhouse Gas (GHG) and improved the overall efficiency as compared to other current approaches to rural development.

Mbodji et al., (2017) developed a computerized methodology based on numerical analysis for the Optimal Design of an Off-Grid Hybrid Solar Photovoltaic-Diesel System for Electrification of a Fishing Village in Morocco. The load profile of the village was evaluated using a power balance, while the optimal capacity of the PV system was determined based on the evaluated load. The PV system was sized and the cost benefit analysis based on quoted system costs for a period of 9 years was performed to determine the economic viability of the proposed system. Simulation results showed that the proposed system design significantly minimize carbon emission, with a relative reduction in overall cost of the system. However, the approach was found to be time consuming.

An approach based on HOMER software for the design of a micro-grid hybrid system to meet the energy demand of a remote locations is presented by Singh & Tiwari, (2017). The off-grid system consists renewable sources such as solar and wind with battery storage system as backup. Individual components of the micro-grid was modeled and optimized using HOMER. The model was implemented on a case study of a typical building in India, comprising of over 100 houses. The most feasible combination of system components was studied and analyzed. Simulation results showed that the hybrid solar-wind-battery system is the most economical of all the system combination considered to meet the energy demand of the location.

Ahamad et al., (2018) presented the optimal design of a grid-connected integrated power system, consisting of PV, wind turbine and a battery for the electrification of an isolated load using HOMER software. The various components of the system were modeled and correspondingly, the performance of the proposed system was analyzed based on its net present cost of the system. The software was also used to optimize

the system and sensitivity analysis was then carried out to determine the response of the system to change in components prices. Simulation results showed that the implementation of micro-grid technologies is an effective solution in meeting the energy demand of the isolated load.

A multi-objective optimal design of a grid-connected Hybrid Power Generation Systems (HPGSs) using whale optimization algorithm and sine-cosine algorithm was proposed by Algabalawy et al., (2018). The components of the HPGS considered include PB modules, wind turbines, battery banks, and has turbines. The components were modeled for power generation in Simulink, an optimization model to minimize total annual cost of the system and carbon emission was developed and optimized using the two proposed algorithm. The obtained results of the proposed model were compared with those obtained using cuckoo search and firefly algorithms to show the robustness of the proposed optimization algorithms.

Khalilnejad et al., (2018) presented the optimal design of a hybrid power system consisting of wind turbine, PV panels and an Electrolyzer using Imperialist Competitive Algorithm (ICA). The various components of the hybrid system was modeled in Simulink and an optimization problem with the objective of minimizing the dump energy and maximizing the penetration of the RE sources and Electrolyzer is formulated and implemented using MATLAB. The meteorological data of a remote location in Miami was used to simulate the hybrid system. Simulation results showed that the optimal system comprises of PV-wind-Electrolyzer, with the Electrolyzer having a higher percentage of penetration.

Bossoufi *et al.*, (2019) proposed the design of a stand-alone hybrid PV-wind-battery energy system using genetic algorithm. The meteorological and load data were collected and assessed for the particular location. Major components of the system and optimization objectives were modeled and an optimal configuration was put in place using a dynamic model of a controlled elitist genetic algorithm for multi-objective optimization. Simulations were carried out using MATLAB/Simulink. The results showed a significant reduction in the life cycle cost of the proposed hybrid energy system. Diemuodeke et al., (2019) presented the optimal design of Hybrid Energy System (HES) consisting of PV modules, wind turbine, energy storage and diesel generator using HOMER software and TOPSIS multi-criteria decision-making algorithm for the electrification of six different location in Nigeria. Feasibility assessment of the locations were carried out to determine the amount of solar and wind resources, as well as the load demand for the selected location. Each of the components were optimally chosen by HOMER software considering the reduction in Cost of Energy (COE) and minimization of carbon emission.

A novel approach for the assessment of the generation reliability of a hybrid mini-grid system for a typical Nigerian community in Kwara State, based on the optimal solution obtained using HOMER software was presented by Esan et al., (2019). The proposed hybrid mini-grid system comprises of solar PV, diesel

generator and battery storage system. Each components of the hybrid mini-grid system was modeled using HOMER software, while the Capacity Outage Probability Table (COPT) was used in validating the reliability of the simulation results obtained. The results showed that there is a significant increase in the reliability and feasibility of the proposed hybrid mini-grid system based on the proposed approach.

Hlal *et al.*, (2019) presented a methodology to size Standalone Hybrid Renewable Energy System (SHRES) which combines solar PV, wind turbines (WT) and Battery Energy Storage (BES) for application in rural areas in Malaysia using (NSGA-II). NSGAII was employed to plot the Pareto front to present the trade-off between the reliability and cost. The optimization was conducted to facilitate the selection of the best configuration across numbers of PV modules, wind turbines and batteries to minimize LPSP and COE. Furthermore, charging/discharging of BES on an hourly basis was investigated to mitigate the intermittency of solar PV/WT output for minimizing energy losses. The results show that the NSGAII optimization of the model is able to determine the best techno-economic sizing for the suggested location.

The optimization of the power generated by a hybrid renewable energy system which consists of Wind turbine, Tidal turbine, PV module and battery using particle swarm optimization was proposed by Mohammed, Amirat and Benbouzid, (2019). The system was designed to satisfy the load demand of a stand-alone area in Brittany. The problem was defined as an economic problem taking into consideration the optimal sizing of the system, high reliability, planning expansion for future development and state of charge of the battery. The total net present cost was introduced as the objective function to represent the minimum fitness value in the particle swarm process. The optimization was carried out using MATLAB software tool. Simulation results showed that the proposed method achieve optimal solution and a reduction in the overall cost with high speed and accuracy.

A framework for the optimal design of a hybrid photovoltaic wind-battery system based on the minimization of total net present cost and loss of load probability for the city of Ahvaz, Iran using Grey wolf optimizer is presented by Naderipour et al., (2019). The number of PV panels, wind turbines and batteries are considered the decision variables in the optimization problem which was formulated to minimize the TNPC and LLOP. The resulting optimization problem was optimized using Grey Wolf Optimizer technique; the performance of the proposed algorithm was demonstrated by comparing its results with that of PSO technique used for the same purpose. Simulation results showed that the proposed algorithm is superior to PSO technique in terms of the optimal solution produced.

A novel methodology based on Satin Bower Bird Optimization (SBBO) to obtain the optimal sizing and power management of hybrid photovoltaic/wind/battery power system was presented by Ranjith Kumar and Surya Kalavathi, (2019). Long term information of the solar irradiation, wind speed and load profile

of the selected site were obtained and used for system modeling. The optimization problem was formulated to minimize system cost and maximize energy availability. The HPS was simulated using MATLAB. Simulation results showed that the proposed approach gives better performance under all operating conditions and power management strategy was also achieved.

Zaki Diab et al., (2019) proposed a simulation model for the operation of a PV/wind/diesel hybrid micro-grid system with battery bank storage for the electrification of Abu-Monqar village located in western desert using Whale Optimization Algorithm (WOA), Water Cycle Algorithm (WCA), Moth-Flame Optimizer (MFO), and Hybrid Particle Swarm-Gravitational Search Algorithm (PSOGSA). The main goal of the study is to meet the load demand of the proposed location with the minimum cost of energy and ensure high reliability of the power supply. The optimal sizing of the system components was carried out using real-time meteorological data of the location. An optimization problem was developed to minimize the cost of energy and increase the reliability and efficiency of the system using loss of power supply probability. The optimization algorithms were applied to obtain the optimal system configuration and determine the capability of each optimization algorithm based on the solution obtained using statistical analysis. Simulation results showed that based on statistical analysis, the WOA produces the most promising performance as compared to other optimization algorithms.

Fioriti et al., (2020) presented an approach for optimal design of hybrid system using a two-stage procedure to minimize the computation requirements of the system. An optimization model was initially developed using a priority-list strategy; and the results of the optimization model are used to refine the second-stage optimization model based on rolling horizon strategy. Simulation results showed that the proposed approach was able to reduce the computational time of system design, as well as negligible reduction in the optimal results as compared to standard iterative approaches.

Ali & Jang, (2020) presented the optimum design of a small hybrid renewable energy system comprising basically of solar and wind generator as primary energy sources for the electrification of a remote island in South Korea using HOMER pro software. Feasibility assessment of the island was done to determine the potential of solar and wind resources, while the hybrid system was modeled using real electricity consumption for a year. The optimum configuration of the proposed hybrid renewable energy system was achieved by modeling two different types of energy storage systems: battery and pumped hydro storage. The levelized cost of energy and net present cost for each configuration were determined to evaluate the most suitable configuration for the electrification of the Island. The results showed that the configuration with the pumped hydro storage system is more feasible compared to that of the battery storage system.

Optimal component sizing of an isolated PV-wind-battery micro-grid for a remote location in India using probabilistic approach and Genetic algorithm is presented by Das, (2020). The deterministic approach was used to determine the values of various energy sources with variation in the load demand based on different time scales. A multi-objective optimization problem based on the minimization of life cycle cost and environmental pollution, and increasing system reliability was formulated and solved using GA technique. Simulation results showed that the proposed approach can be used for the optimal selection of hybrid system components with available time scaled energy sources and load data. Nonetheless, the method was computationally cumbersome and time consuming.

The optimal sizing of a hybrid system consisting of solar PV, wind turbine, battery and fuel cell to meet the energy demand of a location in Kenya based on Monte-Carlo approach is investigated by Fioriti et al., (2020). The hourly uncertainties of the load demand and renewable sources are modeled based on the Monte-Carlo technique. An optimization problem based on the minimization of the net present cost of the system was formulated and optimized using the proposed method. Sensitivity analysis was carried out on the system design to evaluate its performance with variations in components costs. Simulation results showed that an increase in the number of scenarios of the stochastic approach improves the accuracy of the optimal solution. However, the approach was found to be time consuming.

Optimum configuration of hybrid PV/DIESEL/WIND power generation system to supply the energy demand of a research hospital in Kenya using HOMER software was determined by Dursun, Dursun and Aykut, (2020). Numerous HRESs in different configurations of wind turbine, PV panel, diesel generator and battery bank were considered. Moreover, a sensitivity analysis was also performed taking into considerations variations in three important parameters, namely wind speed, diesel price and also solar irradiation. Simulation was carried out using HOMER software and the optimum design was compared with other combination of HRESs. The result clearly showed that the Wind/Diesel/Battery HRES is eco-friendlier than other HRESs combination.

The optimal sizing of hybrid renewable energy system using a Discrete Multi-objective Grey Wolf Optimizer (DMGWO) for rural telecoms towers is presented by Kaur et al., (2020). The components (solar PV, wind turbine, diesel generator and battery system) of the hybrid system are modeled in Simulink; the uncertainty in the renewable sources and the load of the telecom tower is modeled using probability distribution function. A multi-objective optimization problem based on cost of energy, excess energy generation and loss of power supply probability is developed and solved using the proposed algorithm. The Euclidean distance approach was adopted to obtain the optimal solution from the optimal parent front solution obtained using the DMGWO algorithm. Simulation results showed that the developed algorithm

predicted the optimal configuration with corresponding reduction in the cost of energy and excess energy generation.

The optimal design of a hybrid micro-grid consisting of solar PV, wind turbine, diesel generator and battery system using multi-objective particle swarm optimization (MOPSO) for a case study in Rabat and Baghdad in Morocco is presented by Kharrich et al., (2020). An objective function which focuses on the minimization of the Net Present Cost of the system is formulated and solved using the proposed algorithm, taking into consideration system constraints such as loss of power supply probability and energy balance. The results proved that the optimal system configuration is the most feasible economically for the electrification of the selected locations.

Mahdi et al., (2020) developed a sizing optimization model of a stand-alone hybrid photovoltaic/wind turbine/battery system using Ant lion optimizer for the electrification of a remote location comprising of 10 different buildings in Kerman, Iran. The Feasibility study of the proposed location was carried out to determine the potential of the considered RE resources. Thereafter, the mathematical modeling of the various energy generating components was performed in Simulink. An optimization model with an objective to minimize the total investment cost of the system was developed and optimized using the proposed algorithm. The results obtained were compared with those obtained using particle swarm optimization, harmony search, firefly algorithm and differential evolution algorithm for the same purpose to test the effectiveness of the proposed algorithm.

Oladigbolu et al., (2020) examined the potential application of hybrid an optimal configuration of solar PV/hydro/diesel/battery system using HOMER software tool for the electrification of a remote community in Nigeria. The potential of the RE resources in the proposed area was assessed and noted. Four different configuration of the hybrid system were considered with the objectives of minimizing the NPC, COE and carbon emission. The various configurations were simulated and analyzed using HOMER software, simulation results showed that there was a significant reduction in carbon emission with the optimal system configuration.

Sultan et al., (2020) solved the optimization problem of optimal configuration of a hybrid system consisting solar PV, wind turbine and hydroelectric pumped storage system using a recent Metaphor-less Rao Optimization algorithm. Feasibility assessment of the proposed location was conducted to determine the real-time meteorological data of the area. An optimization problem based on the minimization of the cost of energy is formulated and solved using the proposed algorithm. Moreover, statistical analysis was used to validate the accuracy of the proposed technique. Simulation results showed that the proposed algorithm is generate competitive solutions with respect to other recent optimization techniques.

A study on the optimization of cost and carbon emission function of a hybrid energy system comprising of solar PV, wind turbine, battery storage and diesel generator for Aguni Island in Japan using a multi-objective e-constraint and mixed integer linear programming methods is proposed by Akter et al., (2021). The mathematical modeling of the individual components was done in MATLAB, while a multi-objective optimization model to minimize the cost of energy and carbon emission was developed and optimized using the e-constraint and mixed linear programming techniques. The optimal solution from the set of solutions obtained using these techniques was obtained using fuzzy satisfying method. Simulation results showed the applicability of the proposed approach for optimal design of hybrid renewable energy system.

The optimum sizing of a standalone micro-grid system consisting of photovoltaic modules, wind turbines diesel generator and battery banks using Particle Swarm Optimization and Genetic Algorithm for the electrification of a small village in eastern Ethiopia is presented by Ashagire et al., (2021). The weather data of the area was obtained from the necessary authorities to analyze the potential of RE sources. An optimization problem with the aim of minimizing the levelized cost of energy was formulated, GA and PSO was used to solve the problem in several runs taking into consideration the optimization constraints. Simulation results showed that the PSO technique outperform the GA technique in terms of LCOE and RE penetration.

Elbaz & Tahir Guneser, (2021) introduced an optimization technique, named Bat algorithm for the optimal design of a stand-alone hybrid photovoltaic diesel-battery system for the electrification of a small village in southern Libya. The algorithm was used to minimize the annual cost of system subject to controlled electricity restriction and optimal numbers of system components. To demonstrate the effectiveness of the proposed technique, grey wolf search algorithm and particle swarm optimization were used for the same purpose and the results compared. Simulations were carried out using MATLAB software. The results indicated that the proposed method was able to determine the optimal size of the system at the lowest cost as compared to Grey Wolf optimizer and Particle Swarm Optimization algorithm.

Hu et al., (2021) investigated the optimal design of a hybrid renewable energy system with equipment type consideration using a two-step optimization approach. Minimization of the total annual cost of the system is formulated as a single objective optimization problem, the resulting optimization problem is solved using the proposed two step approach. A group of pareto sets were generated after the optimization process and the optimal solution was selected based on the least score of the objective function. Simulation results proved that the proposed method is able to give an optimal system configuration at the least annual cost.

The design and optimization of an off-grid hybrid micro-grid system for the electrification of Barishal and Chattogram divisions in Bangladesh based on different load dispatch strategies is presented by Ishraque et

al., (2021). The hybrid microgrid s consists of wind turbine, storage unit, diesel generator and the load profile of the locations. Each of the components was modeled using HOMER with the aim of minimizing the net present cost, levelized cost of energy, operating cost and carbon emission rate, considering five different dispatch strategies. The power system performance and feasibility of the micro-grid was done using MATLAB software. Simulation results showed that the Load following dispatch strategy gives the best results for the proposed micro-grid.

Kharrich *et al.*, (2021a) proposed the optimal design of hybrid microgrid to feed the electricity demand of an isolated area in Dakhla, Morroco using Equilibrium Optimizer (EO).The hybrid microgrid system consists of photovoltaic (PV), wind turbine (WT), battery and diesel generator taking into considerations several constraints such as the reliability, availability and renewable energy fraction. The impact of wind speed, solar radiation, interest rate, and cost of diesel fuel on the NPC as well as LCOE were analyzed. Similarly, the influence of size variation on LPSP was also analyzed. Simulations were carried out using MATLAB. The optimization results obtained were compared with those obtained by other recent meta-heuristics optimization algorithms such as Harris Hawks Optimizer (HHO), Artificial Electric Field Algorithm (AEFA), Grey Wolf Optimizer (GWO) and Sooty Tern Optimization Algorithm (STOA). The results showed that the EO provided a reduction in the NPC, LCOE, and LPSP; and has fast convergence characteristics when compared with the other optimization algorithms.

The optimal design of hybrid micro-grid using Giza Pyramid Construction optimization algorithm for the electrification of Yanbu region in Saudi Arabia was presented by Kharrich et al., (2021b). The microgrid consists of PV modules, wind turbine and biomass. Different technology used in generating the energy were modeled in Simulink, an optimization model to minimize NPC and LCOE of the system was developed and optimized using the GPC algorithm. The effectiveness of the GPC algorithm was demonstrated by comparing the results obtained with those obtained using artificial electric field and grey wolf optimizer techniques.

Nguyen and Boström, (2021) Presented an optimal design of hybrid wind turbine/PV/battery energy system for a household application in the arctic region of Tromso, Norway using multi-objective optimization approach namely, Particle Swarm Optimization (PSO). Input data for the optimal component sizing of the Hybrid Renewable Energy System (HRES) were measured across the arctic region. Mathematical modeling of the individual components of the HRES as well as the load model was carried out in Simulink. The multi-objective PSO program was written and run using MATLAB software. Optimization results showed that the feasibility of the HRES for a single family housed demand in the region at a reasonable cost.

An approach on the optimal design of Hybrid Renewable Energy System (HRES) for a village in Shinyanga region of Tanzania, using an iterative technique was proposed by Marcel et al., (2021). The HRES consists of solar PV, wind turbine and Battery Energy Storage (BES). The project lifetime was fixed for 25 years and the technique was used to determine the ACS and LCOE of the system that will meet the energy demand of the village and charge the BES system for a whole year. The autonomy days of BES was set at 3 days, while the maximum depth of discharge was set at 50 %. Simulation was results showed that LCOE obtained for the optimized system is cheaper compared to the grid-connected power supply in Tanzania.

An approach to optimize a hybrid micro-grid consisting of PV generator, wind turbine, Diesel generator and battery bank using Particle Swarm Optimization was presented by Priya et al., (2021). The hourly data of solar irradiation, ambient temperature, wind speed as well as the power generated using each of the energy generating sources for one year were modeled in Simulink. An optimization model to minimize the total investment and installation cost under the constraint of LPSP. Simulation was carried out using MATLAB to determine the robustness of the developed model and to obtain the optimal system configuration.

Rashid et al., (2021) developed a hybrid energy system consisting of biomass energy, solar PV, wind turbine, with battery and diesel generator as backups for the electrification of a remote village named Kukri Mukri Island in Bangladesh using Genetic Algorithm and HOMER software. Components modeling was carried out using MATLAB while the optimal sizing and analysis of techno-economic aspects for different system configurations was simulated using HOMER pro software. An optimization model for components sizing was developed with the aim of minimizing the Net Present Cost and Levelized Cost of Energy. The model was simulated and optimized using Genetic Algorithm. Simulation results of the HOMER pro software were compared with those obtained using GA. The results showed that the optimal system configuration consisting of all the five components considered gives the best LCOE. The results also showed that the optimal solution obtained using GA gives a better solution in terms of sustainability and cost effectiveness as compared to those obtained using HOMER software.

A hybrid Harris Hawks Optimizer-Arithmetic Optimization Algorithm (HHO-AOA) for sizing and design of an autonomous micro-grid was proposed by Cetinbas et al., (2022). The proposed approach was aimed at improving the solution diversity obtained using individual algorithm. The approach was implemented on a hybrid system consisting of photovoltaic system, wind turbine system, battery energy storage, diesel generators and a commercial type load with loss of power supply probability and cost of energy as the main objectives. Statistical analysis based on Friedman ranking test and Wilcoxon signed-rank test were performed to illustrate the performance of the proposed hybrid method. All simulation was done using

MATLAB. The results showed that the proposed HHO-AOA generate the most feasible solution when compared to using each of the algorithm individually.

The feasibility of a wind-solar hybrid system for on and off grid application using HOMER software was investigated by Coban et al., (2022). The hybrid system was designed to supply the load demand of a remote location in Somalia. The various components of the system was modeled, optimized and simulated in HOMER software using solar and wind resources of the area. The techno-economic performance of the system was investigated based on the performance of the system in meeting a sampled load demand of the location. Simulation results showed that on-grid solar and wind hybrid system is the most economically feasible of all the system configurations considered.

El Boujdaini et al., (2022) designed a hybrid renewable energy system for remote homes located in Morocco, Spain and Algeria using Particle Swarm Optimization algorithm for a period of 20 years. The hybrid system consists majorly of solar PV, wind turbine, battery and diesel generator. The feasibility assessment of the studied areas was carried out to determine their weather data and load profiles; all system components were modeled in Simulink. The proposed algorithm was used to obtain a system configuration with minimum cost of energy and excess energy, increase renewable fraction and reliability. Optimization was done under varying and fixed load demand and all simulations was carried out using MATLAB. Simulation results showed that the optimal system configuration consisting the four components of the system produce the least cost of energy. The results also showed that the there was a significant increase in the cost of energy under varying load condition as compared to the fixed load demand.

The optimal design of HRES using Particle Swarm Optimization (PSO), hybrid Particle Swarm Optimization-Grey Wolf Optimization (PSOGWO), hybrid Grey-Wolf Optimization-Cuckoo Search (GWOCS) and Sine-Cosine Algorithm (SCA) for the electrification of a multimedia center in Makenene, Cameroon was presented by Hermann et al., (2022). Mathematical modeling of the various components of the HRES were carried out using SIMULINK; an optimization model was developed with the aim of minimizing the Cost of Energy, NPC, and Total Greenhouse gasses emission. Seven different configurations of the HPS were considered and simulated using MATLAB. The results showed that the GWOCS optimized HRES gives the best value of NPC, COE and TGE.

The optimal sizing and simulation of a standalone hybrid energy system consisting of solar PV, wind turbine, gas engine and battery system for a coastal area in Delta State Nigeria was proposed by Kenu et al., (2022). The system components was modeled and simulated based on a funding model using HOMER software. The main objective of the proposed model is to lower the cost of electricity and ensure efficient

usage of the system. Simulation results showed that the system configuration with lowest cost consist of solar PV, wind, gas engine the battery system with respect to other configurations reported in the study.

Mahmoud et al., (2022) investigated the application of Salp Swarm Algorithm (SSA), Grey Wolf Optimizer (GWO), and Improved Grey Wolf Optimizer (IGWO) for the optimal configuration of hybrid power system consisting of PV panels, wind turbines, battery storage system and diesel generators (DGs) as backup. A complete model for the management of the hybrid system was firstly developed in Simulink, subsequently, an optimization model with the objective to reduce the cost of energy and loss of power supply probability was developed using MATLAB. The optimization techniques were applied to obtain the optimal system configuration and to compare their performance stability. Simulation results showed that each of the optimization techniques minimize the cost of energy and loss of power supply probability, with the IGWO technique proving to be the most effective technique among them.

Mohammad-Alikhani et al., (2022) proposed a two-stage multi-objective particle swarm optimization algorithm for the optimal configuration of a hybrid power system comprising of PV arrays, wind turbines, tidal generator, battery banks, flywheels, fuel cells and electrolyzers. A multi-objective problem based on the minimization of levelized cost of electricity and carbon emission was formulated, the problem was solved using a two stage swarm approach. Initially, a first set of swarm was applied to determine which of the system components needs to be optimized, while the second set of swarm was used to optimize the selected components using real annual data in hourly time intervals of the load. Simulation results showed that the proposed approach reduces the susceptibility of the solution to multiple runs with respect to conventional techniques and gives a better optimized power system design.

An investigation on optimization of hybrid renewable energy system for the electrification of a covid-19 based vaccine facility in remote areas of south Africa using HOMER pro software was conducted by Leholo et al., (2022). The hybrid system comprises of PV panels, wind turbine and battery storage as back up. Each of these components is modeled, optimized and simulated using HOMER software and the results of simulation in terms of optimal cost and reduction in greenhouse gas emission are compared with that of using a diesel generator set to meet the demand of the proposed location. A sensitivity analysis was also conducted to determine the effect of varying wind turbine hub height on the overall performance of the hybrid system. The results showed that the proposed hybrid system outperform the diesel generator set. The results also showed that with an increase in the hub height of the wind turbine, a significant reduction in the overall cost of the system was observed.

2.9 Research gap

A critical look at the reviewed literatures on the optimal design of HPS so far showed that most of the work done has been designed to simulate and/or optimize the conventional monofacial PV and wind energy RE sources so as to obtain the best design for a particular location. A bifacial PV module is proposed in this design; the additional energy yield produced from the rear side of the module is expected to benefit the system economically. In addition to that, most reviewed literatures only focus on the use a single large sized generator set as back up to the HPS configuration and there is high probability that the reliability of the system design will be reduced as a result, which could result in corresponding increase in the amount of carbon emission into the atmosphere. Finally, it was also find that the optimal design of HPS comprising of large number of components is a complex task that requires an optimization algorithm capable of handling a large number of control variables present in this type of optimization problem.

Therefore, the main focus of this study is to develop an optimization model capable of finding the optimal design of hybrid HPS consisting of solar bifacial PV, wind energy, split generator set and battery energy storage system at the least life cycle cost, minimum carbon emission and guaranteed reliability. A novel meta-heuristic optimization algorithm, Giza pyramids construction (GPC) was employed to obtain the optimal design of the proposed HPS. The results obtained using the GPC technique were compared with those obtained using FA and WOA techniques to verify the suitability and effectiveness of the algorithm in solving high-dimensional, combinatorial optimization problem. The choice of the GPC optimization algorithm is mainly due to its ability to handle large number of control variables which is a peculiar feature of most HPS designs found in literatures, and fast convergence speed. In order to guarantee that the optimal HPS design is feasible for implementation, the individual components of the HPS were modeled using the database of commercially available.

CHAPTER THREE
SYSTEM MODELING

3.1 Mathematical model of system components

This chapter presents the various mathematical notation used in modeling each of the components of the proposed HPS. The main components of the proposed HPS modeled in this study are bifacial PV module, wind turbine, split diesel generator, battery and the power converter as shown in Figure 3.1. Hence, accurate model of each of the sub-system of the proposed Hybrid Power System (HPS) must be generated in Simulink using their respective mathematical notations (Jha et al., 2018). This section describes the various mathematical models of the energy generating components of the HPS that have been used in literatures to analyze HPS consisting of renewable and non-renewable energy sources.

3.1.1 Mathematical model of solar bifacial PV component

Bifacial PV systems have been reported in many studies to have great potential for energy generation. A bifacial gain of up to 46% has been reported in some studies involving experimental and simulation solutions. This gain is attributed to the ability of the PV module to receive solar energy using both its front and back surfaces (Fajuke & Raji, 2022; Pelaez, Deline, Greenberg, et al., 2019; Pike et al., 2021). However, the modeling of such system is more challenging and requires considering parameters that are not applicable to conventional mono-facial PV systems. Therefore, methods used for mono-facial PV modeling are no longer valid and more precise models have been developed to estimate the extra energy yield of the bifacial modules (Hansen et al., 2017).

In order to properly estimate the total energy output of the bifacial PV system, four important procedures are considered. The first step is to model the irradiance hitting the both sides of the module; and thereafter, modeling the electrical output of the bifacial cell, which is usually done by either implementing the one-diode or two-diode method. The temperature effect of the module is modeled in the third step and finally, the total energy yield of the bifacial module can be estimated (Janssen et al., 2015). A detailed description of each of the steps are subsequently presented.

3.1.1.1 Irradiance model

The first and most difficult step in modeling the energy output of a bifacial PV module is to model the irradiance reaching the front and the back side of the module. Accurate modeling of the front and the back side irradiances will determine the power output of the bifacial PV system. In addition to that, other factors that influence the power output of the bifacial PV system include orientation, mounting height, albedo, tilt angle and temperature (J. A. Louw & Rix, 2019; Onno et al., 2020; Pelaez, Deline, Greenberg, et al., 2019).

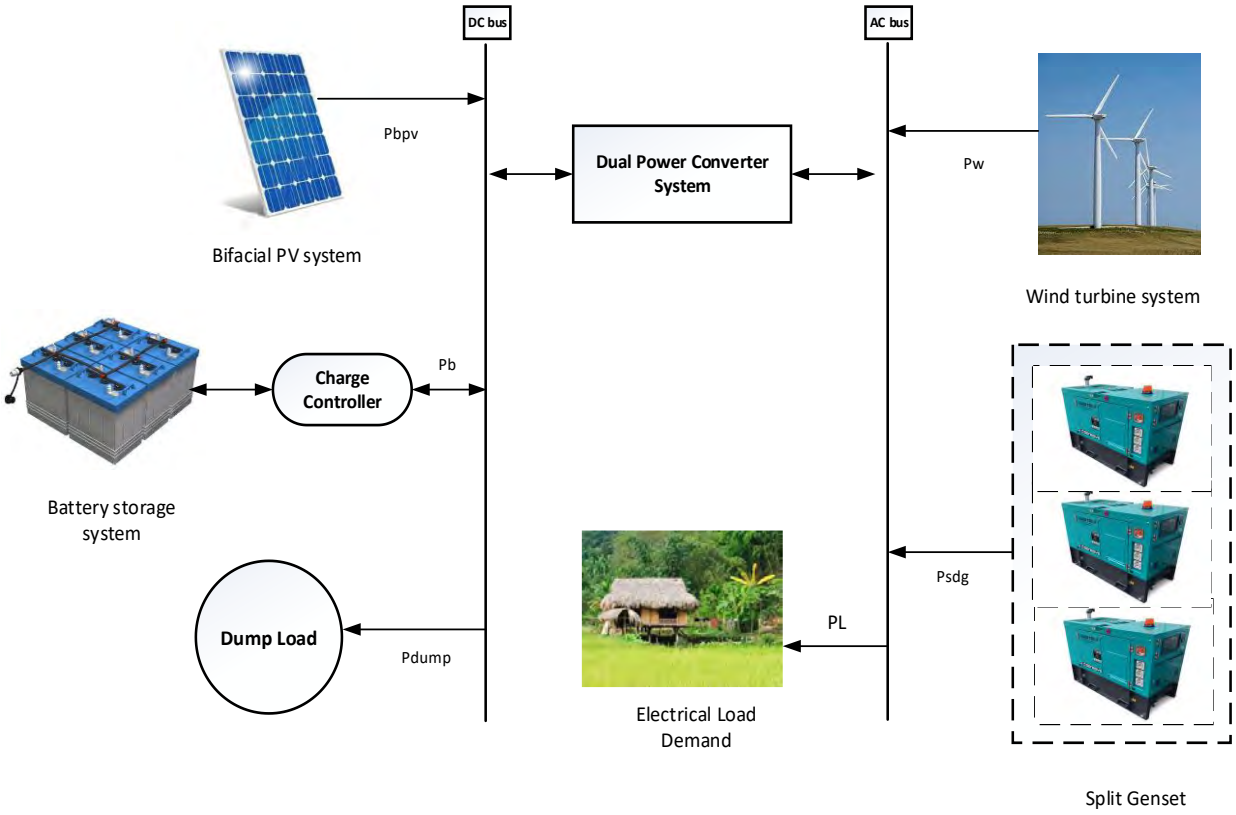

Figure 3.1: Configuration of the proposed hybrid power system

However, for the purpose of this study, the vertical east-west orientation of the PV bifacial module was considered for simulation purposes. It has been reported in various studies that this type of orientation is capable of producing more energy output as compared to the horizontal north-south orientation, and also eliminates the need for complex geometric consideration when developing Simulink models (Baumann et al., 2018; Fajuke & Raji, 2022; Pike et al., 2021).

Generally, the irradiance reaching the front side of the module as described by Jäger et al., (2020) is modeled using equation (3.1).

$$G_f = G_{dir} + G_{diff} + G_{alb} \tag{3.1}$$

where G_{dir}, G_{diff} and G_{alb} are the direct, diffuse and ground albedo irradiances respectively.

For mono-facial modules, the diffuse and albedo irradiance are considered negligible, however, they are the main components that contributes to the energy output of a bifacial module due to the presence of the back side irradiance (Pike et al., 2021). Modeling the back side of a bifacial PV module can be quite challenging and various approaches have been used in literatures to accurately predict the amount of irradiance reaching the back side of the module. The three most common approach that have are well documented in literatures include empirical method, view factor model and the ray tracing model (Carvalho Ganilha, 2017; Hansen et al., 2017; J. A. Louw & Rix, 2019). Table 3.1 presents the comparison of the three most common approach available, while a brief description of each of these models are presented as follow.

I. Empirical method

Empirical methods are simply described as mathematical models that were developed based on the results observed from various experiments. These methods are also known as black box equation, and are used to describe the observations obtained from an experimental setup (Johnson et al., 2012; J. P. Singh et al., 2014). The main problem associated with empirical models is their overdependence on experimental setups, which could results in displacement of important variables at the model development stage and subsequently lead to low accuracy. Nevertheless, this model also has several advantages which include simplification in mathematical expressions, clarity in the behavior of the system under experimentation and ease of implementation for computational simulation. Prism solar, solar world and Bsolar are some of the companies that have developed empirical models to estimate the rear side irradiance of bifacial PV modules (Bsolar, 2020).

Table 3.1: Comparison of approaches used in modeling back side irradiance of bifacial PV

Models	Merits	Demerits
Empirical	Simple mathematical expression Provide a general about module behavior Easy to implement in computational simulation	Experimental dependent, and does not fit all different possibilities Inadequate information on the working principle of the system Could miss important parameters in the formulation of the module
View Factor	Easy to implement in simulation Brings comprehension on the reflected irradiance. Suitable for single configurations	Does not take into consideration the scattering or diffuse effect The geometry becomes complex when there are more complex configuration The model has to be estimated for each cell
Ray Tracing	More realistic estimation Better solution for self-shadow effects Suitable for complex figurations	It is very demanding computationally It is considered too complex for a single module It is also difficult to implement for simulation purposes

Source: (Hansen et al., 2017; Johnson et al., 2012)

I. Ray tracing technique

Ray tracing is a model that uses a 3-D modeling software to calculate the irradiance on a given plane such as the bifacial PV module. It accounts for both reflected and refracted radiations using electromagnetic waves or rays, which are transmitted in such a way that the light is followed from the source toward the subject; this method of transmitting waves or rays is commonly referred to as the forward ray tracing. On the other hand, when the transmitted waves are such that the light is from the subject to the source, it is referred to as the backward or reverse ray tracing (Hansen et al., 2017; J. A. Louw & Rix, 2019; Pelaez, Deline, Greenberg, et al., 2019). The Monte Carlo approach, which employs hundreds to thousands of rays to calculate the irradiance of the geometrical measurements for all weather conditions and mounting orientation is often employed in the model design (Hansen et al., 2016).

Ray tracing approach has been found to be very effective when modeling the irradiance of a bifacial PV module due to its ability to consider many other factors such as mounting height, distance separating two modules, characteristics of the module glass and other optical effects that determine the amount of irradiance hitting the back side of the module (J. Louw & Rix, 2020). Unlike the other modeling approaches, the ray tracing technique is capable of accurately modeling the shading patterns on the ground and accounts for direct and diffuse shading on both front and backside of the module (Hansen et al., 2016). The main drawback of this technique is the complexity in mathematical computation, the difficulty in implementation and the large amount of time it takes to run an annual simulation as compared to the other models. (Carvalho Ganilha, 2017).

II. View factor model

The second type of approach used in modeling the rear side irradiance of a bifacial module, which has been applied in many literatures is known as the view factor or the configuration factor model (Ademola & Qiu, 2020; M. Alam et al., 2021; Hansen et al., 2016). It calculates the amount of radiation scattered or reflected from both surfaces using geometrical notations. Basically, it is based on radiation transfer calculations of the amount of radiation leaving a surface (A) that strikes on the receiving surface (B). The main inputs required to determine the back side irradiance hitting the surface of the plane are the meteorological data, location details of the plane, β, module tilt angle, θ_i, angle of incidence, and solar zenith angle θ_s (M. Alam et al., 2021).

The irradiance reaching the opposite side of the module, G_b is the sum of irradiances from beam and circumsolar diffuse, isotropic diffuse, ground reflected illumination from isotropic diffuse and ground reflected from beam and circumsolar diffuse as given in equation (3.2) to (3.6) (Janssen et al., 2015).

$$G_1 = \left(G_{beam} + G_{diff} A_i\right) R_{b,back} \tag{3.2}$$

$$G_2 = G_{diff}\left(1 - A_i\right)\left(\frac{1+\cos\left(\beta - 180\right)}{2}\right) \tag{3.3}$$

$$G_3 = G_{diff}\left(1 - A_i\right)\gamma_c\left(\frac{1-\cos\left(\beta - 180\right)}{2}\right) \tag{3.4}$$

$$G_4 = \left(G_{alb} + G_{diff} A_i\right)\gamma_c\left(\frac{1-\cos\left(\beta - 180\right)}{2} - F_{v,back}\right) \tag{3.5}$$

$$G_b = G_1 + G_2 + G_3 + G_4 \tag{3.6}$$

where G_{beam} is the reflected (beam) irradiance due to the beam and is given as $DNI\cos\theta_s$; DNI is the direct nominal irradiance from the sun, G_{diff} is the diffuse irradiance and it is given as $G - G_{alb}$; where G_{dir} is the global solar radiation directly to the earth, γ_c is the albedo coefficient of the mounting surface, A_i is the anisotropy index which describes how much of the atmospheric radiation is due to the reflected (beam) radiation on a horizontal surface, R_b is the geometric factor which is given as the beam radiation from a tilted surface to beam radiation to the horizontal surface and F_v is the view factor due to shading effect.

The values of A_i and R_b are assumed to be negligible for this study since the vertical east-west orientation is considered for simulation purpose. However, when considering horizontal north-south orientations, they are to be taken into consideration. In order to account for the shading effect which is produced as a result of the position of the sun, the view factor, F_v must be determined. Considering two surfaces X and Y, the view factor as described by M. Alam et al., (2021 and Hansen et al., (2016) is estimated using the fraction of the radiation received by surface Y, representing the module emitted from surface X (reflected surface) and it is given in equation (3.7)

$$F_{v(X\to Y)} = \frac{1}{Y}\int Y \int X \frac{\cos\theta_1 \cos\theta_2}{\pi s^2} dA dB \tag{3.7}$$

where A is the area of the shadow portion due to the panel on the mounting surface, B is the area of the back side of the module, θ_1 is the incident angle due to the shadow portion on the surface measured to the sky, θ_2 is the incident angle of the module measured to the ground and S is the distance between the center of the module to the center of the shadow area.

The approach is developed at the Institute of Semiconductor Electronics RWTH and ISC Konstanz, and it is the most commonly used approach in many literatures as it estimates the rear side irradiance using the basic principle of heat transfer and takes the effect of shading into consideration (Janssen et al., 2015). Other popular view factor models available are PVSyst, NREL Bifacial VF and the models developed at both Purdue University and University of Geneva. The models developed in Purdue University and University of Geneva also use similar approach to estimate the rear side irradiance of bifacial modules. However, PVSyst applies the basic principle of mono-facial module in calculating the power output of the front side of the module; and then adds the energy generated from the rear side to determine the total power output of the bifacial PV module (PVSyst, 2017).

The view factor model has been applied in many literatures due to its ease of implementation in computational simulation, ability to give a detail description of the reflected radiation and its suitability for individual configurations when implementing a large scale PV power system. However, when considering a large bifacial PV system in horizontal south-north orientation, the geometrical calculations can be quite challenging. In addition to that, the model fails to give a clear description of the effects of diffused radiation (Carvalho Ganilha, 2017; Hansen et al., 2016).

3.1.1.2 Electrical model

Once the front and back side irradiances have been calculated, it is possible to model the electro-thermal model to determine the power output of the bifacial PV module. The sum of these irradiances was used to estimate the power output of the bifacial PV sub-system of the HPS proposed in this study. Once the total irradiance hitting the module has been estimated, the bifacial PV cell can be modelled using the conventional single-diode modeling applied in modeling traditional mono-facial PV cells (Ademola & Qiu, 2020; Carvalho Ganilha, 2017). This is attributed to the fact that the behavior of a solar cell is similar to that of an ideal diode which is connected to a series and shunt resistance. However, for locations with low solar radiation, the double-diode model described in the work of Janssen et al., (2015) can be employed. The equivalent circuit of a solar cell is as shown in Figure 3.2a.

The expression that describes the relationship between the voltage (V) and the current (I) of an ideal diode is obtained from Kirchhoff's current law and is given in equation (3.8) cells (Ademola & Qiu, 2020; Carvalho Ganilha, 2017).

$$I[A] = I_{ph} - I_0\left[\exp\left(\frac{(V + IR_s)}{i_f V_T}\right) - 1\right] - \frac{V + IR_s}{R_{sh}} \qquad 3.8$$

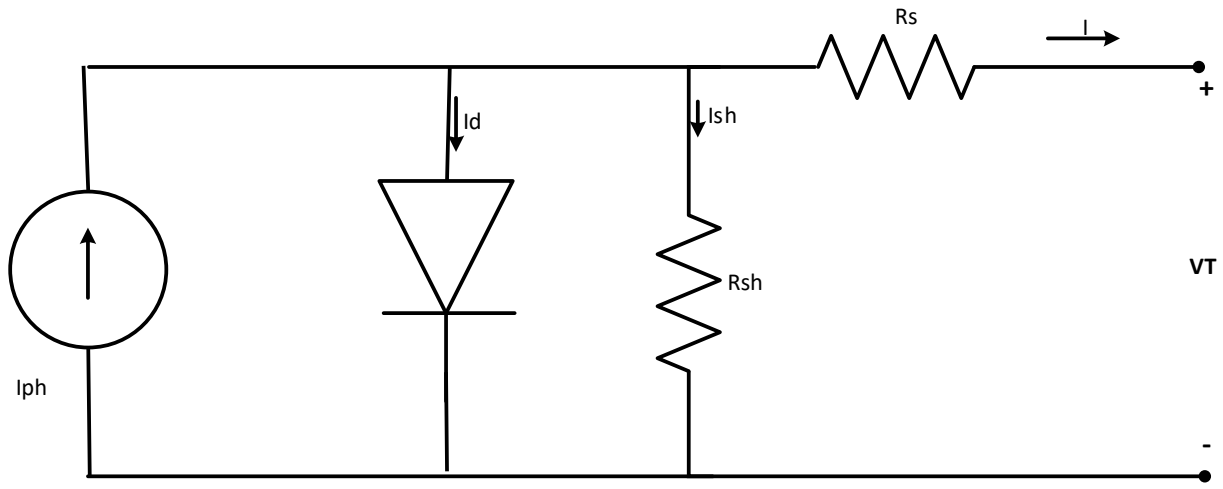

Figure 3.2a: Equivalent circuit of a solar cell

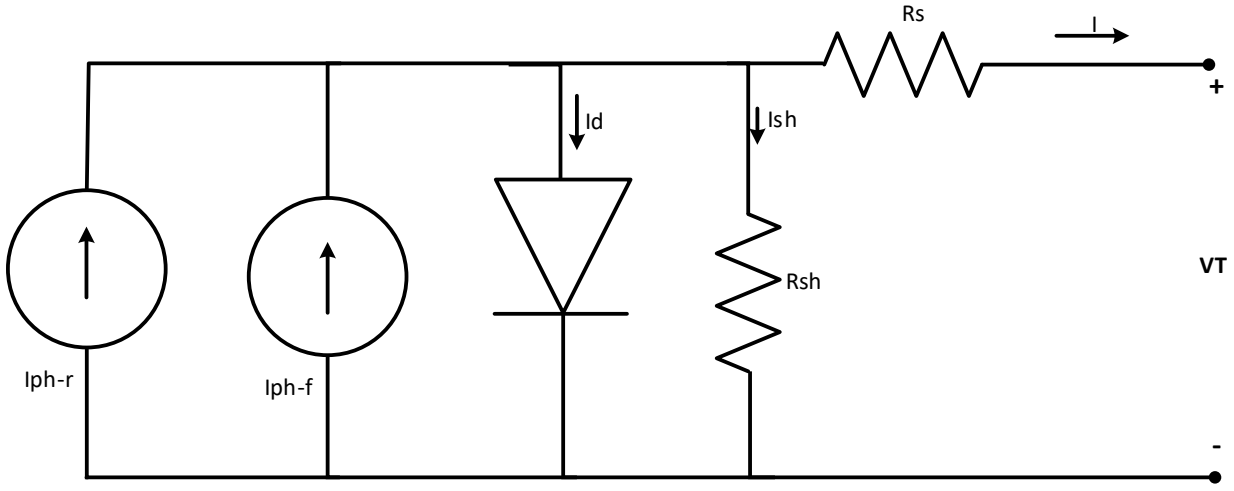

Figure 3.2b: Equivalent circuit representation of bifacial solar cell

Where I_{ph} is the current generated due to the irradiance, I_0 is the diode reverse saturation current, V_T is the thermal voltage which is a function of temperature, i_f is the ideality factor, R_s and R_{sh} are the series and shunt resistances of the diode respectively.

In order to properly understand the electrical characteristics of a bifacial cell, it is usually represented as two mono-facial cells which are connected in parallel as depicted in Figure 3.2b. Applying the same principle of KCL to the equivalent circuit of Figure 3.1b, the I-V characteristics of a bifacial at cell level is given by equation (3.9) (Ademola & Qiu, 2020; Carvalho Ganilha, 2017).

$$I_t[A] = \left(I_{ph-f} + I_{ph-b}\right) - I_0\left[\exp\left(\frac{\left(V + IR_s\right)}{i_f V_T}\right) - 1\right] - \frac{V + IR_s}{R_{sh}} \tag{3.9}$$

It is a known fact that the photon generated current of the two diodes connected in parallel to each other are dependent on the irradiance from the front and back sides of the module, and hence can be estimated using equations (3.10) and (3.11) as follow.

$$I_{ph-f} = \frac{G_f}{G_{ref}}\left[\mu_{bif}\left(T_{bif} - T_{amb}\right) + I_{sc-f}\right] \tag{3.10}$$

$$I_{ph-b} = \frac{G_b}{G_{ref}}\left[\mu_{bif}\left(T_{bif} - T_{amb}\right) + I_{sc-b}\right] \tag{3.11}$$

where I_{ph-f} and I_{ph-b} are the current generated as a result of the front and back side irradiances respectively.

Thus, the V-I characteristics of a bifacial PV at the module level is estimated using equation (3.12) as follows (Ademola & Qiu, 2020; Carvalho Ganilha, 2017).

$$I_T[A] = \left(I_{ph-f} + I_{ph-b}\right) - I_0\left[\exp\left(\frac{\left(V + IR_s\right)}{i_f V_T N_s}\right) - 1\right] - \frac{V + IR_s}{R_{sh}} \tag{3.12}$$

where N_s is the number of cells connected in series for a single bifacial PV module.

The power output of the module as defined by Kadeval, (2021) is simply obtained as the product of the voltage and current obtained at short circuit current and open circuit voltage respectively

3.1.1.3 Effect of temperature on bifacial PV system

The temperature effect on a bifacial PV model is considered and expressed as an energy balance, which states that the rate at which the module transfers heat into the ambient surroundings is equal to the sum of the front and rear irradiance of the module. This expression is related to both the reflection and the electrical

efficiency of the module. Mathematically, the energy balance as described in the work of Janssen et al., (2015) is given in equation (3.13)

$$\mu_{bif}\left(T_{bif}-T_{amb}\right)=\alpha_{bif}\left(G_{total}\right)\left(1-\eta_{bif}\right) \tag{3.13}$$

where μ_{bif} is the heat conductivity of the module, α_{bif} is the reflectance coefficient of the module, η_{bif} is the module efficiency, T_{bif} is the temperature of the module and T_{amb} is the ambient temperature.

3.1.1.4 Power output of bifacial PV system

The total generated power output by a single bifacial PV module at time t is estimated using equation (3.14) while the total capacity of the bifacial PV system required in the HPS is determined according to the load requirement of the location and it is given in equation (3.15).

$$P_{bif}=A_{bif}\times\left|G_f+G_b\right|_{av(t)}\times\eta_{bif} \tag{3.14}$$

$$P_{BPV}=\frac{P_L}{\eta_{BES}\times\eta_{INV}\times T_{cf}} \tag{3.15}$$

where P_{bif} and A_{bif} are the power output and the area of the module respectively, P_L is the load demand of the location, η_{INV} and η_{BES} are the efficiencies of the inverter and battery storage system respectively while T_{cf} is the temperature coefficient factor.

The number of bifacial modules N_m required is estimated using equation (3.16) as follow.

$$N_m=\frac{P_{BPV}}{P_{mpp}} \tag{3.16}$$

3.1.2 Mathematical model of wind turbine component

Wind speed is one of the most important variables in the modeling of a wind energy conversion system. It is the main input that determines the amount of electrical power that can be generated using wind turbines. Consequently, the simulation's accuracy of a wind energy system depends on the representation of wind speed. However, the fluctuating characteristic of the wind requires an accurate understanding of the dynamic behavior of the wind speed for proper system modeling (Singh & Santoso, 2012). Two approaches can be used in this regard; the first approach is to consider measurements of long duration on an actual wind site and the second is representing the wind characteristic by an analytical model. The first solution is obviously more precise and is suitable for simulation purposes, since past wind speed can be obtained from different meteorological databases (Kalmikov, 2017; Olabi et al., 2021). The various steps involved in

modeling the electrical power output of the wind conversion system are discussed in the following subsequent sections.

3.1.2.1 Wind turbine modeling

The output power or torque of a wind turbine is determined by several variables, among which are turbine speed, rotor blade tilt, rotor blade pitch angle, size and shape of turbine, area of turbine, rotor geometry and wind speed as shown in Figure 3.3. The relationship between the output power and the various variables constitute the mathematical model of the wind turbine (Aliprantis & Lafayette, 2014; Masters, 2005; Olabi et al., 2021).

The fundamental principle of the dynamic power of wind is evaluated using Newton's second law of motion. It is a well-known fact that under constant acceleration c_a, the kinetic energy E_k of an object having mass m_o and velocity v_0 is equal to work done W_d, in displacing that object from rest to distance s, under a force F_s; mathematical, this expression is represented as $E_k = W_d = F_s$. The force required to displace the object its initial position as given by Newton is further simplifying as follow (Kalmikov, 2017; Manyonge et al., 2012; Sarkar et al., 2015).

$$F_s = m_o c_a \tag{3.17}$$

Hence, the kinetic energy of the object can then be expressed as;

$$E_k = m_o c_a s \tag{3.18}$$

Applying the basic principle of the kinetic energy of solid motion, where the initial velocity of the object is considered as u_{in}. Therefore, the initial velocity can be estimated using $u_{in}^2 = v_o^2 - 2c_a s$. If the value of the initial velocity is assumed to be zero, which is usually the case; the expression of the constant acceleration c_a becomes $\frac{v_o^2}{2s}$. This expression is substituted in equation (3.18) to obtain the kinetic energy of the moving object as follows (Manyonge et al., 2012).

$$E_k = \frac{1}{2} m_O v_o^2 \tag{3.19}$$

In the case of expression (3.19), it is assumed that the mass of the solid is constant, which is not true for the motion of air. Considering wind as a fluid will definitely results in changes in the density and velocity and subsequently leads to change in mass of air in motion. Thus, it is assumed that the density of air does not vary considerably even with variation in altitude or temperature and the kinetic energy law in equation

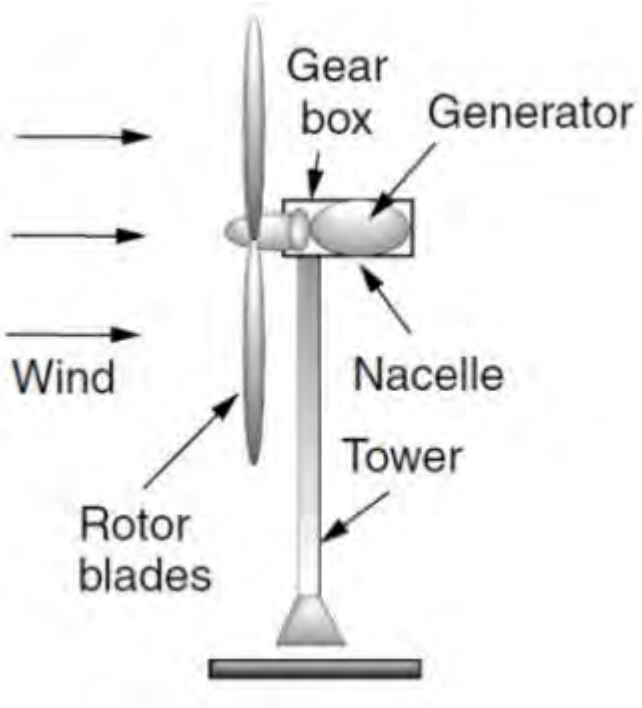

Figure 3.3: Typical horizontal wind turbine (Masters, 2005)

(3.19) is employed. Hence, the kinetic energy in (joules) in air of mass m_a moving with velocity v_w (wind) can be computed using equation (3.19) (Manyonge et al., 2012).The power P_w in wind which is generally described as the rate of change of kinetic energy is mathematically expressed using equation (3.20) (Manyonge et al., 2012; Sarkar et al., 2015).

$$P_w = \frac{dE}{dt} = \frac{1}{2}\frac{dm_a}{dt}v_w^2 \qquad 3.20$$

According to Manyonge et al., (2012), the mass flow rate $\frac{dm}{dt}$ is given as $\rho A v_w$; where A is the area through which the wind is moving and ρ is the density of air in $1.22kg/m^3$. Substituting the given mass flow rate in equation (3.20), the power in the wind thus becomes;

$$P_w = \frac{1}{2}\rho A v_w^3 \qquad 3.21$$

The actual mechanical power $P_{m(w)}$ extracted by the turbine blades as described by Manyonge et al., (2012) is the difference between the upstream and downstream wind powers. This expression is given in equation (3.22) as follows (Manyonge et al., 2012).

$$P_{m(w)} = \frac{1}{2}\rho A v_w \left(v_u^2 - v_d^2\right) \qquad 3.22$$

Where v_u and v_d are the upstream and downstream wind velocities at the entrance and exit of the rotor blade.

Comparing equation (3.22) with the mass flow rate expression results in equation (3.23) (Manyonge et al., 2012).

$$\rho A v_w = \frac{\rho A\left(v_u + v_d\right)}{2} \qquad 3.23$$

The variable v_w is the average of the velocities at the entry and exit of turbine blades. Substituting equation (3.23) into equation (3.22), the mechanical power of the wind is computed as follows (Manyonge et al., 2012).

$$P_{m(w)} = \frac{1}{2}\rho A\left(v_u^2 - v_d^2\right)\frac{\left(v_u + v_d\right)}{2} \qquad 3.24$$

Expression (3.24) can be further simplified to obtain equation (3.25).

$$P_{m(w)} = \frac{1}{2}\left[\rho A\left\{\frac{v_u}{2}\left(v_u^2 - v_d^2\right) + \frac{v_d}{2}\left(v_u^2 - v_d^2\right)\right\}\right]$$

$$= \frac{1}{2}\left[\rho A\left\{\frac{v_u^3}{2} - \frac{v_u v_d^2}{2} + \frac{v_d v_u^2}{2} - \frac{v_d^3}{2}\right\}\right]$$

$$= \frac{1}{2}\left[\rho A v_u^3\left\{\frac{1 - \left(\frac{v_d}{v_u}\right)^2 + \left(\frac{v_d}{v_u}\right) - \left(\frac{v_d}{v_u}\right)^3}{2}\right\}\right]$$

$$P_{m(w)} = \frac{1}{2}\rho A V_u^{\,3} C_p \tag{3.25}$$

The expression C_p is used to describe the turbine power coefficient or the turbine coefficient of performance and can be computed using expression (3.26) or (3.27) as follow (Manyonge et al., 2012; Y. Zhang et al., 2019).

$$C_p = \frac{1 - \left(\frac{v_d}{v_u}\right)^2 + \left(\frac{v_d}{v_u}\right) - \left(\frac{v_d}{v_u}\right)^3}{2} \tag{3.26}$$

$$C_p = \frac{\left(1 + \frac{v_d}{v_u}\right)\left(1 - \left(\frac{v_d}{v_u}\right)^2\right)}{2} \tag{3.27}$$

It should however be noted that the turbine power coefficient or coefficient of performance depends largely on the blade tip speed ratio v_s and the blade pitch angle, λ_p. The blade tip speed ratio is expressed as the ratio of the turbine's angular velocity to the wind speed (Olabi et al., 2021).

However, In order to properly realize a model that follows the typical characteristics of a practical turbine, the following assumptions are implemented (Aliprantis & Lafayette, 2014).

i. If the wind speed range is below the cut-in speed for the turbine, then the output power is assumed to be zero.
ii. If the wind speed range is between the cut-in speed and the rated speed for the turbine, then the power output is the maximum extractable from the wind based on the C_p and wind speed relation for the turbine.
iii. If the wind speed range is between rated and the cut-out speed for the turbine, then the power generated is the rated output of the plant.
iv. If the wind speed range is above the cut-out speed, then the power generated is zero.

Based on the above assumptions, the mechanical power output of the turbine is given

$$P_{m(w)} = \begin{cases} 0 & 0 \le v_u \le_{in} \\ \frac{1}{2}\rho A V_u^3 C_p & v_{in} \le v_u \le v_r \\ P_r & v_r \le v_u \le v_{out} \\ 0 & v_u \ge v_{out} \end{cases} \quad 3.28$$

where;

P_r is the rated power output of the wind turbine

$C_p(v_u)$ is the coefficient of performance of the turbine

v_u is the prevailing incident wind speed adjusted to mass height

v_{in} is the cut-in speed of the wind turbine

v_r is the rated speed of the turbine

v_{out} is the cut-off/out speed of the turbine.

3.1.2.2 Wind generator modeling

The permanent magnet synchronous generator (PMSG) was used in converting the mechanical power of the turbine into useful electrical power. The PMSG has been used in various HPS applications comprising of wind energy system due to its low cost, high starting torque, absence of separate field excitation and limited number of control parameters (Wang et al., 2009; Yaramasu et al., 2015). The model of the PMSG which is readily available in Mathworks was included as part of the wind energy conversion system. Nevertheless, the equivalent circuit of the PMSG shown in Figure 3.4 was used to model the electrical side of the generator as follow.

In accordance with Kirchhoff's voltage law, the output voltage of the generate V_o is given by Sharaf et al., (2007) as;

$$V_o = K_m \omega_m - I_a R_a - L_{aa} \frac{dI_a}{dt} \quad 3.29$$

Where V_o is the output voltage of the generator, K_m is the torque constant, ω_m is the motor speed and I_a, R_a and L_{aa} are the current, resistance and inductance of the armature respectively.

The electromechanical torque developed by the generator on the mechanical side is a function of the armature current I_a and is computed using equation (3.30) (Sharaf et al., 2007).

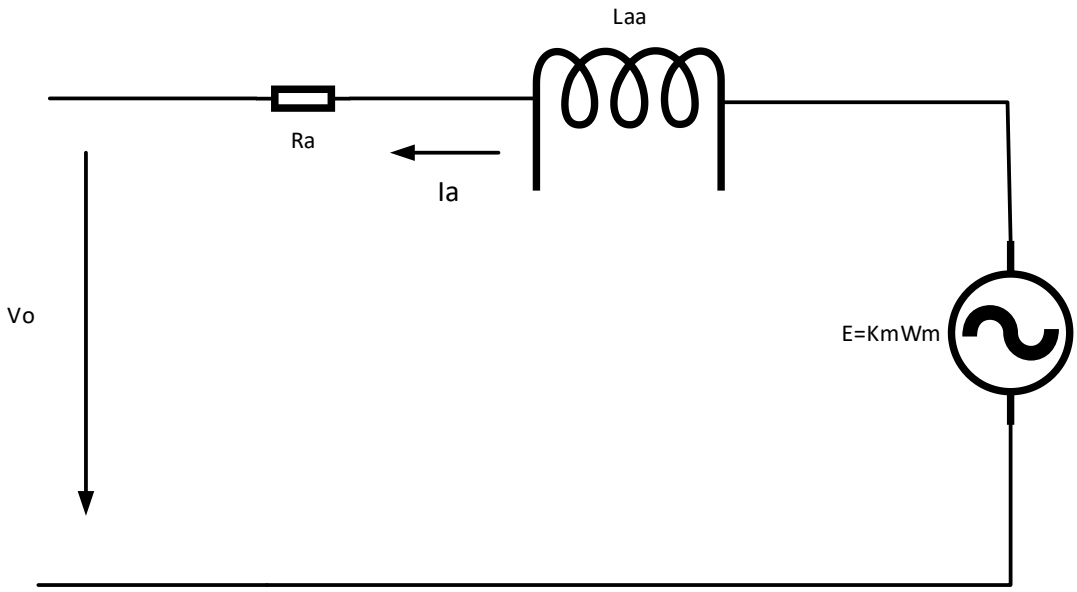

Figure 3.4: Equivalent circuit of PMSG (Sharaf et al., 2007)

$$T_e = K_m I_a \tag{3.30}$$

This torque produces the angular velocity, which is a function of the inertia J_m and frictional force B_m of the machine and the load. The Inertial J_m as described by Sharaf et al., (2007) is estimated using equation (3.31).

$$J_m \frac{d\omega_m}{dt} = T_e - T_L - B_m \omega_m \tag{3.31}$$

Hence, the electrical power output produced by the generator in time t using the mechanical power of a single wind turbine is given in equation (3.32) (Harrouz et al., 2019).

$$P_{E(w)} = P_{m(w)} \times \eta_T \times \eta_{WTG} \tag{3.32}$$

where η_T is the efficiency of the wind turbine and η_{WTG} is the efficiency of the generator.

The total electrical power generated by the wind energy system in time t is estimated according to Ogunjuyigbe et al., (2016) using equation (3.33).

$$P_{T(w)}(t) = P_{m(w)} \times A_w \times \eta_{WTG} \tag{3.33}$$

where $P_{T(w)}$ is the total electrical power output of the wind generator and A_w is the swept area of the wind turbines.

Thus, the number of wind turbines required by the proposed HPS is given using equation (3.34) (Ogunjuyigbe et al., 2016).

$$N_T = \frac{P_L \times S_f}{P_{T(w)}} \tag{3.34}$$

where N_T is the number of wind turbines, S_f is the safety factor and P_L is the load power required at the location.

3.1.3 Mathematical model of diesel generator unit

An efficient model of the diesel generator unit can significantly improve the analysis stage prior to the optimal design of the HPS, as well as its control, identification, performance prediction and diagnosis processes (Benhamed et al., 2016). A diesel generator set comprises a prime mover (diesel engine and governor), a synchronous electrical generator and the automatic voltage regulator (AVR). The diesel engine converts the chemical energy from the fuel into useful mechanical power which is used to drive the generator. The speed governor insures a constant speed operation, while the AVR stabilizes the generated voltage for various loads conditions (Theubou et al., 2012).

Generally, the mathematical models for the DG set are classified into two groups depending on the design approach. When considering small time-steps (seconds) it is necessary to consider the dynamic effects of the engine, and with bigger time steps (hours) a linear or quadratic equation describes the performance with enough accuracy (Belyaev & Gerasimov, 2020). Therefore, since a time step of 1 hour is common in most literatures for techno-economic performance analysis, the linear model is considered in this study simulation purpose. The most common model used to describe the fuel consumption versus electrical power output of diesel generators is given in equation (3.35) (Bilal et al., 2012).

$$P_{dg} = \eta_{ceff} E_{ff} \tag{3.35}$$

where P_{dg} is the electric power generated by the DG from fuel, η_{ceff} is the conversion efficiency and E_{ff} is the total energy content of oil which is approximately proportional to the volume of oil.

However, from control point of view, a diesel engine may be considered as speed-feedback system. The model of the fuel actuator system is usually represented as a first order phase-lag network, which is characterized by gain K_2 and the time constant τ_2 as depicted in Figure 3.5a. The output of the actuator is the transfer function equation described by Luo et al., (2011) is given in equation (3.36).

$$\Phi(s) = \frac{K_3 K_2}{(1+\tau_2)} I(s) \tag{3.36}$$

where $\Phi(s)$ is the fuel flow rate, K_3 is current driver constant and $I(s)$ is the input current.

The fuel flow $\Phi(s)$ rate is then converted into mechanical torque T_s after a pure time delay τ_1 and engine torque constant, K_1 as represented in Figure 3.5b. The transfer function equation of Figure 3.5b as described by Luo et al., (2011) is given in equation (3.37)

$$T_s = \Phi(s) K_1 e^{-\tau_1 s} \tag{3.37}$$

The differential equations for the diesel engine and speed regulation are as given in equation (3.38) and (3.39) respectively (Chen, 2010; Galiullin & Valiev, 2017).

$$\frac{dP_c}{dt} = -\frac{k_1}{\omega_{ref}} \Delta\omega \tag{3.38}$$

$$\frac{dm_B}{dt} = \frac{1}{\Gamma_2}\left(K_2 P_c - \frac{k_2}{\omega_{ref} R_d} \Delta\omega - m_B \right) \tag{3.39}$$

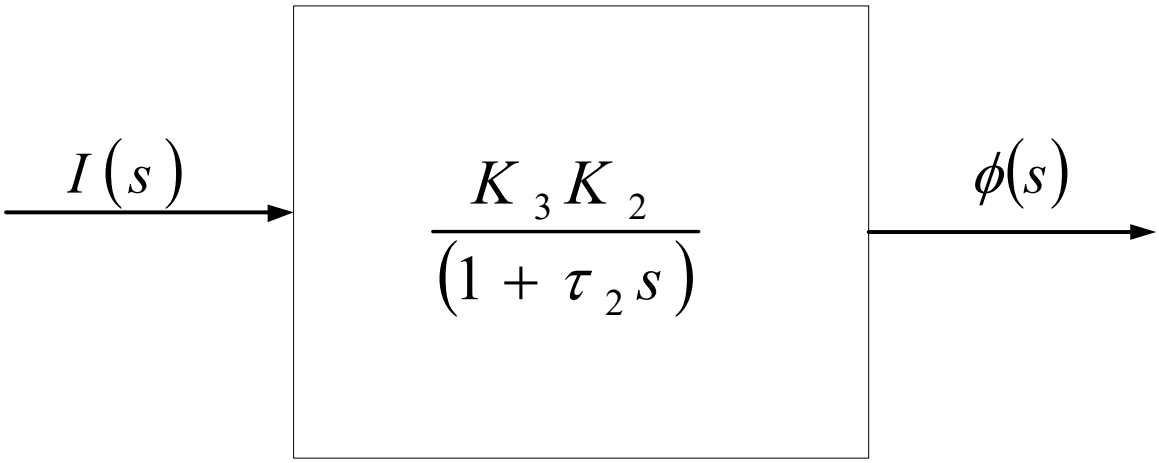

Figure 3.5a: The actuator model (Luo et al., 2011)

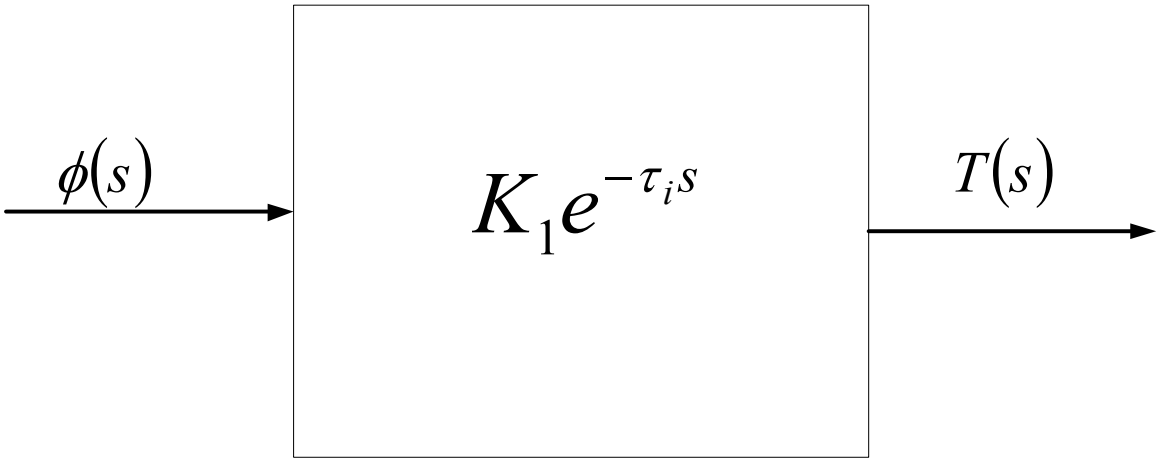

Figure 3.5b: Diesel engine model (Luo et al., 2011)

Where P_c is the compression ratio, k_1 is the governor summing loop amplification factor, R_d is the diesel engine permanent speed droop, ω_{ref} is the engine speed and m_B is the engine fuel consumption rate.

The PMSG model in Mathworks was also used to model the generator side of the DG unit. The generator converts the mechanical torque T_s to the electrical power delivered by the generator. Hence, the power generated by the DG unit in time t is computed using equation (3.40) (Bilal et al., 2012).

$$P_{dg} = P_{nom}\eta_{dg} \tag{3.40}$$

where P_{dg}, P_{nom} and η_{dg} represent the power output, the nominal power and the efficiency of the DG unit respectively.

Since a number of small sized DG set is considered in this study as compared to using a single large sized DG unit common with most HPS applications, it is important to model the total power output of the split genset system. The main reason for using a split DG set in this study is to be able to match the variations in load during the period of power deficit from other generating sources. Subsequently, this will result to low fuel consumption, low carbon emission and improved overall reliability of the HPS. The total power output of the DG set system is modeled in accordance with the model developed in the work of Ayodele et al., (2017). A typical configuration of the split genset considered in this study is depicted in Figure 3.6.

Each of the DG unit in the configuration is equipped with a control switch S_w which is assigned binary digit 0 and 1 to control the power output of the split DG set. The possible arrangements of the DG units required to supply a load at any time t is determined using Boolean logic conditions. Hence, for n number of switches, the number of possible configurations of the DG set is computed using "$2^n - 1$". For the purpose of this study, three split DG units were considered in the configuration of the DG set; using the Boolean logic combination rule, the DG set can supply the load in seven different configurations. Hence, the total power output from the DG set at any time t is expressed as (Ayodele et al., 2017);

$$P_{(sdg)}(t) = S_{w1}P_{1nom} + S_{w2}P_{2nom} + S_{w3}P_{3nom} \tag{3.41}$$

3.1.4 Mathematical model of battery storage device

The Battery Energy Storage (BES) is an important sub-system of the HPS. It is commonly used as backup energy sources due to the intermittent nature of the RE generating sources. Several studies have reported on the use of lead acid batteries for different HPS designs due to their reasonable, however, for the purpose of this study, the lithium ion battery was used due to its high efficiency and reliability (Kiehbadroudinezhad & Merabet, 2022).

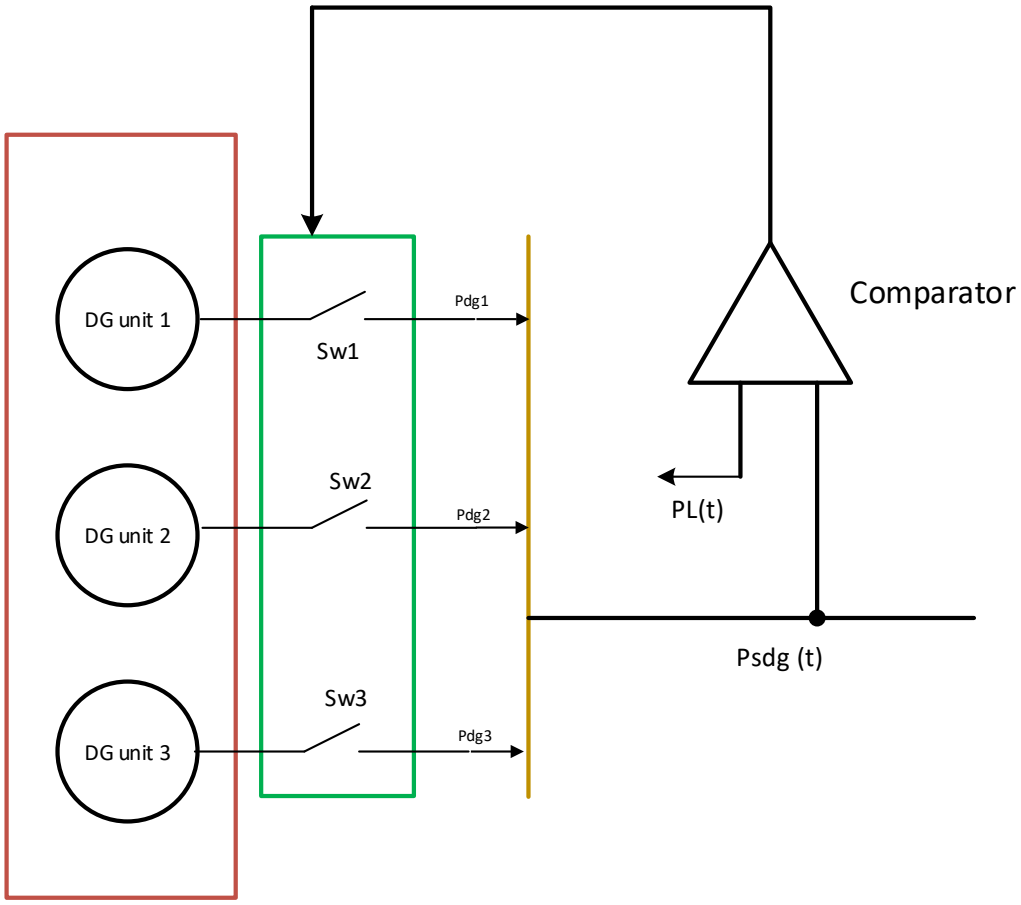

Figure 3.6: Split genset model (Ayodele et al., 2017)

The Lithium ion battery used in this study is modeled based on controlled voltage source connected in series with a constant resistance as depicted in Figure 3.7. The model was modeled by shepherd in 1969; it was adopted due to its simplicity and the availability of model variables, which are easily specified in the manufacturer's datasheet (Tremblay & Dessaint, 2009). Basically, the shepherd model represents accurately the voltage dynamics when there is variation in the current and also consider the open circuit voltage relative to the state of charge (SOC) of the battery As a result, a non-linear term, referred to as polarization resistance was introduced to the discharge model equation for better accuracy. The polarization resistance as described by shepherd is given in equation (3.42), while the voltage of the BES during discharge period is modeled using equation (3.43) (Hinz, 2019; Tremblay & Dessaint, 2009).

$$R_{pol} = \left(K \frac{Q}{Q - it} it \right) \tag{3.42}$$

$$V_{BES}(DOD) = E_0 - K \frac{Q}{Q - it} it - Ri - K \frac{Q}{Q - it} i^* + A_v \exp(-B_t it) \tag{3.43}$$

Where E_0 represents the battery constant voltage, K is used to describe the polarization constant, Q represents the maximum battery capacity, it $\left(\int idt\right)$ represents the main charge of the battery, R represents the internal resistance, i is a term describing the battery current, i^* represents the current dynamics of the battery at low frequency, A_v describes the voltage drop of the battery during the exponential zone period and B_t represents the time constant during the exponential zone.

On the other hand, during the charge period, the voltage of the BES will rise rapidly and hence, there is a corresponding change in the polarization resistance as given in equation (3.44) (Hinz, 2019; Tremblay & Dessaint, 2009).

$$R_{pol} = \left(K \frac{Q}{it} \right) \tag{3.44}$$

The polarization resistance term described in equation (3.44) will continue to increase until the battery is fully charged, that is, when the current is equal to zero. However, this may not be achievable in real life applications, hence, in his experiment, shepherd assume that only 90 % of the battery capacity is fully charged and the remaining 10 % was shifted towards the polarization resistance. Therefore, the new polarization resistance as expressed by shepherd is given in equation (3.45) (Hinz, 2019; Tremblay & Dessaint, 2009).

$$R_{pol} = \left(K \frac{Q}{it + 0.1Q} \right) \tag{3.45}$$

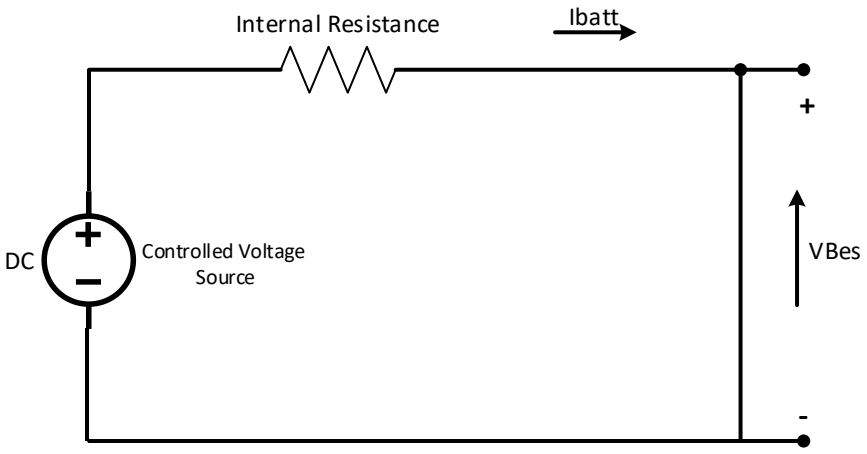

Figure 3.7: Equivalent circuit of lithium ion battery model (Hinz, 2019)

Hence, voltage of the BES during the charging cycle using the RE either of the RE generating sources is given in equation (3.46) (Hinz, 2019; Tremblay & Dessaint, 2009).

$$V_{BES}(SOC) = E_0 - K\frac{Q}{Q-it}it - Ri - K\frac{Q}{it+0.1Q}i^* + A_v\exp(-B_t it) \quad 3.46$$

At full charge, the voltage of the BES is computed using equation (3.47) as follows.

$$V_{BES(full)} = E_0 - (R*i) + A_v \quad 3.47$$

At the end of the discharge period, the reverse voltage of the BES as described by shepherd is computed by replacing the time constant B_t with an approximate term, $\left(\frac{3}{Q_{\exp}}\right)$ using equation (3.48) while the nominal voltage of the battery is computed using equation (3.49) as follow (Hinz, 2019; Tremblay & Dessaint, 2009).

$$V_{BES(\exp)} = E_0 - K\frac{Q}{Q-Q_{\exp}}(Q_{\exp}+i) - Ri + A_v\exp\left(-\frac{3}{Q_{\exp}}Q_{\exp}\right) \quad 3.48$$

$$V_{BES(nom)} = E_0 - K\frac{Q}{Q-Q_{nom}}(Q_{nom}+i) - Ri + A_v\exp\left(-\frac{3}{Q_{\exp}}Q_{nom}\right) \quad 3.49$$

The capacity of the BES system required in the proposed HPS is largely dependent on the autonomy days. The BES autonomy days is defined as the total number of days the BES system is able to supply the load without being recharged. A period of five days have been used in many literatures HPS design and was also used in this study. Hence the nominal capacity of the BES system in this study is computed using equation (3.50) (Adebanji et al., 2020; Ogunjuyigbe et al., 2016).

$$C_{BES} = \frac{P_L \times A_{.d}}{V_{BES}\cdot DOD_{\max}\cdot\eta_{BES}\cdot\eta_{INV}} \quad 3.50$$

where C_{BES} is the nominal capacity of the BES, V_{BES} is the voltage of the BES at maximum permissible depth of discharge and A_d is the battery autonomy days.

The SOC of the BES system at any time t is thus expressed using equation (3.51) as follows (Abedi et al., 2012).

$$SOC(t) = SOC(t-1) \pm \frac{P_{BES}.\eta_{BES}}{C_{BES}} \times 100 \quad 3.51$$

$SOC(t)$ and $SOC(t-1)$ represent the state of charge of the BES in time step t and $t-1$, the positive and negative signs indicates the charging and discharging mode of the BES respectively and P_{BES} is the power charged or discharged from the battery at any time t.

3.1.5 Mathematical model of power converter system

The configuration of many HPS designs usually contains a bi-directional converter which consists of both rectifier and inverter (Aditi & Pandey, 2016). The inverter converts the DC power components from the DC bus to the AC form at the desired load voltage and frequency while the rectifier converts the AC components from the AC bus back to the DC form used in charging the battery. The bidirectional inverter is modeled in two modes namely the rectifier mode and the inverter mode (Bissey et al., 2018; Rashid et al., 2021).

In the rectifier mode, the power output of the bi-directional converter at any time t is modeled as follows (Rashid et al., 2021).

$$P_{rec-out}(t) = P_{rec-in} \cdot \eta_{INV}(t) \tag{3.52}$$

However, when the converter is operated in the inverter mode, the power output of the bi-directional converter is computed using equation (3.53) (Rashid et al., 2021).

$$P_{inv-out}(t) = P_{inv-in} \cdot \eta_{INV}(t) \tag{3.53}$$

where $P_{rec-out}$ and P_{rec-in} are the output and input power of the bidirectional converter in the rectifier mode respectively, while $P_{inv-out}$ and P_{inv-in} are the output and input power of the bidirectional converter in the inverter mode respectively.

3.2 Power dispatch strategy of the proposed HPS

The power output of the wind turbine generator was estimated equation (3.33), taking the average hourly wind speed as input. Also, the power output of the bifacial PV panel system was estimated at an hourly basis according to equation (3.15), using the estimated average hourly front and back irradiances as inputs. The total hourly generated power from the renewable energy sources is added together and compared with the hourly load demand. The battery energy storage is operated only when there is excess or insufficient output power from the renewable sources. When the power generated from the renewable energy sources are in excess compared to the power demanded by the load, the excess power is used to charge the battery until it reaches its maximum state of charge $soc_{\max}$, however, when there is shortage of power from the renewable energy sources, the battery is discharged to meet the deficit until it reaches its maximum depth of discharge $DOD_{\max}$. The split genset is operated when there is shortage of power from the renewable

sources and the battery energy storage is at maximum depth of discharge, and unable to deliver power to the load. The comparator model in Figure 3.6 is usually used to check for the amount of deficit power in order to determine which of the DG unit has to be turned on. The first DG unit is then turned on to serve the load; however, if the power demanded by the load is greater than the capacity of the first DG unit, the second DG unit is operated in parallel with the first to supply power to the load, if the power demanded by the load is still unmet, the split genset is operated at its rated capacity. The stepwise procedure of the dispatch strategy is outlined as follows.

Step 1 Calculate the power generated by the Bifacial PV and wind turbine systems at time t using equation (3.15) and (3.33) respectively, and calculate the total power generated from the renewable energy sources using $P_{REs}(t) = P_{BPV}(t) + P_{WTG}(t)$ and evaluate the power required by the load in one hour step.

Step 2 Compare the total power generated by the renewable sources and battery state of charge with the power required by the load at every hour.

Step 3 Check if $\left[P_{REs} > P_L(t)/\eta_{INV}\right]$ and $\left[soc(t-1) < soc_{\max}\right]$; supply power to the load and charge the battery.

Step 4 Check if $\left[P_{REs} > P_L(t)/\eta_{INV}\right]$ and $\left[soc(t-1) > soc_{\max}\right]$; supply power to the load, stop charging the battery and update the battery state of charge.

Step 5 Check if $\left[P_{REs} = P_L(t)/\eta_{INV}\right]$; supply power to the load only.

Step 6 Check if $\left[P_{REs} < P_L(t)/\eta_{INV}\right]$ and $\left[DOD(t-1) < DOD_{\max}\right]$; supply power to the load by discharging the battery to meet the power shortage. The power supplied by the battery at this step is calculated using the expression, $\left[P_{BES}(t) = P_L(t)/\eta_{INV} - P_{REs}(t)\right]$.

Step 7 Check If $\left[P_{REs} < P_L(t)/\eta_{INV}\right]$ and $\left[DOD(t) \geq DOD_{\max}\right]$; stop discharging the battery, update the battery depth of discharge and evaluate the power deficit.

Step 8 Check if $\left[P_{REs} < P_L(t)/\eta_{INV}\right]$ and $\left[DOD(t) \geq DOD_{\max}\right]$, supply the power deficit using by switch on DG unit 1

Step 9 Check if $\left[P_{REs} < P_L(t)/\eta_{INV}\right]$, $\left[DOD(t) \geq DOD_{\max}\right]$ and $\left[P_L/\eta_{INV} > P_{dg1}\right]$, supply the power deficit using DG units 1 and 2.

Step 10 Check if $\left[P_{REs} < P_L(t)/\eta_{INV}\right]$, $\left[DOD(t) \geq DOD_{\max}\right]$ and $\left[P_L/\eta_{INV} > P_{dg1} + P_{dg2}\right]$, supply the load using the rated capacity of the split genset and dump any excess energy.

The flowchart of the power dispatch strategy described above is as shown in Figure 3.8.

3.3 Summary

The mathematical expression of each components of the proposed HPS is presented in this chapter. It begins by presenting the various techniques used in modeling the irradiance reaching both the front and back side of the bifacial PV module. This is preceded by the mathematical modeling of the wind turbine power output, diesel generator set, battery storage scheme and the converter system. The step by step procedure of the power dispatch strategy of the HPS concludes the chapter.

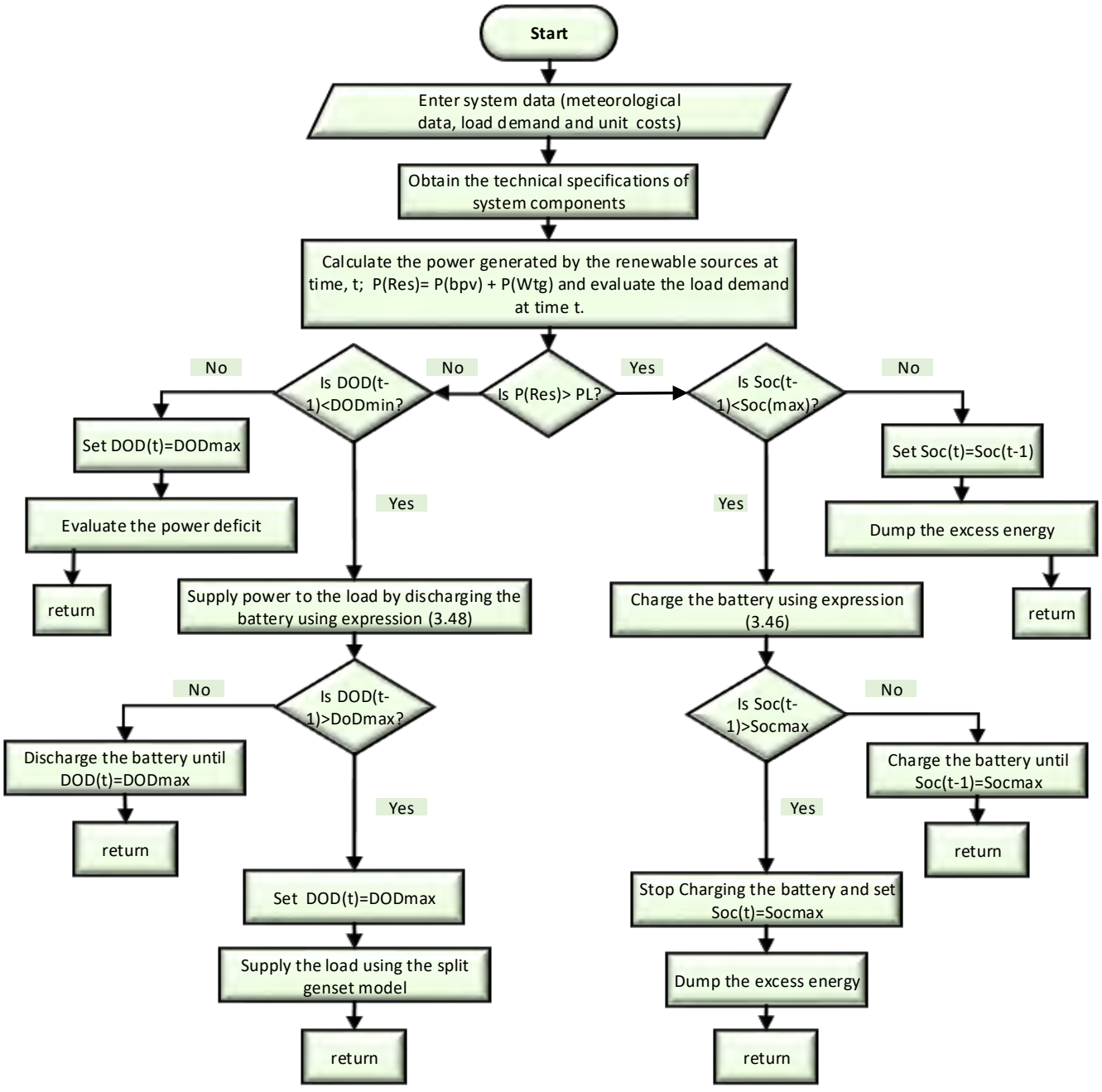

Figure 3.8: Flowchart of the power dispatch strategy for the proposed HPS

CHAPTER FOUR
DESIGN METHODOLOGY

4.1 Research approach

This study is focused on the optimal design of HPS consisting of bifacial PV, wind turbine, battery energy storage and split gensets. A multi-objective optimization solution method was employed to find the optimal design of the proposed off-grid HPS that guarantees reliable and continuous supply of electrical power at the least Life Cycle Cost and total environmental pollution. The proposed HPS consists of bifacial PV, wind turbine, battery system and split genset. Mathematical modeling of the individual components of the proposed HPS was carried out using Simulink software; in order to properly evaluate the performance of the bifacial PV, two orientation states namely vertical east-west and horizontal north-south are considered during the simulation process. For the vertical east-west orientation, the bifacial module was assumed to be installed with the front side facing the direction of the sun and the irradiance reaching the back side were estimated using the mathematical model of expression (3.20). On the other hand, for the horizontal north-south orientation, the module was assumed to be tilted at an optimized angle of twenty degrees, and the irradiance reaching the back side is also estimated in accordance with expression (3.28). Each of the component models is then integrated together in a single HPS model.

An optimization problem based on Life Cycle Cost (LCC) and Total Environmental Pollution (TEP) is developed and optimized using Giza Pyramid Construction (GPC) algorithm, Firefly Algorithm (FA) and Whale Optimization Algorithm (WOA) techniques. Optimization of the system is achieved not only by selecting an appropriate system configuration, but also by implementing a suitable dispatch strategy to control the flow of power in each of the energy generating sources. The proposed model is applied to a remote village in northern part of Nigeria in order to demonstrate the effectiveness of the proposed algorithms in terms of simulation run time, convergence speed and quality of solution. All simulation are done using MATLAB (R2021a) to check for the most feasible solution after the application of each optimization technique. The block diagram of Figure 4.1 shows the basic steps in achieving the optimal system design.

4.2 Problem formulation

The design process of any optimization problem includes defining the objective function(s), identifying the decision variables and defining the constraints. The ability to understand the link among these three elements is significant to achieving an optimal solution to a problem. Generally, a multi-objective optimization problem as described by Bouaouda & Sayouti, (2022)) is formulated in accordance with equation (4.1) to (4.4).

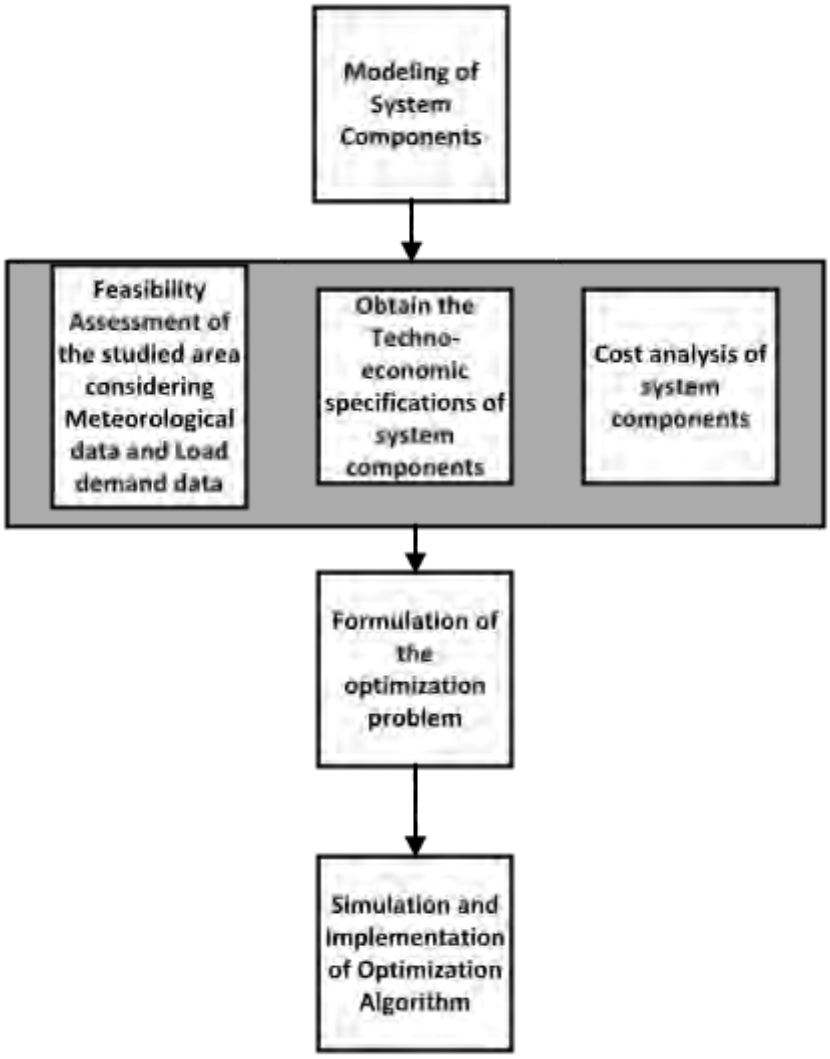

Figure 4.1: Framework of the system design

$$\text{Minimize } F(x) = (f_1(x), \ldots\ldots\ldots f_o(x))^T \quad 4.1$$

subject to;

$$h_i(x) = 0, \quad i = 1, \ldots\ldots\ldots, m, \quad 4.2$$

$$g_j(x) \leq 0, \quad j = 1, \ldots\ldots\ldots, k, \quad 4.3$$

$$x_L \leq x \leq x_U \quad 4.4$$

Where $(f_1 \ldots\ldots\ldots f_0)$ represent all the specified objective functions, x denotes the vector of all the decision variables, $(h_1 \ldots\ldots\ldots h_m)$ is used to denote the equality constraints and $(g_1 \ldots\ldots\ldots g_k)$ represent the inequality constraints, while x_L and x_U are the lower and upper limits on the decision variables respectively. A weighted sum method was employed to convert the multi-objective function to a single function F, where the pareto optimal solutions of the original multi-objective problem is defined as;

$$\text{Minimize } F(x) = \{f_1(x_1), f_2(x_2)\} \quad 4.5$$

Applying the weighted sum method to equation (4.5), the single objective function is thus expressed using equation (4.6) as follows;

$$F(x) = (w_1 \times f_1) + (w_2 \times f_2) \quad 4.6$$

where w_1 and w_2 represent the importance of the two objective functions f_1 and f_2 respectively, such that;

$$w_1 + w_2 = 1 \quad \text{for } w_1, w_2 \geq 0 \quad 4.7$$

The optimal design of the proposed HPS was aimed at minimizing two objective functions, the LCC and TEP of the system with respect to the decision variables and subject to the associated equality and inequality constraints. The objective functions, decision variables, as well as the design constraints are presented in the following sub-sections.

4.2.1 Objective function

The objective functions considered in this study are the LCC and TEP of the system, f_1 is used to denote the LCC, while the TEP is denoted by f_2. A detail evaluation of the two objective functions are presented as follows.

4.2.1.1 Life cycle cost (LCC)

The life cycle cost of the system is used to describe the total amount spent on the system during its entire lifespan. The total amount spent include the initial capital cost, operation and maintenance cost, replacement cost and fuel cost of the split genset. The LCC is described mathematically as follows.

$$f_1 = LCC = IC_c + OM_c + R_c + F_{c(sdg)} \tag{4.8}$$

where IC_c is the initial capital cost, OM_c is the operation and maintenance cost, R_c is the replacement cost and $F_{c(sdg)}$ is the fuel cost of the split genset.

The initial capital cost is the sum of the capital cost of all the components of the system and is given in equation (4.9) as;

$$IC_c = CC_{bif}.N_{bif} + CC_{WTG}.N_{WTG} + CC_{BES}.N_{BES} + CC_{dg1} + CC_{dg2} + CC_{dg3} \tag{4.9}$$

Where CC_{bif} is the capital cost of one bifacial PV module, N_{bif} is the number of bifacial PV modules required by the system, CC_{WTG} is the capital cost of a wind turbine generator, N_{WTG} is the number of wind turbines, CC_{BES} is the capital cost of a single battery, N_{BES} is the number of batteries selected, CC_{dg1}, CC_{dg2} and CC_{dg3} are the capital costs of the DG units 1, 2 and 3 respectively.

Moreover, the operation and maintenance cost of the proposed HPS is the sum of the individual components of the system and it is expressed as;

$$OM_c = OM_{c(BPV)} + OM_{c(WTG)} + OM_{c(BES)} + OM_{c(sdg)} \tag{4.10}$$

The operation and maintenance costs individual components are estimated using equations (4.11) to (4.14) as follow.

$$OM_{c(bpv)} = C_{ann(bif)} \times N_{bif} \times \sum_{i=1}^{N} \left(\frac{1+f_r}{1+i_r} \right)^i \tag{4.11}$$

$$OM_{c(WTG)} = C_{ann(WTG)} \times N_{WTG} \times \sum_{i=1}^{N} \left(\frac{1+f_r}{1+i_r} \right)^i \tag{4.12}$$

$$OM_{c(BES)} = C_{ann(BES)} \times N_{BES} \times \sum_{i=1}^{N} \left(\frac{1+f_r}{1+i_r} \right)^i \tag{4.13}$$

$$OM_{c(sdg)} = C_{ann(sdg)} \times N_{oh} \times \sum_{i=1}^{N} \left(\frac{1+f_r}{1+i_r} \right)^i \tag{4.14}$$

where $C_{ann(bif)}$, $C_{ann(WTG)}$, $C_{ann(BES)}$, and $C_{ann(sdg)}$ are the annual operation and maintenance costs of the bifacial PV system, wind turbine, battery system and the split genset respectively, N is the project lifetime

which is set to 30 years based on the lifespan of the bifacial PV module, f_r is the inflation rate, i_r is the interest rate and N_{oh} is the number of hours the split genset was operated during the project lifetime.

The replacement cost is considered for the split genset and the battery energy storage system only. The replacement cost of these two components is estimated using equation (4.15) as follows.

$$R_c = C_u \times C_{nom} \times \sum_{i=1}^{N_r} \left(\frac{1+f_r}{1+i_r} \right)^{\frac{N_i}{N_r+1}} \tag{4.15}$$

where C_u is the cost of a single component to be replaced, N_r is the number of times the components must be replaced, N_i is the number of components to be replaced and C_{nom} is the nominal capacity of the component to be replaced.

The total fuel cost of the split genset is also estimated using equation (4.16) as follows.

$$F_{c(sdg)} = \sum_{t=1}^{8760} C_{ann(f)}(t) \times \sum_{i=1}^{N} \left(\frac{1+f_r}{1+i_r} \right)^{i} \tag{4.16}$$

The annual fuel cost, $C_{ann(f)}$, annual fuel consumption of the split genset, $F_{sdg}(t)$ and the annual fuel consumption of each DG unit F_{dg} are estimated using equations (4.17) to (4.19) respectively.

$$C_{ann(f)} = f_c \times F_{sdg} \tag{4.17}$$

$$F_{sdg}(t) = F_{dg1} + F_{dg2} + F_{dg3} \tag{4.18}$$

$$F_{dg} = a_g P_{dg} + b_g P_r \tag{4.19}$$

Where f_c is the fuel cost, F_{dg1}, F_{dg2} and F_{dg3} are the annual fuel consumption of the DG unit 1, 2 and 3, P_{dg} and P_r are the output power and rated power of each DG unit, while a_g and b_g represent the coefficient of fuel consumption can be found in the manufacturer's datasheet.

4.2.1.2 Total environmental pollution (TEP)

The total environmental pollution (TEP) represents an objective function used to describe the emission of harmful gases into the environment throughout the entire lifespan of the system and denoted as f_2. The main component responsible for the emission of these gases is the split genset system. During the operation of the split genset, gases such as CO_2, SO_2 and NO_x are emitted into the atmosphere, the accumulation of these gases are included in the TEP objective and is estimated using equation 4.20 as follows.

$$f_2 = TEP = \sum_{t=1}^{N} \left[\left(\varpi CO_2 + \varpi SO_2 + \varpi NO_x \right) \times P_{sdg}(t) \right] \quad 4.20$$

Where ϖCO_2, ϖSO_2 and ϖNO_x are the emission factors of gases CO_2, SO_2 and NO_x respectively and $P_{sdg}(t)$ represents the split genset output power at time t

4.2.2 Design constraints

The objective functions under consideration are subjected to the following equality and inequality constraints. Equality constraints are the type of constraints that must be obeyed by system at all time during the optimization process while inequality constraints are constraints that can either be obeyed or sidestepped by the system. The various equality and inequality constraints considered in the design process of the proposed HPS are presented as follow.

4.2.2.1 Equality constraints

1. The power balance relation

At any instant t, the total power delivered by the proposed HPS must be greater than or equal to the total power required by the load at the specified location as expressed in equation (4.21).

$$P_{REs}(t) + P_{BES}(t) + P_{sdg}(t) - P_L(t) = 0 \quad 4.21$$

4.2.2.2 Inequality constraints

1. The Reliability Objective Constraint

The reliability objective considered is referred to as the Loss of Power Supply Probability (LPSP). The LPSP is a criteria used in literatures to measure the portion of the load at a specific location that the system is unable to supply at any point in time. For standalone applications, the value of the LPSP should be around 0.01. Hence the LPSP of the proposed HPS is considered an inequality constraints which must be satisfied at all time and it is adopted from the work of Bhandari *et al*., (2015) and given in equation (4.22).

$$LPSP \angle 0.01 \quad 4.22$$

The value of the LPSP is determined using equation (4.23) as follows.

$$LPSP = \frac{\sum \left(P_L - P_{REs} + P_{BES} soc_{\min} + P_{sdg} \right)}{\sum P_L} \quad 4.23$$

2. The constraint on number of system components

The minimum and maximum number of components in the proposed HPS is also considered as an inequality constraint and it is expressed as;

$$N_{c(\min)} \leq N_c \leq N_{c(\max)} \quad 4.24$$

where N_c represents the Number of components, c required by the system, $N_{c(\min)}$ and $N_{c(\max)}$ represent the minimum and maximum number of components required by the proposed HPS. For the purpose of this study, the system is designed to select a minimum of one (1) component, while the maximum number of components is estimated according to the peak power demand of the specific location using equation (4.25).

$$N_c = \frac{P_{L(peak)}}{P_{c(\min)}} \tag{4.25}$$

where $P_{L(peak)}$ is the daily peak power required by the load and $P_{c(\min)}$ is the minimum power output that can be generated from a single component.

3. The battery energy storage capacity constraint

Some limits should be considered during charging and discharging of the planned battery energy storage (BES) as the state of charge (SOC) of the batteries (should not exceed the capacity of the storage batteries but to overdo the minimum permissible storage level. Hence, the BES capacity is constrained using equation (4.26), while the SOC of the battery is constrained using equation (4.27).

$$P_{BES(\min)} \leq P_{BES(cap)} \leq P_{BES(\max)} \tag{4.26}$$

$$soc_{\min} \leq soc(t) \leq soc_{\max} \tag{4.27}$$

4. The constraints on split genset

In order to avoid collapse and damages to each generating unit, the hourly generation of each generating unit was bounded between the minimum and maximum generation as given in equation (4.28).

$$P_{dg(\min)} \leq P_{dg}(t) \leq P_{dg(\max)} \tag{4.28}$$

5. Non-negativity constraints

Since electrical power can only flow in one direction, all the energy generating components are expected to be non-negative and are constrained using equation (4.29).

$$1 \leq P_c \leq P_{\max,c} \tag{4.29}$$

where P_c is the power generated by each of the components and $P_{mac,c}$ is the maximum power output of the components.

4.2.3 Design variables

The decision variables in any optimization problem are quantities that can be controlled by the decision-maker. Their optimal values must be determined to achieve an optimal solution to the problem. In this study, four decision variables that are considered are presented as follows;

i. the number of bifacial PV modules (N_{bif})

ii. the number of wind turbines (N_{WTG})

iii. the number of batteries (N_{BES})

iv. the rated capacity of each DG unit (P_r)

4.3 Implementation of Optimization Algorithm

The optimal design of any HPS is a complex problem due to the various differing objectives such as cost, reliability, environmental pollution and many others. Hence, the concept of multi-objective solution method is well documented in solving problems with differing objectives. Nevertheless, the main issue associated with this kind of solution methodology is the issue of convergence and simulation run time. Thus, an optimization algorithm with the ability to produce quality solution at a faster convergence rate and minimal simulation run time is usually required. In this study, the implementation of the various optimization algorithms is discussed in this section. Three optimization techniques are applied to the optimization problem developed in section 4.2 to obtain the optimal system design with the least life cycle cost and total environmental pollution for a period of 30 years; and their performance were compared with one another.

However, it is important to state that for most complex system designs such as the proposed HPS considered in this study, the mathematical modeling of the system described in chapter three (3) of this study plays a significant role in producing the optimal solution to the optimization problem. Therefore, the system is first simulated using the various mathematical models of the sub-systems described in sections 3.1 to 3.4 to accommodate uncertainties and gives true representation of the proposed HPS. Thereafter, the three optimization techniques are then applied to search for the most appropriate representation of the system and produce the optimal solution in a reasonable simulation run time. In order to properly evaluate the performance of the optimization algorithms, equal number of population size and number of iterations are selected for each algorithm. The implementation procedure of each of the optimization algorithms considered in this study is subsequently presented.

4.3.1 Implementation of Firefly Algorithm

For the optimal design of the proposed HPS, Firefly Algorithm (FA) is one of the optimization algorithms employed to obtain a system design that minimizes the life cycle cost and total environmental pollution produced by the system. FA is a meta-heuristic, nature-inspired optimization algorithm which is based on the social flashing behavior of fireflies. It has been applied to solve many engineering optimization problems due to its ability to achieve global optimum solution in limited simulation run time and its fast convergence speed.

The objective function, which also determines the fitness/light intensity of a firefly, the design constraints, design variables, components are all defined in the firefly algorithm. At the inception stage, a population of fireflies (f_p) is generated and distributed evenly in a search medium according to expression (4.30) as follows.

$$f_p = \left[f_1, f_2, f_3, f_{4,} \ldots\ldots\ldots f_N \right] \quad 4.30$$

where N represents the number of fireflies in the population.

Moreover, other basic parameters of the firefly algorithm such as such as the randomness factor (σ), the initial attractiveness of a firefly (β_0), the light absorption coefficient of medium (γ) and light intensity (L) are also initialized. The design variables which represent the capacity of each sub-systems of the proposed HPS are defined in a vector named firefly as described using expression (4.31) as follows.

$$f_i = \left| N_{bif} \times P_{bif}, N_{WTG} \times P_{E(w)}, N_{BES} \times P_{BES}, P_{dg1}.h_1, P_{dg2}.h_2, P_{dg3}.h_3 \right| \quad 4.31$$

where f_i is the ith firefly, P_{dg1}, P_{dg2} and P_{dg3} are the selected capacities of the DG units 1, 2 and 3 respectively during the entire lifespan of the system and h_1, h_2 and h_3 are hours of operation of each DG units during the entire lifespan of the system.

In other words, each firefly represents a potential configuration of the proposed HPS. For every possible configuration, the light intensity (fitness value) of each firefly is simulated to check its feasibility based on the objective function of equation (4.5) subject to the various design constraints presented in section 4.2.2 of this study. At the simulation stage, the mathematical expression of the various components of the proposed HPS described in section 3.1 is used to predict their output in each time period (one hour) based on the weather data of the proposed location. The simulation is run for 30 years to evaluate the performance of each firefly in the population. The simulation process simultaneously estimates the life cycle cost and the total environmental pollution for each possible configuration.

At the optimization stage, each firefly is evaluated based on its light intensity (fitness value). The algorithm is run for 50 iterations, and in each iteration, the fitness value of one firefly is compared to another firefly in the search medium. Each of the firefly is made to fly in the search medium according to the number of the design variables. The movement of a firefly with a less fitness value is adjusted towards a firefly with a higher fitness value using equation (2.7). The process is repeated for each iteration until there is no firefly with a higher fitness value in the population or maximum number of iterations has been reached. The firefly with the best fitness value (the least life cycle cost and total environmental pollution) represents the optimal design of the proposed HPS. The flowchart of the optimization process is depicted in Figure 4.2.

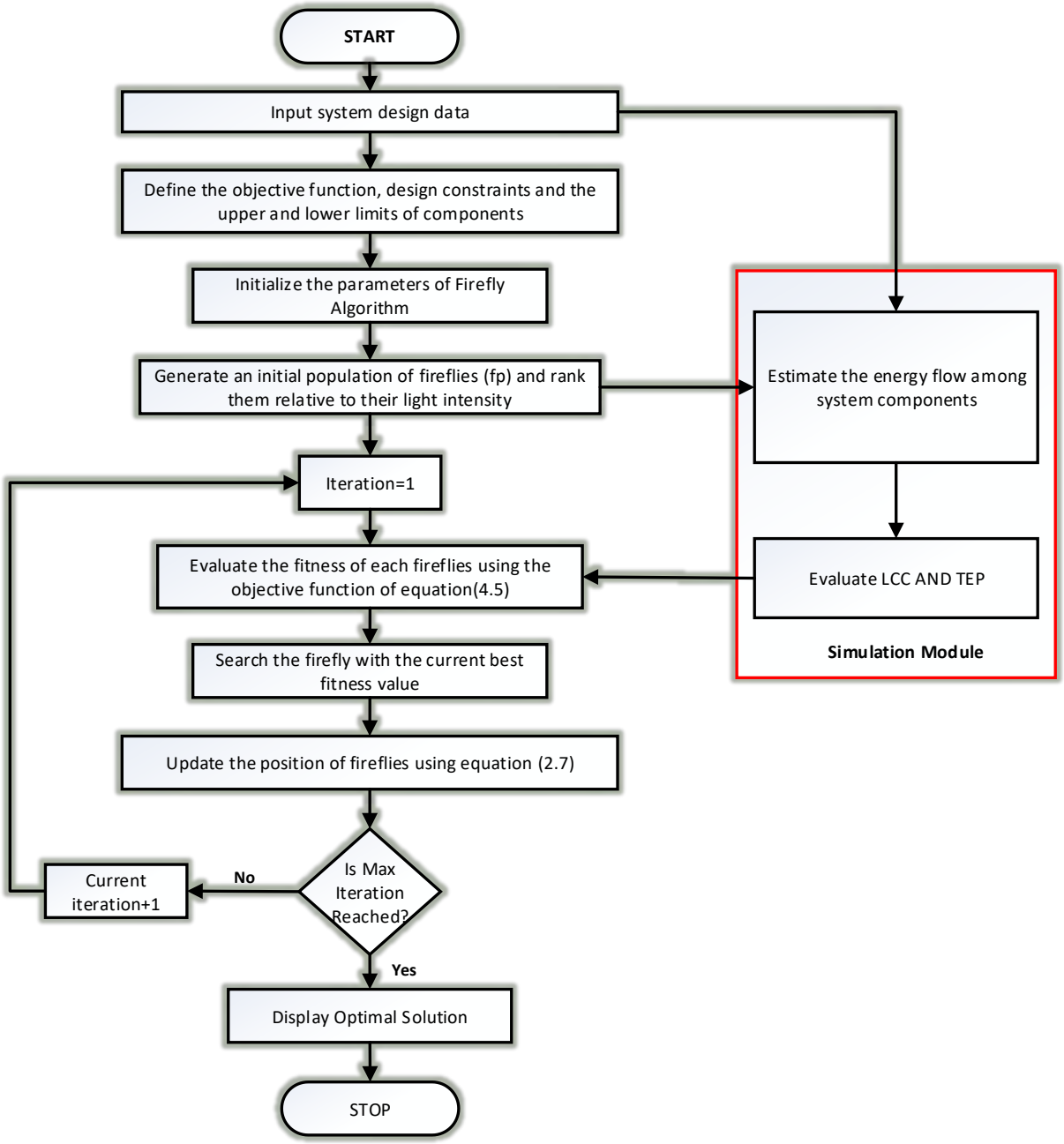

Figure 4.2: Flowchart of Firefly Algorithm for optimal design of the proposed HPS

4.3.2 Implementation of Whale Optimization Algorithm

The optimal design of the proposed HPS was also carried out using Whale Optimization Algorithm (WOA). The algorithm was also implemented to obtain a system design with the least life cycle cost and total environmental pollution. Whale optimization algorithm is known for its intelligence capability when solving multi-dimensional optimization problems as it is inspired by the intelligent movement of humpback whales when hunting for their prey.

In the implementation of the WOA technique, the objective function of equation (4.5) determines the target prey, which is assumed as the whale with the best fitness value in the population. Hence, the objective function along with the design constraints and design variables are all defined in the algorithm. At the inception stage, a number of humpback whales (W_p) is generated according to expression (4.32).

$$W_p = \left[W_1, W_2, W_3, W_{4,} \ldots\ldots W_N\right] \tag{4.32}$$

where N represents the number of whales in the population.

The basic parameters of the WOA technique such as such as the coefficient vectors (A) and (C), movement probability (p_m) and randomization number (l) are all initialized. The design variables which represent the capacity of each sub-systems of the proposed HPS are defined in a vector named whale as described using expression (4.33) as follows.

$$W_i = \left|N_{bif} \times P_{bif}, N_{WTG} \times P_{E(w)}, N_{BES} \times P_{BES}, P_{dg1}.h_1, P_{dg2}.h_2, P_{dg3}.h_3\right| \tag{4.33}$$

where W_i represents the ith whale in the population.

Basically, each humpback whale denotes a possible combination of the design variables. Hence, for every possible combination, the fitness of each whale is simulated to check its feasibility based on the objective function of equation (4.5) subject to the various design constraints presented in section 4.2.2 of this study. At the simulation stage, the mathematical expression of the various components of the proposed HPS described in section 3.1 is obviously used to predict their output in each time period (one hour) based on the weather data of the proposed location. The simulation is also run for 30 years to evaluate the performance of each whale in the population. The simulation process simultaneously estimates the life cycle cost and the total environmental pollution of for every possible combination of the design variables.

At the optimization stage, the fitness value of each whale also referred to as search agent is evaluated based on the encoded objective function. At each iteration, the algorithm undergo three basic steps. The first step is to randomly search for the whale with the best fitness value within the population and identify it as the target prey using expression (2.9). The target prey in this study is denoted using equation (4.34) as follows.

$$W_i^* = \left| N_{bif} \times P_{bif}, N_{WTG} \times P_{E(w)}, N_{BES} \times P_{BES}, P_{dg1}.h_1, P_{dg2}.h_2, P_{dg3}.h_3 \right| \quad 4.34$$

Once the target prey has been identified, the next step is for other search agents in the population to encircle the target prey using expression (2.11). The final step of the algorithm is to attack the prey using the bubble-net attacking method described in expression (2.12). During the attacking process, the movement probability (p_m) is used to decide either to encircle the target prey using the shrinking or spiral method. The position of each search agents in the population is then updated relative to the position of the target prey using expression (2.11). In order to obtain the optimal solution, the target prey is randomly selected in the population at every iteration using expression (2.14) until the maximum number of iteration is reached or convergence is achieved. The search agent with the same position as the target prey represents the optimal design of the proposed HPS. That is, the system design with the least life cycle cost and total environmental pollution. The flowchart of the optimization process is depicted in Figure 4.3.

4.3.3 Implementation of Giza Pyramid Construction Algorithm

The optimal design of the proposed HPS was also done using a recently introduced meta-heuristic optimization technique known as Giza Pyramid Construction (GPC) algorithm. The algorithm was applied to obtain a system design or configuration with the least life cycle cost and total environmental pollution. In its application to series of optimization problems including the optimal design of hybrid power system, GPC has been reported to have efficient capability in dealing with complex and multi-dimensional optimization problems such as the optimal design of the HPS proposed in this study.

In a similar way to other optimization algorithms proposed in this study, the objective function, the design constraints, design variables, are all defined in the algorithm. At the initialization stage, a population of workers or stone blocks denoted using G_p, is randomly generated and distributed evenly in a search medium according to expression (4.35) as follows.

$$G_p = \left[G_1, G_2, G_3, G_{4,} \ldots\ldots\ldots G_N \right] \quad 4.35$$

where N represents the number of workers or stone blocks in the population.

In addition to that, the basic parameters of the GPC algorithm such as such as the gravity (g), ramp angle (θ), frictional force (f_f), co-efficient of frictional force (μ_f), as well as the substitution probability (ψ_k) were all set at the inception stage. The design variables which represent the capacity of each sub-systems of the proposed system are defined in a vector named worker or stone block as described using expression

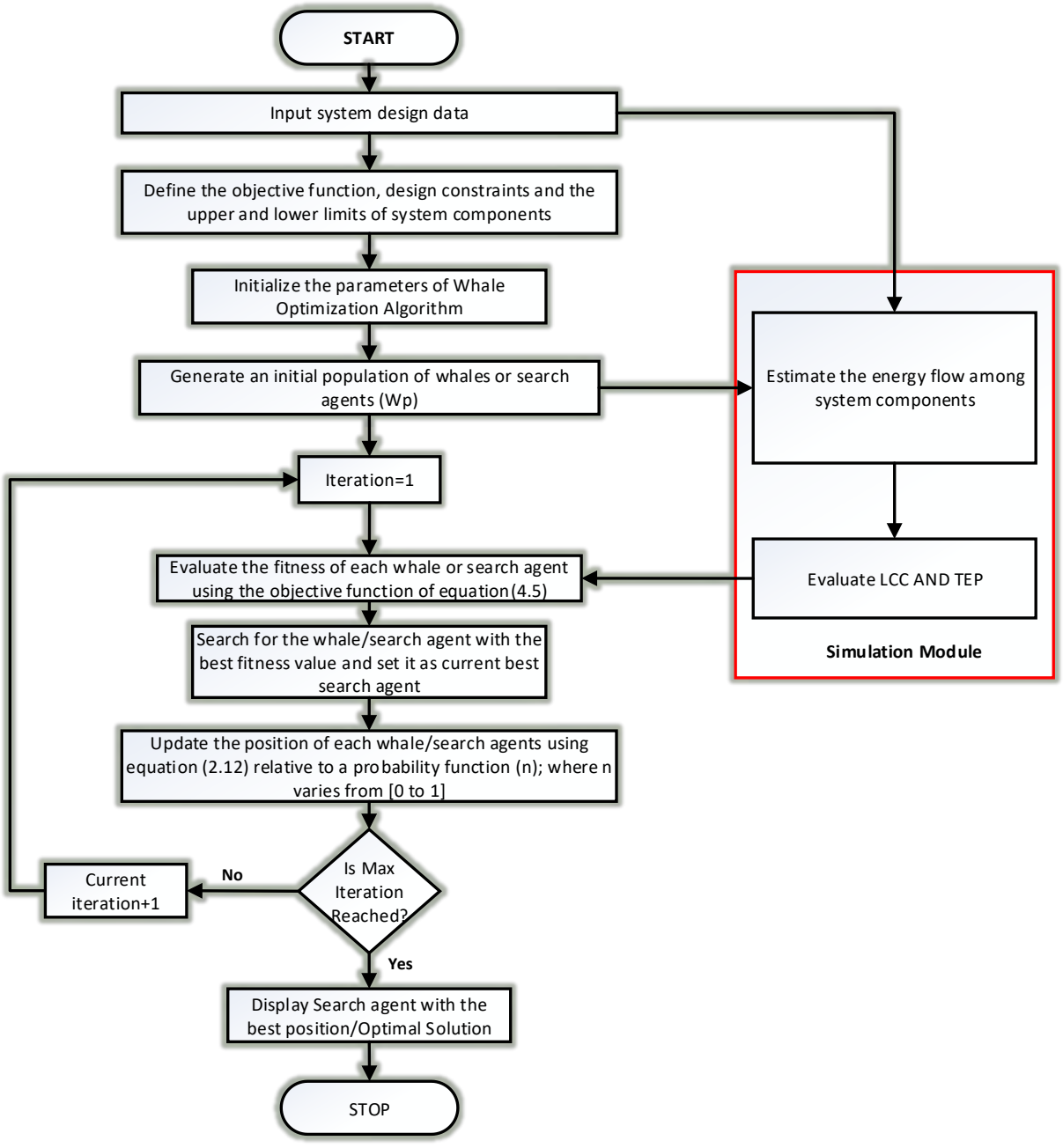

Figure 4.3: Flowchart of Whale Optimization Algorithm for optimal design of the proposed HPS

(4.36) as follows.

$$G_i = \left| N_{bif} \times P_{bif}, N_{WTG} \times P_{E(w)}, N_{BES} \times P_{BES}, P_{dg1}.h_1, P_{dg2}.h_2, P_{dg3}.h_3 \right| \quad 4.36$$

where G_i is the ith worker or stone block in the population.

According to expression (4.36), every worker or stone block in the population represents a possible configuration of the proposed HPS. The stone block or worker with the best fitness value (least life cycle cost and total environmental pollution) is the optimal solution to the optimization problem. Subsequently, the fitness value of each worker or stone block in the population is simulated to check its feasibility based on the objective function of equation (4.5) subject to the various design constraints described in section 4.2.2 of this study. At the simulation stage, the mathematical expression of the various components of the proposed HPS described in section 3.1 is also used to predict their output in each time period (one hour) based on the weather data of the proposed location. The simulation is also run for 30 years to evaluate the performance of the stone blocks or workers in the population. The simulation process simultaneously estimates the life cycle cost and the total environmental pollution for each worker or stone block and sends it to the optimization module for evaluation.

At the optimization stage, individual worker or stone block is evaluated based on its fitness value. The fitness value of individual stone block or worker in the search space is estimated and the worker or stone block with the best fitness value is set as a as Pharaoh's agent in the search space and saved in an external module. The selected Pharaoh's agent guides the worker in updating their movement in order to displace the stone block. Each of the worker in the population continues to adjust their movement until there is a displacement in the stone block. In relation to the optimal design process, each worker is made to search for the optimal system design in accordance with the number of design variables.

At the updating stage, the amount of stone block displacement or the amount of worker's movement is calculated using expressions (2.18) or (2.19) respectively. Hence, new positions of each stone block or workers are estimated using expression (2.20). Furthermore, the probability of substituting a tired worker among the population during the search process is investigated using equation (2.21). Finally, new fitness value is calculated for each worker and compared with the fitness of the current Pharaoh's agent in the external module. Once a worker with a fitness value that dominates the current Pharaoh's agent in the external module is identified, it is set as new Pharaoh's agent. The process is repeated for each iteration until there is no worker with a better fitness value than the current Pharaoh's agent or maximum number of iterations has been reached. The current Pharaoh's agent with the best fitness value (the least life cycle cost

and total environmental pollution) represents the optimal design of the proposed HPS. The flowchart of the optimization process is depicted in Figure 4.4.

4.4 Performance metrics

In addition to evaluating the performance of the optimization algorithms using the set optimization objectives (life cycle cost and total environmental pollution), the quality of the generated solutions using each of the proposed optimization techniques were numerically measured using their respective worst and best fitness score. The mean, median and standard deviation of the fitness score of each technique are obtained at each iteration of the optimization process, this numerical analysis is important to properly evaluate the performance of the optimization algorithms and determine the most efficient technique for the optimal design of the proposed HPS.

While the mean and median were estimated using basic statistical expressions, the standard deviation and efficiency of each of the reported optimization techniques are estimated using equation (4.37) and (4.38) respectively.

$$S_d = \sqrt{\frac{\sum_{i=1}^{n_r}\left(F_{v(b)} - \vec{F}_v\right)}{n_r - 1}} \tag{4.37}$$

$$Efficiency = \frac{F_{v(b)} - F_{v(w)}}{F_{v(b)}} \times \frac{100}{1} \tag{4.38}$$

where S_d represent the standard deviation, $F_{v(b)}$, represents the best fitness value/score, $F_{v(w)}$ represents the worst fitness value/score, $\vec{F}_v$ represents the mean fitness value/score and n_r represents the number of runs.

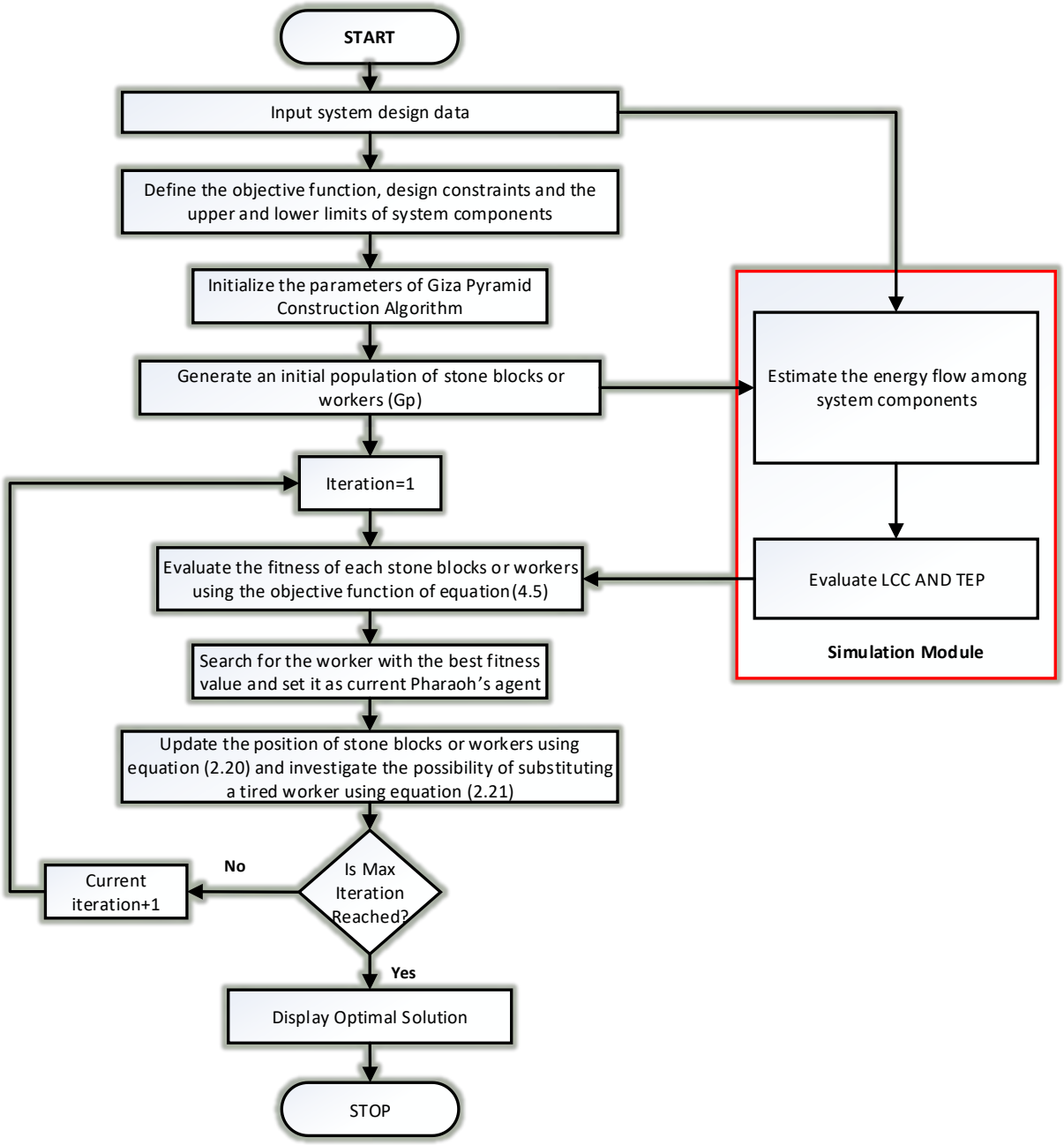

Figure 4.4: Flowchart of Giza Pyramid Construction for optimal design of the proposed HPS

CHAPTER FIVE
RESULTS AND DISCUSSION

5.1 Results of feasibility assessment of the studied area

The results of the feasibility assessment of the studied area for the implementation of the proposed HPS model is presented and discussed in this section. It provides basic information such as the hourly load demand data, as well as solar and wind resources of the area used in evaluating the performance of the proposed optimization algorithms. These information are necessary in making unbiased decision on the viability of the energy generating system.

5.1.1 Load demand of the studied area

A remote community located in the northern part of Nigeria is selected as the studied area for implementation of the proposed HPS model. The community, named Bara is located at ($8^0412^{'}$N, $9^0373^{'}$ E), Kirfi Local Government area of Bauchi state, Nigeria, and has a population of over 500 residents. The feasibility assessment of the area was done to determine the hourly load demand of the community; this information was obtained via a survey conducted among some of the residents in the community for a period of three days. The hourly energy usage profile of the community for one day period is depicted in Figure 5.1, with an average hourly demand of 17.29 kw/h. Based on the information contained in Figure 5.1, the hourly peak load demand of the area occurred around 10:00 pm when most of the residents are back in their respective houses. It decreases slightly until midnight when it reaches the minimum load demand. It remains almost constant for up to six hours when most of the residents are asleep and rises steadily in the early mornings when the residents are awake, until it reaches its peak value again in the evening.

5.1.2 Solar resource data of the studied area

The hourly solar resource data of the community for a period of one year is obtained from an existing database of the Power Data Access Viewer of National Aeronautic and Space Administration (NASA). Based on the existing data database, the average hourly temperature of the selected village is 21.14 ^0C, and the average hourly horizontal solar irradiance is 246 $W/m^2/day$. The direct horizontal solar irradiance was used as inputs to estimate the irradiance reaching the back side of the module. The hourly solar irradiance reaching the front side of the module, temperature and clearness index of the studied area for a period of two days are depicted in Figures 5.2, 5.3a and 5.3b respectively. It can be deduced from Figure 5.2a that the peak solar irradiance occurred from 11:00 pm to 1:00 pm in the afternoon, which can be regarded as the peak sunshine hours. However, during the early mornings and late evenings, the solar irradiances at these periods are observed to be at their minimum value due to the intermittent nature of the solar energy resources.

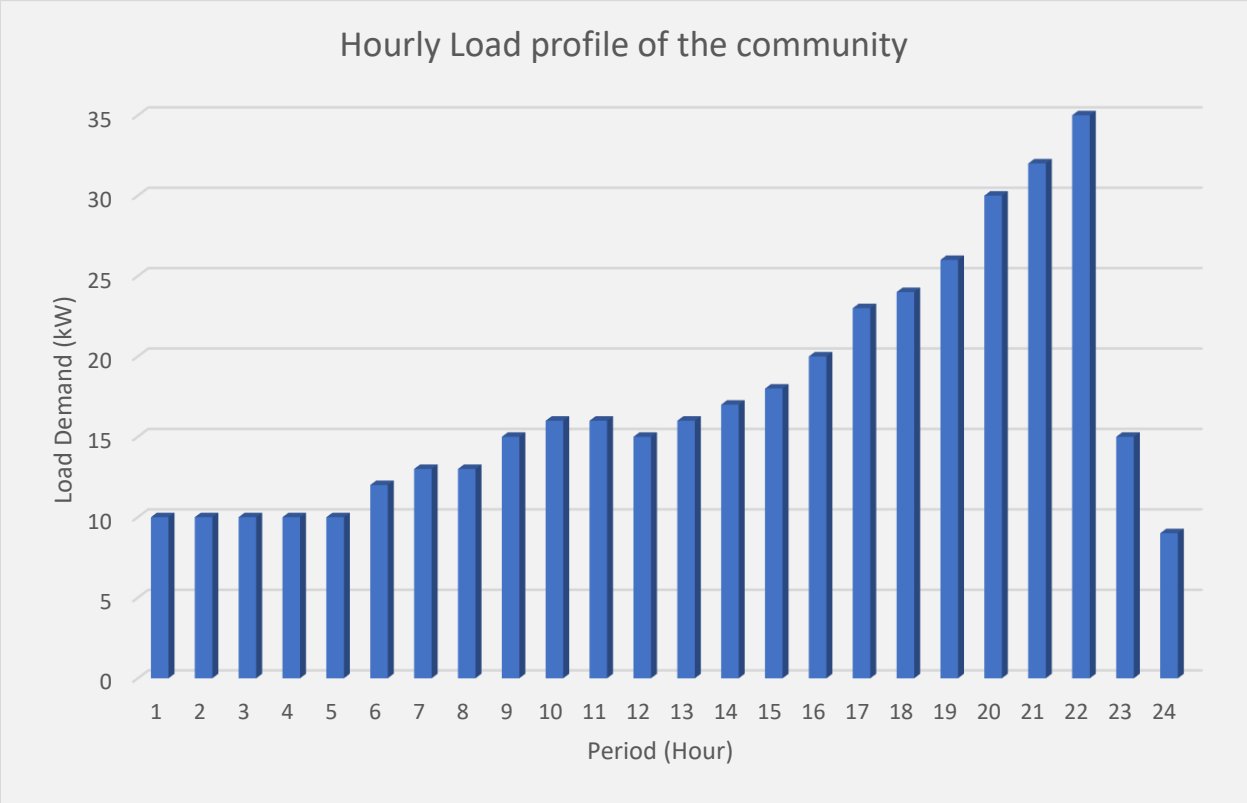

Figure 5.1: Hourly load profile of the studied area

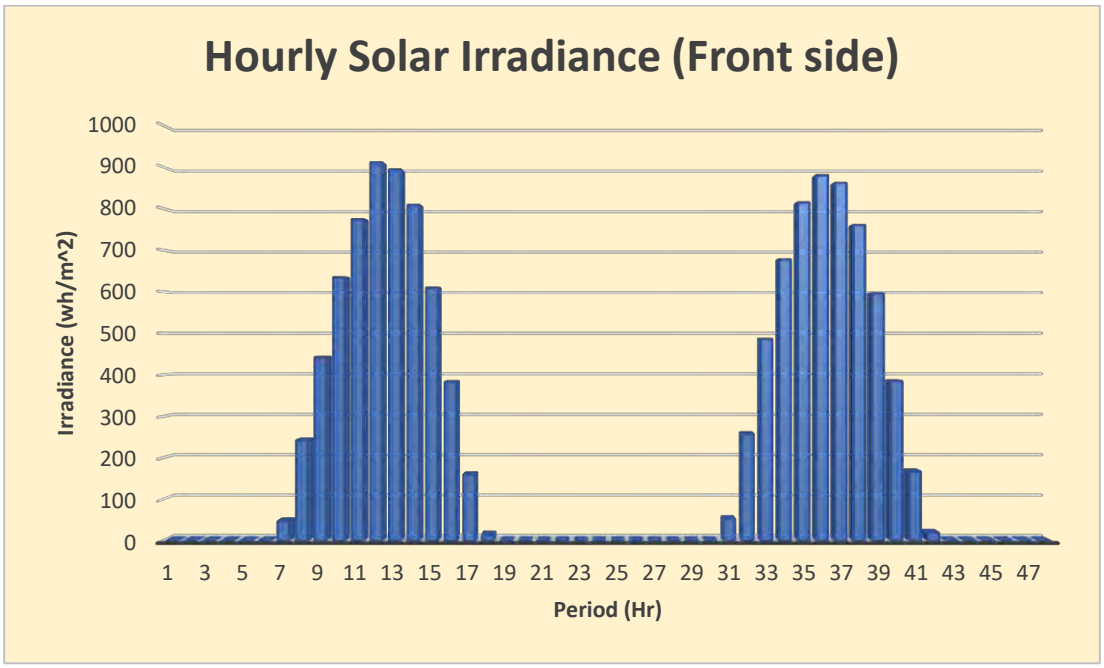

Figure 5.2: Hourly solar irradiance of the studied area

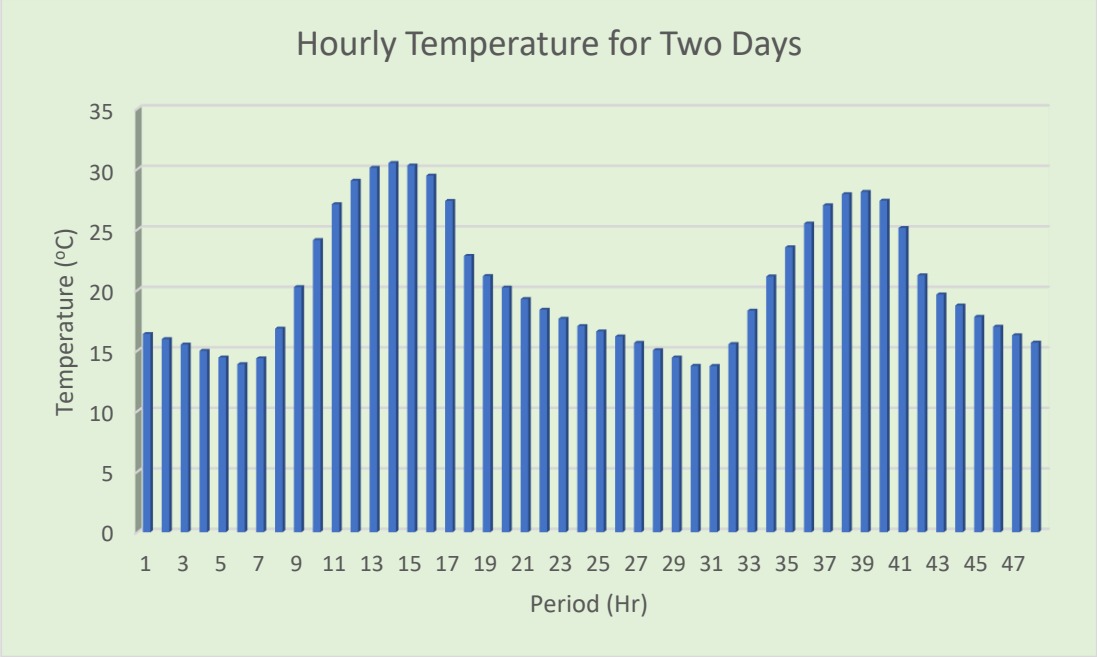

Figure 5.3a: Hourly temperature of the studied area

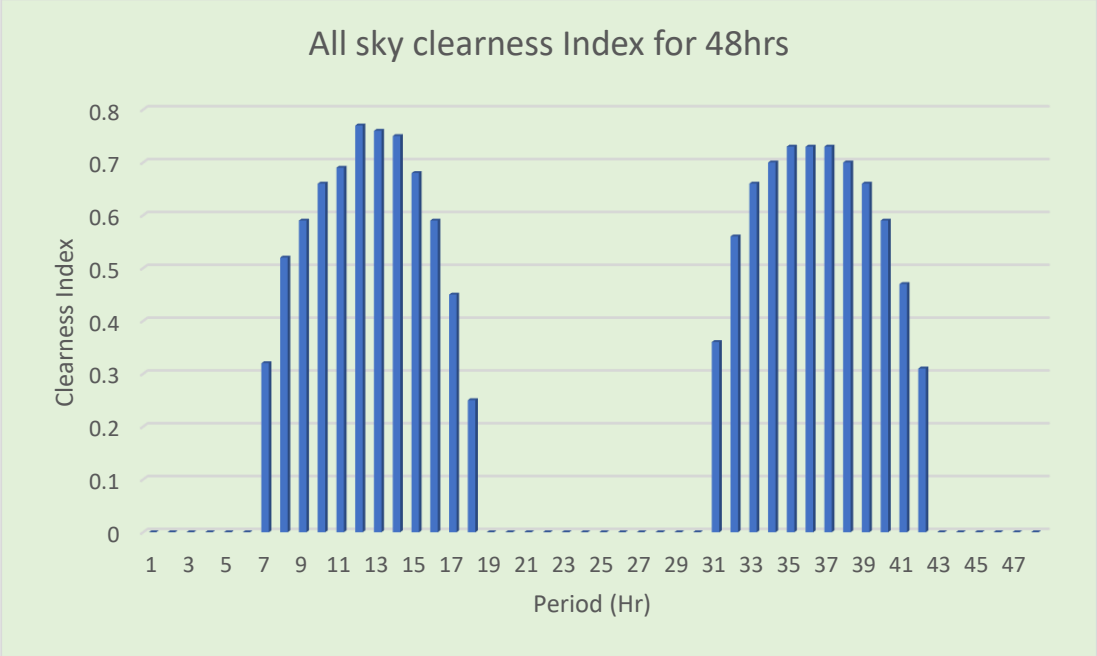

Figure 5.3b: Hourly clearness index of the studied area

5.1.3 Wind resource data of the studied area

Similar to the solar resource data, the hourly wind resource data of the community for a period of one year was also obtained from an existing database of the Power Data Access Viewer of NASA. Based on the existing data database, the hourly wind speed of the studied area for a period of two days is as shown in Figure 5.4. It can be observed from Figure 5.4 that the studied area is moderately blessed with wind energy resources. The maximum wind speed of the area was observed at the early hours of the morning, while the minimum wind speed occur at the hourly hours of the evening. The average hourly wind speed of the community at a height of 30 m above the ground is 4.7 ms^{-1}. However, for simulation purposes, the cut in speed was set at 3.4 ms^{-1} while the cut-out speed was set at 20 ms^{-1}.

5.2 Simulation results of major system components

The output waveforms results obtained from the simulation models of bifacial module and wind turbine generator discussed in chapter three (3) of this study are presented in this section. The solar irradiance and wind speed data of the studied area is used in simulating the performance of the bifacial module and wind turbine generator for a period of forty-eight (48) hours; the corresponding power output waveforms obtained for each component are subsequently presented.

5.2.1 Power output of bifacial PV module

The power output produced by each of the orientation states of the bifacial PV module are presented in this sub-section. The estimated irradiance reaching the front and back side of the module for both orientation states is used in simulating the power produced by each orientation states.

The power output waveform obtained for the front and back sides of the module for the horizontal north-south orientation state is as depicted in Figure 5.5. From the result of Figure 5.5, it was observed that an increase in the value of the solar irradiance reaching the front and back sides of the module leads to a corresponding increase in the magnitude of the power output and vice versa.. The maximum power generated from the front side of the module is approximately 250 W, while the maximum power generated from the back side of the module is approximately 50 W. Consequently, the total power output waveform of a single bifacial PV module in the horizontal north-south orientation state is depicted in Figure 5.5b. It can be deduced from the plot of Figure 5.5b that the total maximum power extractable from a single bifacial module in horizontal north-south orientation state is approximately 300 W.

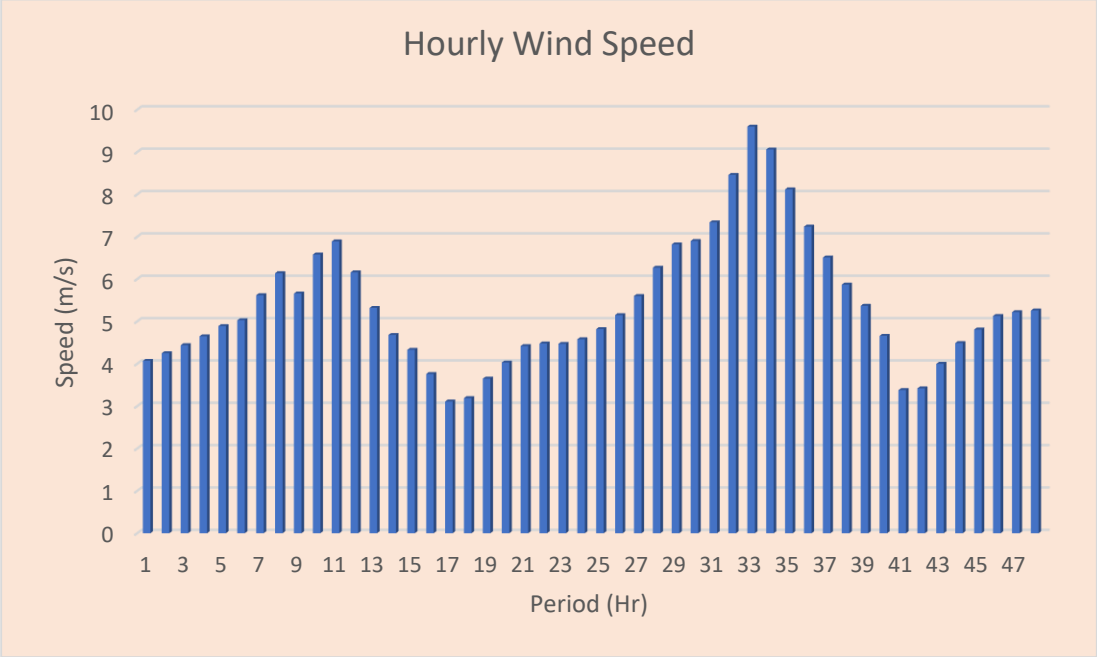

Figure 5.4: Hourly wind speed of the studied area

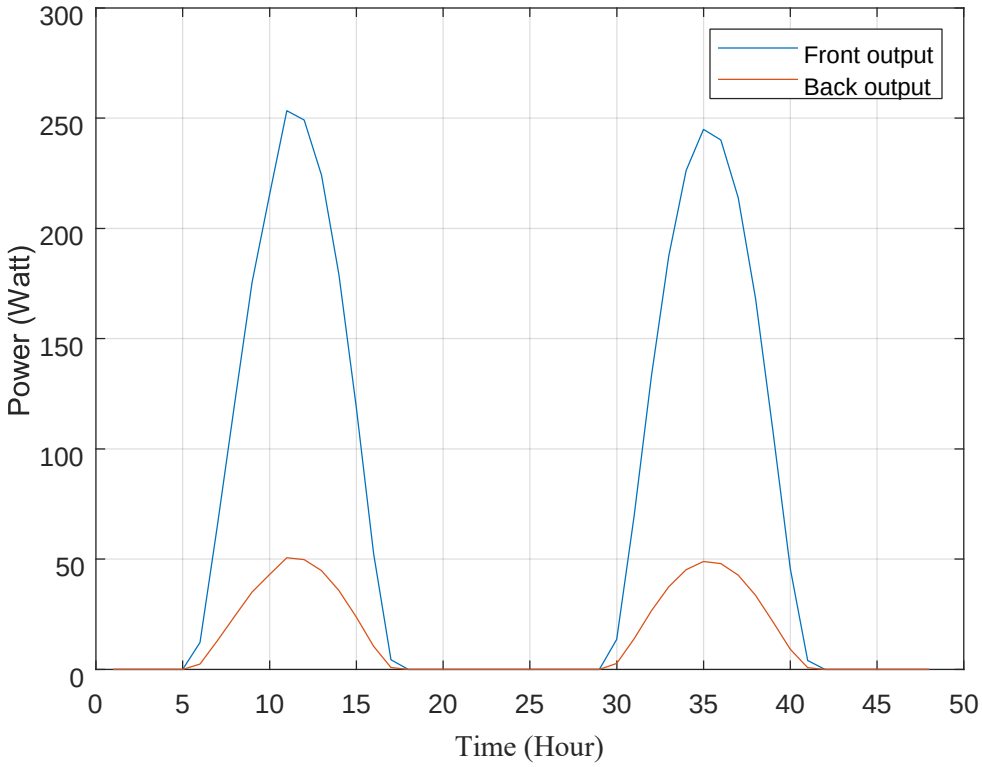

Figure 5.5a: Hourly power output of the front and back side of bifacial PV in horizontal north-south orientation state

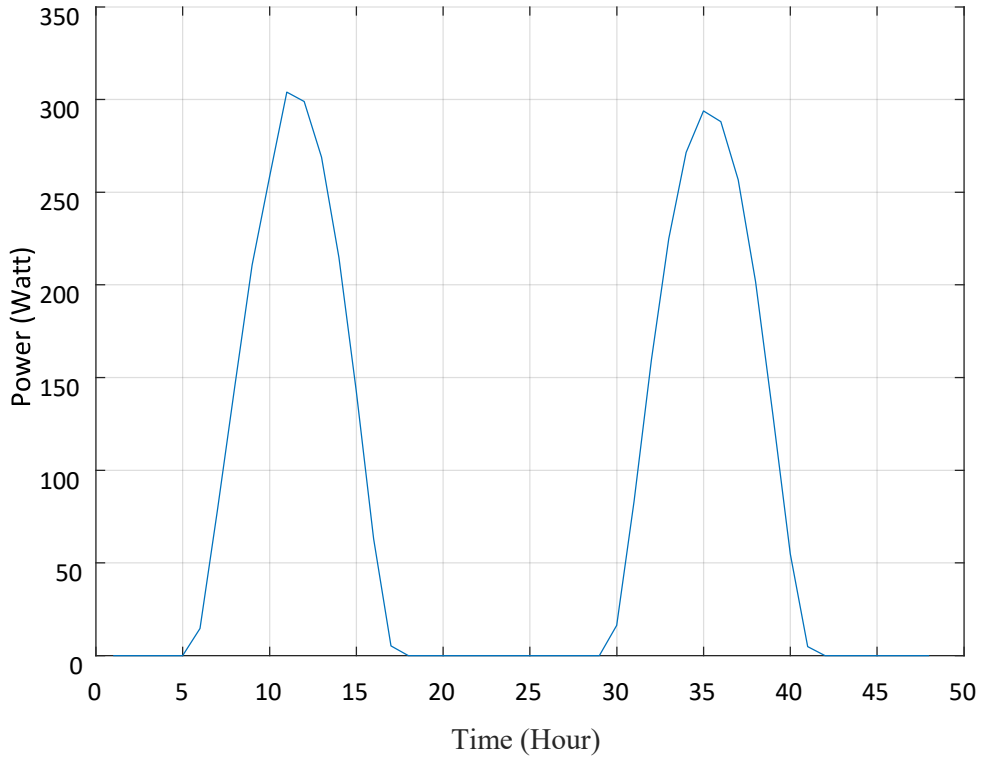

Figure 5.5b: Hourly total output power of a bifacial PV in horizontal north-south orientation state

For the vertical east-west orientation, the power output waveform obtained from the front and back sides of the module is as depicted in Figure 5.6. From the result of Figure 5.6a, the maximum power output observed for the front side of the module is approximately 250 W, while the maximum power out from the back side of the module is approximately 75 W. It was observed that the maximum power output produced from the back side of the module for vertical east-west orientation state is 33.33 % more than the maximum power produced from the back side of the module for horizontal north-south orientation state. The total power output waveform of a single bifacial PV module in the horizontal north-south orientation state is depicted in Figure 5.6b. It can be deduced from the plot of Figure 5.6b that the total maximum power extractable from a single bifacial module in the vertical east-west orientation state is approximately 330 W.

5.2.2 Power output of wind turbine generator

The power output waveform for a single wind turbine generator for a period of forty-eight (48) hours is depicted in Figure 5.7. It was observed that the power output produced by the wind turbine fluctuates throughout the day due to the intermittent nature of the resources at the studied area. The maximum and minimum power outputs for the first day is approximately 275 W and 40 W respectively; while the maximum and minimum power output for the second day is approximately 450 W and 60 W respectively.

5.3 Simulation results of optimal system design

Simulation results of optimal system design, as well as the different combination of energy generating sources considered to meet the energy demand of the studied area are presented and discussed in this section. The techno-economic specifications of each of the sub-system of the proposed HPS, which also serve as part of the input data used for system design and optimization are presented in Table 5.1 to Table 5.5, while the parameters of the optimization algorithms are given in Table 5.6a to Table 5.6c. In order to demonstrate the viability of the proposed HPS for electrification of the studied area in terms of LCC and TEP, the optimal design of the system is carried out for three different hybrid configurations using each of the proposed optimization techniques; and the results are compared with a system configuration of three (3) split genset only. The optimal design of the system was carried out for each orientation state of the bifacial module. The various combination of energy systems considered are categorized under four (4) case studies as follow.

i. Case one: Three split genset only
ii. Case two: Hybrid Wind turbine/Battery/split genset
iii. Case three: Hybrid Bifacial PV/Battery/split genset
iv. Case four: Hybrid Bifacial PV/wind turbine/Battery/split genset

In each case, the LCC and TEP of each of the various combination are noted for comparison.

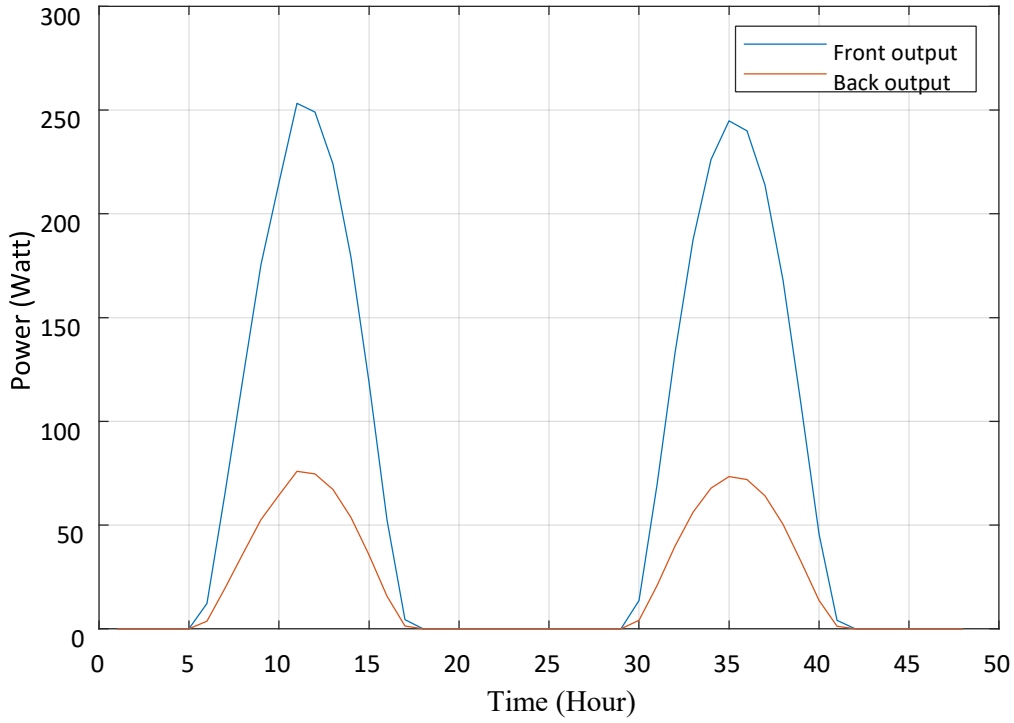

Figure 5.6a: Hourly power output of the front and back side of bifacial PV in the vertical-east west orientation state

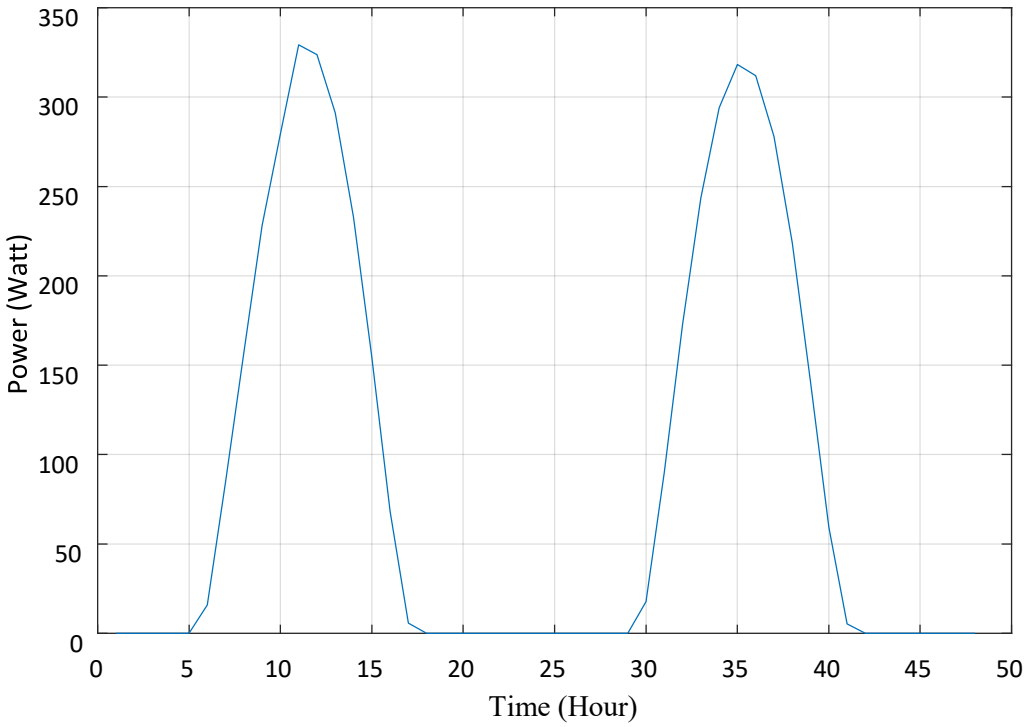

Figure 5.6b: Hourly total output power of a bifacial PV in the vertical east-west orientation state

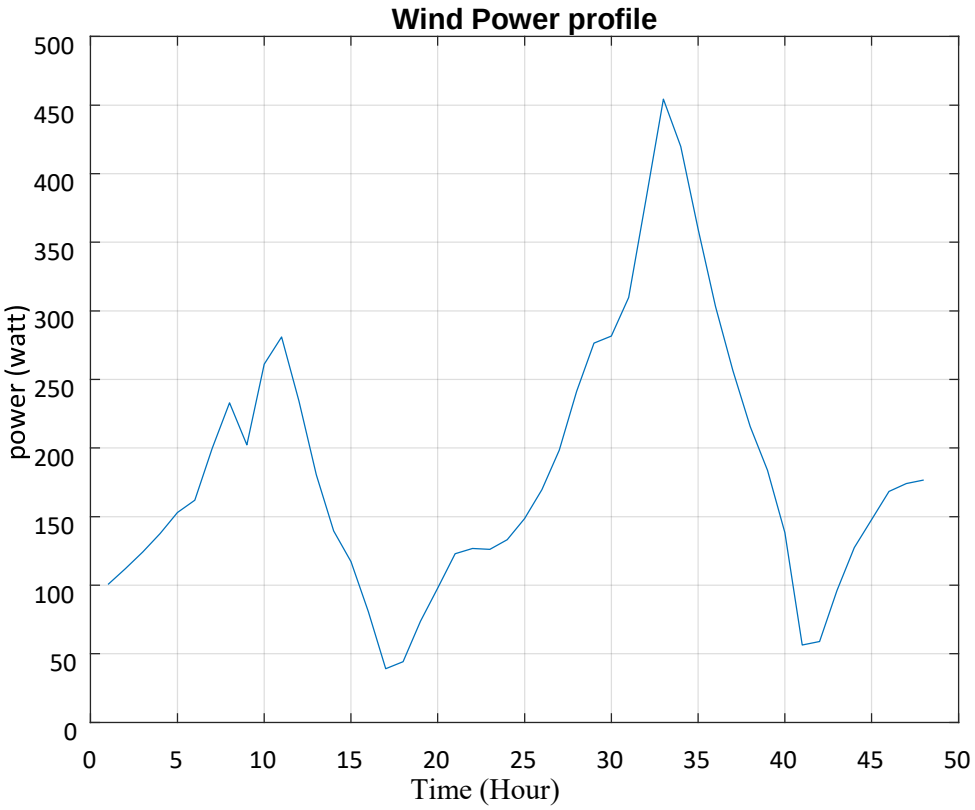

Figure 5.7: Hourly power output of the wind turbine

Table 5.1: Techno-economic specification of the bifacial PV module

Parameters	Values	Unit
Model	PERC JKM385M-72H-BDVP	N/A
Maximum power	385	Watts
Maximum power current	9.56	A
Maximum power voltage	40.3	V
Module efficiency	18.81	%
Module temperature	45	^0C
Module dimension	$2031 \times 1008 \times 30$	mm
Temperature co-efficient	0.35	$\%/^0C$
Bifaciality factor	75	%
Initial cost	500	US Dollars
Annual O & M	1	%
Interest rate	9	%
Inflation rate	6	%
Lifecycle	30	Years

Table 5.2: Techno-economic specifications of the wind turbine

Parameters	Values	Unit
Model	SI-172625	N/A
Rated power	500	Watts
Rated voltage	24	V
Rotor diameter	1.44	m
Cut-in wind speed	2.5	m/s
Rated wind speed	10	m/s
Cut-out wind speed	30	m/s
Hub height	12	meters
Efficiency	96	%
Initial cost/unit	500	US Dollars
Annual O & M/unit	3	%
Interest rate	9	%
Inflation rate	6	%
Lifecycle	25	Years

Table 5.3: Techno-economic specifications of the battery storage system

Parameters	Values	Unit
Model	KJ24360	N/A
Size of a single battery	360	Ah
Autonomy days	3	Days
Depth of discharge (DOD)	80	%
Minimum state of charge (soc)	20	%
Battery efficiency	90	%
Inverter efficiency	80	%
Battery voltage	24	V
Initial cost/unit	300	US Dollars
Annual O & M cost	3	%
Replacement cost/unit	300	US Dollars
Interest rate	9	%
Inflation rate	6	%
Lifecycle	10	Years

Table 5.4: Techno-economic specifications of each of the DG unit

Parameters	Values	Unit
Model	K20U-IV-SDMO	N/A
Rated Power of each DG unit	20	kVA
Rated voltage	220	V
Initial Cost/kW	500	US Dollars
Annual O & M/kW	40	US Dollars
Replacement cost/kW	500	%
Fuel Cost/litre	1.5	US Dollars
Interest rate	9	%
Inflation rate	6	%
Lifecycle	10	Years
Power Factor	0.85	N/A

Table 5.5: Emission factors of harmful gases

Gases	Emission rate (g/kWh)
CO_2	697
SO_2	0.5
NO_x	0.22

Table 5.6a: Optimization Parameters of Firefly Algorithm

S/N	Parameter	Value
1	Maximum Iteration	20
2	Number of Fireflies	50
3	Light absorption coefficient	100
4	Randomness factor	100
5	Initial attractiveness	50
6	Light Intensity	30

Table 5.6b: Optimization Parameters of Whale Optimization Algorithm

S/N	Parameter	Value
1	Maximum Iteration	20
2	Number of Search Agents	50
3	Coefficient Vector A	100
4	Coefficient Vector C	100
5	Movement Probability	0.5
6	Randomness Parameter	10

Table 5.6c: Optimization Parameters of Giza Pyramid Construction

S/N	Parameter	Value
1	Maximum Iteration	20
2	Number of stone blocks or workers	50
3	Acceleration due to gravity	100
4	Ramp angle	100
5	Substitution probability	0.5
6	Frictional force	6
7	Co-efficient of frictional force	10

5.3.1 Case one: Three split genset only

For case study one, a system configuration of three split genset only is used to supply the energy demand of the studied area for a period of 30 years. The split genset is sized to supply 120 % of the village's hourly peak energy requirement, with each DG unit contributing 40 % of the total capacity of the split genset. The operational behavior of the system for a period of 48 hours and ten (10) days is as shown in Figures 5.8a and 5.8b respectively. It can be inferred from Figure 5.8a that each DG unit in the split genset configuration is operated based on the hourly energy requirement of the area. Moreover, the performance in terms of LCC and TEP are presented in Table 5.7, a LCC of $1,830,752.40 and TEP of 3,241,987 kg are recorded for the entire lifespan of the system. The high emission value indicates the environmental implications of using diesel generator only in meeting the energy requirement of the area.

5.3.2 Case two: Hybrid Wind turbine/Battery/split genset

For Case study two, three energy generating sources comprising of wind turbine generator, battery energy system and the split genset are considered to meet the energy demand of the studied area for a period of 30 years. The optimal design of the hybrid system is done using each of the proposed optimization techniques. The performance of the system in terms of the evaluated values of LCC and TEP of each optimization techniques are noted for comparison. The optimal design results of each optimization techniques are presented in the following sub-sub-sections.

5.3.2.1 Optimal design result using Firefly Algorithm (FA)

Firefly Algorithm (FA) is implemented to determine the most appropriate components combination of the system configuration; a combination of 97 wind turbines and 21 batteries, in addition with the operational hours of the split genset are selected by the algorithm to meet the energy demand of the studied area. The operational behavior of the system for a period of forty-eight (48) hours and ten (10) days is depicted in Figures 5.9a and 5.9b respectively. It can be inferred from Figure 5.9a that the SOC of the battery increases slightly in accordance with an increase in the hourly power output of the wind turbine between the hours of 12:00 midnight and 1:00pm until it reaches its peak value at 2:00 pm. It decreases gradually from 2:00 pm until 4:00 pm when it reaches it minimum DOD. At this period, the split genset is switched on to cover the deficit in energy. The performance in terms of LCC and TEP are presented in Table 5.8a. A LCC of $1,518,636.76 and TEP of 2,564,611.03 kg were recorded for the hybrid system using FA. The high values of LCC and TEP for the configuration indicates a high commitment of the split genset during the lifespan of the system

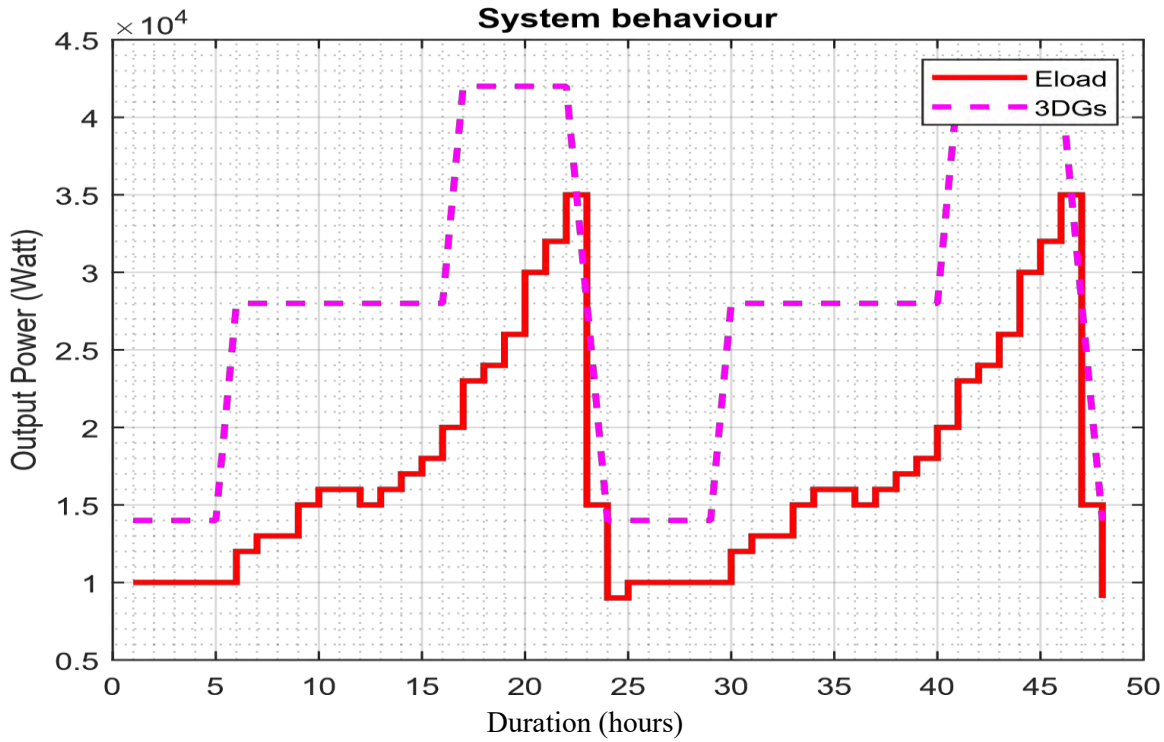

Figure 5.8a: System behavior of three split genset configuration for a period of 48 hours

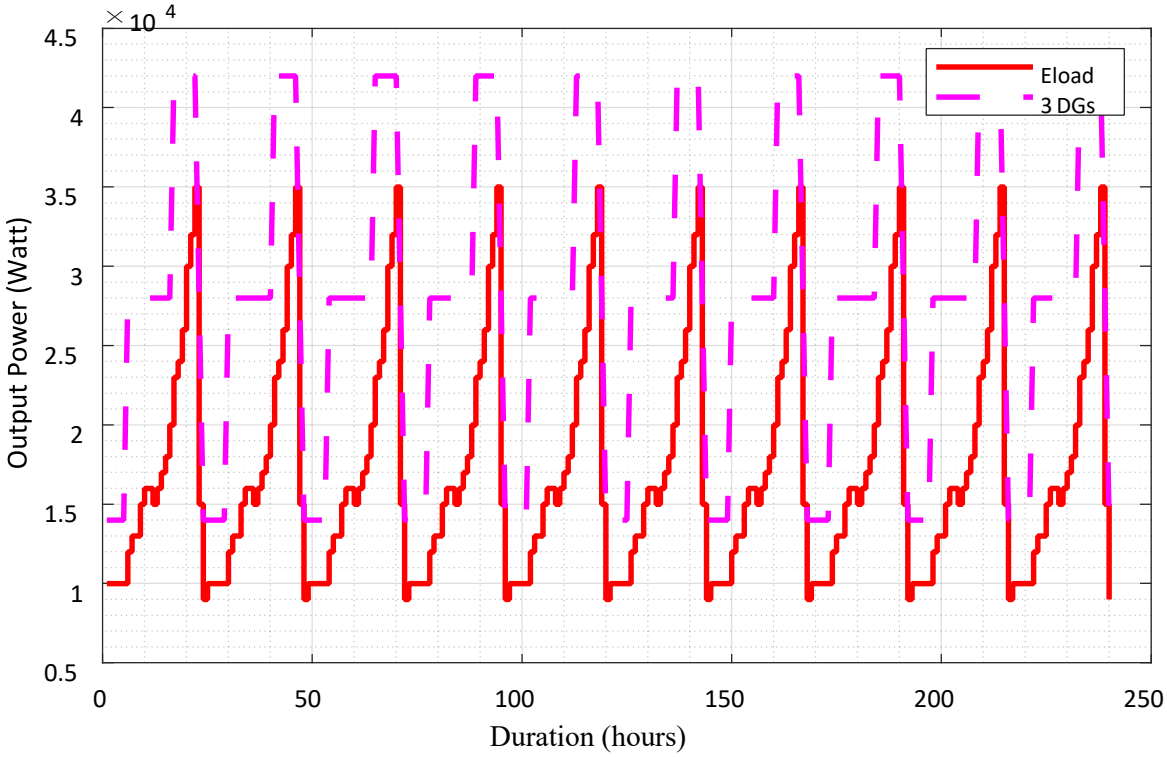

Figure 5.8b: System behavior of three split genset configuration for a period of 10 days

Table 5.7: Performance of three split genset configuration

Particulars	System Configuration		
	Three Split Genset Only		
	DG unit 1	DG unit 2	DG unit 3
Hours of Operation	262,800	197,100	65,700
LCC	**$1,830,752.40**		
TEP	**3,241,987.00 kg**		

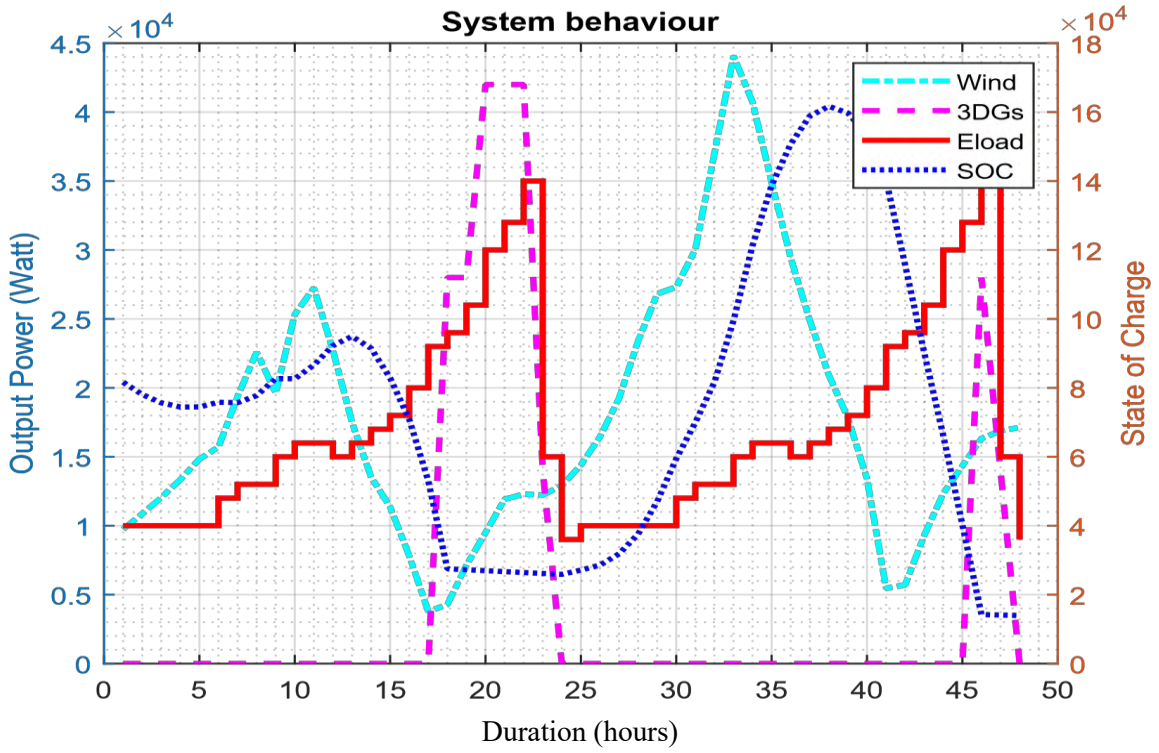

Figure 5.9a: System behavior of wind/battery/split genset configuration using FA for a period of 48 hours

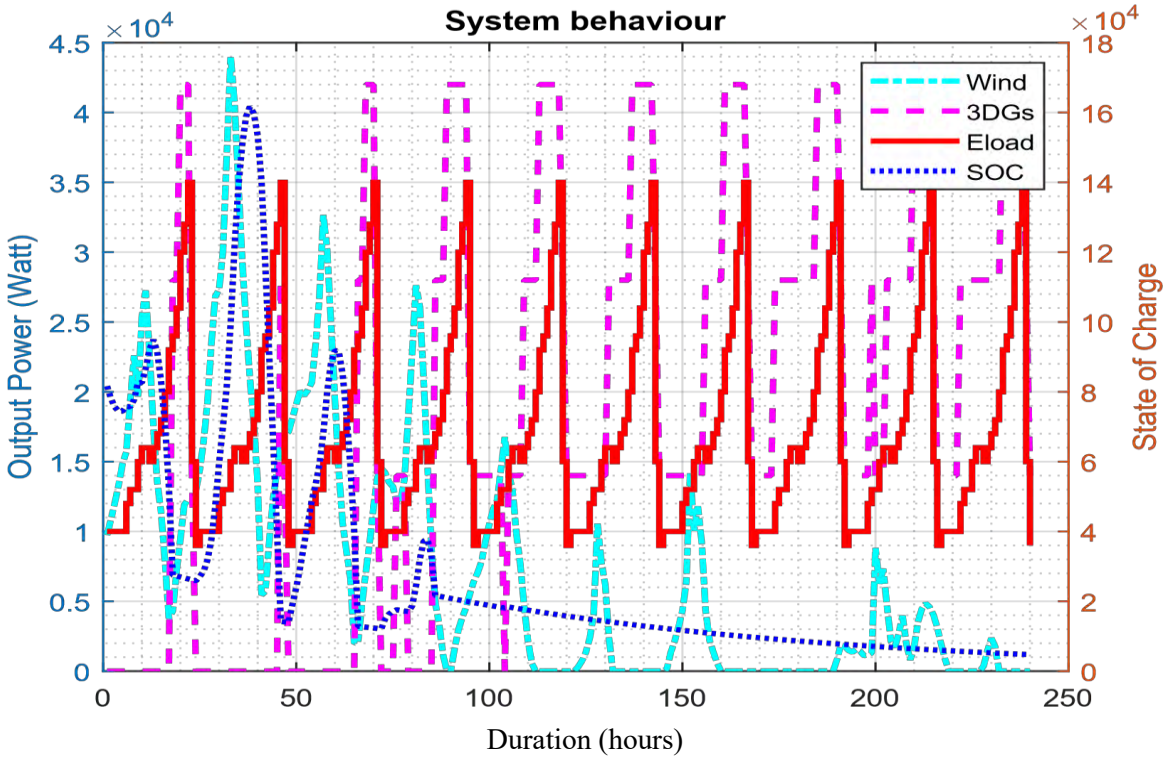

Figure 5.9b: System behavior of wind/battery/split genset configuration using FA for a period of 10 days

Table 5.8a: Performance of the hybrid wind/battery/split genset system using FA

Particulars	System Configuration				
	Hybrid Wind Turbine/Battery/Split Genset				
Components	Wind Turbine	Battery	Split Genset		
Number of Components	97	21	DG unit 1	DG unit 2	DG unit 3
Hours of Operation	N/A	N/A	251156	135107	55844
LCC			**$1,518,636.76**		
TEP			**2,564,611.03 kg**		

Table 5.8b: Performance of the hybrid wind/battery/split genset system using WOA

Particulars	System Configuration				
	Hybrid Wind Turbine/Battery/Split Genset				
Components	Wind Turbine	Battery	Split Genset		
Number of components	122	32	DG unit 1	DG unit 2	DG unit 3
Hours of Operation	N/A	N/A	237903	127852	53452
LCC			**$1,468,379.89**		
TEP			**2,431,264.13 kg**		

Table 5.8c: Performance of the hybrid wind/battery/split genset system using GPC technique

Particulars	System Configuration				
	Hybrid Wind Turbine/Battery/Split Genset				
Components	Wind Turbine	Battery	Split Genset		
Number of Components	111	32	DG unit 1	DG unit 2	DG unit 3
Hours of Operation	N/A	N/A	244859	130997	54679
LCC			**$1,495,747.57**		
TEP			**2,490,797.21 kg**		

5.3.2.2 Optimal design result using Whale Optimization Algorithm (WOA)

Whale Optimization Algorithm (WOA) is also implemented to determine the most appropriate components combination of the system configuration for case study two. A combination of 122 wind turbines and 32 batteries, in addition with the operational hours of the split genset are selected by the algorithm to meet the energy demand of the studied area. The operational behavior of the system for a period of forty-eight (48) hours and ten (10) days is depicted in Figures 5.10a and 5.10b respectively. It can be inferred from Figure 5.10a that there is an increase in the SOC of the battery due to an increase in the power output of the wind turbine, it increases betwthe hours of 1:00 am and 1:00 pm until it reaches its peak value at 2:00 pm. It decreases gradually from 2:00 pm until 8:00 pm when it reaches it minimum DOD. At this period, the split genset is switched on to cover the deficit in energy. The performance in terms of LCC and TEP are presented in Table 5.8b. A LCC of $1,468,379.89 and TEP of 2,431,264.13 kg are also recorded for the hybrid system using WOA. The corresponding reduction in the values of LCC and TEP as compared to that of FA technique indicates a decrease in the hourly commitment of the split genset during the lifespan of the system.

5.3.2.3 Optimal design result using Giza Pyramid Construction (GPC) Algorithm

The GPC technique is also implemented to determine the most appropriate components combination of the system configuration for case study two. A combination of 111 wind turbines and 32 batteries, in addition with the operational hours of the split genset are selected by the algorithm to meet the energy demand of the studied area. The operational behavior of the system for a period of forty-eight (48) hours and ten (10) days is depicted in Figures 5.11a and 5.11b respectively. It can be seen from Figure 5.11a that there is an increase in the SOC of the battery due to an increase in the power output of the wind turbine, it increases betwthe hours of 1:00 am and 1:00 pm until it reaches its peak value at 2:00 pm. It decreases gradually from 2:00 pm until 6:00 pm when it reaches it minimum DOD. At this period, the split genset is switched on to cover the deficit in energy. The performance in terms of LCC and TEP are presented in Table 5.8c. A LCC of $1,495,747.57 and TEP of 2,490,797.21 kg are as well recorded for the hybrid system using GPC. Similar to WOA technique, the corresponding reduction in the values of LCC and TEP as compared to that of FA technique indicates a decrease in the commitment of the split genset during the lifespan of the system.

5.3.3 Case three: Hybrid Bifacial PV/Battery/split genset

For Case study three, three energy generating sources comprising of bifacial PV module, battery energy system and the split genset are considered to meet the energy demand of the studied area for a period of 30 years. In order to evaluate the performance of the bifacial PV on optimal system design, the two

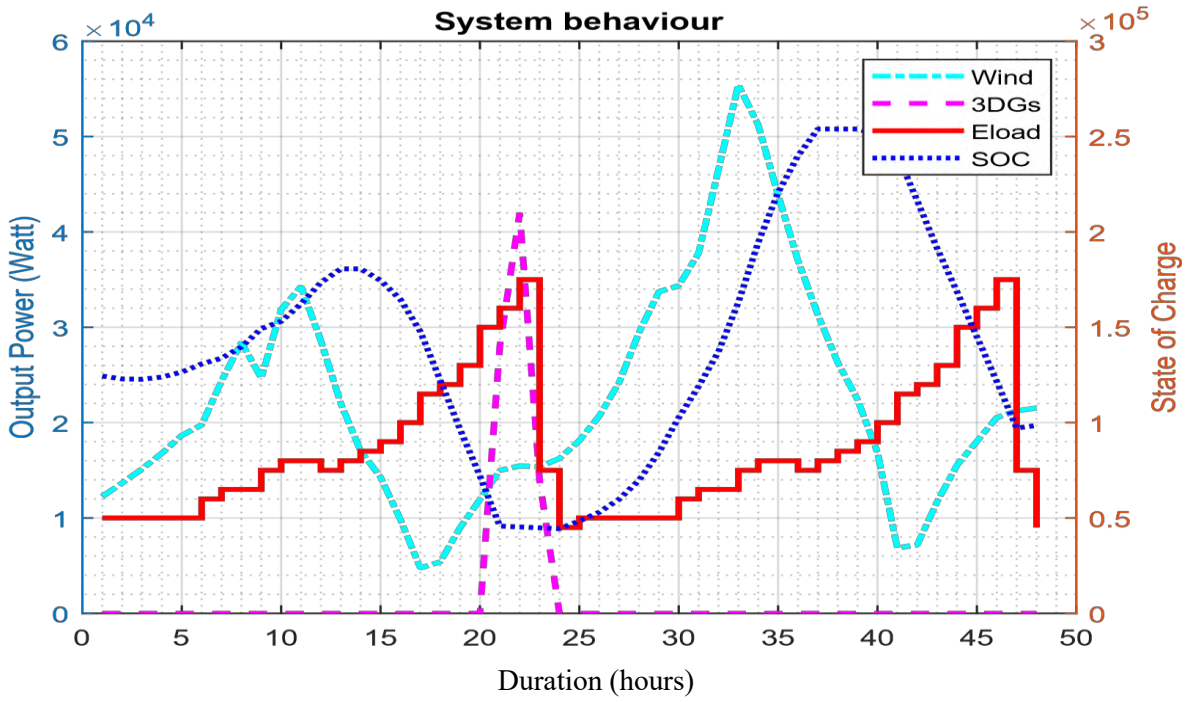

Figure 5.10a: System behavior of wind/battery/split genset configuration using WOA for a period of 48 hours

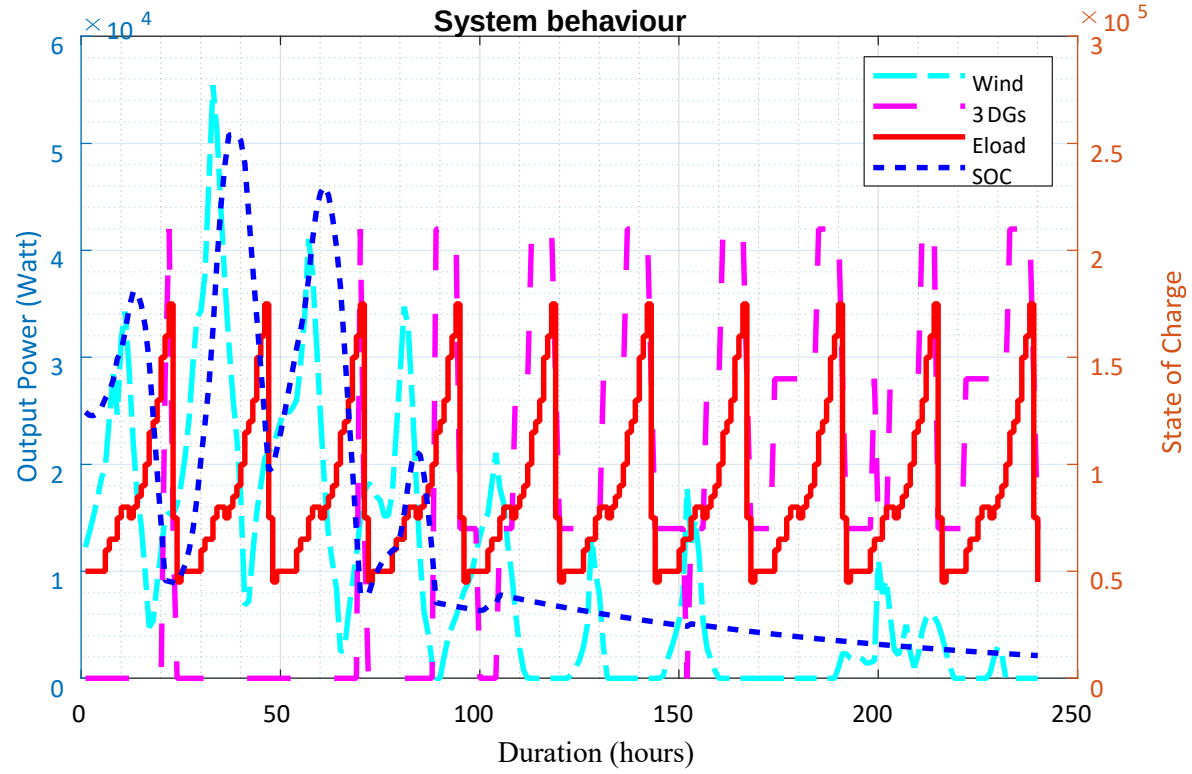

Figure 5.10b: System behavior of wind/battery/split genset configuration using WOA for a period of 10 days

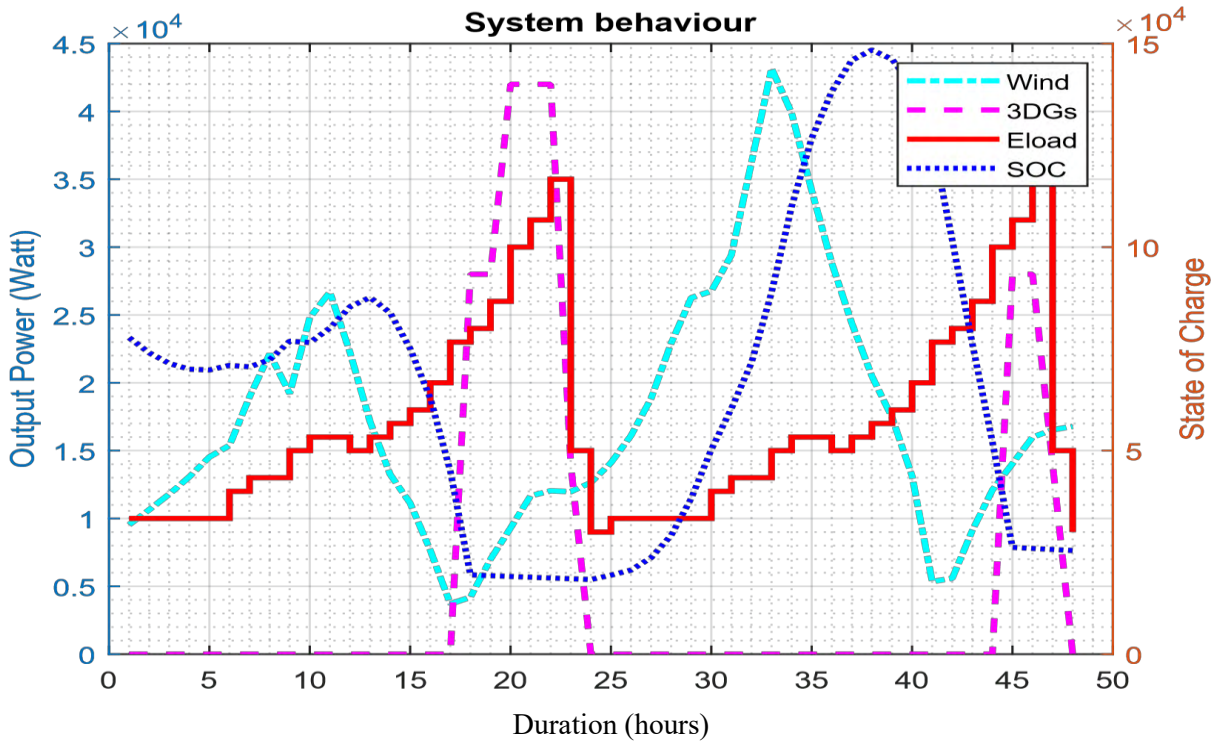

Figure 5.11a: System behavior of wind/battery/split genset configuration using GPC for a period of 48 hours

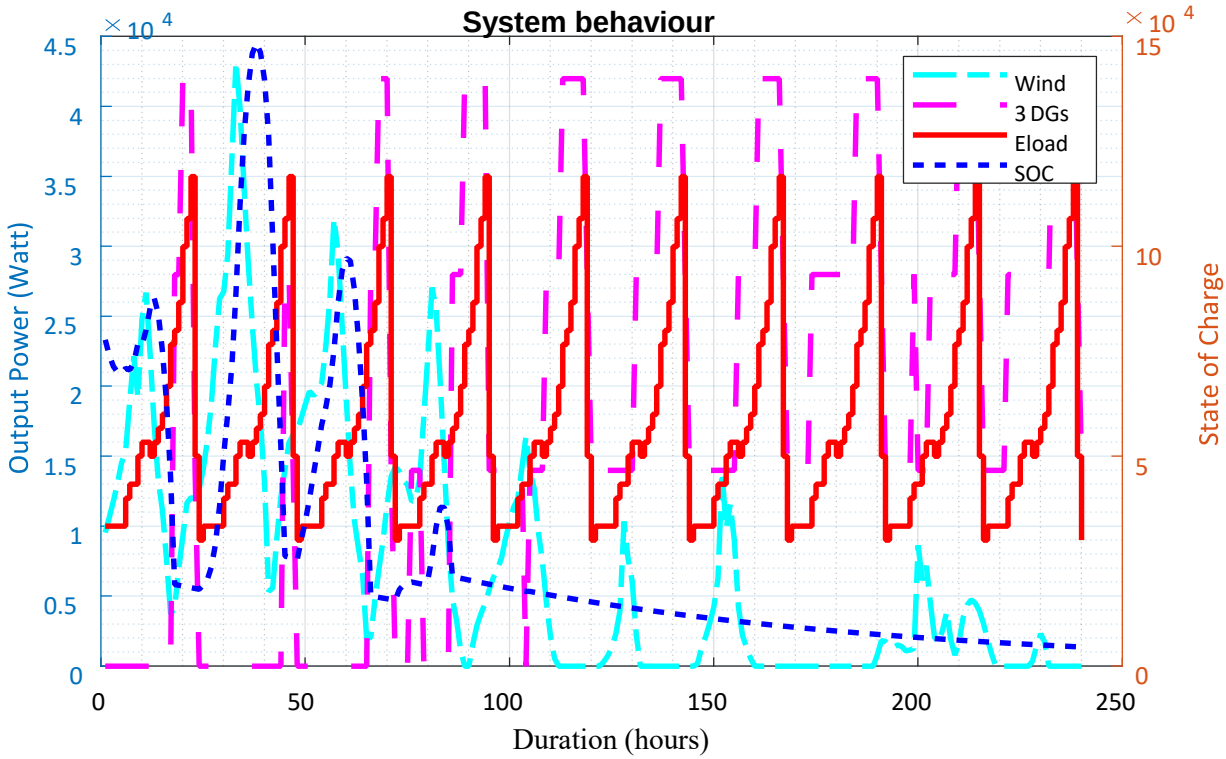

Figure 5.11b: System behavior of Wind/battery/split genset configuration using GPC for a period of 10 days

orientation states are considered in the optimization process. The optimal design of the hybrid system is also carried out using each of the proposed optimization techniques. The performance of the system in terms of the evaluated values of LCC and TEP of each optimization techniques are noted for comparison. The optimal design results of each optimization techniques are presented in the following sub-sections.

5.3.3.1 Optimal design results using Firefly Algorithm (FA)

Firefly Algorithm (FA) is implemented to determine the most appropriate components combination of the system configuration for each orientation states. For vertical east-west orientation state, a combination of 152 bifacial PV modules and 29 batteries, in addition with the operational hours of the split genset are selected by the algorithm to meet the energy demand of the studied area. The operational behavior of the system for a period of forty-eight (48) hours and ten (10) days is depicted in Figures 5.12a and 5.12b respectively. It can be inferred from Figure 5.12a that there is an increase in the SOC of the battery between the hours of 9:00 am and 1:00 pm. The increase in the SOC of the battery can be attributed to daytime period when there is abundance of solar radiation. It reaches its peak value at 2:00 pm, and decreases gradually from that period until 8:00 pm when it reaches its minimum DOD. At this period, the split genset is switched on to cover the deficit in energy.

The performance in terms of LCC and TEP are presented in Table 5.9a. A LCC of $859,936.15 and TEP of 1,326,259.09 kg are recorded for the hybrid system using FA. It is observed that there was a significant drop in the values of LCC and TEP for this configuration as compared to the wind turbine/battery/split genset configuration. This reduction can be attributed to lesser commitment of the split genset during the lifespan of the system.

Moreover, the algorithm is also implemented for the horizontal north-south orientation state; a combination of 161 bifacial PV modules and 31 batteries, in addition with the operational hours of the split genset are selected to meet the energy demand of the studied area. The operational behavior of the system for a period of forty-eight (48) hours and ten (10) days is depicted in Figures 5.13a and 5.13b respectively. The operational behavior of the system for the horizontal north-south orientation is quite similar to that of the vertical east-west orientation. The only difference is the increase in the number of bifacial PV modules and battery units selected by the algorithm. The performance in terms of LCC and TEP are presented in Table 5.9b. A LCC of $879,568.94 and TEP of 1,346,022.01 kg are recorded for the hybrid system using FA. It is observed that there is a slight increase in the values of LCC and TEP obtained for the horizontal north-south orientation state as compared to the vertical east-west orientation state. The increment may be attributed to the difference in the additional energy produced by the module for both orientation states.

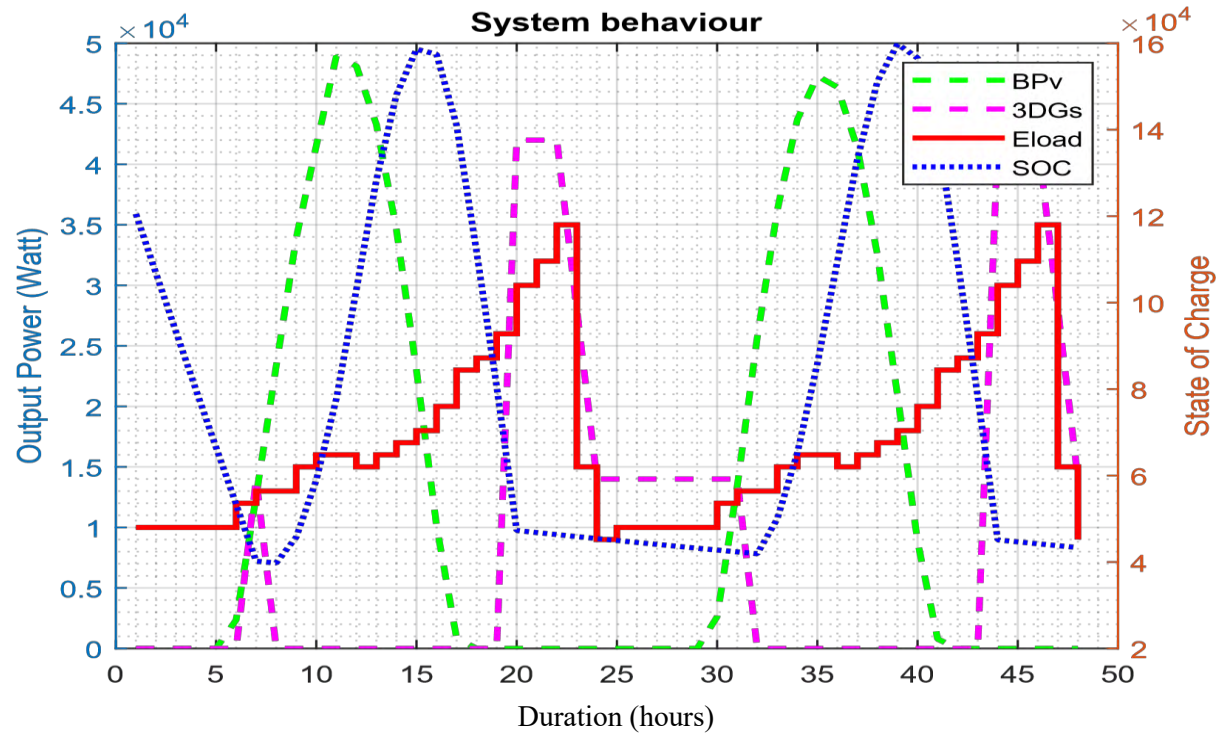

Figure 5.12a: System behavior of bifacial PV/battery/split genset configuration using FA for a period of 48 hours for vertical east-west orientation state

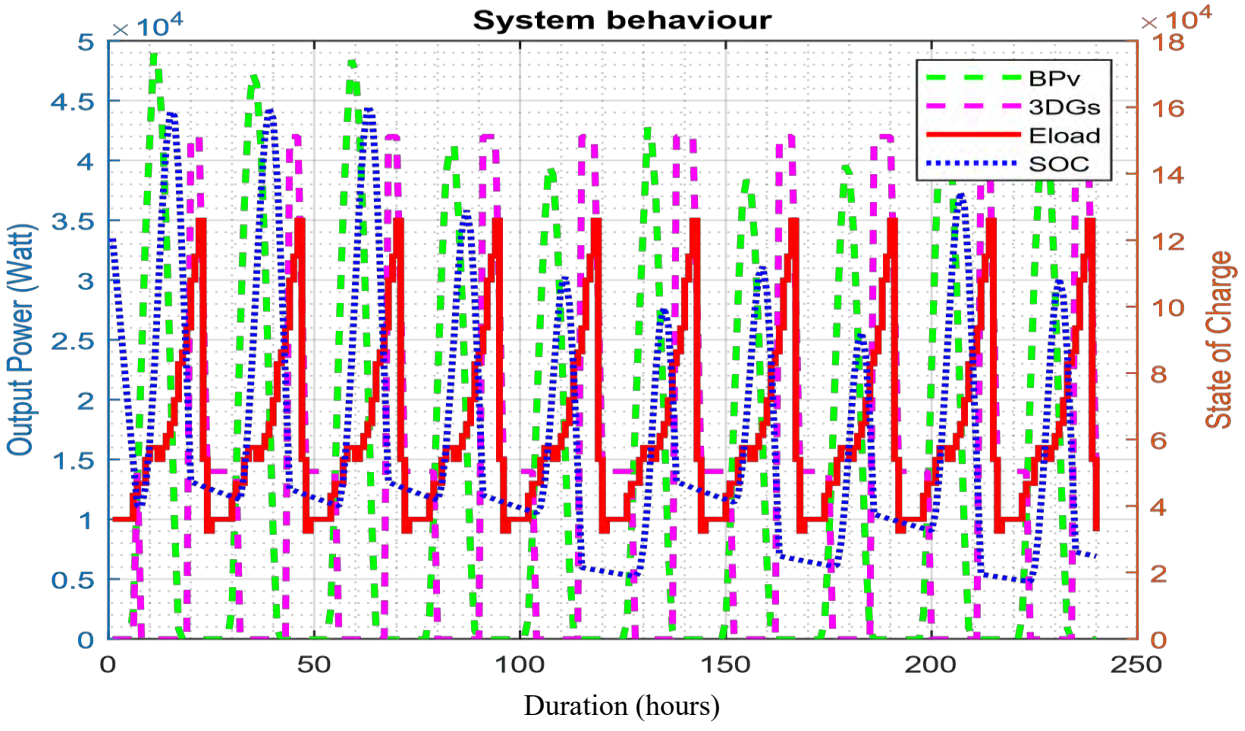

Figure 5.12b: System behavior of bifacial PV/battery/split genset configuration using FA for a period of 10 days for vertical east-west orientation state

Table 5.9a: Performance of the hybrid bifacial PV/battery/split genset system using FA for vertical east west orientation state

Particulars	System Configuration				
	Hybrid Bifacial PV/Battery/Split Genset				
Components	Bifacial PV	Battery	Split Genset		
Number of Components	152	29	DG unit 1	DG unit 2	DG unit 3
Hours of Operation	N/A	N/A	113819	65234	26560
LCC			**$859,936.15**		
TEP			**1,326,259.09 kg**		

Table 5.9b: Table 5.3a: Performance of the hybrid bifacial PV/battery/split genset system using FA for horizontal north-south orientation state

Particulars	System Configuration				
	Hybrid Bifacial PV/Battery/Split Genset				
Components	Bifacial PV	Battery	Split Genset		
Number of components	161	31	DG unit 1	DG unit 2	DG unit 3
Hours of Operation	N/A	N/A	113819	68645	29367
LCC			**$879,568.94**		
TEP			**1,346,022.01 kg**		

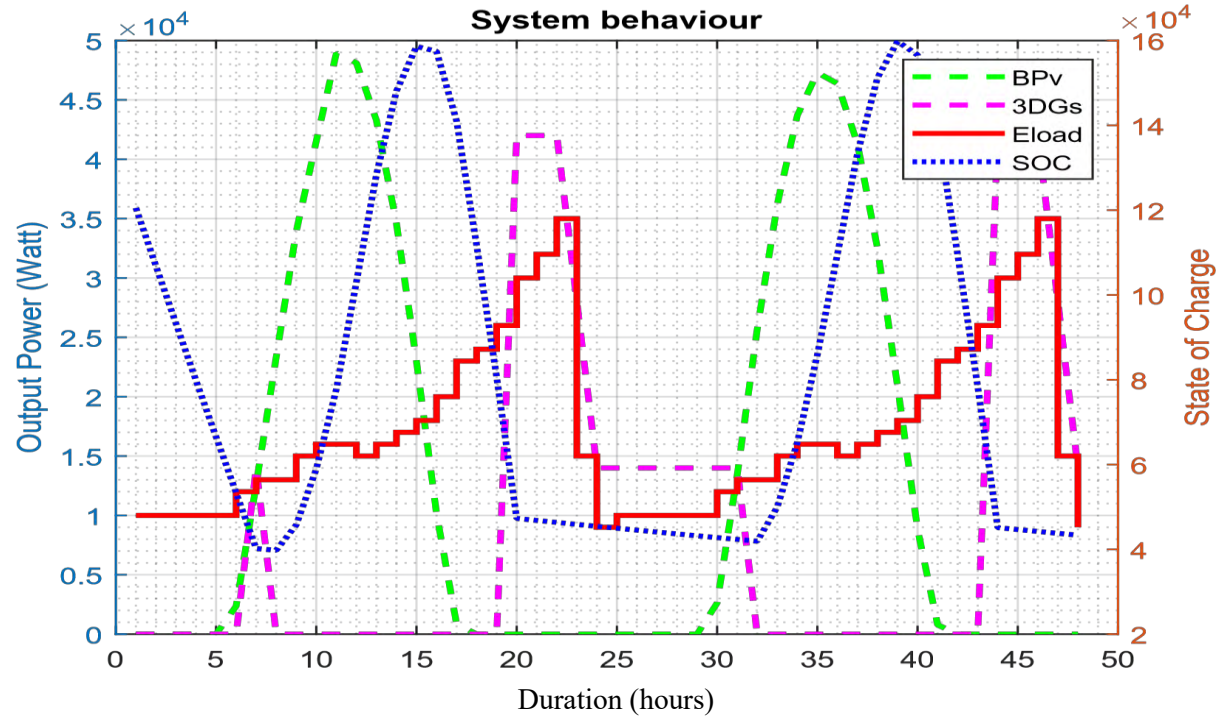

Figure 5.13a: System behavior of bifacial PV/battery/split genset configuration using FA for a period of 48 hours for horizontal north-south orientation state

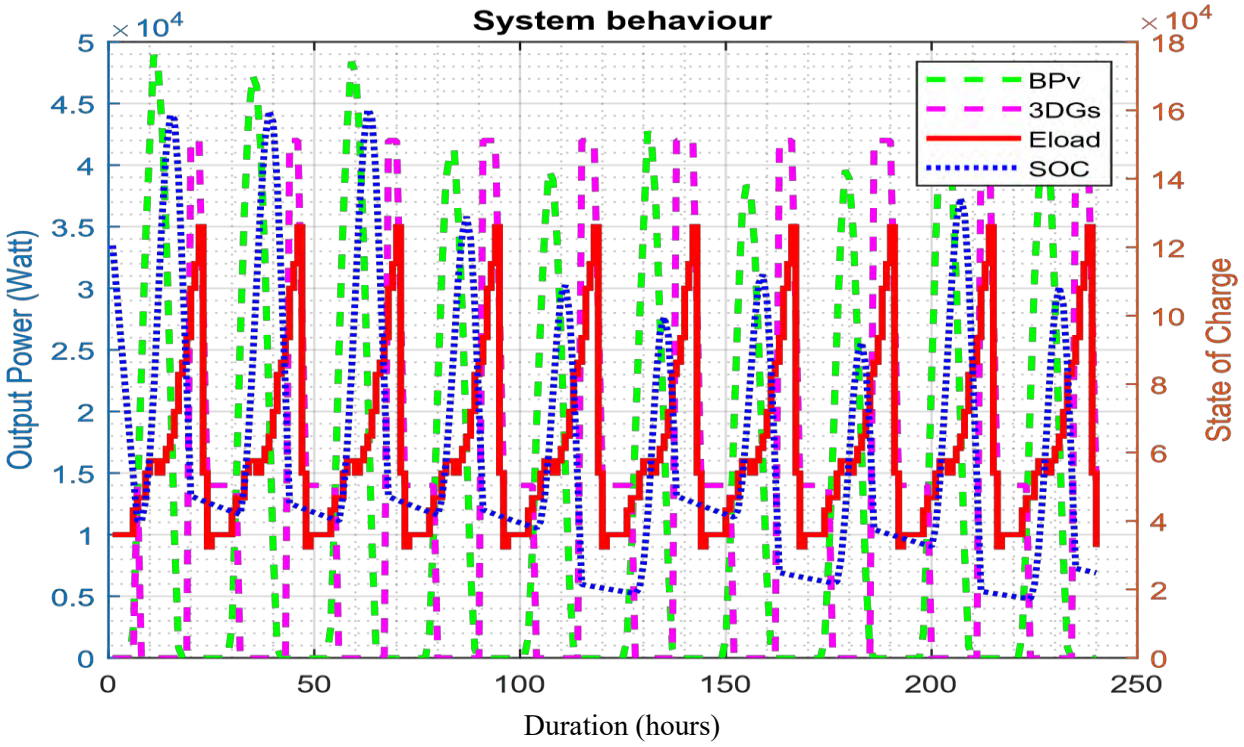

Figure 5.13b: System behavior of bifacial PV/battery/split genset configuration using FA for a period of 10 days for horizontal north-south orientation state

5.3.3.2 Optimal design results using Whale Optimization Algorithm (WOA)

The Whale Optimization Algorithm (WOA) is also implemented to determine the most appropriate components combination of the system configuration for each orientation states. For vertical east-west orientation state, a combination of 160 bifacial PV modules and 30 batteries, in addition with the operational hours of the split genset are selected by the algorithm to meet the energy demand of the studied area. The operational behavior of the system for a period of forty-eight (48) hours and ten (10) days is depicted in Figures 5.14a and 5.14b respectively. It can be inferred from Figure 5.14a that there is an increase in the SOC of the battery between the hours of 7:00 am and 2:00 pm. The increase in the SOC of the battery can be attributed to daytime period when there is abundance of solar radiation. It reaches its peak value at 3:00 pm, and decreases gradually from that period until 8:00 pm when it reaches its minimum DOD. At this period, the split genset is switched on to cover the deficit in energy.

The performance in terms of LCC and TEP are presented in Table 5.10a. A LCC of $831,253.17 and TEP of 1,215,065.23 kg are recorded for the hybrid system using WOA. It was observed that there was a further reduction in the values of LCC and TEP as compared to those obtained using FA technique. This is because the WOA technique selected more bifacial PV modules, leading to more power output from the bifacial PV system and a corresponding reduction in the commitment hours of the split genset during the lifespan of the system.

Similarly, the algorithm is also implemented for the horizontal north-south orientation state; a combination of 167 bifacial PV modules and 32 batteries, in addition with the operational hours of the split genset are selected to meet the energy demand of the studied area. The operational behavior of the system for a period of forty-eight (48) hours and ten (10) days is depicted in Figures 5.15a and 5.15b respectively. The operational behavior of the system for the horizontal north-south orientation is quite similar to that of the vertical east-west orientation. The only difference is the increase in the number of bifacial PV modules and battery units selected by the WOA algorithm. The performance in terms of LCC and TEP are also presented in Table 5.10b. A LCC of $846,101.39 and TEP of 1,278,536.47 kg are recorded for the hybrid system using WOA. It is also observed that there is a slight increase in the values of LCC and TEP obtained for the horizontal north-south orientation state as compared to the vertical east-west orientation state. The increment may be attributed to the difference in the additional energy produced by the module for both orientation states.

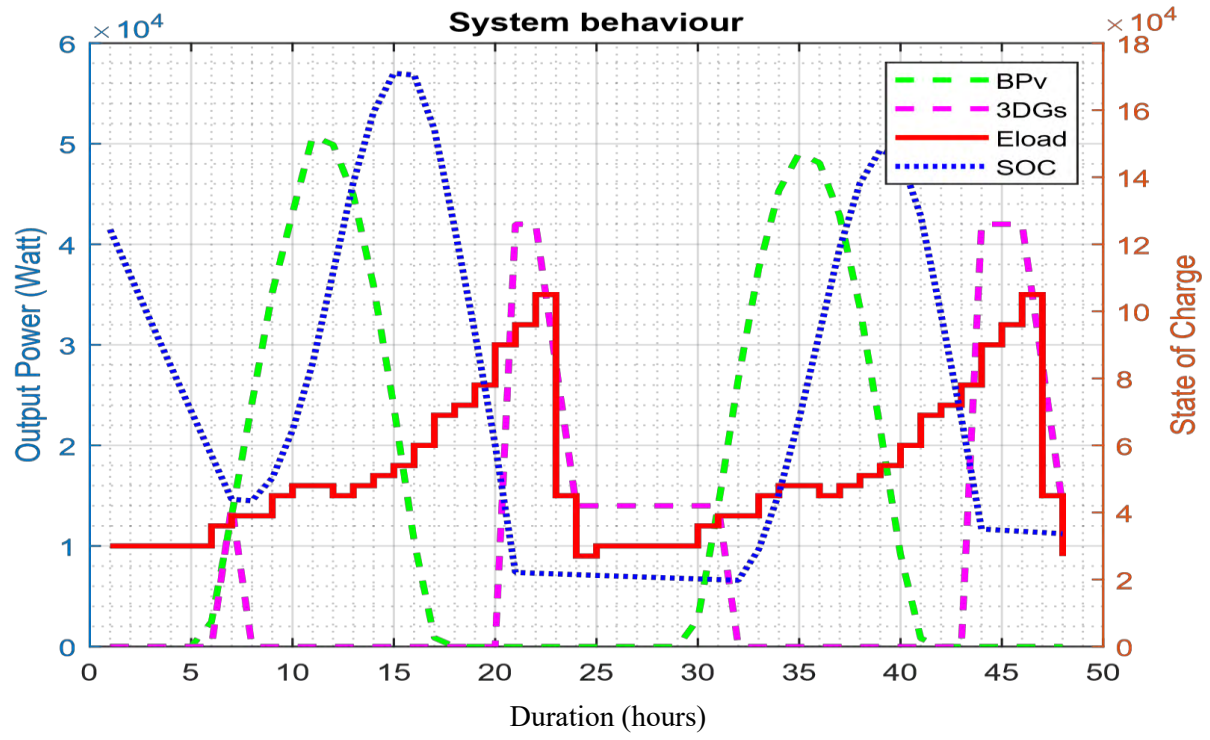

Figure 5.14a: System behavior of bifacial PV/battery/split genset configuration using WOA for a period of 48 hours for vertical east-west orientation state

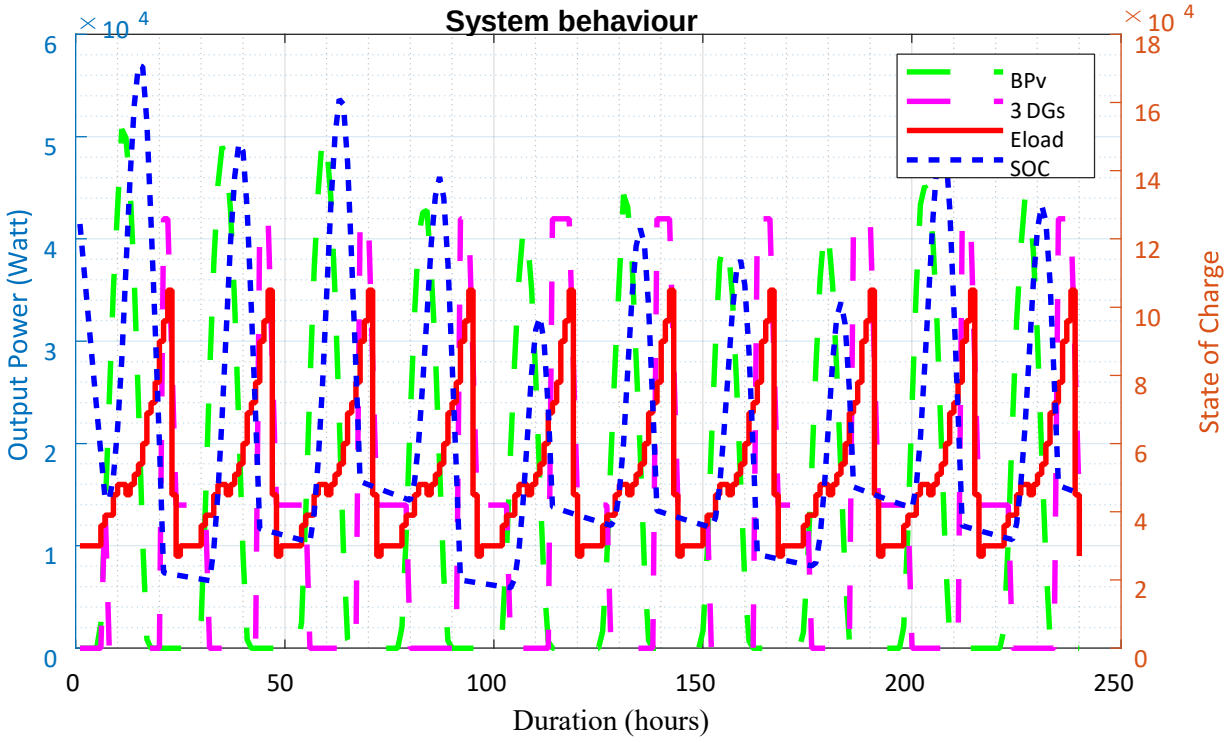

Figure 5.14b: System behavior of bifacial PV/battery/split genset configuration using WOA for a period of 10 days for vertical east-west orientation state

Table 5.10a: Performance of the hybrid bifacial PV/battery/split genset system using WOA for vertical east west orientation state

Particulars	System Configuration				
	Hybrid Bifacial PV/Battery/Split Genset				
Components	Bifacial PV	Battery	Split Genset		
Number of components	160	30	DG unit 1	DG unit 2	DG unit 3
Hours of Operation	N/A	N/A	108842	63220	25320
LCC			**$831,253.17**		
TEP			**1,215,065.23 kg**		

Table 5.10b: Performance of the hybrid bifacial PV/battery/split genset system using WOA for horizontal north-south orientation state

Particulars	System Configuration				
	Hybrid Bifacial PV/Battery/Split Genset				
Components	Bifacial PV	Battery	Split Genset		
Number of components	167	32	DG unit 1	DG unit 2	DG unit 3
Hours of Operation	N/A	N/A	108842	65060	27441
LCC			**$846,101.39**		
TEP			**1,278,536.47 kg**		

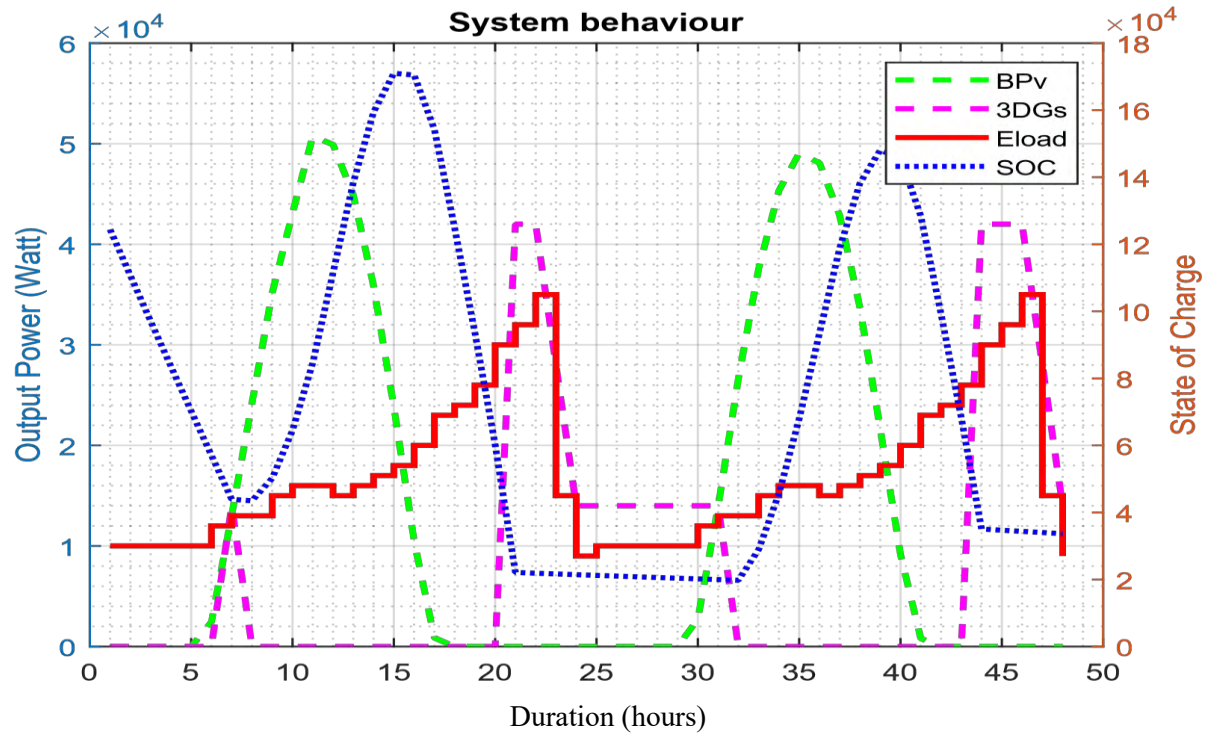

Figure 5.15a: System behavior of bifacial PV/battery/split genset configuration using WOA for a period of 48 hours for horizontal north-south orientation state

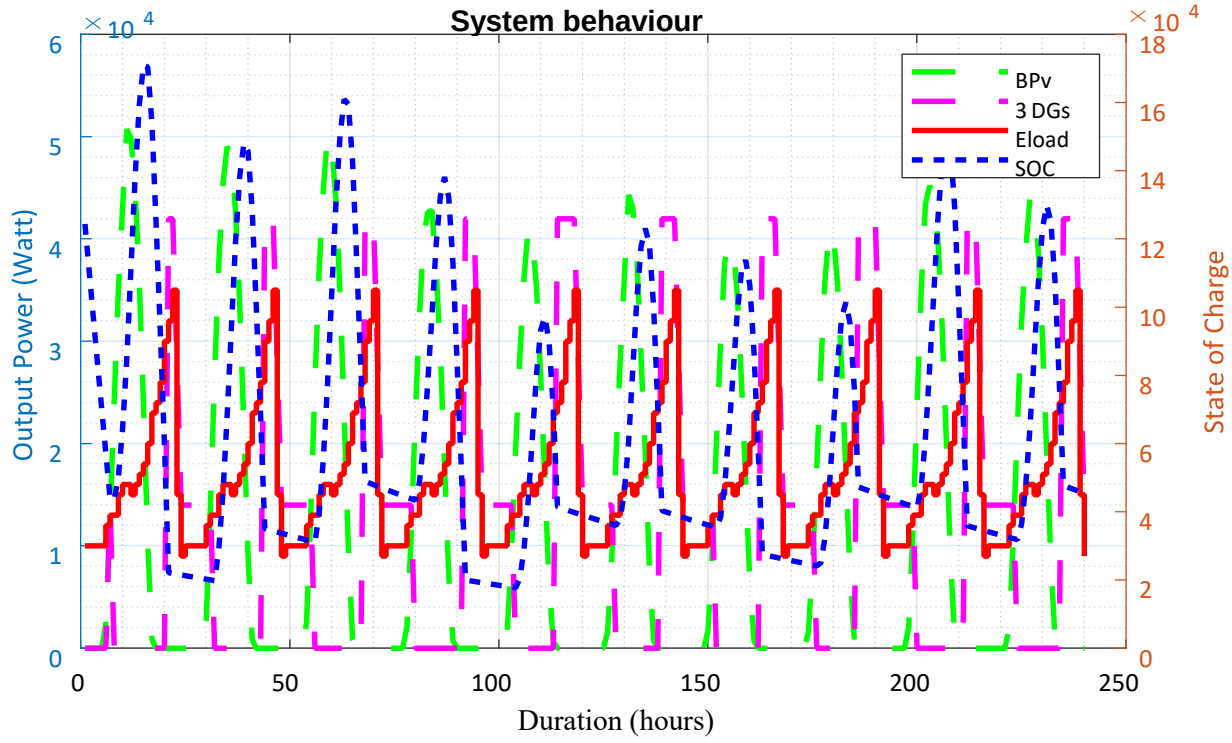

Figure 5.15b: System behavior of bifacial PV/battery/split genset configuration using WOA for a period of 10 days for horizontal north-south orientation state

5.3.3.3 Optimal design results using Giza Pyramid Construction (GPC) Algorithm

Giza Pyramid Constriction (GPC) algorithm is also used to determine the most appropriate components combination of case study three for each orientation states. For vertical east-west orientation state, a combination of 159 bifacial PV modules and 31 batteries, in addition with the operational hours of the split genset are selected by the algorithm to meet the energy demand of the studied area. The operational behavior of the system for a period of forty-eight (48) hours and ten (10) days is depicted in Figures 5.16a and 5.16b respectively. The operational behavior for case study three (3) using GPC algorithm is quite similar to that of WOA algorithm. However, the performance in terms of LCC and TEP presented in Table 5.11a are slightly different. A LCC of $842,253.17 and TEP of 1,225,619.08 kg are recorded for the hybrid system using GPC. These values are only slightly higher than those obtained using the WOA algorithm.

Moreover, the algorithm is also implemented for the horizontal north-south orientation state; a combination of 165 bifacial modules and 29 batteries, in addition with the operational hours of the split genset were selected to meet the energy demand of the studied area. The operational behavior of the system for a period of forty-eight (48) hours and ten (10) days is depicted in Figures 5.17a and 5.17b respectively. The operational behavior of the system for the horizontal north-south orientation is also quite similar to that of the vertical east-west orientation. The only difference is the increase in the number of bifacial PV modules and battery units selected by the GPC algorithm. The performance in terms of LCC and TEP are presented in Table 5.11b. A LCC of $867,545.91 and TEP of 1,299,700.43 kg are recorded for the hybrid system using GPC. A slight increase in the values of LCC and TEP obtained for the horizontal north-south orientation state as compared to the vertical east-west orientation is also observed.

5.3.4 Case four: Proposed Bifacial PV//Wind/Battery/split genset configuration

The results of optimal design of the proposed HPS is presented in this sub-section. The system configuration comprising of all the energy generating sources (bifacial bifacial PV module, wind turbine, battery energy system and the split genset) are considered to meet the energy demand of the studied area for a period of 30 years. The performance of the bifacial PV module on the optimal system design is also evaluated for the two orientation states of the system configuration. The optimal design of the proposed HPS is done using each of the proposed optimization techniques, and the performance of the system in terms of LCC and TEP for each optimization techniques are noted for comparison. The optimal design results of each optimization techniques are subsequently presented.

5.3.4.1 Optimal design results of the proposed HPS using Firefly Algorithm (FA)

Firefly Algorithm (FA) is implemented to determine the most appropriate components combination of the system configuration for the two orientation states of the bifacial PV module. For the vertical east-west

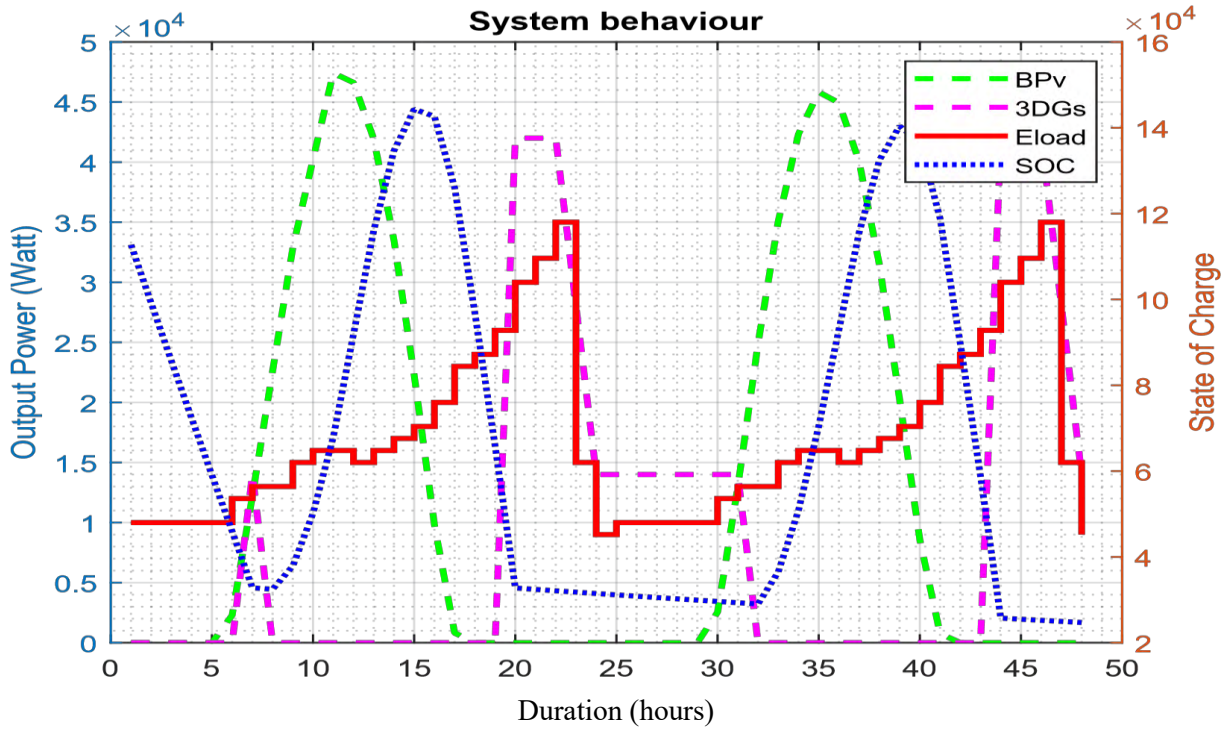

Figure 5.16a: System behavior of bifacial PV/battery/split genset configuration using GPC for a period of 48 hours for vertical east-west orientation state

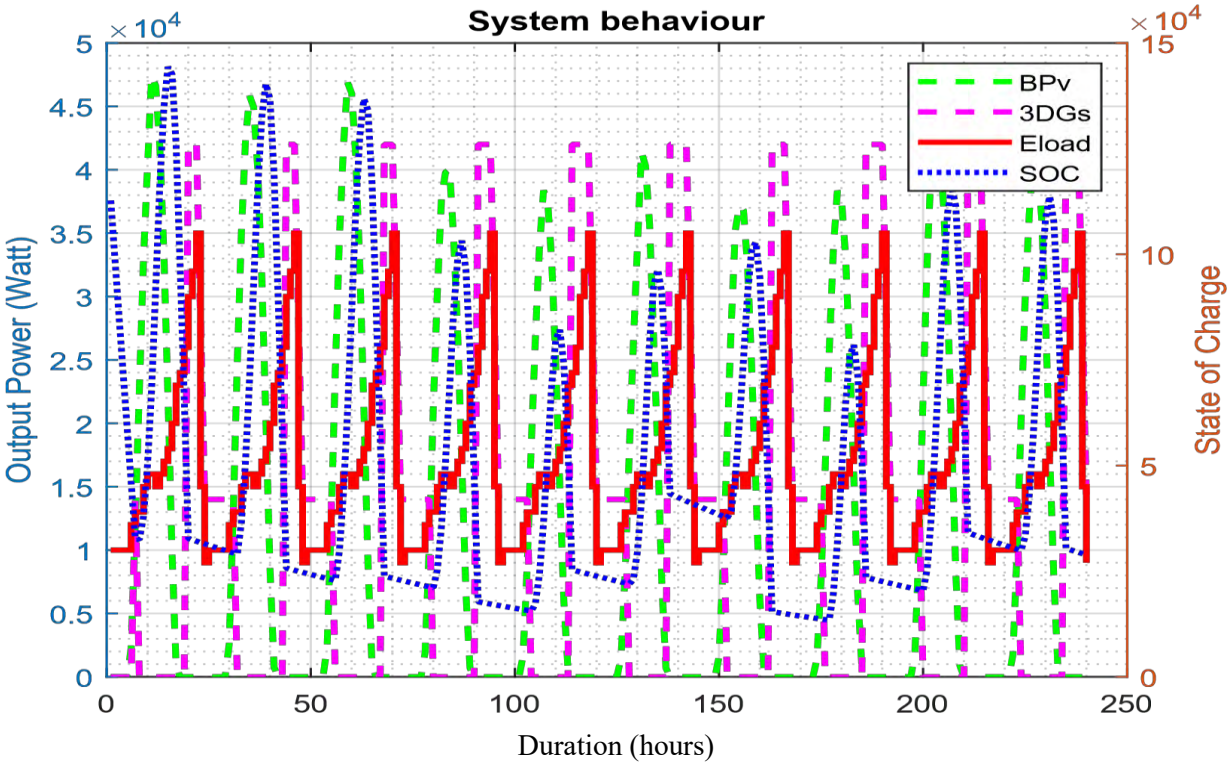

Figure 5.16b: System behavior of bifacial PV/battery/split genset configuration using GPC for a period of 10 days for vertical east-west orientation state

Table 5.11a: Performance of the hybrid bifacial PV/battery/split genset system using GPC algorithm for vertical east west orientation state

Particulars	System Configuration				
	Hybrid Bifacial PV/Battery/Split Genset				
Components	Bifacial PV	Battery	Split Genset		
Number of components	159	31	DG unit 1	DG unit 2	DG unit 3
Hours of Operation	N/A	N/A	111895	65201	26142
LCC			**$842,253.17**		
TEP			**1,225,619.08 kg**		

Table 5.11b: Performance of the hybrid bifacial PV/battery/split genset system using GPC algorithm for horizontal north-south orientation state

Particulars	System Configuration				
	Hybrid Bifacial PV/Battery/Split Genset				
Components	Bifacial PV	Battery	Split Genset		
Number of components	165	29	DG unit 1	DG unit 2	DG unit 3
Hours of Operation	N/A	N/A	111895	67561	29123
LCC			**$867,545.91**		
TEP			**1,299,700.43 kg**		

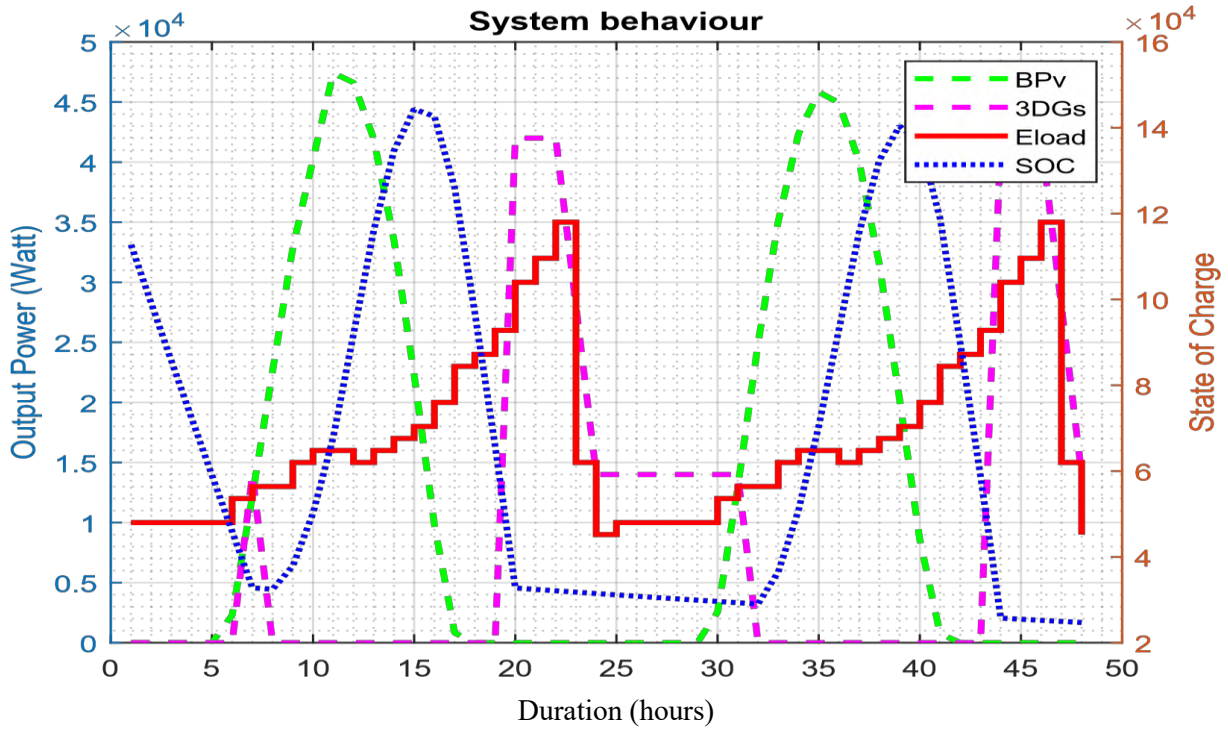

Figure 5.17a: System behavior of bifacial PV/battery/split genset configuration using GPC for a period of 48 hours for horizontal north-south orientation state

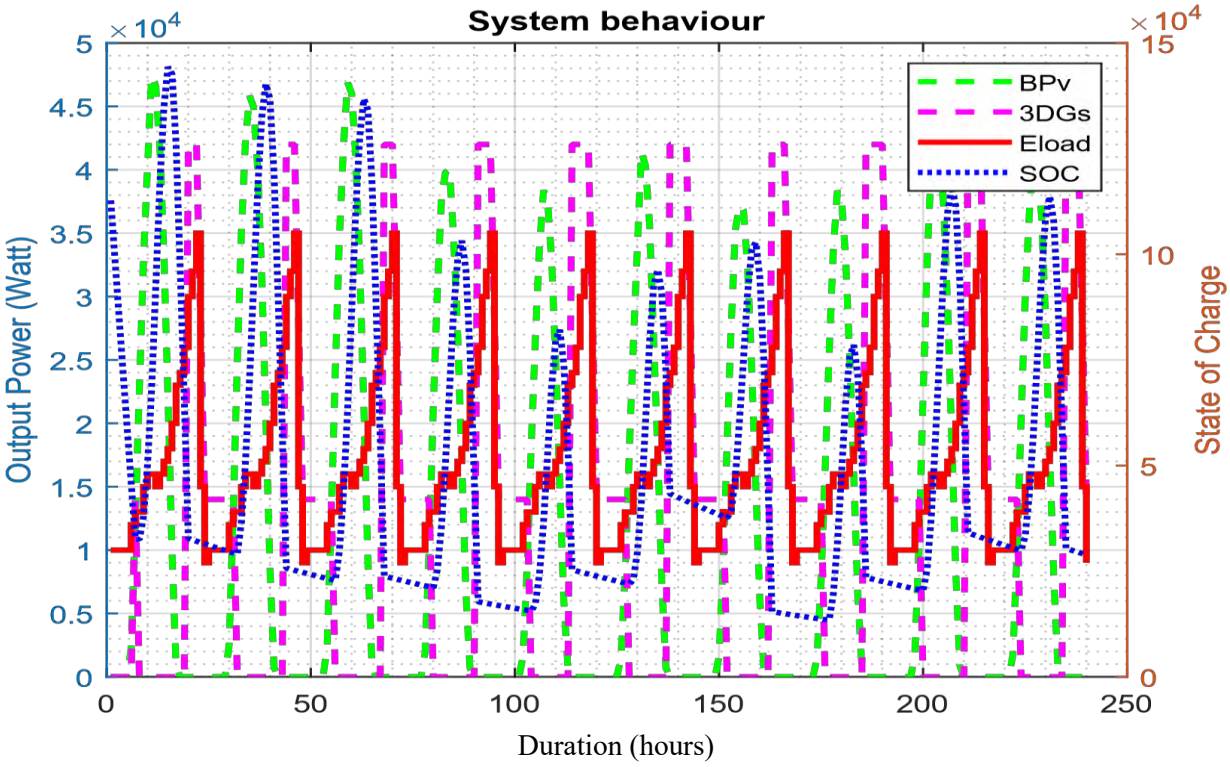

Figure 5.17b: System behavior of bifacial PV/battery/split genset configuration using GPC for a period of 10 days for horizontal north-south orientation state

orientation state, a combination of 125 bifacial PV modules, 23 wind turbines and 25 batteries; in addition with the operational hours of the split genset are selected by the algorithm to meet the energy demand of the studied area. The operational behavior of the system for a period of forty-eight (48) hours and ten (10) days is depicted in Figures 5.18a and 5.18b respectively. It can be seen from Figure 5.18a that the SOC of the battery start to increase from 6:30 am in the morning due to the excess energy contributed from the two renewable sources. It reaches its maximum value at about 3:00 pm and decreases from that period until about 9:00 pm. It remains constant from 9:00 pm to around 8:00 am; this period corresponds to late evenings and early mornings when there is neither enough solar radiation nor wind speed to generate power to meet the load demand or charge the battery. The energy deficit during this period is covered by the split genset.

The performance in terms of LCC and TEP are presented in Table 5.12a. From the results of Table 5.12a, it can be seen that the proposed HPS recorded the least values of LCC and TEP ($836,135.65 and 1,469,829.44 kg) as compared to other system configurations considered in this study. This reduction can be attributed to lesser commitment of the split genset during the lifespan of the system as more energy is made available to the system from the two renewable energy sources.

The algorithm is also implemented for the horizontal north-south orientation state; a combination of 142 bifacial PV modules and 12 wind turbines, 26 batteries, in addition with the operational hours of the split genset are selected to meet the energy demand of the studied area. The operational behavior of the system for a period of forty-eight (48) hours and ten (10) days is depicted in Figures 5.19a and 5.19b respectively. The operational behavior of the system for the horizontal north-south orientation is quite similar to that of the vertical east-west orientation. The main difference is in the number of components selected by the algorithm, which may be due to a reduction in the power output of the bifacial PV system. The performance in terms of the LCC and TEP are also presented in Table 5.12b. A LCC of $840,804.82 and TEP of 1,471,239.30 kg are recorded for the system in the horizontal north south orientation state, which is higher than the values obtained for the vertical east-west orientation state. This may be attributed to an increase in the hourly commitment of the split genset to meet the deficit energy

5.3.4.2 Optimal design results of the proposed HPS using Whale Optimization Algorithm (WOA)

The Whale Optimization Algorithm (WOA) is also implemented to determine the most appropriate components combination of the system configuration for each orientation states orientation states of the bifacial PV module. For vertical east-west orientation state, a combination of 147 bifacial PV modules, 26 wind turbines and 32 batteries; in addition with the operational hours of the split genset are selected by

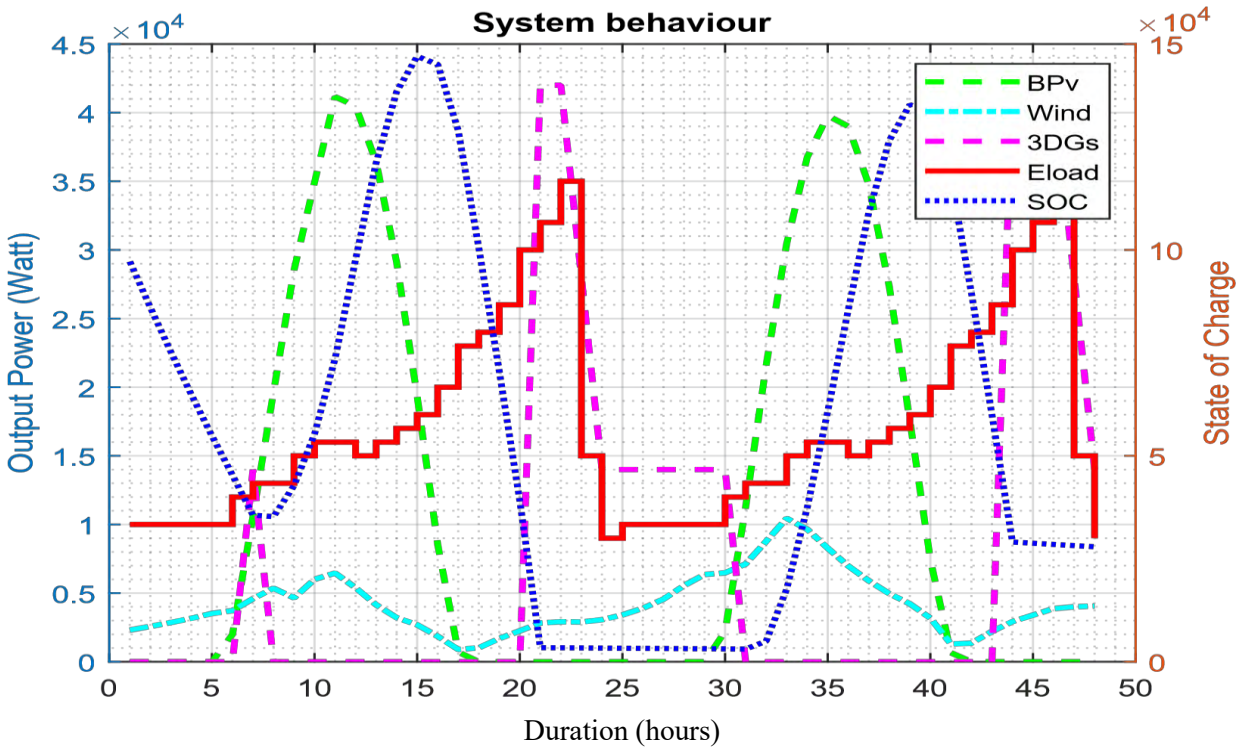

Figure 5.18a: System behavior of bifacial PV/wind turbine/battery/split genset configuration using FA for a period of 48 hours for vertical east-west orientation state

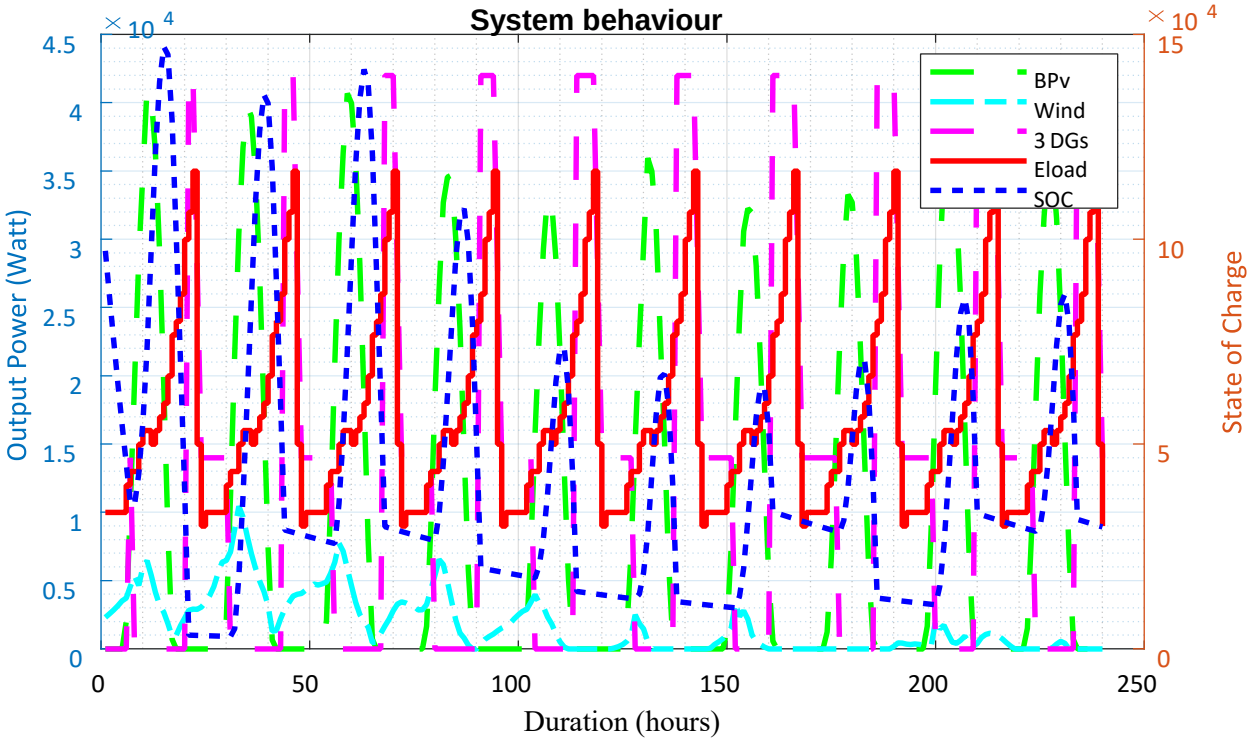

Figure 5.18b: System behavior of bifacial PV/wind turbine/battery/split genset configuration using FA for a period of 10 days for vertical east-west orientation state

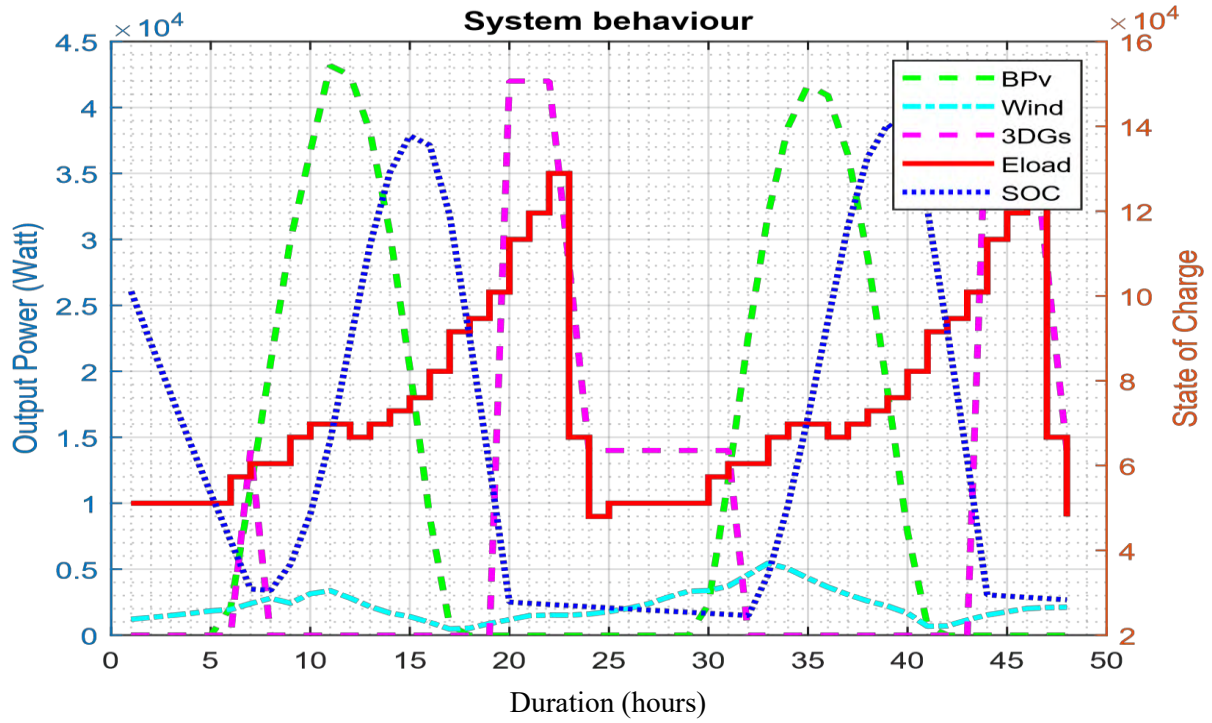

Figure 5.19a: System behavior of bifacial PV/wind turbine/battery/split genset configuration using FA for a period of 48 hours for horizontal north-south orientation state

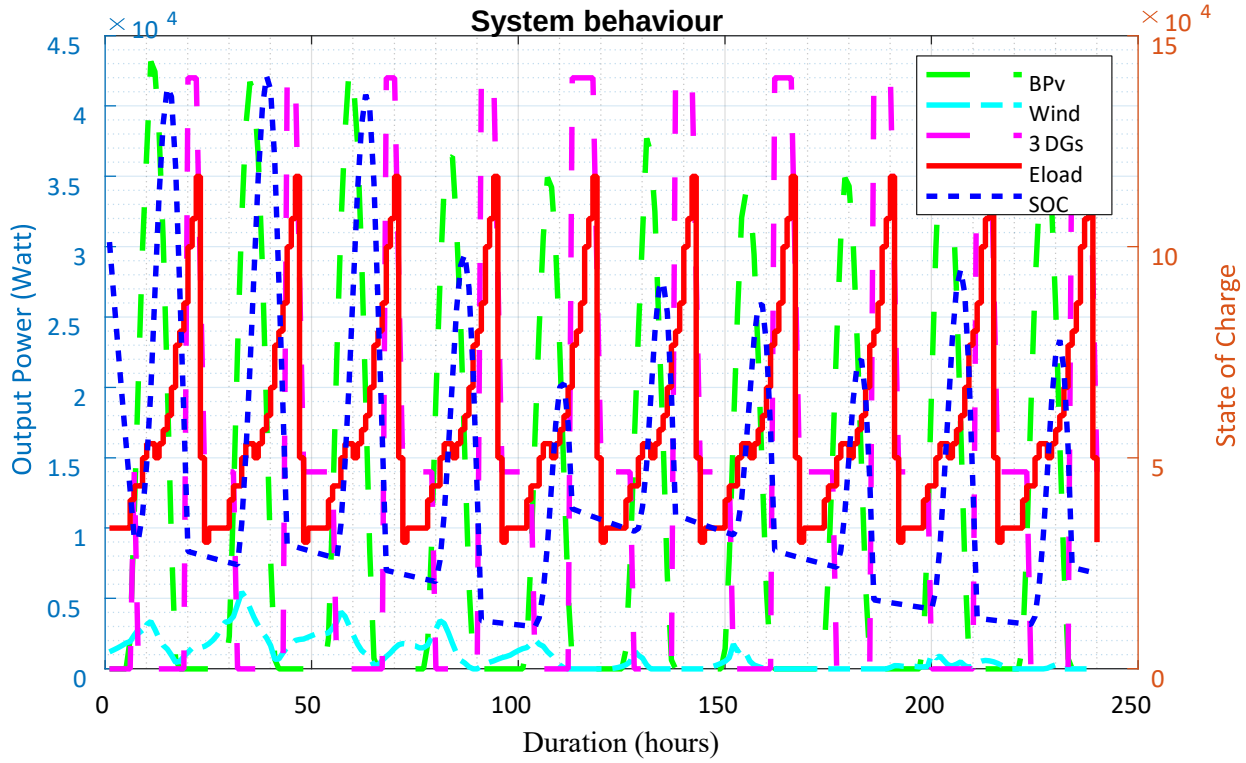

Figure 5.19b: System behavior of bifacial PV/wind turbine/battery/split genset configuration using FA for a period of 10 days for horizontal north-south orientation state

Table 5.12a: Performance of the hybrid bifacial PV/wind turbine/battery/split genset system using FA for vertical east west orientation state

Particulars	System Configuration					
	Hybrid Bifacial PV/Wind Turbine/Battery/Split Genset					
Components	Bifacial PV	Wind Turbine	Battery	Split Genset		
Number of components	125	23	25	DG unit 1	DG unit 2	DG unit 3
Hours of Operation	N/A	N/A	N/A	129554	74710	33772
LCC	**$836,135.65**					
TEP	**1,469,829.44 kg**					

Table 5.12b: Performance of the hybrid bifacial PV/wind turbine/battery/split genset system using FA for horizontal north-south orientation state

Particulars	System Configuration					
	Hybrid Bifacial PV/Wind Turbine/Battery/Split Genset					
Components	Bifacial PV	Wind Turbine	Battery	Split Genset		
Number of components	142	12	26	DG unit 1	DG unit 2	DG unit 3
Hours of Operation	N/A	N/A	N/A	126752	76107	33463
LCC	**$840,804.82**					
TEP	**1,471,239.30 kg**					

the algorithm to meet the energy demand of the studied area. The operational behavior of the system for a period of forty-eight (48) hours and ten (10) days is depicted in Figures 5.20a and 5.20b respectively. It can be seen from Figure 5.20a that the SOC of the battery start to increase from 7:00 am in the morning due to the excess energy contributed from the two renewable sources. It reaches its maximum value at about 3:00 pm and remains constant till about 4:00 pm. It starts to decrease from 3:30 pm until about 9:00 pm. It remains constant from 9:00 pm to about 7:00 am; this period corresponds to late evenings and early mornings when there is neither enough solar radiation nor wind speed to generate power to supply the load or charge the battery. The energy deficit during this period is covered by the split genset.

The performance in terms of LCC and TEP are presented in Table 5.13a. A LCC of $799,243.58 and TEP of 1,188,139.91 kg are recorded for the hybrid system using WOA. It is observed that the values of the LCC and TEP obtained using WOA technique were further reduced as compared to those obtained using FA technique. This reduction can be attributed to an even allocation of renewable energy sources and battery system, which corresponds to a lesser commitment of the split genset during the lifespan of the system.

Moreover, the algorithm was is implemented for the horizontal north-south orientation state; a combination of 156 bifacial PV modules, 30 wind turbines and 32 batteries; in addition with the operational hours of the split genset are selected to meet the energy demand of the studied area. The operational behavior of the system for a period of forty-eight (48) hours and ten (10) days is depicted in Figures 5.21a and 5.22b respectively. The operational behavior of the system for the horizontal north-south orientation is quite similar to that of the vertical east-west orientation. The main difference is in the number of components selected by the algorithm, which may be due to a reduction in the power output of the bifacial PV system. The performance in terms of LCC and TEP are presented in Table 5.13b. A LCC of $811,863.39 and TEP of 1,198,919.95 kg are recorded for the hybrid system in the horizontal north south orientation state, which is higher than the values obtained for the vertical east-west orientation state. This may be attributed to an increase in the hourly commitment of the split genset to cover the deficit energy

5.3.4.3 Optimal design results of the proposed HPS using Giza Pyramid Construction (GPC)

Giza Pyramid Constriction (GPC) algorithm is also used to determine the most appropriate components combination of case study three for each orientation states of the bifacial PV module. For vertical east-west orientation state, a combination of 127 bifacial PV modules, 37 wind turbines and 32 batteries; in addition with the operational hours of the split genset were selected by the algorithm to meet the energy demand of

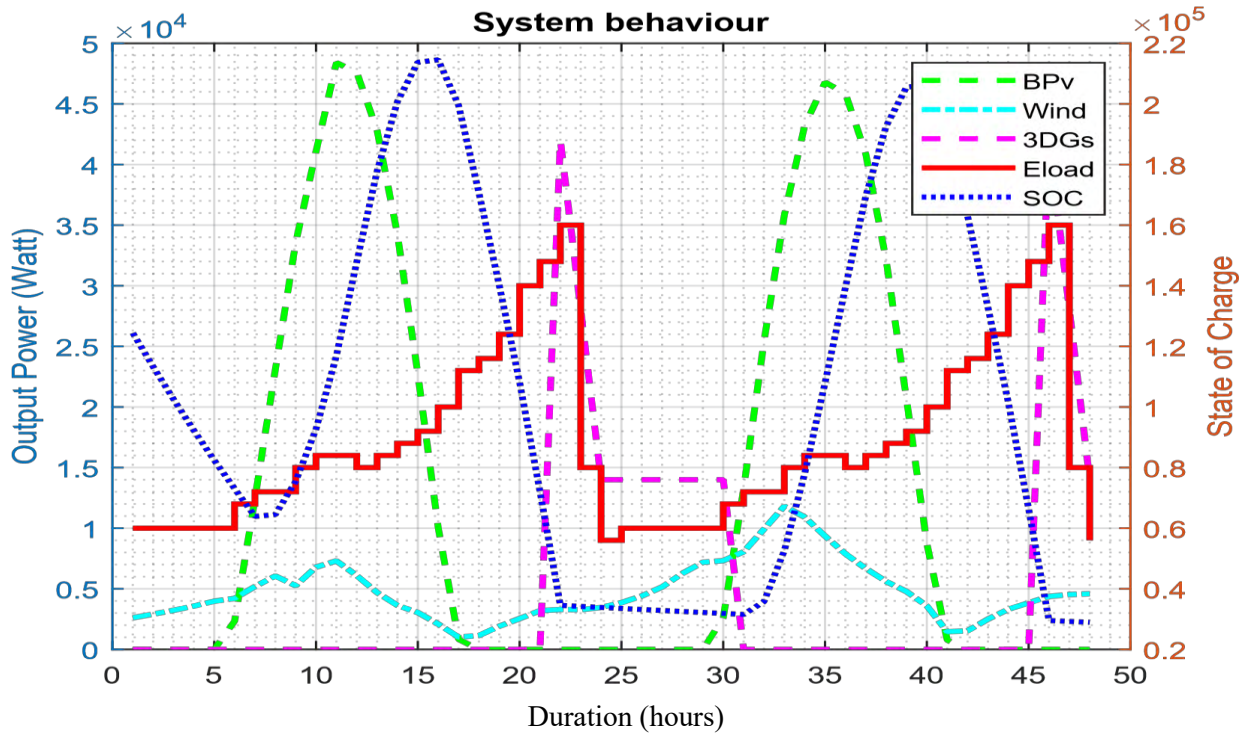

Figure 5.20a: System behavior of bifacial PV/wind turbine/battery/split genset configuration using WOA for a period of 48 hours for vertical east-west orientation state

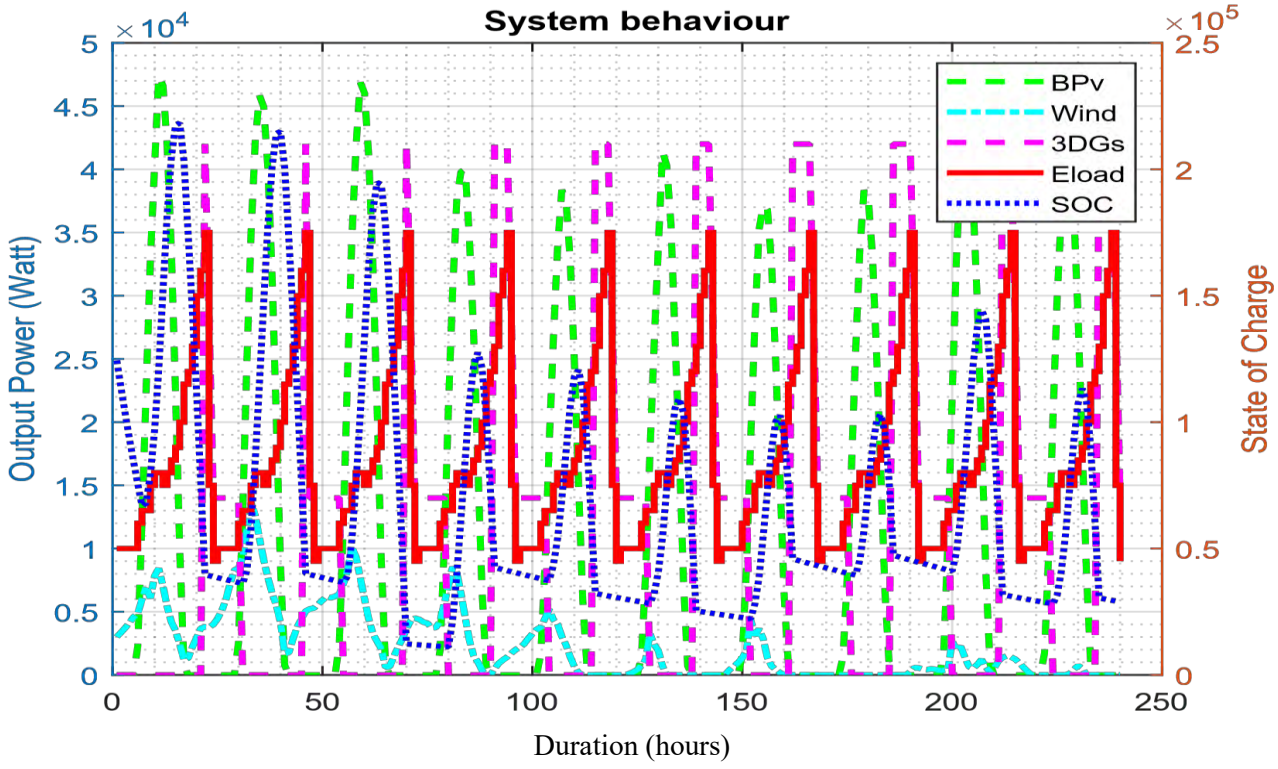

Figure 5.20b: System behavior of bifacial PV/wind turbine/battery/split genset configuration using WOA for a period of 10 days for vertical east-west orientation state

Table 5.13a: Performance of the hybrid bifacial PV/wind turbine/battery/split genset system using WOA for vertical east west orientation state

Particulars	System Configuration					
	Hybrid Bifacial PV/Wind Turbine/Battery/Split Genset					
Components	Bifacial PV	Wind Turbine	Battery	Split Genset		
Number of components	147	26	32	DG unit 1	DG unit 2	DG unit 3
Hours of Operation	N/A	N/A	N/A	107632	59310	25692
LCC	**$799,243.58**					
TEP	**1,188,139.91 kg**					

Table 5.13b: Performance of the hybrid bifacial PV/wind turbine/battery/split genset system using WOA for horizontal north-south orientation state

Particulars	System Configuration					
	Hybrid Bifacial PV/Wind Turbine/Battery/Split Genset					
Components	Bifacial PV	Wind Turbine	Battery	Split Genset		
Number of components	156	30	32	DG unit 1	DG unit 2	DG unit 3
Hours of Operation	N/A	N/A	N/A	109280	59189	26108
LCC	**$811,863.39**					
TEP	**1,198,919.95 kg**					

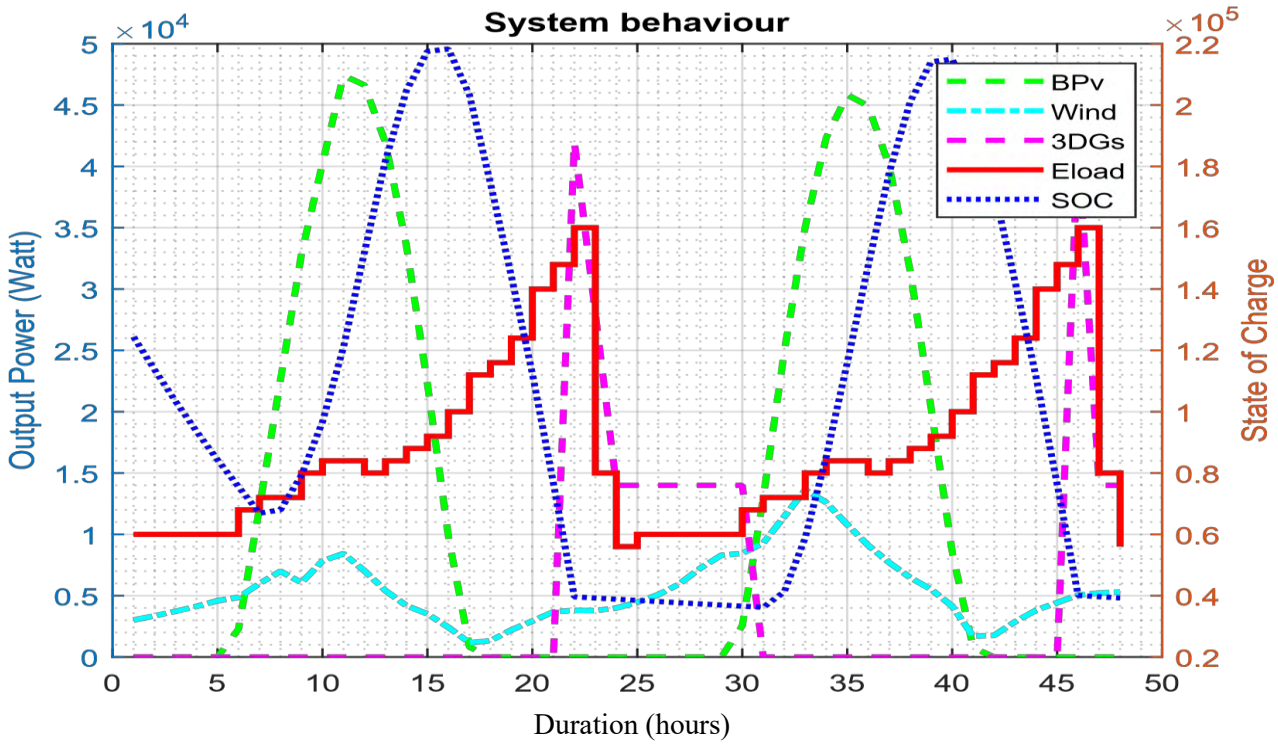

Figure 5.21a: System behavior of bifacial PV/wind turbine/battery/split genset configuration using WOA for a period of 48 hours for horizontal north-south orientation state

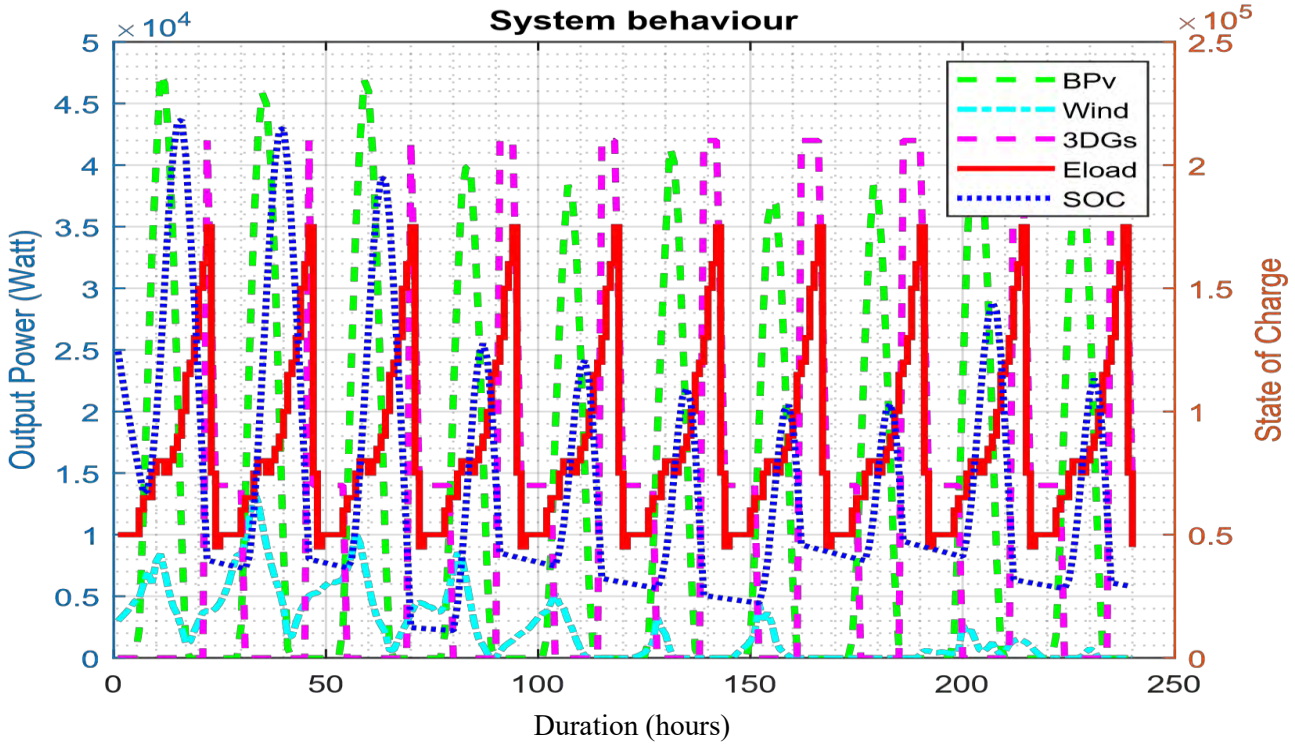

Figure 5.21b: System behavior of bifacial PV/wind turbine/battery/split genset configuration using WOA for a period of 10 days for horizontal north-south orientation state

the studied area. The operational behavior of the system for a period of forty-eight (48) hours and ten (10) days is depicted in Figures 5.22a and 5.22b respectively. It can be seen from Figure 5.22a that the SOC of the battery start to increase from 7:00 am in the morning due to the excess energy contributed from the two renewable sources. It reaches its maximum value at about 3:00 pm and remains constant till about 4:00 pm. It starts to decrease from 3:30 pm until about 10:00 pm. It remains constant from 9:00 pm till about 6:30 am; this period corresponds to late evenings and early mornings when there is neither enough solar radiation nor wind speed to generate power to supply the load or charge the battery. The energy deficit during this period is covered by the split genset.

The performance in terms of LCC and TEP are presented in Table 5.14a. A LCC of $803,599.09 and TEP of 1,265,933.58 kg are recorded for the hybrid system using GPC. It was observed that the values of the LCC and TEP obtained using GPC technique are close to those obtained using WOA technique. Thus, illustrating the ability of the algorithm to evenly allocate the components of the system in meeting the energy demand of the studied area.

Moreover, the algorithm is also implemented for the horizontal north-south orientation state; a combination of 147 bifacial PV modules, 40 wind turbines and 32 batteries; in addition with the operational hours of the split genset are selected to meet the energy demand of the studied area. The operational behavior of the system for a period of forty-eight (48) hours and ten (10) days is depicted in Figures 5.23a and 5.23b respectively. The operational behavior of the system for the horizontal north-south orientation is also very similar to that of the vertical east-west orientation. The main difference is in the number of components selected by the algorithm, which may be due to a reduction in the power output of the bifacial PV system. The performance in terms of LCC and TEP are presented in Table 5.14b. A LCC of $833,991.90 and TEP of 1,237,614.39 kg are recorded for the hybrid system in the horizontal north-south orientation state, which are higher than the values obtained for the vertical east-west orientation state. This may be attributed to an increase in the hourly commitment of the split genset to cover the deficit energy.

Generally, it is observed that an increase in the hourly commitment of the split genset corresponds to an increase in the values of the LCC and TEP for all system configurations; which is due to the high operation and maintenance cost of the split genset.

5.4 Performance comparison of different system configuration

The performance comparison of various system configuration/case studies is presented in this section. A summary of the results obtained for both orientation states of the bifacial PV module are presented in Table 5.15a and 5.15b respectively. However, for comparison purposes, the results obtained using the vertical east-west orientation of the module is used to demonstrate the feasibility of the proposed HPS, since it

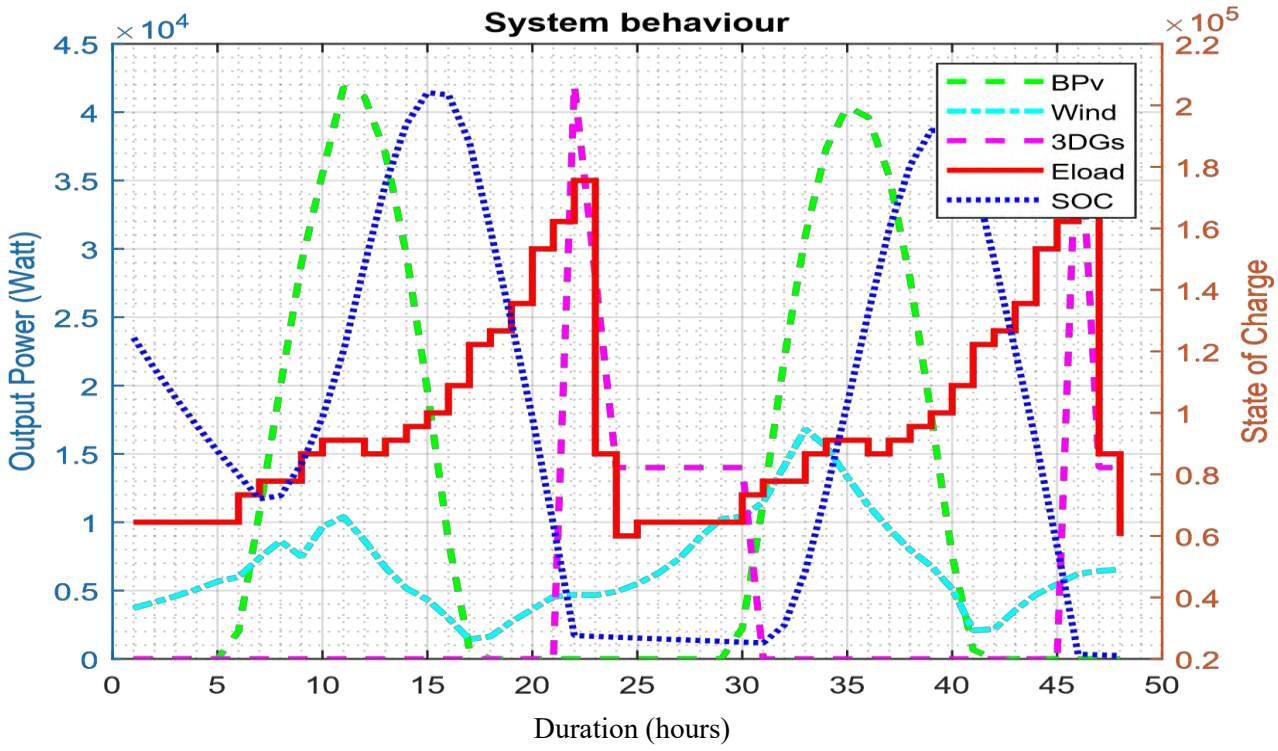

Figure 5.22a: System behavior of bifacial PV/wind turbine/battery/split genset configuration using GPC algorithm for a period of 48 hours for vertical east-west orientation state

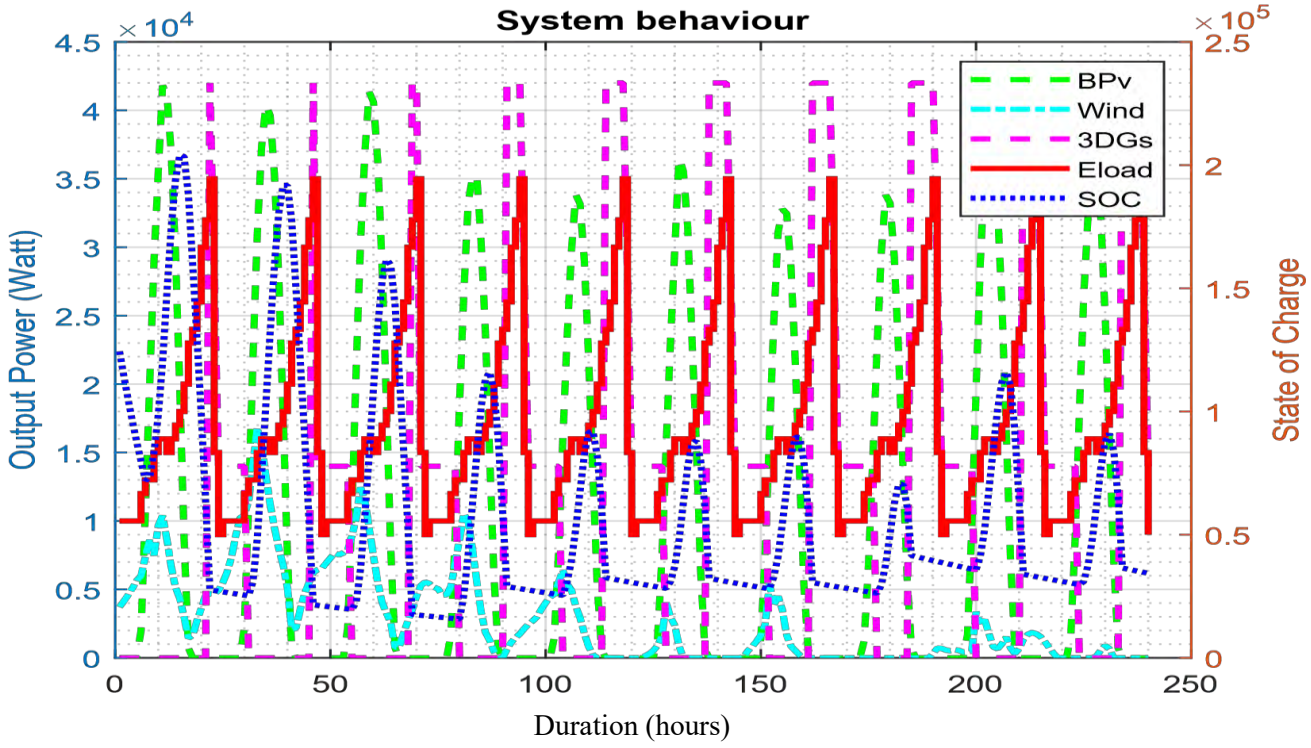

Figure 5.22b: System behavior of bifacial PV/wind turbine/battery/split genset configuration using GPC algorithm for a period of 10 days for vertical east-west orientation state

Table 5.14a: Performance of the hybrid bifacial PV/wind turbine/battery/split genset system using GPC for vertical east west orientation state

Particulars	System Configuration					
	Hybrid Bifacial PV/Wind Turbine/Battery/Split Genset					
Components	Bifacial PV	Wind Turbine	Battery	Split Genset		
Number of components	127	37	32	DG unit 1	DG unit 2	DG unit 3
Hours of Operation	N/A	N/A	N/A	114181	60848	27116
LCC	**$803,599.09**					
TEP	**1,265,933.58 kg**					

Table 5.14b: Performance of the hybrid bifacial PV/wind turbine/battery/split genset system using GPC for horizontal north-south orientation state

Particulars	System Configuration					
	Hybrid Bifacial PV/Wind Turbine/Battery/Split Genset					
Components	Bifacial PV	Wind Turbine	Battery	Split Genset		
Number of components	147	40	32	DG unit 1	DG unit 2	DG unit 3
Hours of Operation	N/A	N/A	N/A	114313	60932	27481
LCC	**$833,991.90**					
TEP	**1,237,614.39 kg**					

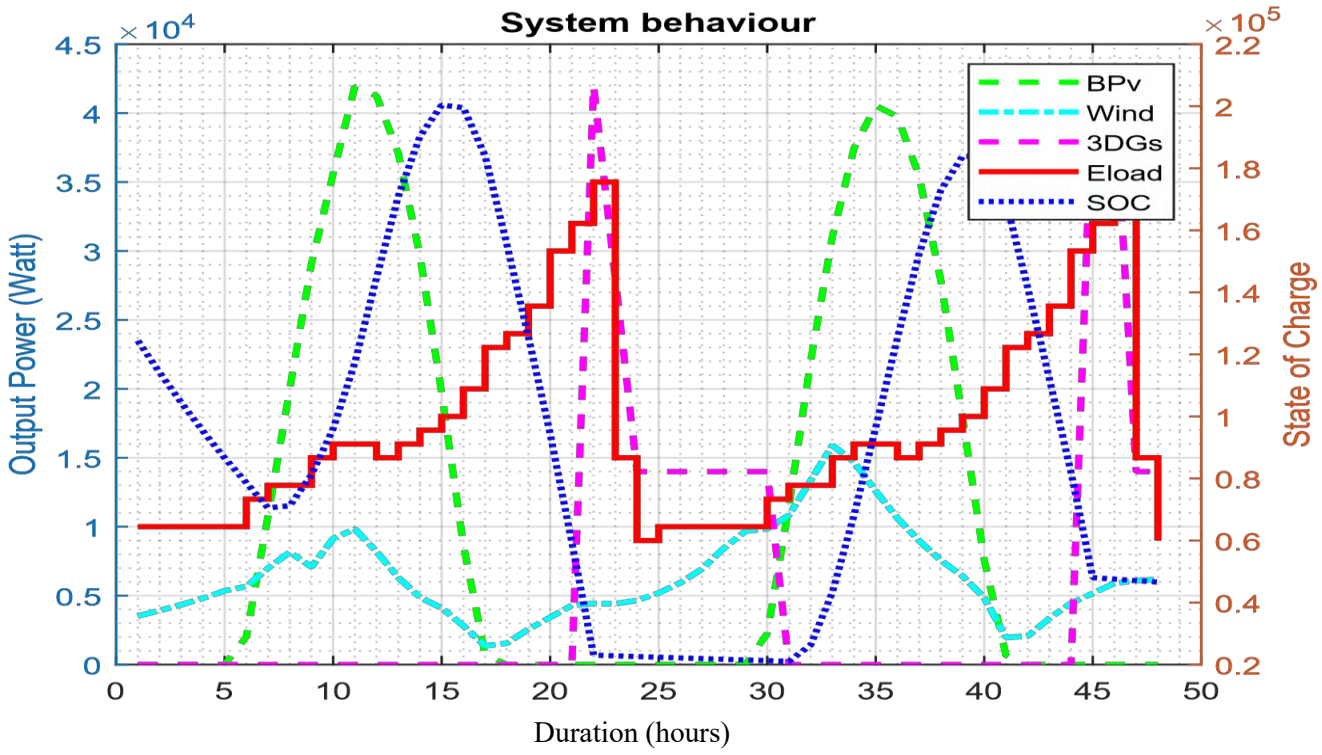

Figure 5.23a: System behavior of bifacial PV/wind turbine/battery/split genset configuration using GPC algorithm for a period of 48 hours for horizontal north-south orientation state

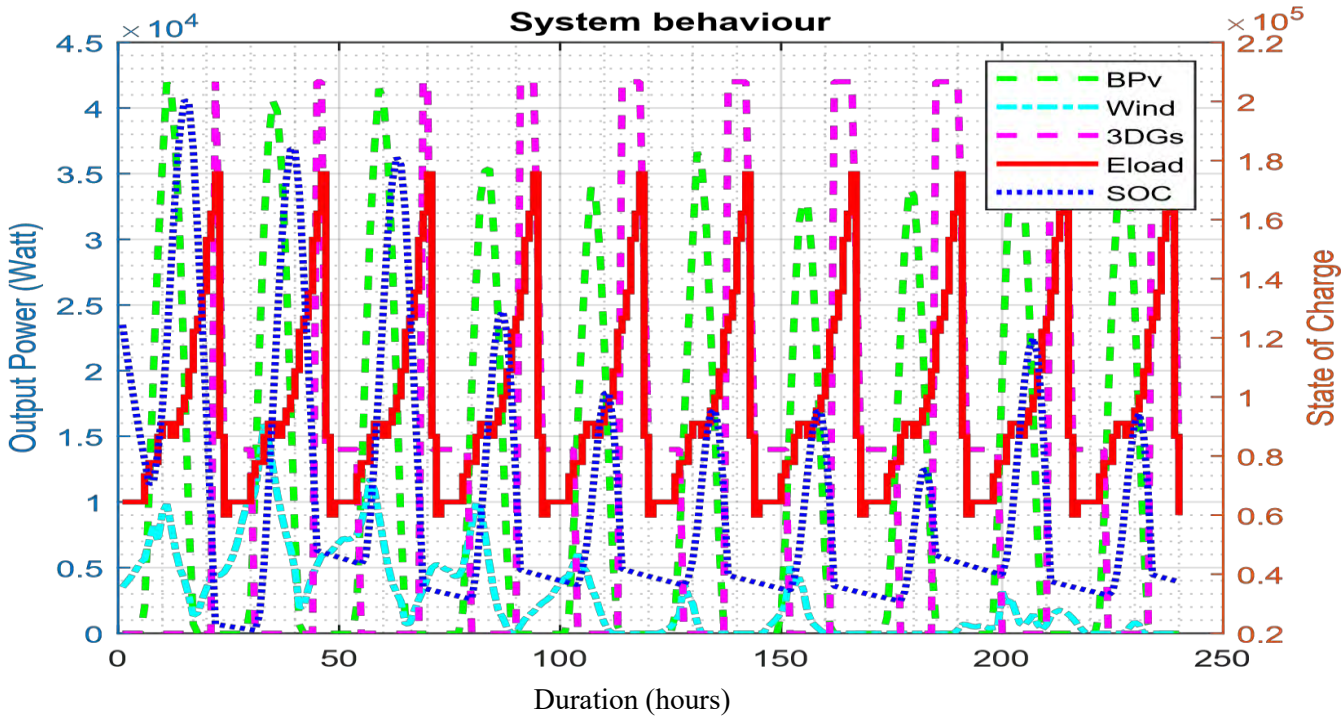

Figure 5.23b: System behavior of bifacial PV/wind turbine/battery/split genset configuration using GPC algorithm for a period of 10 days for horizontal north-south orientation state

Table 5.15a: Comparison of various system configurations for vertical east-west orientation state

System Configuration	Algorithm	No of Bpv	No of WT	No of Batt	No of DG units	LCC (US$)	TEP (kg)
Split Genset Only	**N/A**	**N/A**	**N/A**	**N/A**	**3**	**1,830,752.40**	**3,241,987.00**
Wind/Battery/Splt Genset	FA	N/A	97	21	3	1,518,636.76	2,564,611.03
	WOA	N/A	122	32	3	1,468,379.89	2,431,264.13
	GPC	N/A	111	32	3	1,495,747.57	2,490,797.21
Bifacial PV/Battery/Split Genset	FA	152		29	3	859,936.15	1,326,259.09
	WOA	160	N/A	30	3	831,253.17	1,215,065.23
	GPC	159	N/A	31	3	842,253.17	1,225,619.08
Optimal system configuration	FA	125	23	25	3	836,135.65	1,469,829.44
	WOA	**147**	**26**	**32**	**3**	**799,243.58**	**1,188,139.91**
	GPC	127	37	32	3	803,599.09	1,265,933.58

Table 5.15b: Comparison of various system configurations for horizontal north-south orientation

System Configuration	Algorithm	No of Bpv	No of WT	No of Batt	No of DG units	LCC(US$)	TEP (kg)
Split Genset Only	**N/A**	**N/A**	**N/A**	**N/A**	**3**	**1,830,752.40**	**3,241,987.00**
Wind/Battery/Splt Genset	FA	N/A	97	21	3	1,518,636.76	2,564,611.03
	WOA	N/A	122	32	3	1,468,379.89	2,431,264.13
	GPC	N/A	111	32	3	1,495,747.57	2,490,797.21
Bifacial PV/Battery/Split Genset	FA	161	N/A	31	3	879,568.94	1,346,022.01
	WOA	167	N/A	32	3	846,101.39	1,278,536.47
	GPC	165	N/A	29	3	867,545.91	1,299,700.43
Optimal system configuration	FA	142	12	26	3	840,804.82	1,471,239.30
	WOA	**156**	**30**	**32**	**3**	**811,863.39**	**1,198,919.95**
	GPC	147	40	32	3	833,991.90	1,237,614.39

generates more additional energy as compared to the horizontal north-south orientation state. The comparison is done using the LCC and TEP recorded for each system configuration using each of the optimization algorithms.

From the results of Table 5.15a, it is observed that the LCC and TEP of the proposed optimal system configuration using FA technique are considerably low ($836,135.65 and 1,469,829.44 kg) as compared to the other system configurations considered in this study, which include bifacial PV/Battery/split genset ($859,936.15 and 1,326,259.09 kg), Wind/Battery/split genset ($1,518,636.76 and 2,564,611.03 kg) and three split genset only ($1,830,752.40 and 3,241,987.00 kg). In addition, the percentage reduction in terms of LCC and TEP of each of the optimized system configurations are evaluated and compared with the LCC and TEP of using a three split genset configuration only. A 54.33 % and 54.66 % reduction in LCC and TEP respectively are obtained for the proposed system configuration, as compared to 53.03 % and 59.09 %, and 17.04 % and 20.89 % obtained for both bifacial PV/Battery/split genset and Wind/Battery/split genset configurations respectively.

Similarly, the LCC and TEP of the proposed optimal system configuration using WOA technique are significantly low ($799,243.58 and 1,188,139.91 kg) as compared to the other system configurations considered in this study, which include bifacial PV/Battery/split genset ($831,253.17 and 1,215,065.23 kg), Wind/Battery/split genset ($1,468,379.89 and 2,431,264.13 kg) and three split genset only ($1,830,752.40 and 3,241,987.00 kg). Moreover, the percentage reduction in terms of LCC and TEP of each of the optimized system configurations are also evaluated and compared with the LCC and TEP of using a three split genset configuration only. A 56.34 % and 63.35 % reduction in LCC and TEP respectively are obtained for the proposed system configuration, as compared to 54.59 % and 62.52 % and 19.79 % and 25.00 % obtained for both bifacial PV/Battery/split genset and Wind/Battery/split genset configurations respectively.

Correspondingly, the LCC and TEP of the proposed optimal system configuration using GPC technique are also significantly low ($803,599.09 and 1,265,933.58 kg) as compared to the other system configurations considered in this study, which include bifacial PV/Battery/split genset ($842,253.17and 1,225,619.08 kg), Wind/Battery/split genset ($1,495,747.57 and 2,490,797.21 kg) and three split genset only ($1,830,752.40) and 3,241,987.00 kg). Moreover, the percentage reduction in terms of LCC and TEP of each of the optimized system configurations are also evaluated and compared with the LCC and TEP of using a three split genset configuration only. 56.10 % and 60.95 % reduction in LCC and TEP respectively are obtained for the proposed system configuration, as compared to 53.99 % and 62.19 % and 18.30 % and 23.17 %

obtained for both bifacial PV/Battery/split genset and Wind/Battery/split genset configurations respectively.

Although, the bifacial PV/Battery/split genset configuration proves to be the most environmentally friendly as it gives the lowest value of TEP as compared to other optimized system configuration, the LCC is slightly higher than the optimal system configuration. On the other hand, it is observed that there is a higher percentage reduction in values of both the LCC and TEP for the optimal system configuration using each of the optimization techniques. This high reduction can be attributed to the corresponding reduction in capital cost, operation and maintenance cost and replacement cost of the proposed HPS, which is due to the uniformity in resource allocation as compared to other configuration of energy systems designed to meet the load requirement of the studied area. The plot of Figures 5.24a and 5.24b show the respective LCC and TEP comparison of the various system configuration using each of the optimization algorithms.

5.5 Performance comparison of the optimization algorithms

The performance comparison of each of the optimization algorithms in the optimal design of the proposed bifacial PV/Wind turbine/Battery/Split genset is presented in this section. The comparison was is done using the simulation results obtained for the vertical east-west orientation state of the bifacial module. Simulation results of optimal design of the proposed HPS in terms of LCC and TEP using each of the optimization algorithms are presented in Table 5.16.

From the results of Table 5.16, it can be observed that the WOA technique predicts the least LCC and TEP of the proposed HPS configuration. The algorithm selected a combination of 147 bifacial PV modules, 26 wind turbines, 32 battery units and 192,634 operational hours of the split genset to attain a LCC of $799,243.58 and TEP of 1,188,139.91 kg. Nevertheless, the LCC and TEP predicted by the GPC technique is not too far behind, as the algorithm selected a combination of 127 bifacial PV modules, 37 wind turbines, 32 battery units and 202,145 operational hours of the split genset to attain a LCC of $803,599.09 and TEP of 1,265,933.58 kg. On the contrary, the FA technique predicts the highest LCC and TEP; the algorithm selected a combination 125 bifacial PV modules, 23 wind turbines, 25 battery units and 238,036 operational hours of the split genset to achieve a LCC of $836,135.65 and TEP of 1,469,829.44 kg. The comparison in terms of the LCC and TEP obtained using each of the optimization algorithm is clearly depicted in Figures 5.25a and 5.25b respectively.

Furthermore, the performance comparison of each of the optimization algorithm was also done based on statistical analysis of the simulation results obtained after implementing each of the algorithms over twenty (20) iterations. Simulation results of optimal design of the proposed HPS in terms of the best objective

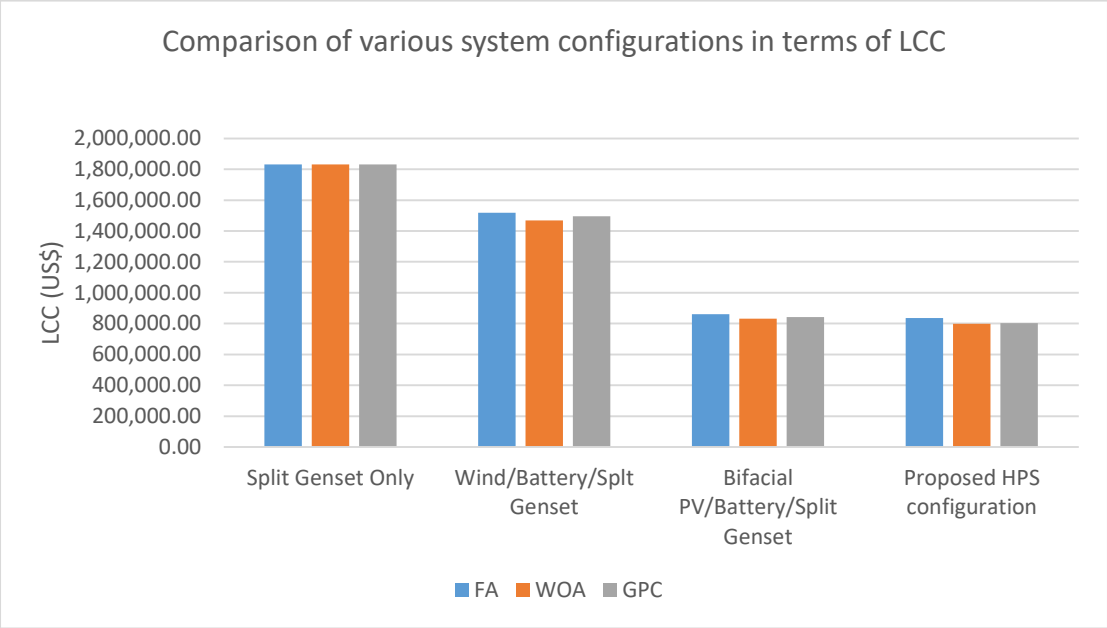

Figure 5.24a: Comparison of the LCC for various system configurations

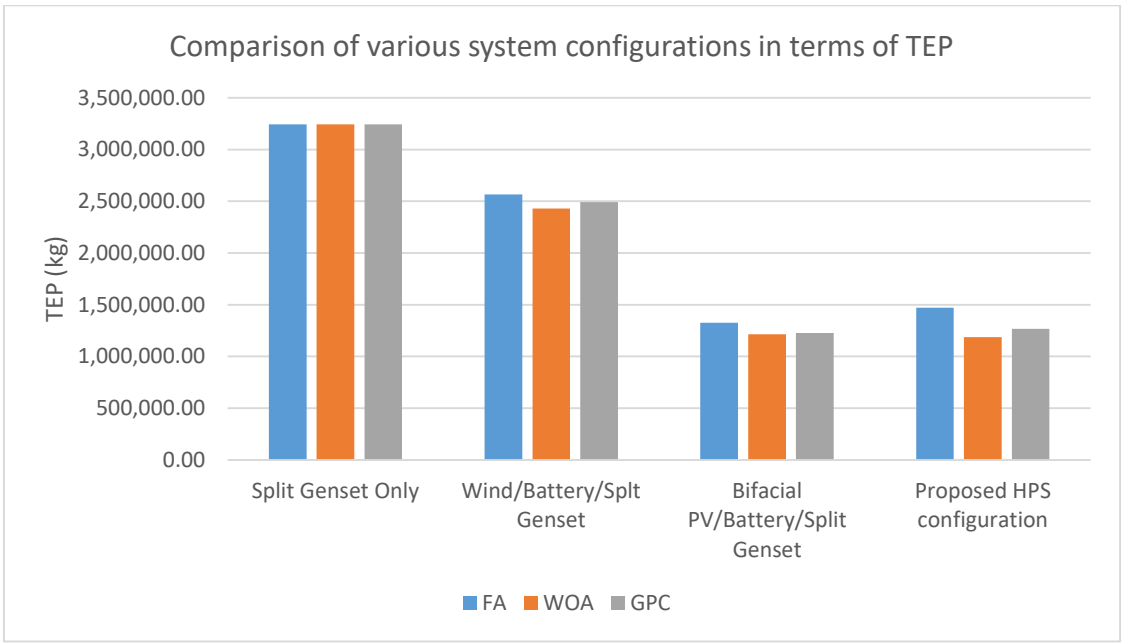

Figure 5.24b: Comparison of the TEP for various system configurations

Table 5.16: Performance comparison of the optimization techniques in terms of optimal solution

System Configuration	Algorithm	No of Bpv	No of WT	No of Batt	No of DG units	LCC(US$)	TEP (kg)
Optimal system configuration	FA	125	23	25	3	836,135.65	1,469,829.44
	WOA	147	26	32	3	799,243.58	1,188,139.91
	GPC	127	37	32	3	803,599.09	1,265,933.58

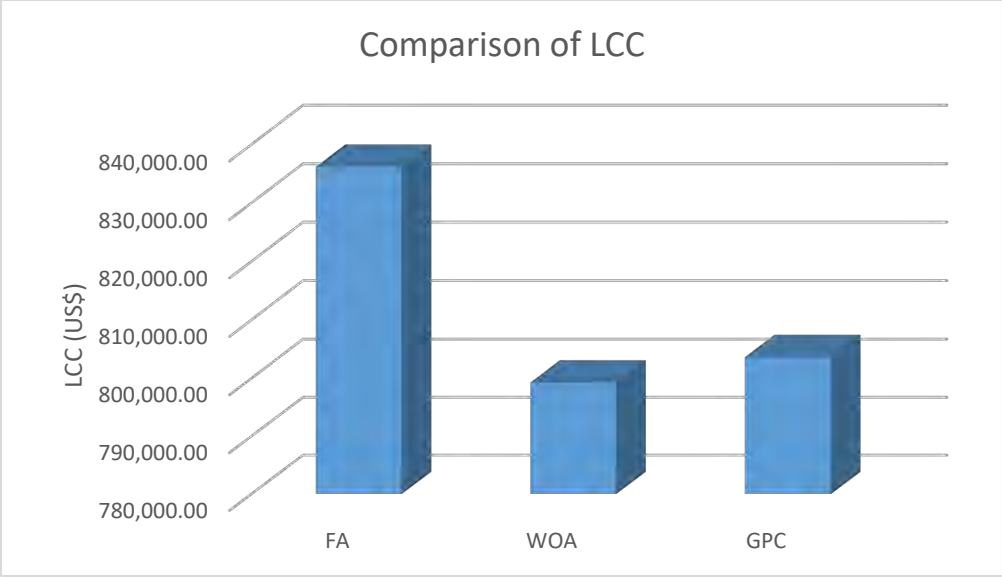

Figure 5.25a: Performance comparison of optimization algorithm in terms of LCC

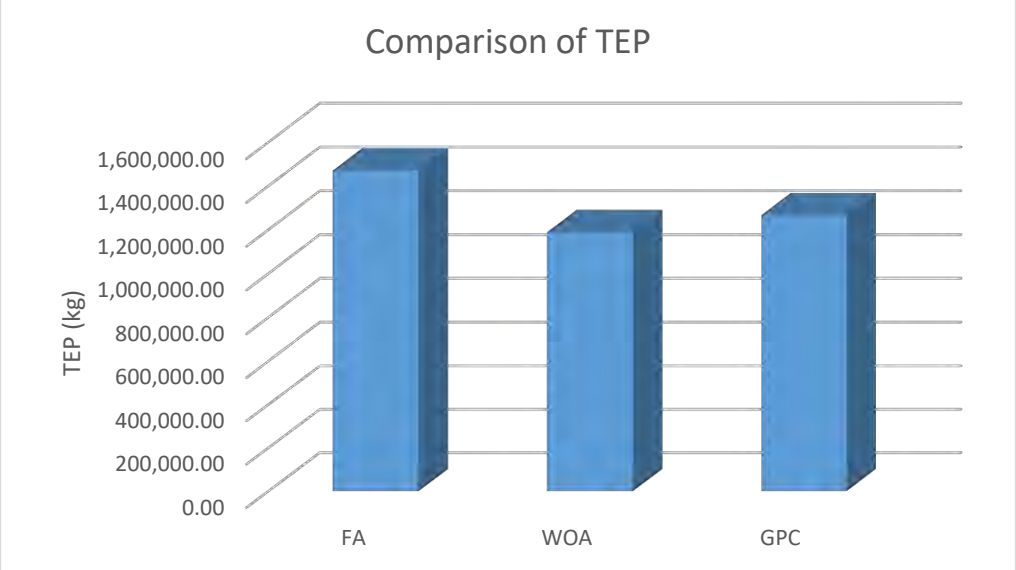

Figure 5.25b: Performance comparison of optimization algorithm in terms of TEP

score, worst objective score, mean score, median score, standard deviation, efficiency and simulation run time using each of the optimization algorithms are presented in Table 5.17.

From the results of Table 5.17, it can be seen that that FA technique, despite its high value of efficiency has a high simulation run time. On the other hand, the WOA technique has the lowest efficiency but with a reasonable simulation run time as compared to the FA technique. However, the GPC technique has a considerable efficiency and the lowest simulation run time in reaching the optimal solution. In addition to that, the minimum values of standard deviation obtained for both FA and GPC techniques indicate their high stability in reaching the optimal solution as compared to WOA technique. Nevertheless, the quality of the optimal solution obtained using the FA technique is much lower than that of the GPC technique. The comparison of the simulation run time and efficiency of each of the proposed optimization techniques is depicted in Figure 5.26a and 5.26b, while their convergence characteristics comparison plot is depicted in Figure 5.27. It can be inferred from the Figure 5.27 that the GPC technique converges faster, followed by the FA and WOA techniques respectively.

Generally, the results showed that despite the high efficiency and stability of the FA technique, the quality of its optimal solution in terms of LCC and TEP are below par when compared to both WOA and GPC techniques. On the contrary, the WOA technique, which gives the best quality solution in terms of the LCC and TEP lags behind in terms of efficiency, stability, simulation run time and convergence speed as compared to the GPC technique. The GPC technique however, produces considerably quality solution in terms of LCC and TEP, has reasonable efficiency and stability, lowest simulation run time and converges faster than both FA and WOA techniques. Thus confirming the robustness and suitability of the proposed GPC algorithm in the optimal design of bifacial PV/wind turbine/battery/split genset hybrid power system for the electrification of remote locations, critical facilities, among others.

Table 5.17: Performance comparison of the optimization techniques based on statistical analysis

Optimization technique	Worst score	Best score	Mean score	Median score	Standard deviation	Efficiency (%)	Simulation run time (minutes)
FA	541125	526841	528983.6	526841	0.7142	97.36	12.28
WOA	541125	471295	475688	471295	3.4915	87.09	10.59
GPC	541125	520933	523292	541125	1.0096	96.28	9.78

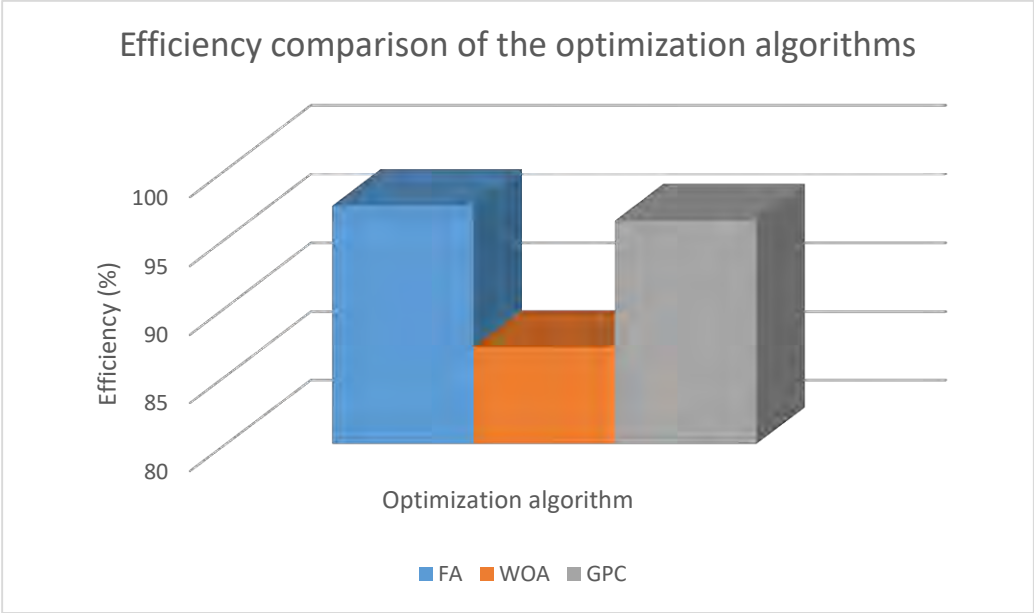

Figure 5.26a: Performance comparison of optimization algorithms in terms of efficiency

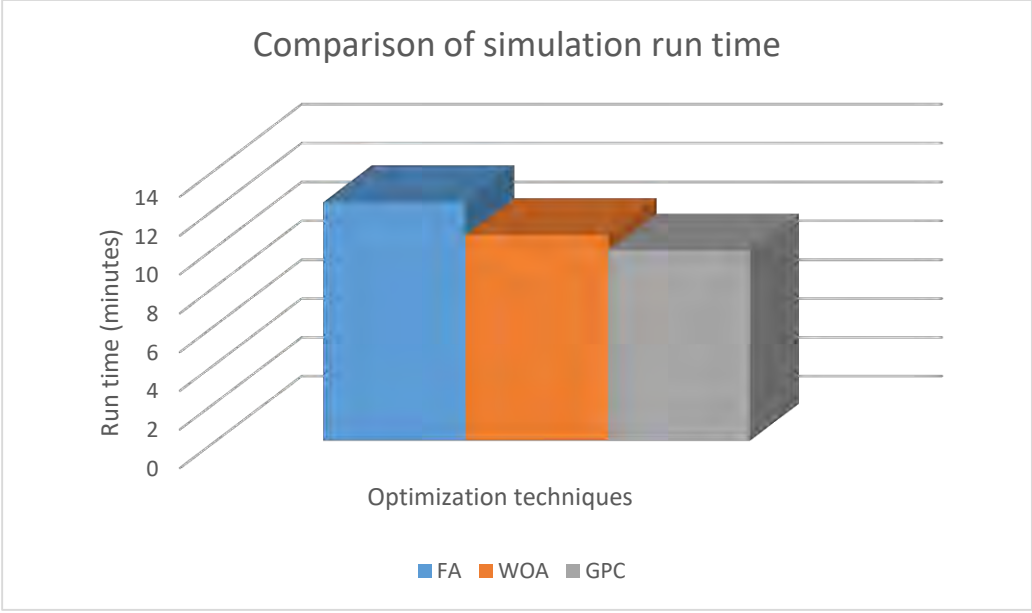

Figure 5.26b: Performance comparison of optimization algorithms in terms of simulation run time

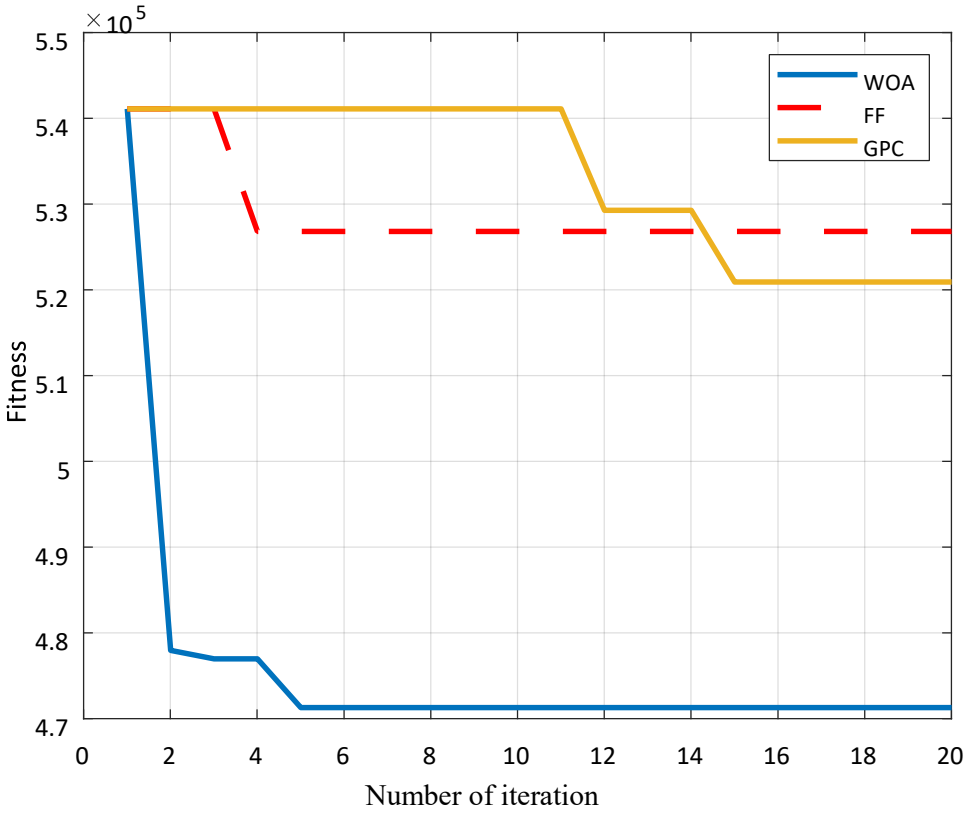

Figure 5.27: Comparison of convergence characteristics curve of the optimization algorithms

CHAPTER SIX
CONCLUSION AND RECOMMENDATIONS

6.1 Conclusion

The optimal design of a hybrid power system consisting of bifacial PV, wind turbine, battery energy storage and split genset using Giza Pyramid Construction optimization algorithm is presented in this study. The main objective of the design is to simultaneously minimize the Life Cycle Cost and Total Environmental Pollution of the system. A multi-objective solution method is employed to find the appropriate components combination of off-grid HPS that guarantees reliable and continuous supply of electrical energy.

Simulink models of each components of the HPS are developed in Simulink environment using their respective mathematical expressions; each of the model is integrated together to generate a single HPS model so as to give a true representation of the hybrid system. The performance of the bifacial PV module in the system is evaluated by estimating the additional energy yield for both orientation states. Generally, it was observed that the vertical east-west orientation state yielded more additional energy compared to the horizontal north-south state. Hence, the viability of the proposed HPS design is evaluated based on the vertical east-west orientation state of the module.

An optimization problem based on Life Cycle Cost (LCC) and Total Environmental Pollution (TEP) was developed and optimized using Giza Pyramid Construction (GPC) algorithm, Firefly Algorithm (FA) and Whale Optimization Algorithm (WOA) techniques. The proposed method was applied to a remote village in northern part of Nigeria using hourly solar irradiance, hourly wind speed and hourly energy requirement of the area as inputs to the algorithm. The performance of the proposed HPS was demonstrated by comparing its results with three other system configurations designed to meet the load requirement of the location. Each of the system configurations is simulated for a period of 30 years and the results in terms of LCC and TEP are documented. From an optimization perspective, the performance of the optimization algorithms in terms of quality of the optimal solutions, simulation run time and convergence speed after 20 iterations are also noted for comparison. Moreover, statistical analysis was used to evaluate the performance of the proposed optimization algorithm and its results were compared with the two other algorithms reported in this study.

The optimization results showed that the proposed system configuration is the most feasible in terms of LCC and TEP. The results also showed that the WOA technique gives the best value of the objective function representing the least LCC value of $799,243.58 and TEP value of 1,188,139.91 kg. The GPC technique predicted a competitive LCC value of $803, 599.09 and TEP of 1,265,933.58 kg. However, the values of LCC and TEP obtained using FA technique are much higher than those predicted using WOA and

GPC techniques, the algorithm predicted the highest LCC value of $836,135.65 and TEP value of 1,469,829.44 kg. It should however be noted that the values of LCC and TEP predicted by the three optimization techniques illustrate that the proposed hybrid system configuration is more feasible when compared to other system configurations considered in this study to meet the energy requirement of the studied location.

The optimization results also showed that the GPC algorithm has the least simulation run time and converges faster than both the WOA and FA techniques. In addition to that, by comparing the results of statistical analysis of the proposed algorithm with the two other optimization algorithms; it can be concluded that the standard deviation of 1.0096 and efficiency of 96.28 obtained for the proposed algorithm are much better than those obtained for WOA technique, and quite competitive with those obtained using FA technique. Thereby demonstrating the accuracy and stability, in addition to the fast simulation run time and convergence speed of the proposed algorithm in solving multi-dimensional optimization problems such as the optimal design of HPS consisting of renewable and non-renewable energy sources.

6.2 Contributions to knowledge

This study has made the following contributions to knowledge in the field of hybrid renewable energy system.

1. The result of this study have made it possible to identify the most appropriate orientation state of the bifacial PV module capable of generating more additional energy; identifying the right orientation of the module during installation will help improve the total power output that can be extracted from a bifacial PV system and subsequently increasing the share of renewable energy in the system.
2. The result of this study has also demonstrated the effectiveness of the Giza Pyramid Construction optimization algorithm as compared to FA and WOA algorithms in solving optimal design problems of hybrid power system consisting of renewable and non-renewable energy sources. An optimization model based on the proposed algorithm has been developed. The model, which is capable of accepting input variables and returning an optimal solution in terms of life cycle cost and total environmental pollution can be used by government agencies, decision makers and energy solution companies to optimally size and analyze the components of HPS before implementation.

6.3 Recommendations

The following recommendations are suggested for future research.

1. It is recommended that the amount of the additional energy contributed by the back side of a bifacial module under different albedo values for both orientation states should be investigated and incorporated into the optimal design of hybrid power system.

2. Future work on the inclusion of other types of renewable energy sources such as biomass, geothermal, fuel cell, ocean wave and small hydro should also be conducted.
3. The response of the developed HPS under small and large signal disturbances can be investigated to determine its impact on existing grid.
4. Different optimization methods such as Political Optimizer, Equilibrium Optimizer, Corona virus algorithm and many other recent optimization algorithms should be applied to the optimal design of HPS consisting of bifacial PV modules, wind turbine, split genset, as well as battery system, and the results should be compared with the proposed algorithm used in this study for the same purpose.

Bibliography

Abaye, A. E. (2018). System Analysis and Optimization of photovoltaic-wind hybrid system: Review. *International Research Journal of Engineering and Technology*, *5*(1), 197–201. www.irjet.net

Abedi, S., Alimardani, A., Gharehpetian, G. B., Riahy, G. H., & Hosseinian, S. H. (2012). A comprehensive method for optimal power management and design of hybrid RES-based autonomous energy systems. *Renewable and Sustainable Energy Reviews*, *16*(3), 1577–1587. https://doi.org/10.1016/j.rser.2011.11.030

Achkari, O., & Fadar, A. El. (2018). Renewable Energy Storage Technologies-A Review. *Conference Internationale En Automatique & Traitement de Signal*, *35*, 69–79.

Adebanji, B., Adepoju, G. A., Olulope, P., Fasina, T., & Adetan, O. (2020). Feasibility and optimal design of a hybrid power system for rural electrification for a small village. *International Journal of Electrical and Computer Engineering*, *10*(6), 6214–6224. https://doi.org/10.11591/IJECE.V10I6.PP6214-6224

Adebanji, B., Adepoju, G. A., Oni, J. O., & Olulope, P. K. (2017). *Optimal Sizing Of An Off-Grid Small Hydro- Photovoltaic-Diesel Generator Hybrid Power System For A Distant Village*. *6*(08).

Ademola, S., & Qiu, Y. (2020). *Potential of Bifacial PV Installation and Optimization*. *11*(12), 558–565.

Aditi, & Ashok Kumar Pandey. (2016). A Review Paper on Hybrid Power System with Different Controllers and Tracking Methods. *International Journal of Engineering Research And*, *V5*(01), 6–9. https://doi.org/10.17577/ijertv5is010022

Ahamad, N. B., Othman, M., Vasquez, J. C., Guerrero, J. M., & Su, C. L. (2018). Optimal sizing and performance evaluation of a renewable energy based microgrid in future seaports. *Proceedings of the IEEE International Conference on Industrial Technology*, *2018-February*, 1043–1048. https://doi.org/10.1109/ICIT.2018.8352322

Akter, H., Howlader, H. O. R., Saber, A. Y., Mandal, P., Takahashi, H., & Senjyu, T. (2021). Optimal sizing of hybrid microgrid in a remote island considering advanced direct load control for demand response and low carbon emission. *Energies*, *14*(22). https://doi.org/10.3390/en14227599

AL Shaqsi, A. Z., Sopian, K., & Al-Hinai, A. (2020). Review of energy storage services, applications, limitations, and benefits. *Energy Reports*, *6*, 288–306. https://doi.org/10.1016/j.egyr.2020.07.028

Alam, A., & Mehar, M. V. (2021). Hybrid Renewable Energy System Integration with Grid – A Review. *Smart Moves Journal Ijoscience*, *7*(5), 78–82. https://doi.org/10.24113/ijoscience.v7i11.459

Alam, M., Gul, M. S., & Muneer, T. (2021). Self-shadow analysis of bifacial solar photovoltaic and its implication on view factor computation. *2021 IEEE Green Energy and Smart Systems Conference, IGESSC 2021*, *2*, 2–6. https://doi.org/10.1109/IGESSC53124.2021.9618684

Algabalawy, M. A., Abdelaziz, A. Y., Mekhamer, S. F., & Aleem, S. H. E. A. (2018). Considerations on optimal design of hybrid power generation systems using whale and sine cosine optimization algorithms Considerations on optimal design of hybrid power generation systems using whale and sine cosine optimization algorithms. *Journal of Electrical Systems and Information Technology*, *5*(3), 312–325. https://doi.org/10.1016/j.jesit.2018.03.004

Ali, N., Othman, M. A., Husain, M. N., & Misran, M. H. (2014). A review of firefly algorithm. *ARPN Journal of Engineering and Applied Sciences*, *9*(10), 1732–1736.

Ali, S., & Jang, C. M. (2020). Optimum design of hybrid renewable energy system for sustainable energy supply to a remote Island. *Sustainability (Switzerland)*, *12*(3). https://doi.org/10.3390/su12031280

Aliprantis, D. C., & Lafayette, W. (2014). *Fundamentals of Wind Energy Conversion for Electrical Engineers*. 46.

Alrikabi, N. K. M. A. (2014a). Renewable Energy Types. *Journal of Clean Energy Technologies*, *January 2014*, 61–64. https://doi.org/10.7763/jocet.2014.v2.92

Alrikabi, N. K. M. A. (2014b). Renewable Energy Types. *Journal of Clean Energy Technologies*, *2*(1), 61–64. https://doi.org/10.7763/jocet.2014.v2.92

Altherwi, A. (2020). Application of the Firefly Algorithm for Optimal Production and Demand Forecasting at Selected Industrial Plant. *Open Journal of Business and Management*, *08*(06), 2451–2459. https://doi.org/10.4236/ojbm.2020.86151

Amer, M., Namaane, A., & M'Sirdi, N. K. (2013). Optimization of hybrid renewable energy systems (HRES) using PSO for cost reduction. *Energy Procedia*, *42*, 318–327. https://doi.org/10.1016/j.egypro.2013.11.032

Ammari, C., Belatrache, D., Touhami, B., & Makhloufi, S. (2021). Sizing, optimization, control and energy management of hybrid renewable energy system—A review. *Energy and Built Environment*, *December 2020*. https://doi.org/10.1016/j.enbenv.2021.04.002

An, L. N., Quoc-Tuan, T., Seddik, B., & Be, N. (2014). Optimal design of an isolated photovoltaic-diesel-battery hybrid system by using an iterative algorithm. *IEEE Power and Energy Society General Meeting*, *2014-October*(October), 0–4. https://doi.org/10.1109/PESGM.2014.6939171

Aneke, M., & Wang, M. (2016). Energy storage technologies and real life applications – A state of the art review. *Applied Energy*, *179*, 350–377. https://doi.org/10.1016/j.apenergy.2016.06.097

Ardakani, F. J., Riahy, G., & Abedi, M. (2010). Optimal sizing of a grid-connected hybrid system for north-west of Iran-case study. *2010 9th Conference on Environment and Electrical Engineering, EEEIC 2010*, 29–32. https://doi.org/10.1109/EEEIC.2010.5490006

Arifin, Z., Triyono, N. A., & Supriyanto, E. (2021). Technology Selection of Solar PV for Household and Small Industries in Indonesia. *Proceedings - ICCTEIE 2021: 2021 International Conference on Converging Technology in Electrical and Information Engineering: Converging Technology for Sustainable Society*, 97–101. https://doi.org/10.1109/ICCTEIE54047.2021.9650625

Arun, S. L., Kumaravel, S., & Selvan, M. P. (2014). Unit size optimization of Hybrid Energy System. *2014 IEEE Innovative Smart Grid Technologies - Asia, ISGT ASIA 2014*, 79–83. https://doi.org/10.1109/ISGT-Asia.2014.6873768

Ashagire, A. A., Adjallah, K. H., & Bekele, G. (2021). Optimal sizing of hybrid energy sources by using genetic algorithm and particle swarm optimization algorithms considering life cycle cost. *International Conference on Electrical, Computer, Communications and Mechatronics Engineering, ICECCME 2021*, *October*, 7–8. https://doi.org/10.1109/ICECCME52200.2021.9590952

Atia, R., & Yamada, N. (2016). Sizing and Analysis of Renewable Energy and Battery Systems in Residential Microgrids. *IEEE Transactions on Smart Grid*, *7*(3), 1204–1213. https://doi.org/10.1109/TSG.2016.2519541

Ayodele, T. R., Ogunjuyigbe, A. S. O., & Akinola, O. A. (2017). n-split generator model: An approach to

reducing fuel consumption, LCC, CO2 emission and dump energy in a captive power environment. *Sustainable Production and Consumption*, *12*(July), 193–205. https://doi.org/10.1016/j.spc.2017.07.006

B.Eteiba, M., T. El Shenawy, E., H. Shazly, J., & Z. Hafez, A. (2013). A Photovoltaic (Cell, Module, Array) Simulation and Monitoring Model using MATLAB®/GUI Interface. *International Journal of Computer Applications*, *69*(6), 14–28. https://doi.org/10.5120/11845-7579

Babatunde, O. M., Munda, J. L., & Hamam, Y. (2020). A Comprehensive State-of-the-Art Survey on Hybrid Renewable Energy System Operations and Planning. *IEEE Access*, *8*, 75313–75346. https://doi.org/10.1109/ACCESS.2020.2988397

Babu, B., & Divya, S. (2017). Comparative study of different types of generators used in wind turbine and reactive power compensation. *IOSR Journal of Electrical and Electronics Engineering*, 2320–3331. www.iosrjournals.org

Badejani, M. M., Masoum, M. A. S., & Kalanta, M. (2007). Optimal design and modeling of stand-alone hybrid PV-wind systems. *2007 Australasian Universities Power Engineering Conference, AUPEC*, 1–6. https://doi.org/10.1109/AUPEC.2007.4548134

Bahtiyar Dursun, Sibel Dursun, & Ercan Aykut. (2020). An Assessment of Renewable Energy Options for Somalia Turkey Hospital. *J. of Electrical Engineering*, *8*(1), 27–45. https://doi.org/10.17265/2328-2223/2020.01.005

BALARAJU, V., & Chengaiah, C. (2020). Mathematical Analysis of Solar Photovoltaic Array Configurations with Partial Shaded Modules. *Trends in Renewable Energy*, *6*(2), 121–143. https://doi.org/10.17737/tre.2020.6.2.00115

Bandaru, S., & Deb, K. (2016). Metaheuristic techniques. *Decision Sciences: Theory and Practice*, 693–749. https://doi.org/10.1201/9781315183176

Bansal, A. K., Gupta, R. A., & Kumar, R. (2011). Optimization of hybrid PV/wind energy system using Meta Particle Swarm Optimization (MPSO). *India International Conference on Power Electronics, IICPE 2010*. https://doi.org/10.1109/IICPE.2011.5728079

Baumann, T., Carigiet, F., Knecht, R., Klenk, M., Dreisiebner, A., Nussbaumer, H., & Baumgartner, F. (2018). Performance Analysis of Vertically Mounted Bifacial PV Modules on Green Roof System. *35th European Photovoltaic Solar Energy Conference and Exhibition (EU PVSEC 2018), Brussels*, *September*, 2–7.

Behabtu, H. A., Messagie, M., Coosemans, T., Berecibar, M., Fante, K. A., Kebede, A. A., & Van Mierlo, J. (2020). A review of energy storage technologies' application potentials in renewable energy sources grid integration. *Sustainability (Switzerland)*, *12*(24), 1–20. https://doi.org/10.3390/su122410511

Belyaev, M. E., & Gerasimov, D. (2020). *Design of Diesel Engine Mathematical Model Oriented to Speed Control Design of Diesel Engine Mathematical Model Oriented to Speed Control*. *August*. https://doi.org/10.1134/S1064230718040044

Benhamed, S., Ibrahim, H., Belmokhtar, K., Hosni, H., Ilinca, A., Rousse, D., Chandra, A., & Ramdenee, D. (2016). Dynamic modeling of diesel generator based on electrical and mechanical aspects. *2016 IEEE Electrical Power and Energy Conference, EPEC 2016*. https://doi.org/10.1109/EPEC.2016.7771756

Bhaskar, M. A., & Jimoh, A. A. (2016). Wk ,qwhuqdwlrqdo &rqihuhqfh rq 5hqhzdeoh (qhuj\ 5hvhdufk dqg $ssolfdwlrqv 1ry %luplqjkdp 8. *5th International Conference on Renewable Energy Research and Applications*, *5*, 14–17.

Bhikabhai, Y. (2005). Hybrid Power Systems and Their. *Energy*, *August*, 1–48. https://docs.niwa.co.nz/library/public/SMR406.pdf

Bilal, B. O., Sambou, V., Kébé, C. M. F., Ndiaye, P. A., & Ndongo, M. (2012). *Energy Procedia Methodology to Size an Optimal Stand-Alone PV / wind / diesel / battery System Minimizing the Levelized cost of Energy and the CO 2 Emissions*. *14*(December), 1636–1647. https://doi.org/10.1016/j.egypro.2011.12.1145

Bissey, S., Jacques, S., Reymond, C., & Bunetel, J. Le. (2018). *An Innovative Bidirectional DC-AC Converter to Improve Power Quality in a Grid-Connected Microgrid*. *July*, 1–18. https://doi.org/10.20944/preprints201807.0252.v1

Bordry, F., & Aguglia, D. (2015). *Definition of Power Converters*. *003*(May 2014), 7–14.

Bossoufi, B., Lamnadi, M., Trihi, M., & Boulezhar, A. (2019). Optimal design of stand-alone hybrid power system using wind and solar energy sources. *International Journal of Energy Technology and Policy*, *15*(2/3), 280. https://doi.org/10.1504/ijetp.2019.10019646

Bouaouda, A., & Sayouti, Y. (2022). Hybrid Meta-Heuristic Algorithms for Optimal Sizing of Hybrid Renewable Energy System: A Review of the State-of-the-Art. In *Archives of Computational Methods in Engineering* (Issue 0123456789). Springer Netherlands. https://doi.org/10.1007/s11831-022-09730-x

Bourennani, F., Rahnamayan, S., & Naterer, G. F. (2015). Optimal design methods for hybrid renewable energy systems. *International Journal of Green Energy*, *12*(2), 148–159. https://doi.org/10.1080/15435075.2014.888999

Bright, R. (2008). Selecting cable strain reliefs. *Electronic Products (Garden City, New York)*, *50*(3).

Bsolar, Commercial test sites and outdoor field results, http://www.b solar.com/Technology.aspx?Sel=Field%20Results, Accessed: 2022-05-29.

Cao, W., Xie, Y., & T, Z. (2012). Wind Turbine Generator Technologies. *Advances in Wind Power*. https://doi.org/10.5772/51780

Carvalho Ganilha, S. (2017). *Potential of bifacial PV installation and its integration with storage solutions*.

Cetinbas, I., Tamyurek, B., & Demirtas, M. (2022). The Hybrid Harris Hawks Optimizer-Arithmetic Optimization Algorithm: A New Hybrid Algorithm for Sizing Optimization and Design of Microgrids. *IEEE Access*, *10*, 19254–19283. https://doi.org/10.1109/ACCESS.2022.3151119

Chandrashekhar, P. K., Managuli, S., & Shashank, A. (2019). Design of small scale vertical axis wind turbine. *1st International Conference on Power Electronics Applications and Technology in Present Energy Scenario, PETPES 2019 - Proceedings*. https://doi.org/10.1109/PETPES47060.2019.9003999

Chen, A. (2010). Speed regulator of diesel-generator based on model free adaptive control. *Proceedings - 2010 2nd WRI Global Congress on Intelligent Systems, GCIS 2010*, *3*(3), 193–196. https://doi.org/10.1109/GCIS.2010.257

Chen, H., Cong, T. N., Yang, W., Tan, C., Li, Y., & Ding, Y. (2009). Progress in electrical energy storage system: A critical review. *Progress in Natural Science*, *19*(3), 291–312. https://doi.org/10.1016/j.pnsc.2008.07.014

Clark, R., Cronje, W., & Wyk, M. A. Van. (2015). Design optimization of a hybrid energy system through fast convex programming. *Proceedings - International Conference on Intelligent Systems, Modelling and Simulation, ISMS*, *2015-Septe*, 423–428. https://doi.org/10.1109/ISMS.2014.78

Coban, H. H., Rehman, A., & Mohamed, A. (2022). Technical and Economical Investigation of a Centralized and Decentralized Hybrid Renewable Energy System in Cadaado, Somalia. *Processes*, *10*(4). https://doi.org/10.3390/pr10040667

crystals12. (2012). *Various Wind Turbine TechnologiesSeptember 2012*. *September*, 1–30. papers3://publication/uuid/60644B6F-0F28-45D6-89EA-D110C81DA1BF

Das, J. (2020). Optimal Component Sizing of an Isolated PV-Wind-Battery Microgrid in India using Multi Objective Optimisation. *2020 IEEE 17th India Council International Conference, INDICON 2020*, *1*. https://doi.org/10.1109/INDICON49873.2020.9342122

Davis, M. S., Jafarian, A., Ferdowsi, F., & Madani, M. R. (2021). Wind energy harvesting capability of a novel cascaded dual-rotor horizontal-axis wind turbine. *International Conference on Electrical, Computer, Communications and Mechatronics Engineering, ICECCME 2021*, *October*, 7–8. https://doi.org/10.1109/ICECCME52200.2021.9590963

Deb, S., Ghosh, D., & Mohanta, D. K. (2017). Optimal configuration of stand-alone hybrid microgrid considering cost, reliability and environmental factors. *International Conference on Signal Processing, Communication, Power and Embedded System, SCOPES 2016 - Proceedings*, 48–53. https://doi.org/10.1109/SCOPES.2016.7955878

del Moral, J. S., & Egido, M. A. (2012). Simulation of AC, DC, and AC-DC coupled mini-grids. In search of the most efficient system. *Proceedings of the 6th European Conference on PV Hybrids an Mini Grids*, 0–20. http://oa.upm.es/19167/

Delgado, C., & Dominguez-Navarro, J. A. (2014). Optimal design of a hybrid renewable energy system. *2014 9th International Conference on Ecological Vehicles and Renewable Energies, EVER 2014*. https://doi.org/10.1109/EVER.2014.6844008

Deline, C., Macalpine, S., Marion, B., Toor, F., Asgharzadeh, A., & Stein, J. S. (2017). Evaluation and field assessment of bifacial photovoltaic module power rating methodologies. *2017 IEEE 44th Photovoltaic Specialist Conference, PVSC 2017*, *7*(2), 1–6. https://doi.org/10.1109/PVSC.2017.8366887

Deng, W., Chen, D., Xiong, Z., Verlinden, P. J., Member, S., Dong, J., Ye, F., Li, H., Zhu, H., Zhong, M., Yang, Y., Chen, Y., Feng, Z., & Altermatt, P. (2015). P-Type Multicrystalline Silicon Substrate. *IEEE Journal of Photovoltaics*, *6*(1), 1–7.

Diemuodeke, E. O., Addo, A., Oko, C. O. C., Mulugetta, Y., & Ojapah, M. M. (2019). Optimal mapping of hybrid renewable energy systems for locations using multi-criteria decision-making algorithm. *Renewable Energy*, *134*, 461–477. https://doi.org/10.1016/j.renene.2018.11.055

Dodo, U. A., Ashigwuike, E. C., Gafai, N. B., Eronu, E. M., Sada, A. Y., & Dodo, M. A. (2020). Optimization of an Autonomous Hybrid Power System for an Academic Institution. *European Journal of Engineering Research and Science*, *5*(10), 1160–1167.

https://doi.org/10.24018/ejers.2020.5.10.2157

Dukes, S., Shohoud, O., & Welch, T. (2021). *Exploring the Great Pyramid : Detector Technical Design Report with Stand-Alone Monte Carlo Simulations Introduction*.

Edenhofer, O., Madruga, R. P., Sokona, Y., Seyboth, K., Matschoss, P., Kadner, S., Zwickel, T., Eickemeier, P., Hansen, G., Schlömer, S., & von Stechow, C. (2011). Renewable energy sources and climate change mitigation: Special report of the intergovernmental panel on climate change. In *Renewable Energy Sources and Climate Change Mitigation: Special Report of the Intergovernmental Panel on Climate Change*. https://doi.org/10.1017/CBO9781139151153

El Boujdaini, L., Mezrhab, A., Moussaoui, M. A., Jurado, F., & Vera, D. (2022). Sizing of a stand-alone PV–wind–battery–diesel hybrid energy system and optimal combination using a particle swarm optimization algorithm. *Electrical Engineering*. https://doi.org/10.1007/s00202-022-01529-0

El Chaar, L., Lamont, L. A., & Elzein, N. (2011). Wind energy technology - Industrial update. *IEEE Power and Energy Society General Meeting*, *m*, 1–5. https://doi.org/10.1109/PES.2011.6039575

Elbaz, A., & Tahir Guneser, M. (2021). Algorithms to model and optimize a stand-alone photovoltaic-diesel-battery system: An application in rural libya. *Tehnicki Vjesnik*, *28*(2), 523–529. https://doi.org/10.17559/TV-20200530094834

Ellabban, O., Abu-Rub, H., & Blaabjerg, F. (2014). Renewable energy resources: Current status, future prospects and their enabling technology. *Renewable and Sustainable Energy Reviews*, *39*, 748–764. https://doi.org/10.1016/j.rser.2014.07.113

Elmanakhly, D. A., Saleh, M. M., & Rashed, E. A. (2021). An Improved Equilibrium Optimizer Algorithm for Features Selection: Methods and Analysis. *IEEE Access*, *9*, 120309–120327. https://doi.org/10.1109/ACCESS.2021.3108097

Energy Education [EE], Accessed: 06/21/2022, from https://energyeducation.ca/encyclopedia/Wind_power#cite_note-1.

Esan, A. B., Agbetuyi, A. F., Oghorada, O., Ogbeide, K., Awelewa, A. A., & Afolabi, A. E. (2019). Reliability assessments of an islanded hybrid PV-diesel-battery system for a typical rural community in Nigeria. *Heliyon*, *5*(5), e01632. https://doi.org/10.1016/j.heliyon.2019.e01632

Fajuke, I. D., & Raji, A. K. (2022). Firefly Algorithm-Based Optimization of the Additional Energy Yield of Bifacial PV Modules. *Energies*, *15*(7). https://doi.org/10.3390/en15072651

Farahani, S. M., Abshouri, A. A., Nasiri, B., & Meybodi, M. R. (2011). A Gaussian Firefly Algorithm. *International Journal of Machine Learning and Computing*, *1*(5), 448–453. https://doi.org/10.7763/ijmlc.2011.v1.67

Fioriti, D., Lutzemberger, G., Poli, D., & Micangeli, A. (2020). Optimal sizing and operation of isolated microgrids for developing countries: Hedging uncertainties with Monte Carlo techniques. *IEEE PES Innovative Smart Grid Technologies Conference Europe*, *2020-October*, 744–748. https://doi.org/10.1109/ISGT-Europe47291.2020.9248897

Frp, V. J., Vhq, U., & Df, G. (2021). *5Hylhz Rq Wkh Ghyhorsphqw Vfhqdulr Ri Uhqhzdeoh Hqhuj \ Lq Gliihuhqw Frxqwu *. 28–29.

Fullerton, D. G., Bruce, N., & Gordon, S. B. (2008). Linking Renewable Energy to Rural Development. *Transactions of the Royal Society of Tropical Medicine and Hygiene*, *102*(9), 843–851.

http://dx.doi.org/10.1016/j.enpol.2011.04.070%5Cnhttp://dx.doi.org/10.1016/j.apenergy.2012.07.032%5Cnhttp://dx.doi.org/10.1016/j.esd.2013.12.005%5Cnhttp://dx.doi.org/10.1016/j.enpol.2013.11.042%5Cnhttp://dx.doi.org/10.1016/j.biombioe.2012.12.028%5Cnhttp:/

Galiullin, L. A., & Valiev, R. A. (2017). *Mathematical Modelling of Diesel Engine Testing and Diagnostic Regimes*. *December*, 1864–1871.

Girma, Z. (2013). Hybrid renewable energy design for rural electrification in Ethiopia. *Journal of Energy Technologies and Policy*, *3*(13), 38–53. http://www.iiste.org/Journals/index.php/JETP/article/viewFile/9765/9972

Graefenhain, M., Fiedler, F., & Tsanakas, I. (2017). Energy Yield Simulation Analysis of Bifacial PV Installations in the Nordic Climate. *European Solar Engineering School*, *221*.

Gray, J. L. (2011). The Physics of the Solar Cell. In *Handbook of Photovoltaic Science and Engineering*. https://doi.org/10.1002/9780470974704.ch3

H-Tec Education [HTE], Retrieved May 6, 2022, from http://www.htec.com/fileadmin/content/edu/Lehrmaterialien/Transparencies.pdf

Hansen, C. W., Stein, J. S., Deline, C., Macalpine, S., Marion, B., Asgharzadeh, A., & Toor, F. (2016). Analysis of irradiance models for bifacial PV modules. *Conference Record of the IEEE Photovoltaic Specialists Conference*, *2016-Novem*(June), 138–143. https://doi.org/10.1109/PVSC.2016.7749564

Hansen, C. W., Stein, J. S., Deline, C., Macalpine, S., Marion, B., Asgharzadeh, A., & Toor, F. (2017). Analysis of irradiance models for bifacial PV modules. *2017 IEEE 44th Photovoltaic Specialist Conference, PVSC 2017*, 1376–1380. https://doi.org/10.1109/PVSC.2017.8366322

Harifi, S., Khalilian, M., Mohammadzadeh, J., & Ebrahimnejad, S. (2020). New generation of metaheuristics by inspiration from ancient. *2020 10h International Conference on Computer and Knowledge Engineering, ICCKE 2020*, 256–261. https://doi.org/10.1109/ICCKE50421.2020.9303653

Harifi, S., Mohammadzadeh, J., Khalilian, M., & Ebrahimnejad, S. (2020). Giza Pyramids Construction: an ancient-inspired metaheuristic algorithm for optimization. *Evolutionary Intelligence*, *0123456789*. https://doi.org/10.1007/s12065-020-00451-3

Harifi, S., Mohammadzadeh, J., Khalilian, M., & Ebrahimnejad, S. (2021a). Giza Pyramids Construction: an ancient-inspired metaheuristic algorithm for optimization. *Evolutionary Intelligence*, *14*(4), 1743–1761. https://doi.org/10.1007/s12065-020-00451-3

Harifi, S., Mohammadzadeh, J., Khalilian, M., & Ebrahimnejad, S. (2021b). Giza Pyramids Construction: an ancient-inspired metaheuristic algorithm for optimization. *Evolutionary Intelligence*, *14*(4), 1743–1761. https://doi.org/10.1007/s12065-020-00451-3

Harrouz, A. (2019). *(QHUJ \ 0RGHOLQJ 2XWSXW RI : LQG 6 \ VWHP EDVHG RQ : LQG 6SHHG*. *2019*, 63–68.

Hassan, Q., Jaszczur, M., & Abdulateef, J. (2016). Optimization of PV/WIND/DIESEL Hybrid Power System in HOMER for Rural Electrification. *Journal of Physics: Conference Series*, *745*(3). https://doi.org/10.1088/1742-6596/745/3/032006

Hassanzadehfard, H., Moghaddas-Tafreshi, S. M., & Hakimi, S. M. (2011). Optimal Sizing of an Islanded Micro-Grid for an Area in North-West Iran Using Particle Swarm Optimization Based on Reliability

Concept. *Proceedings of the World Renewable Energy Congress – Sweden, 8–13 May, 2011, Linköping, Sweden*, *57*, 2969–2976. https://doi.org/10.3384/ecp110572969

Hawass, Z. (1998). Pyramid Construction New Evidence Discovered at Giza. *Stationen: Beitrage Zur Kulturgeschichte Agyptens; Rainer Stadelmann Gewidmet*, 53–66.

He, G. X., Cheng, L., Xu, J., Chen, L., & Tao, W. Q. (2017). Optimal configuration of a wind/PV/battery hybrid energy system using HOMER software. *Chemical Engineering Transactions*, *61*, 1507–1512. https://doi.org/10.3303/CET1761249

Heemels, W. P. M. H., Lehmann, D., Lunze, J., & De Schutter, B. (2011). Introduction to hybrid systems. *Handbook of Hybrid Systems Control*, *May*, 3–30. https://doi.org/10.1017/cbo9780511807930.002

Helal, A., El-Mohr, R., & Eldosouki, H. (2012). Optimal design of hybrid renewable energy system for electrification of a remote village in Egypt. *2nd International Conference on Communications Computing and Control Applications, CCCA 2012*. https://doi.org/10.1109/CCCA.2012.6417901

Hermann, D. T., Franck Armel, T. K., René, T., & Donatien, N. (2022). Consideration of some optimization techniques to design a hybrid energy system for a building in Cameroon. *Energy and Built Environment*, *3*(2), 233–249. https://doi.org/10.1016/j.enbenv.2021.01.007

Hinz, H. (2019). Comparison of Lithium-Ion Battery Models. *Inventions*, *41*(4).

Hlal, I. M., Ramachandaramurthy, V. K., Hafiz Nagi, F., & Bin Tuan Abdullah, T. A. R. (2019). Optimal Techno-Economic Design of Standalone Hybrid Renewable Energy System Using Genetic Algorithm. *IOP Conference Series: Earth and Environmental Science*, *268*(1). https://doi.org/10.1088/1755-1315/268/1/012012

Holt, A., & Pengelly, I. J. (2008). ITS and renewable energy. *15th World Congress on Intelligent Transport Systems and ITS America Annual Meeting 2008*, *6*, 3854–3862. https://doi.org/10.1049/ic.2008.0789

How Stuff Works [HSW], Retrieved Nov 11, 2021, from http://electronics.howstuffworks.com/everyday-tech/lithium-ion-battery1.htm

Hu, Y., Zhu, Z., Xiao, G., Zhou, B., Zou, T., & Zhang, R. (2021). Optimal design of hybrid renewable energy system considering equipment performance and annual cost. *Conference Digest - 2021 International Conference on Security, Pattern Analysis, and Cybernetics, SPAC 2021*, 71–75. https://doi.org/10.1109/SPAC53836.2021.9539917

Huang, M., Fu, L., Zhang, Y., & Gao, X. (2017). *Optimal Design of an Island Microgrid with Considering Scheduling Optimization*. 0–5.

Ibrahim, M., Khair, A., & Ansari, S. (2011). A Review of Hybrid Renewable / Alternative Energy Systems for Electric Power Generation : *IEEE Transactions on Sustainable Energy*, *2*(4), 392–403. https://doi.org/10.1109/TSTE.2011.2157540

International Energy Outlook [IEO] 2013 [Online]. Available at: http://www.eia.gov/forecasts/ieo/pdf/0484(2013).pdf. [Accessed: 01-July-2022].

IRENA. (2013). Pacific Lighthouses: Hybrid power systems. *Irena*.

IRENA. (2016). Wind power - technology Brief. *Energy*, *16*, 1–24.

Ishraque, M. F., Shezan, S. A., Rashid, M. M., Bhadra, A. B., Hossain, M. A., Chakrabortty, R. K., Ryan, M. J., Fahim, S. R., Sarker, S. K., & Das, S. K. (2021). Techno-Economic and Power System Optimization of a Renewable Rich Islanded Microgrid Considering Different Dispatch Strategies. *IEEE Access*, *9*, 77325–77340. https://doi.org/10.1109/ACCESS.2021.3082538

Jäger, K., Tillmann, P., & Becker, C. (2020). Detailed illumination model for bifacial solar cells. *Optics Express*, *28*(4), 4751. https://doi.org/10.1364/oe.383570

Janssen, G. J. M., Van Aken, B. B., Carr, A. J., & Mewe, A. A. (2015). Outdoor Performance of Bifacial Modules by Measurements and Modelling. *Energy Procedia*, *77*, 364–373. https://doi.org/10.1016/j.egypro.2015.07.051

Jarraya, B., & Bouri, A. (2012). Metaheuristic Optimization Backgrounds: A Literature Review. *International Journal of Contemporary Business Studies*, *3*(12), 2156–7506. http://www.akpinsight.webs.com

Jha, V. N., Karn, S. K., & Kumar, K. (2018). Review on the Role of Mathematical Modeling in Energy Sectors. *International Journal of Engineering Science Invention (IJESI)*, *6*(12), 18. www.ijesi.org

Johari, N. F., Zain, A. M., Mustaffa, N. H., & Udin, A. (2013). Firefly algorithm for optimization problem. *Applied Mechanics and Materials*, *421*(April), 512–517. https://doi.org/10.4028/www.scientific.net/AMM.421.512

Johnson, J., Yoon, D., & Baghzouz, Y. (2012). Modeling and analysis of a bifacial grid-connected photovoltaic system. *IEEE Power and Energy Society General Meeting*, 1–6. https://doi.org/10.1109/PESGM.2012.6345266

Kaabeche, A., Diaf, S., & Ibtiouen, R. (2017). Firefly-inspired algorithm for optimal sizing of renewable hybrid system considering reliability criteria. *Solar Energy*, *155*, 727–738. https://doi.org/10.1016/j.solener.2017.06.070

Kadeval, H. N. (2021). *Mathematical modelling for solar cell , panel and array for photovoltaic system*. *9411*.

Kalantari, N. T., Ahangari Hassas, M., & Pourhossein, K. (2018). Bibliographic Review and Comparison of Optimal Sizing Methods for Hybrid Renewable Energy Systems. *Journal of Energy Management and Technology (JEMT)*, *2*(2), 66. http://dx.doi.org/10.22109/jemt.2018.102306.1039

Kalmikov, A. (2017). Wind Power Fundamentals. *Wind Energy Engineering: A Handbook for Onshore and Offshore Wind Turbines*, 17–24. https://doi.org/10.1016/B978-0-12-809451-8.00002-3

Kamjoo, A., Maheri, A., Dizqah, A. M., & Putrus, G. A. (2016). Multi-objective design under uncertainties of hybrid renewable energy system using NSGA-II and chance constrained programming. *International Journal of Electrical Power and Energy Systems*, *74*, 187–194. https://doi.org/10.1016/j.ijepes.2015.07.007

Katsigiannis, Y. A., Georgilakis, P. S., & Karapidakis, E. S. (2012). Hybrid simulated annealing-tabu search method for optimal sizing of autonomous power systems with renewables. *IEEE Transactions on Sustainable Energy*, *3*(3), 330–338. https://doi.org/10.1109/TSTE.2012.2184840

Kaur, R., Krishnasamy, V., Kandasamy, N. K., & Kumar, S. (2020). Discrete Multiobjective Grey Wolf Algorithm Based Optimal Sizing and Sensitivity Analysis of PV-Wind-Battery System for Rural Telecom Towers. *IEEE Systems Journal*, *14*(1), 729–737.

https://doi.org/10.1109/JSYST.2019.2912899

Kenu, E. S., Uhunmwangho, R., & Okafor, E. N. C. (2022). Optimal sizing and simulation of a sustainable off-grid hybrid energy system: A case study of the coastal areas of Delta State. *Nigerian Journal of Technology*, *41*(2), 291–301. https://doi.org/10.4314/njt.v41i2.11

Khalilnejad, A., Sundararajan, A., & Sarwat, A. I. (2018). Optimal design of hybrid wind/photovoltaic electrolyzer for maximum hydrogen production using imperialist competitive algorithm. *Journal of Modern Power Systems and Clean Energy*, *6*(1), 40–49. https://doi.org/10.1007/s40565-017-0293-0

Kharrich, M., Kamel, S., Abdeen, M., Mohammed, O. H., Akherraz, M., Khurshaid, T., & Rhee, S. B. (2021). Developed approach based on equilibrium optimizer for optimal design of hybrid PV/Wind/Diesel/Battery Microgrid in Dakhla, Morocco. *IEEE Access*, *9*, 13655–13670. https://doi.org/10.1109/ACCESS.2021.3051573

Kharrich, M., Kamel, S., Alghamdi, A. S., Eid, A., Mosaad, M. I., Akherraz, M., & Abdel-Akher, M. (2021). Optimal design of an isolated hybrid microgrid for enhanced deployment of renewable energy sources in Saudi Arabia. *Sustainability (Switzerland)*, *13*(9), 1–26. https://doi.org/10.3390/su13094708

Kharrich, M., Mohammed, O. H., & Akherraz, M. (2020). Design of hybrid microgrid PV/wind/diesel/battery system: Case study for rabat and baghdad. *EAI Endorsed Transactions on Energy Web*, *7*(26), 1–9. https://doi.org/10.4108/eai.13-7-2018.162692

Kiehbadroudinezhad, M., & Merabet, A. (2022). *clean technologies Review of Latest Advances and Prospects of Energy Storage Systems : Considering Economic , Reliability , Sizing , and Environmental Impacts Approach*. 477–501.

Kim, E. S., Song, B. M., & Lee, K. Y. (2010). Modeling and analysis of a grid-connected wind energy conversion system using PSCAD/EMTDC. *Innovative Smart Grid Technologies Conference, ISGT 2010*, 1–6. https://doi.org/10.1109/ISGT.2010.5434756

Knudsen, J. (2017). *Aalborg Universitet Modeling , Control , and Optimization for Diesel-Driven Generator Sets Knudsen , Jesper Viese Publication date :*

Kopecek, R., & Libal, J. (2021). Bifacial photovoltaics 2021: Status, opportunities and challenges. *Energies*, *14*(8). https://doi.org/10.3390/en14082076

Koutroulis, E., Kolokotsa, D., Potirakis, A., & Kalaitzakis, K. (2006). Methodology for optimal sizing of stand-alone photovoltaic/wind-generator systems using genetic algorithms. *Solar Energy*, *80*(9), 1072–1088. https://doi.org/10.1016/j.solener.2005.11.002

Kumar, A. (2021). A Novel Meta-Heuristic Gizza Pyramid Construction Optimization Approach for Image Encryption using Logistic Map and DNA Encoding. *Journal of Soft Computing and Engineering …*, *2*(1), 33–44. https://srkpublication.org/files/archives/1639634353_4 Kumar-2021.pdf

Kushida, T., & Abe, R. (2016). Optimal design of a grid connected PV-diesel hybrid system. *EEEIC 2016 - International Conference on Environment and Electrical Engineering*, 2–5. https://doi.org/10.1109/EEEIC.2016.7555493

Larsson, M. (2009). Global Energy Transformation. In *Global Energy Transformation*. https://doi.org/10.1057/9780230244092

Lassalle, J. M., Martínez, D. F., & Fernández, L. V. (2022). Optimisation of hybrid renewable energy systems on islands: A review. *Island Studies Journal*, *17*(1), 221–242. https://doi.org/10.24043/isj.167

Leholo, S. T., Owolawi, P. A., & Akindeji, K. T. (2022). Optimisation of a RE-Based Hybrid System for Covid-19 Vaccine Cold Storage Facility. *Proceedings - 30th Southern African Universities Power Engineering Conference, SAUPEC 2022*, 8–13. https://doi.org/10.1109/SAUPEC55179.2022.9730741

Louw, J. A., & Rix, A. J. (2019). Irradiance modelling for bi-facial PV modules using the ray tracing technique. *Proceedings - 2019 Southern African Universities Power Engineering Conference/Robotics and Mechatronics/Pattern Recognition Association of South Africa, SAUPEC/RobMech/PRASA 2019*, 383–388. https://doi.org/10.1109/RoboMech.2019.8704817

Louw, J., & Rix, A. J. (2020). *Modelling and simulation of bifacial PV modules by implementing the ray tracing technique*. *March*. https://scholar.sun.ac.za

Luo, L., Gao, L., & Fu, H. (2011). The Control and Modeling of Diesel Generator Set in Electric Propulsion Ship. *International Journal of Information Technology and Computer Science*, *3*(2), 31–37. https://doi.org/10.5815/ijitcs.2011.02.05

Mahdi, S., Baygi, H., & Farzaneh, J. (2020). Application of Artificial intelligence techniques for optimum design of hybrid grid-independent PV / WT / battery power system. *International Journal of Industrial Electronics, Control and Optimization*, *3*(3), 275–289.

Maheshwari, Z., & Ramakumar, R. (2017). Smart Integrated Renewable Energy Systems (SIRES): A novel approach for sustainable development. *Energies*, *10*(8), 1–22. https://doi.org/10.3390/en10081145

Mahmoud, F. S., Diab, A. A. Z., Ali, Z. M., El-Sayed, A. H. M., Alquthami, T., Ahmed, M., & Ramadan, H. A. (2022). Optimal sizing of smart hybrid renewable energy system using different optimization algorithms. *Energy Reports*, *8*, 4935–4956. https://doi.org/10.1016/j.egyr.2022.03.197

Mahmud, N. (2013). *System for St . Martin Island Using HOMER*.

Mallikarjuna, A., Balachandra, J. C., Potli, M., & Venugopal, N. (2016). Optimal sizing of Wind/Solar/Hydro in an isolated power system using SMFFT based Cuckoo Search Algorithm. *2016 IEEE 6th International Conference on Power Systems, ICPS 2016*. https://doi.org/10.1109/ICPES.2016.7584107

Mandal, S., Mandal, K. K., & Tudu, B. (2015). Optimal design of a hybrid power system using a new improved particle swarm optimization technique. *IET Conference Publications*, *2015*(CP683), 494–499. https://doi.org/10.1049/cp.2015.1682

Manyonge, A. W., Ochieng, R. M., Onyango, F. N., & Shichikha, J. M. (2012). Mathematical modelling of wind turbine in a wind energy conversion system: Power coefficient analysis. *Applied Mathematical Sciences*, *6*(89–92), 4527–4536.

Marcel, E. T., Mutale, J., & Mushi, A. T. (2021). Optimal Design of Hybrid Renewable Energy for Tanzania Rural Communities. *Tanzania Journal of Science*, *47*(5), 1716–1727. https://doi.org/10.4314/tjs.v47i5.19

Martins, A., Madaleno, M., & Dias, M. F. (2019). *Energy Literacy*. 494–499.

https://doi.org/10.1145/3362789.3362938

Masters, G. M. (2005). Renewable and efficient electric power systems. In *Choice Reviews Online* (Vol. 42, Issue 06). https://doi.org/10.5860/choice.42-3448

Mbodji, N., Arisily, T. A. A., Hajji, A., Ababou, K., & Heddouch, A. (2017). Optimal design of an off-grid hybrid solar photovoltaic-diesel system in community electrification of a fishing village in Morocco. *Proceedings of 2016 International Renewable and Sustainable Energy Conference, IRSEC 2016*, 946–955. https://doi.org/10.1109/IRSEC.2016.7983984

Mekhamer, S. F., Abdelaziz, A. Y., Badr, M. A. L., & Algabalawy, M. A. (2015a). *Hybrid Power Generation Systems : A Holistic View*. *6*(5), 1905–1912.

Mekhamer, S. F., Abdelaziz, A. Y., Badr, M. A. L., & Algabalawy, M. A. (2015b). Optimal Multi-Criteria Design of Hybrid Power Generation Systems: A New Contribution. *International Journal of Computer Applications*, *129*(2), 13–24. https://doi.org/10.5120/ijca2015906819

Mesquita, D. D. B., Lucas De Silva, J., Moreira, H. S., Kitayama, M., & Villalva, M. G. (2019). A review and analysis of technologies applied in PV modules. *2019 IEEE PES Conference on Innovative Smart Grid Technologies, ISGT Latin America 2019*, *December*. https://doi.org/10.1109/ISGT-LA.2019.8895369

Mira, M. C., Zhang, Z., Knott, A., & Andersen, M. A. E. (2017). Analysis, Design, Modeling, and Control of an Interleaved-Boost Full-Bridge Three-Port Converter for Hybrid Renewable Energy Systems. *IEEE Transactions on Power Electronics*, *32*(2), 1138–1155. https://doi.org/10.1109/TPEL.2016.2549015

Mirjalili, S., & Lewis, A. (2016). Advances in Engineering Software The Whale Optimization Algorithm. *Advances in Engineering Software*, *95*, 51–67. https://doi.org/10.1016/j.advengsoft.2016.01.008

Mobarra, M., Rezkallah, M., & Ilinca, A. (2022). Variable Speed Diesel Generators: Performance and Characteristic Comparison. *Energies*, *15*(2). https://doi.org/10.3390/en15020592

Moehlecke, A., Da Conceição Osório, V., & Zanesco, I. (2014). Analysis of thin bifacial silicon solar cells with locally diffused and selective back surface field. *Materials Research*, *17*(5), 1328–1335. https://doi.org/10.1590/1516-1439.294614

Mohamed, A., & Khatib, T. (2013). Optimal sizing of a PV/wind/diesel hybrid energy system for Malaysia. *Proceedings of the IEEE International Conference on Industrial Technology*, 752–757. https://doi.org/10.1109/ICIT.2013.6505766

Mohammad-Alikhani, A., Mahmoudi, A., Khezri, R., & Kahourzade, S. (2022). Multiobjective Optimization of System Configuration and Component Capacity in an AC Minigrid Hybrid Power System. *IEEE Transactions on Industry Applications*, *58*(3), 4158–4170. https://doi.org/10.1109/TIA.2022.3160411

Mohammed, H. M., Umar, S. U., & Rashid, T. A. (2019). *A Systematic and Meta-Analysis Survey of Whale Optimization Algorithm*.

Mohammed, O. H., Amirat, Y., & Benbouzid, M. (2019). Particle swarm optimization of a hybrid wind/tidal/PV/battery energy system. Application to a remote area in Bretagne, France. *Energy Procedia*, *162*(April), 87–96. https://doi.org/10.1016/j.egypro.2019.04.010

Nabipour-Afrouzi, H., Wen Yii, S. H., Ahmad, J., & Tabassum, M. (2018). Comprehensive review on

appropriate sizing and optimization technique of hybrid PV-wind system. *Asia-Pacific Power and Energy Engineering Conference, APPEEC*, *2018-Octob*, 364–369. https://doi.org/10.1109/APPEEC.2018.8566269

Naderipour, A., Abdul-Malek, Z., Zahedi Vahid, M., Mirzaei Seifabad, Z., Hajivand, M., & Arabi-Nowdeh, S. (2019). Optimal, Reliable and Cost-Effective Framework of Photovoltaic-Wind-Battery Energy System Design Considering Outage Concept Using Grey Wolf Optimizer Algorithm - Case Study for Iran. *IEEE Access*, *7*, 182611–182623. https://doi.org/10.1109/ACCESS.2019.2958964

Nair, A., Murali, K., Anbuudayasankar, S. P., & Arjunan, C. V. (2017). Modelling and Optimising the Value of a Hybrid Solar-Wind System. *IOP Conference Series: Materials Science and Engineering*, *197*(1). https://doi.org/10.1088/1757-899X/197/1/012035

Nehrir, M. H., Wang, C., Strunz, K., Aki, H., Ramakumar, R., Bing, J., Miao, Z., & Salameh, Z. (2011). A review of hybrid renewable/alternative energy systems for electric power generation: Configurations, control, and applications. *IEEE Transactions on Sustainable Energy*, *2*(4), 392–403. https://doi.org/10.1109/TSTE.2011.2157540

Nguyen, T.-T., & Boström, T. (2021). Multiobjective Optimization of a Hybrid Wind/Solar Battery Energy System in the Arctic. *Journal of Renewable Energy*, *2021*, 1–11. https://doi.org/10.1155/2021/8829561

NRC - E111 - Chapter 9. (2011). *Emergency Diesel Generator - The Generator, Exciter, and Voltage Regulation 9.0*. 1–34.

Nssibi, M., Manita, G., & Korbaa, O. (2021). Binary Giza pyramids construction for feature selection. *Procedia Computer Science*, *192*, 676–687. https://doi.org/10.1016/j.procs.2021.08.070

Ogunjuyigbe, A. S. O., Ayodele, T. R., & Akinola, O. A. (2016). Optimal allocation and sizing of PV/Wind/Split-diesel/Battery hybrid energy system for minimizing life cycle cost, carbon emission and dump energy of remote residential building. *Applied Energy*, *171*, 153–171. https://doi.org/10.1016/j.apenergy.2016.03.051

Okere, A., & Tariq Iqbal, M. (2021). Techno-economic Comparison of Emerging Solar PV modules for Utility Scale PV installation. *2021 IEEE 12th Annual Information Technology, Electronics and Mobile Communication Conference, IEMCON 2021*, 827–833. https://doi.org/10.1109/IEMCON53756.2021.9623086

Okinda, V., Odero, N. A., Okinda, V. O., & Odero, N. A. (2016). Modelling, Simulation and Optimal Sizing of a Hybrid Wind, Solar PV Power System in Northern Kenya multi objective dynamic economic dispatch with renewable energy cost functions View project Renewable Energy View project Modelling, Simulation and Optimal. *INTERNATIONAL JOURNAL of RENEWABLE ENERGY RESEARCH V. Okinda and N.Odero*, *6*(4). https://www.researchgate.net/publication/319165281

Olabi, A. G., Wilberforce, T., Elsaid, K., Salameh, T., Sayed, E. T., Husain, K. S., & Abdelkareem, M. A. (2021). Selection guidelines for wind energy technologies. *Energies*, *14*(11), 1–34. https://doi.org/10.3390/en14113244

Oladigbolu, J. O., Ramli, M. A. M., & Al-Turki, Y. A. (2020). Optimal design of a hybrid pv solar/micro-hydro/diesel/battery energy system for a remote rural village under tropical climate conditions. *Electronics (Switzerland)*, *9*(9), 1–22. https://doi.org/10.3390/electronics9091491

Oliveti, G., Marletta, L., Arcuri, N., De Simone, M., Bruno, R., & Evola, G. (2014). Solar energy. *Green Energy and Technology*, *0*(9783319030739), 159–214. https://doi.org/10.1007/978-3-319-03074-6_4

Onno, A., Rodkey, N., Asgharzadeh, A., Manzoor, S., Yu, Z. J., Toor, F., & Holman, Z. C. (2020). Predicted Power Output of Silicon-Based Bifacial Tandem Photovoltaic Systems. *Joule*, *4*(3), 580–596. https://doi.org/10.1016/j.joule.2019.12.017

Palej, P., Qusay, H., Kleszcz, S., Hanus, R., & Jaszczur, M. (2019). Analysis and optimization of hybrid renewable energy systems. *Polityka Energetyczna*, *22*(2), 107–120. https://doi.org/10.33223/epj/109911

Pan, W., Gao, W., & Muljadi, E. (2009). The dynamic performance and effect of hybrid renewable power system with diesel/wind/PV/battery. *1st International Conference on Sustainable Power Generation and Supply, SUPERGEN '09*, *38505*, 1–5. https://doi.org/10.1109/SUPERGEN.2009.5348178

Paper, C., Andy, T., Tameghe, T., & Kamwa, I. (2012). *Dynamic model of diesel generator set for hybrid wind-diesel small grids applications DYNAMIC MODEL OF DIESEL GENERATOR SET FOR HYBRID WIND-DIESEL SMALL GRIDS APPLICATIONS*. *April*, 10–14. https://doi.org/10.1109/CCECE.2012.6334849

Pelaez, S. A., Deline, C., Greenberg, P., Stein, J. S., & Kostuk, R. K. (2019). Model and Validation of Single-Axis Tracking with Bifacial PV. *IEEE Journal of Photovoltaics*, *9*(3), 715–721. https://doi.org/10.1109/JPHOTOV.2019.2892872

Pelaez, S. A., Deline, C., Macalpine, S. M., Marion, B., Stein, J. S., & Kostuk, R. K. (2019). Comparison of Bifacial Solar Irradiance Model Predictions with Field Validation. *IEEE Journal of Photovoltaics*, *9*(1), 82–88. https://doi.org/10.1109/JPHOTOV.2018.2877000

Pham, Q., Mirjalili, S., Kumar, N., Alazab, M., & Hwang, W. (2020). *Whale Optimization Algorithm with Applications to Resource Allocation in Wireless Networks*.

Pike, C., Whitney, E., Wilber, M., & Stein, J. S. (2021). Field performance of south-facing and east-west facing bifacial modules in the arctic. *Energies*, *14*(4), 1–15. https://doi.org/10.3390/en14041210

Priya, R., Valli, R., Pushpa, B., & Santhanakrishnan, P. L. (2021). Optimal Sizing of Hybrid Micro Grid System Using PSO Technique for Rural Electrification. *2021 International Conference on System, Computation, Automation and Networking, ICSCAN 2021*, 3–8. https://doi.org/10.1109/ICSCAN53069.2021.9526536

Qi, X., Zhu, S., & Zhang, H. (2017). A hybrid firefly algorithm. *Proceedings of 2017 IEEE 2nd Advanced Information Technology, Electronic and Automation Control Conference, IAEAC 2017*, 287–291. https://doi.org/10.1109/IAEAC.2017.8054023

Raji, A. K., & Luta, D. N. (2019). Modeling and optimization of a community microgrid components. *Energy Procedia*, *156*(September 2018), 406–411. https://doi.org/10.1016/j.egypro.2018.11.103

Raji, A., & Kahn, M. T. (2012). Analysis of distributed energy resources for domestic electricity users. *Journal of Energy in Southern Africa*, *23*(2), 50–55. https://doi.org/10.17159/2413-3051/2012/v23i2a3163

Ranjith Kumar, K., & Surya Kalavathi, M. (2019). Optimal sizing of grid connected hybrid PV/wind/battery power system using satin bowerbird optimization. *International Journal of*

Innovative Technology and Exploring Engineering, *8*(4), 412–418.

Rashid, F., Hoque, M. E., Aziz, M., Sakib, T. N., Islam, M. T., & Robin, R. M. (2021). Investigation of optimal hybrid energy systems using available energy sources in a rural area of bangladesh. *Energies*, *14*(18). https://doi.org/10.3390/en14185794

Razongles, G., Sicot, L., Joanny, M., Gerritsen, E., Lefillastre, P., Schroder, S., & Lay, P. (2016). Bifacial Photovoltaic Modules: Measurement Challenges. *Energy Procedia*, *92*, 188–198. https://doi.org/10.1016/j.egypro.2016.07.056

Rehman, S., Habib, H. U. R., Wang, S., Buker, M. S., Alhems, L. M., & Al Garni, H. Z. (2020). Optimal Design and Model Predictive Control of Standalone HRES: A Real Case Study for Residential Demand Side Management. *IEEE Access*, *8*, 29767–29814. https://doi.org/10.1109/ACCESS.2020.2972302

Reinemann, D., & Heinzen, J. (2014). Graphic design How Do Wind Turbines Generate Electricity? *Midwest Rural Energy Council*, 1–2. www.mrec.org

Renewable Energy Policy Network for the 21 Century [REN21], Accessed May 25, 2022, from http:// sustainablejohn.com/?p=213.

Rigby, J. (n.d.). *Building The Great Pyramid At Giza: Investigating Ramp Models*. 1–13.

Roy, P., He, J., Zhao, T., & Singh, Y. V. (2022). Recent Advances of Wind-Solar Hybrid Renewable Energy Systems for Power Generation: A Review. *IEEE Open Journal of the Industrial Electronics Society*, *3*(January), 81–104. https://doi.org/10.1109/OJIES.2022.3144093

Russell, T. C. R., Saive, R., Augusto, A., Bowden, S. G., & Atwater, H. A. (2017). The Influence of Spectral Albedo on Bifacial Solar Cells: A Theoretical and Experimental Study. *IEEE Journal of Photovoltaics*, *7*(6), 1611–1618. https://doi.org/10.1109/JPHOTOV.2017.2756068

Saif, A., Elrab, K. G., Zeineldin, H. H., Kennedy, S., & Kirtley, J. L. (2010). Multi-objective capacity planning of a PV-wind-diesel-battery hybrid power system. *2010 IEEE International Energy Conference and Exhibition, EnergyCon 2010*, 217–222. https://doi.org/10.1109/ENERGYCON.2010.5771679

Salloom, A., Abdulrazzaq, O., & Ismail, B. (2018). Assessment of the Performance of Bifacial Solar Panels. *International Journal of Engineering and Technical Research*, *8*(7), 13–17. https://www.erpublication.org/published_paper/IJETR2634.pdf

Sarkar, M. R., Julai, S., Tong, C. W., Chao, O. Z., & Rahman, M. (2015). Mathematical modelling and simulation of induction generator based wind turbine in MATLAB/SIMULINK. *ARPN Journal of Engineering and Applied Sciences*, *10*(22), 17276–17280.

Sateesh Kumar, M., Pavan Kumar, Y. V., John Pradeep, D., & Reddy, C. P. (2020). Analysis on the Effectiveness of Vertical Axis Wind Turbine for Domestic Consumers. *2020 International Symposium on Advanced Electrical and Communication Technologies, ISAECT 2020*, *c*, 1–6. https://doi.org/10.1109/ISAECT50560.2020.9523698

Sawle, Y., Gupta, S. C., & Bohre, A. K. (2016a). PV-wind hybrid system: A review with case study. *Cogent Engineering*, *3*(1), 1–31. https://doi.org/10.1080/23311916.2016.1189305

Sawle, Y., Gupta, S. C., & Bohre, A. K. (2016b). PV-wind hybrid system: A review with case study. *Cogent Engineering*, *3*(1). https://doi.org/10.1080/23311916.2016.1189305

Sengupta, N., Das, K., Jayram, T. S., & Seetharam, D. P. (2012). Optimal allocation of land area for a hybrid solar wind power plant. *2012 IEEE 3rd International Conference on Smart Grid Communications, SmartGridComm 2012*, 522–527. https://doi.org/10.1109/SmartGridComm.2012.6486038

Sharaf, A. M., Elbakush, B., & Altas, I. H. (2007). Novel control strategies for photovoltaic powered PMDC motor drives. *2007 IEEE Canada Electrical Power Conference, EPC 2007*, 461–466. https://doi.org/10.1109/EPC.2007.4520376

Shayeghi, H., Moradzadeh, M., Hashemi, Y., Saif, M., & Vandevelde, L. (2016). Wind-PV-storage optimal environomic design using multi-objective Artificial Bee Colony. *Asia-Pacific Power and Energy Engineering Conference, APPEEC*, *2016-January*. https://doi.org/10.1109/APPEEC.2015.7381057

Shi, Z. S., Wang, R., Zhang, X. Y., Zhang, Y., & Zhang, T. (2017). Optimal design of grid-connected hybrid renewable energy systems using multi-objective evolutionary algorithm. *Scientia Iranica*, *24*(6), 3148–3156. https://doi.org/10.24200/sci.2017.4578

Siddique, Z. Bin, Yadav, G. D., & Gadhauli, Y. (2016). Standalone Power Generation System using Renewable Energy Sources : A Review. *International Research Journal of Engineering and Technology (IRJET) e-ISSN:*, *3*(9), 1176–1182.

Singh, G., & Tiwari, A. N. (2017). Optimization of a smart grid distributed generation: Designing of a hybrid solar system for a building. *2017 1st International Conference on Electronics, Materials Engineering and Nano-Technology, IEMENTech 2017*. https://doi.org/10.1109/IEMENTECH.2017.8077007

Singh, J. P., Aberle, A. G., & Walsh, T. M. (2014). Electrical characterization method for bifacial photovoltaic modules. *Solar Energy Materials and Solar Cells*, *127*, 136–142. https://doi.org/10.1016/j.solmat.2014.04.017

Singh, M., & Santoso, S. (2012). Dynamic models for wind turbines and wind power plants. *Wind Power: Systems Engineering Applications and Design Models*, *October*, 93–204.

Solarworld. (2015). Calculating the Additional Energy Yield of Bifacial Solar Modules. *White Paper*, 1–8. https://www.solarworld-usa.com/~/media/www/files/white-papers/calculating-additional-energy-yield-through-bifacial-solar-technology-sw9002us.pdf?la=en

Starlight Power [SP], retrieved June 29, 2022, from https://www.dieselgeneratortech.com/generator-sets/basic-structure-and-application-of-diesel-generator-set.html

Sulaiman, M. H., Mustafa, M. W., Zakaria, Z. N., Aliman, O., & Abdul Rahim, S. R. (2012). Firefly algorithm technique for solving economic dispatch problem. *2012 IEEE International Power Engineering and Optimization Conference, PEOCO 2012 - Conference Proceedings*, *June*, 90–95. https://doi.org/10.1109/PEOCO.2012.6230841

Sultan, H. M., Kuznetsov, O. N., Menesy, A. S., & Kamel, S. (2020). Optimal Configuration of a Grid-Connected Hybrid PV/Wind/Hydro-Pumped Storage Power System Based on a Novel Optimization Algorithm. *Proceedings of the 2nd 2020 International Youth Conference on Radio Electronics, Electrical and Power Engineering, REEPE 2020*. https://doi.org/10.1109/REEPE49198.2020.9059189

Sun, X., Khan, M. R., Deline, C., & Alam, M. A. (2018). Optimization and performance of bifacial solar

modules: A global perspective. *Applied Energy*, *212*(September), 1601–1610. https://doi.org/10.1016/j.apenergy.2017.12.041

Suryoatmojo, H., Hiyama, T., Elbaset, A. A., & Ashari, M. (2009). Optimal design of wind-PV-diesel-battery system using genetic algorithm. *IEEJ Transactions on Power and Energy*, *129*(3), 413–420. https://doi.org/10.1541/ieejpes.129.413

Syafaruddin, & Zinger, D. S. (2020). A review of hybrid power generation: Modelling-simulation, control strategy and future trend development. *Journal of Engineering Science and Technology Review*, *13*(4), 249–263. https://doi.org/10.25103/jestr.134.26

Tahir, S., & Khaliq, A. (2018). Control of grid connected DC-coupled hybrid microgrid. *Proceedings of 2017 International Multi-Topic Conference, INMIC 2017*, *2018-Janua*, 1–6. https://doi.org/10.1109/INMIC.2017.8289457

Tan, Y., Lv, Z., & Li, S. (2015). Stand-alone micro-grid distributed generator optimization with different battery technologies. *Chinese Control Conference, CCC*, *2015-September*, 2651–2656. https://doi.org/10.1109/ChiCC.2015.7260045

TeacherGeek.com. (2006). Type of Wind Turbines. *TeacherGeek.Com*, 1–7. https://teachergeek.org/wind_turbine_types.pdf

Tégani, I., Aboubou, A., Ayad, M. Y., Becherif, M., Saadi, R., & Kraa, O. (2014). Optimal sizing design and energy management of stand-alone photovoltaic/wind generator systems. *Energy Procedia*, *50*(0), 163–170. https://doi.org/10.1016/j.egypro.2014.06.020

Theubou, T., Wamkeue, R., & Kamwa, I. (2012). *DYNAMIC MODEL OF DIESEL GENERATOR SET FOR HYBRID WIND-DIESEL SMALL GRIDS APPLICATIONS T . Theubou , R . Wamkeue , Senior Member , IEEE Universit ´ e du Qu ´ ebec en Abitibi-T ´ emiscamingue (UQAT) 445 boul . de l ' universit ´ e , J9X5E4 , QC , Canada a*. *1*, 11–14.

Tito, M. S. R., Lie, T. T., & Anderson, T. (2013). A Simple Sizing Optimization Method for Wind-Photovoltaic-Battery Hybrid Renewable Energy Systems. *20th Electronics New Zealand Conference*, 8–12. http://aut.researchgateway.ac.nz/bitstream/handle/10292/5650/A Simple Sizing Optimization Method.pdf?sequence=4

Tremblay, O., & Dessaint, L. A. (2009). Experimental validation of a battery dynamic model for EV applications. *24th International Battery, Hybrid and Fuel Cell Electric Vehicle Symposium and Exhibition 2009, EVS 24*, *2*, 930–939.

Tywoniuk, A., Skorupka, Z. (2018). Wind Power Plants - Types, Design and Operation Principles. *Journal of KONES*, *25*(3). https://doi.org/10.5604/01.3001.0012.4371

Vishakha, V., Vardwaj, V., Jadoun, V. K., Jayalaksmi, S. N., & Agarwal, A. (2020). Review of Optimization Techniques for Hybrid Wind PV-ESS System. *2020 International Conference on Power Electronics and IoT Applications in Renewable Energy and Its Control, PARC 2020*, 202–207. https://doi.org/10.1109/PARC49193.2020.236593

Wang, C., & Chu, X. (2019). An Improved Firefly Algorithm with Specific Probability and Its Engineering Application. *IEEE Access*, *7*(2), 57424–57439. https://doi.org/10.1109/ACCESS.2019.2914534

Wang, J., Ma, Y., Hu, Z., & Yang, X. (2009). Modeling and real-time simulation of non-grid-connected

wind energy conversion system. *WNWEC 2009 - 2009 World Non-Grid-Connected Wind Power and Energy Conference*, 216–220. https://doi.org/10.1109/WNWEC.2009.5335815

Wang, L., & Singh, C. (2009). Multicriteria design of hybrid power generation systems based on a modified particle swarm optimization algorithm. *IEEE Transactions on Energy Conversion*, *24*(1), 163–172. https://doi.org/10.1109/TEC.2008.2005280

Wang, L., Wei, J., Wang, X., & Zhang, X. (2009). The development and prospect of offshore wind power technology in the world. *WNWEC 2009 - 2009 World Non-Grid-Connected Wind Power and Energy Conference*, 439–442. https://doi.org/10.1109/WNWEC.2009.5335761

Wang, R., Zhang, F., & Zhang, T. (2015). Multi-Objective Optimal Design of Hybrid. *11th International Conference on Natural Computation*, 1196–1200.

Wang, S., Wilkie, O., Lam, J., Steeman, R., Zhang, W., Khoo, K. S., Siong, S. C., & Rostan, H. (2015). Bifacial Photovoltaic Systems Energy Yield Modelling. *Energy Procedia*, *77*, 428–433. https://doi.org/10.1016/j.egypro.2015.07.060

Wang, Z., Qin, C., Wan, B., & Song, W. W. (2021). A comparative study of common nature-inspired algorithms for continuous function optimization. *Entropy*, *23*(7), 1–40. https://doi.org/10.3390/e23070874

WESL. (2016). Chapter 1 Wind Turbine Components. *Wind Turbine*, 1–9.

Wind Energy Development. (May 21, 2022). Wind Energy Basics [Online], Available at: http://windeis.anl.gov/guide/basics/

Yadav, D. K., Girimaji, S. P., & Bhatti, T. S. (2012). Optimal hybrid power system design for rural electrification. *ICPCES 2012 - 2012 2nd International Conference on Power, Control and Embedded Systems*. https://doi.org/10.1109/ICPCES.2012.6508125

Yang, X., & Bai, K. (2010). Development and prospects of offshore wind power. *Proceedings of 2010 World Non-Grid-Connected Wind Power and Energy Conference, WNWEC 2010*, 127–130. https://doi.org/10.1109/WNWEC.2010.5673138

Yang, X. S. (2009). Firefly algorithms for multimodal optimization. *Lecture Notes in Computer Science (Including Subseries Lecture Notes in Artificial Intelligence and Lecture Notes in Bioinformatics)*, *5792 LNCS*, 169–178. https://doi.org/10.1007/978-3-642-04944-6_14

Yang, X. S. (2014). Preface. *Studies in Computational Intelligence*, *585*, v–vi. https://doi.org/10.1007/978-3-319-02141-6

Yang, X. S., & He, X. (2013). Firefly algorithm: recent advances and applications. *International Journal of Swarm Intelligence*, *1*(1), 36. https://doi.org/10.1504/ijsi.2013.055801

Yang, Z. (2020). *Application of Improve Whale Optimization Algorithm to the Distribution Network Reconfiguration with Distributed Generation*. *2*(3), 109–113.

Yaramasu, V., Wu, B., Sen, P. C., Kouro, S., & Narimani, M. (2015). High-power wind energy conversion systems: State-of-the-art and emerging technologies. *Proceedings of the IEEE*, *103*(5), 740–788. https://doi.org/10.1109/JPROC.2014.2378692

Yuan, X., Huang, B., Xu, J., Liu, H., & Yao, Q. (2018). *Application of Demand Response Strategy in Optimal Configuration of a Standalone Wind-Solar-Battery System*. *April*, 1–14.

https://doi.org/10.20944/preprints201804.0303.v1

Zaki Diab, A. A., Sultan, H. M., Mohamed, I. S., Kuznetsov Oleg, N., & Do, T. D. (2019). Application of different optimization algorithms for optimal sizing of pv/wind/diesel/battery storage stand-alone hybrid microgrid. *IEEE Access*, *7*, 119223–119245. https://doi.org/10.1109/ACCESS.2019.2936656

Zhang, L., Barakat, G., & Yassine, A. (2012). Design and optimal sizing of hybrid PV/wind/diesel system with battery storage by using DIRECT search algorithm. *15th International Power Electronics and Motion Control Conference and Exposition, EPE-PEMC 2012 ECCE Europe*, 1–7. https://doi.org/10.1109/EPEPEMC.2012.6397335

Zhang, N., Sun, Z., Zhang, J., Ma, T., & Wang, J. (2011). Optimal design for stand-alone wind/solar hybrid power system. *2011 International Conference on Electronics, Communications and Control, ICECC 2011 - Proceedings*, 4415–4418. https://doi.org/10.1109/ICECC.2011.6067613

Zhang, Y., Lin, M., Zou, B., Yin, X., Liu, T., & Zhou, W. (2019). Preliminary Analysis of Wind Resources and Wind Energy Reserves in the off-Shore Region of Guangdong Province. *International Geoscience and Remote Sensing Symposium (IGARSS)*, 8209–8212. https://doi.org/10.1109/IGARSS.2019.8899218

Zhou, W., Lou, C., Li, Z., Lu, L., & Yang, H. (2010). Current status of research on optimum sizing of stand-alone hybrid solar-wind power generation systems. *Applied Energy*, *87*(2), 380–389. https://doi.org/10.1016/j.apenergy.2009.08.012

Zinoviev, G. (2008). *Overview of Power Electronics Converters and Controls Overview of Power Electronics Converters and Controls* (Issue February 2016). https://doi.org/10.1007/978-1-84800-318-7

Энергии, В. И., & Sleptsov, A. A. (2017). *Мировой Опыт Развития Альтернативных (Renewable) Energy Sources*. 58–63.

Appendix A: Matlab codes

General functions

```
function Positions=initialization(SearchAgents_no,dim,ub,lb)

Boundary_no= size(ub,2); % numnber of boundaries

% If the boundaries of all variables are equal and user enter a signle
% number for both ub and lb
if Boundary_no==1
    Positions=rand(SearchAgents_no,dim).*(ub-lb)+lb;
end

% If each variable has a different lb and ub
if Boundary_no>1
    for i=1:dim
        ub_i=ub(i);
        lb_i=lb(i);
        Positions(:,i)=rand(SearchAgents_no,1).*(ub_i-lb_i)+lb_i;
    end
end


function Mbatt= battery_capacity(Eren)
Ad=3;
eff_batt=0.9;
eff_inv=0.8;
DoD=0.8;
Vs=24;
Mbatt=((Ad*Eren)/(eff_batt*eff_inv*DoD*Vs));


  function avail_batt= battery_module
batt_capacity=250;
DOD=0.6;
Vs=12;
batt_effi=0.9;
inv_effi=0.9;
avail_batt=batt_capacity*batt_effi*inv_effi*DOD*Vs;
    end


%load demand
function [El,peak_El]=load_demand
%E=[350,350,350,350,350,560,560,530,530,530,430,330,330,330,330,330,330,400,4
00,400,530,530,350,350];
E=[10 10 10 10 10 12 13 13 15 16 16 15 16 17 18 20 23 24 26 30 32 35 15 9];
El=E*1000;
for ii=1:14
El=[El, El];
end
peak_El=max(El);
end
```

```
%load profile plot
close all
clear all

[wind_speed,solar_irradiance]=speed_irradiance_data;
H=solar_irradiance;
v=wind_speed;
for mm=1:4
    H=[H;H];
    v=[v;v];
end
h=solar_irradiance;
V=wind_speed;
for mn=1:4
    h=[h;h];
    V=[V;V];
end
% Hh=irradiance_data0;
Hh=[H;h];
vV=[v;V];
% vV=v;
%initialize soc
% soc=zeros(1,(365*24*n));
for t=2:2410
Ppv=pvmodule(Hh(t-1));
PPv(t-1)=Ppv*1.20;
PPv_main(t-1)=Ppv*1;
PPv_back(t-1)=Ppv*0.20;
Pwind(t-1)=wt_module(vV(t-1));
end
tt=1:48;
figure
plot(tt, PPv(tt));
title('Bifacial PV Power profile')
ylabel('power (watt)')
xlabel('Time (Hour)')
grid on
figure
plot(tt, Pwind(tt));
title('Wind Power profile')
ylabel('power (watt)')
xlabel('Time (Hour)')
grid on
figure
plot(tt, PPv_main(tt));
hold on
plot(tt, PPv_back(tt));
hold off
title('Back and Front output of Bifacial PV')
ylabel('power (watt)')
xlabel('Time (Hour)')
grid on
legend('Front output','Back output')
ttt=0:47;
dg_out=[42 42 42 42 42 42 42 42 42 42 42 42 42 42 42 42 42 42 42 42 42 42
42 42 42 42 42 42 42 42 42 42 42 42 42 42 42 42 42 42 42 42 42 42 42 42
42 42 42 42 42 42 42 42].*1000;
```

```
plot(ttt, dg_out(tt));
ylim([0 45000])
title('DG Output Power profile')
ylabel('power (watt)')
xlabel('Time (Hour)')
grid on




    function avail_pv= pvmodule(Ht)
%Apv=(0.0254*78.15)*(0.0254*38.98); % A=lxb %1inch=0.0254m, LxBxH=
78.15*38.98*1.81
Apv=(2031*1008)/1000000;
pv_effi=0.1881;
eff_inv=0.8;
eff_batt=0.9;
%Ht=0.622*5.630*1000;  solar irradiance
avail_pv= Apv*Ht*pv_effi*eff_inv*eff_batt;
    end




function Crep= Replacement_cost(N_hr,n,Cint)
Nrep=(n*365*24)/N_hr;
Nrep=round(Nrep);
%Egen is the capacity of the generator
kd=8;
fo=4;
if Nrep<1
    Crep_coeff=0;
else
for Ni=1:Nrep
    Crep_coeff(Ni)=((1+fo)/(1+kd))^(Ni/(Nrep+1));
end
end
Crep=Cint*(sum(Crep_coeff));

function
[Cinit,Crep,Cmaint,fuel_cost,LCC,Eco2,T_Dump,Hgen1,Hgen2,Hgen3,Egen,Ewind,EPv
,soc,El]=Results(x)

x=round(x);
x1=x(1);
x2=x(2);
x3=x(3);
x4=x(4);
x5=x(5);
x6=x(6);

[El,El_peak]=load_demand;
n=30;
Egen1=0.40*El_peak;
Egen2=0.40*El_peak;
```

```
Egen3=0.40*El_peak;
Hgen1=0; Hgen2=0; Hgen3=0;
Eco2=0; %initialize Eco2
f=0;
Dump=0;
E_sup_DG1=0; E_sup_DG2=0; E_sup_DG3=0;
Cunit_pv=500;
Cunit_wind=500;
Cunit_gen1=0.3*Egen1; % in $
Cunit_gen2=0.3*Egen2;  % in $
Cunit_gen3=0.3*Egen3;  % in $
Cunit_battery=300;
Cfuel_per_l=1.5;

eff_inv=0.8;
eff_batt=0.9;
batt_Ah=360;
Vs=24;
s_dis_r=0.01;
CB=batt_Ah*Vs*eff_batt*x6;
soc=0.5*CB;
DoD=0.8;
soc_min=(1-DoD)*CB;
soc_max=CB;

%load input data
[wind_speed,solar_irradiance]=speed_irradiance_data;
H=solar_irradiance;
v=wind_speed;

for mm=1:8
    H=[H;H];
    v=[v;v];
end
h=solar_irradiance;
V=wind_speed;
for mn=1:8
    h=[h;h];
    V=[V;V];
end
Hh=[H;h];
vV=[v;V];
num_year_h=((365*24*n)+1);
for t=2:num_year_h
Ppv=pvmodule(Hh(t-1));
Ppv=Ppv*1.20;
EPv(t-1)=Ppv*x1;
Pwind=wt_module(vV(t-1));
Ewind(t-1)=Pwind*x2;
Eren=Ppv*x1+Pwind*x2;
%soc(t)=soc(t-1);
Edx=Eren-(El(t-1)/eff_inv);
if Edx>0     %i.e if their is excess energy
    if soc(t-1)<soc_max
        %for charging
         soc(t)=soc(t-1)*(1-s_dis_r)+(Eren-(El(t-1)/eff_inv))*eff_batt;
```

```
    else
        Dump(t)=abs(Edx);
        soc(t)=soc(t-1);
    end
elseif Edx<0  %i.e if their is deficit energy
    if soc(t-1)>soc_min
        %for discharging
        soc(t)=soc(t-1)*(1-s_dis_r)-((El(t-1)/eff_inv)-Eren);
    else
        %Generator selection scheme
        if abs(Edx)<(x3*Egen1)
            s1=1; s2=0; s3=0;
        elseif abs(Edx)<((x3*Egen1)+(x4*Egen2))

            s1=1; s2=1; s3=0;
        else
            s1=1;
            s2=1;
            s3=1;
        end
        Egen(t-1)=s1*Egen1*x3+s2*Egen2*x4+s3*Egen3*x5;

        if s1==1
            E_sup_DG1(t-1)= ((abs(Edx))/1000);
            f1(t-1)= E_sup_DG1(t-1)*0.145;
            Hgen1=Hgen1+1;
        else
            f1(t-1)=0;
        end
        if s2==1
            E_sup_DG2(t-1)= (((abs(Edx))-Egen1)/1000);
            f2(t-1)= E_sup_DG2(t-1)*0.145;
            Hgen2=Hgen2+1;
            else
            f2(t-1)=0;
        end
        if s3==1
            E_sup_DG3(t-1)= (((abs(Edx))-(Egen1+Egen2))/1000);
            f3(t-1)= E_sup_DG3(t-1)*0.145;
            Hgen3=Hgen3+1;
            else
            f3(t-1)=0;
        end
        f(t-1)= f1(t-1)+f2(t-1)+f3(t-1);
        Seco2=2.7; %kg/l
        Eco2(t-1)=Seco2*f(t-1);

        soc(t)=soc(t-1)*(1-s_dis_r);
    end
end
end
Eco2=sum(Eco2);
fuel=sum(f);
fuel_cost=fuel*Cfuel_per_l;
% Total intial cost
```

```
Cinit=x1*Cunit_pv+x2*Cunit_wind+x3*Cunit_gen1+x4*Cunit_gen2+x5*Cunit_gen3+x6*
Cunit_battery;

N_year_wind=25*365*24;
N_year_batt=10*365*24;
n_gen=10*365*24;
if Hgen1>n_gen

Crep_gen1=Replacement_cost(Hgen1,n,Cunit_gen1);
else
Crep_gen1=0;
end
if Hgen2>n_gen
Crep_gen2=Replacement_cost(Hgen2,n,Cunit_gen2);
else
Crep_gen2=0;
end
if Hgen3>n_gen

Crep_gen3=Replacement_cost(Hgen3,n,Cunit_gen3);
else
Crep_gen3=0;
end

Crep_wind=0;
Crep_batt=Replacement_cost(N_year_batt,n,Cunit_battery);
Crep=Crep_wind*x2+Crep_batt*x6+Crep_gen1*x3+Crep_gen2*x4+Crep_gen3*x5;

fo=4;
kd=8;
Com_pv=0.01*Cunit_pv*x1*((1+fo)/(kd-fo))*(1-((1+fo)/(1+kd))^n);
Com_wind=0.03*Cunit_wind*x2*((1+fo)/(kd-fo))*(1-((1+fo)/(1+kd))^n);
Com_gen1=0.05*Cunit_gen1*x3*((1+fo)/(kd-fo))*(1-((1+fo)/(1+kd))^n);
Com_gen2=0.05*Cunit_gen2*x4*((1+fo)/(kd-fo))*(1-((1+fo)/(1+kd))^n);
Com_gen3=0.05*Cunit_gen3*x5*((1+fo)/(kd-fo))*(1-((1+fo)/(1+kd))^n);
Com_batt=0.03*Cunit_battery*x6*((1+fo)/(kd-fo))*(1-((1+fo)/(1+kd))^n);
Cmaint=Com_pv+Com_wind+Com_gen1+Com_gen2+Com_gen3+Com_batt;
T_Dump=sum(Dump);

LCC=Cinit+Crep+Cmaint+fuel_cost;


function Pwind_out=wt_module(v)

%v=6; %m/s
v_rated=10; %m/s
vc_in=2.5; % cut in speed m/s
vc_off=30;  % cut out speed m/s
pwt_rated=500; %watt
r=1.44; %m
eff_wt=0.96; %efficiency of wind turbine
if v<vc_in || v>vc_off
    pwt_watt=0;
elseif v>=vc_in && v<=v_rated
    pwt_watt=pwt_rated*((v-vc_in)/(v_rated-vc_in));
```

```
elseif v>=v_rated && v<=vc_off
    pwt_watt=pwt_rated;
end
Aw=(22/7)*(r^2); %area= pie*r^2
% Pwind_out=pwt_watt*Aw*eff_wt;
Pwind_out=pwt_watt*eff_wt;
```

Firefly

```
% =========================================================== %
% Files of the Matlab programs included in the book:        %
% Xin-She Yang, Nature-Inspired Metaheuristic Algorithms,   %
% Second Edition, Luniver Press, (2010).   www.luniver.com %
%programmer: Engr. Convenience
%Date:23-10-2021
%Code version: Improved Version
%Improved in MATLAB R2021a
% =========================================================== %

% ----------------------------------------------------------- %


function fa_ndim
% parameters [n N_iteration alpha betamin gamma]
para=[50 20 0.5 0.2 1];

help fa_ndim.m
tic
% Simple bounds/limits for d-dimensional problems

        %the primary source
        batt_rated=360;   %battery capacity in AH
       SF=1.5; %safety factor
       rated_pv=385; %watt
       rated_wind=500; %watt
       [~,peak_El]=load_demand;
       u_pv=peak_El*SF/rated_pv;
       u_wind=peak_El*SF/rated_wind;
       u_batt=(battery_capacity(peak_El))/batt_rated;
        Lb=[1 1 1 1 1 1];
        Ub=[round(u_pv*SF) round(u_wind*SF) 1 1 1 round(u_batt*SF)];
        %ub=[5000 5000 1 1 1 1000]


% Initial random guess
%load position
load Positions
uo=Positions;
u0=uo(1,:);
[u,fval,fitbest]=ffa_mincon(@cost,u0,Lb,Ub,para);

% Display results
```

```
bestojb=fval;
Best_pos = u;
[Cinit,Crep,Cmaint,fuel_cost,LCC,Eco2,T_Dump,Hgen1,Hgen2,Hgen3,Egen,Ewind,EPv
,soc,El]=Results(Best_pos);
toc
fprintf('_____________________________________________\n')
fprintf('----------Simulation Results-----------------\n')
fprintf('PV Modules:           %6d \n',round(Best_pos(1)))
fprintf('Wind Turbine Modules: %6d \n',round(Best_pos(2)))
fprintf('Battery Modules:      %6d \n',round(Best_pos(6)))
fprintf('DG Set1 Module:       %6d \n',round(Best_pos(3)))
fprintf('Hour of operation of DG1:       %6d \n',round(Hgen1))
fprintf('DG Set2 Module:       %6d \n',round(Best_pos(4)))
fprintf('Hour of operation of DG2:       %6d \n',round(Hgen2))
fprintf('DG Set3 Module:       %6d \n',round(Best_pos(5)))
fprintf('Hour of operation of DG3:       %6d \n',round(Hgen3))
fprintf('Initial Capital cost:     %8.2f $ \n',Cinit)
fprintf('Replacement cost:         %8.2f $ \n',Crep)
fprintf('OP and Maintenance cost:  %8.2f $ \n',Cmaint)
fprintf('Fuel cost:                %8.2f $ \n',fuel_cost)
fprintf('Life cycle cost:          %8.2f $ \n',LCC)
fprintf('Total CO2 Emission:            %8.2f kg \n',Eco2)
fprintf('Dump Energy:              %8.2f Watt \n',T_Dump)
fprintf('_____________________________________________\n')
figure;
%plot(BestCost,'LineWidth',2);
semilogy(fitbest,'LineWidth',2);
xlabel('Iteration');
ylabel('Best Cost');
grid on;
figure
%plot hourly output of the hps for 48hrs
TT=1:48;
yyaxis left
plot(TT,EPv(TT),'--g','LineWidth',2)
hold on
plot(TT,Ewind(TT),'-.c','LineWidth',2)
plot(TT,Egen(TT),'--m','LineWidth',2)
stairs(TT,El(TT),'-r','LineWidth',2)
hold off
ylabel('Output Power (Watt)')
xlabel('Duration (Hr)')
yyaxis right
plot(TT,soc(TT),':b','LineWidth',2)
ylabel('State of Charge')
title('System behaviour')
legend('BPv','Wind','3DGs','Eload','SOC')
grid on
grid minor
%plot hourly output of the hps for 10day
figure
T=1:240;
yyaxis left
plot(T,EPv(T),'--g','LineWidth',2)
hold on
plot(T,Ewind(T),'-.c','LineWidth',2)
plot(T,Egen(T),'--m','LineWidth',2)
```

```
stairs(T,El(T),'-r','LineWidth',2)
hold off
ylabel('Output Power (Watt)')
xlabel('Duration (Hr)')
yyaxis right
plot(T,soc(T),':b','LineWidth',2)
ylabel('State of Charge')
title('System behaviour')
legend('BPv','Wind','3DGs','Eload','SOC')
grid on
grid minor

%%% Put your own cost/objective function here --------%%%
%% Cost or Objective function
 function z=cost(x)
x=round(x);
x1=x(1);
x2=x(2);
x3=x(3);
x4=x(4);
x5=x(5);
x6=x(6);

[El,El_peak]=load_demand;
n=30;
Egen1=0.40*El_peak;
Egen2=0.40*El_peak;
Egen3=0.40*El_peak;
Hgen1=0; Hgen2=0; Hgen3=0;
Eco2=0;
f=0;
Dump=0;
E_sup_DG1=0; E_sup_DG2=0; E_sup_DG3=0;

Cunit_pv=500;
Cunit_wind=500;
Cunit_gen1=0.3*Egen1; %
Cunit_gen2=0.3*Egen2;
Cunit_gen3=0.3*Egen3;
Cunit_battery=300;
Cfuel_per_l=1.5;

eff_inv=0.8;
eff_batt=0.9;
batt_Ah=360;
Vs=24;
s_dis_r=0.01;
CB=batt_Ah*Vs*eff_batt*x6;
soc=0.5*CB;
DoD=0.8;
soc_min=(1-DoD)*CB;
soc_max=CB;

[wind_speed,solar_irradiance]=speed_irradiance_data;
H=solar_irradiance;
v=wind_speed;
```

```
for mm=1:8
    H=[H;H];
    v=[v;v];
end
h=solar_irradiance;
V=wind_speed;
for mn=1:8
    h=[h;h];
    V=[V;V];
end
Hh=[H;h];
vV=[v;V];
%initialize soc
% soc=zeros(1,(365*24*n));
for t=2:365*24*n
Ppv=pvmodule(Hh(t-1));
Ppv=Ppv*1.30;
Pwind=wt_module(vV(t-1)); %loaded wind speed data is accessed here
Eren=Ppv*x1+Pwind*x2;

Edx=Eren-(El(t-1)/eff_inv);
if Edx>0     %i.e if their is excess energy
    if soc(t-1)<soc_max
        %for charging
         soc(t)=soc(t-1)*(1-s_dis_r)+(Eren-(El(t-1)/eff_inv))*eff_batt;
    else
        Dump(t)=abs(Edx);
        soc(t)=soc(t-1);
    end
elseif Edx<0
    if soc(t-1)>soc_min
        %for discharging
        soc(t)=soc(t-1)*(1-s_dis_r)-((El(t-1)/eff_inv)-Eren);
    else
        %Generator
        if abs(Edx)<(x3*Egen1)
            s1=1; s2=0; s3=0;
        elseif abs(Edx)<((x3*Egen1)+(x4*Egen2))

            s1=1; s2=1; s3=0;
        else
            s1=1;
            s2=1;
            s3=1;
        end
        Egen(t-1)=s1*Egen1*x3+s2*Egen2*x4+s3*Egen3*x5;


        if s1==1
            E_sup_DG1(t-1)= ((abs(Edx))/1000);
            f1(t-1)= E_sup_DG1(t-1)*0.145;
            Hgen1=Hgen1+1;
        else
            f1(t-1)=0;
        end
```

```
        if s2==1
            E_sup_DG2(t-1)= (((abs(Edx))-Egen1)/1000);
            f2(t-1)= E_sup_DG2(t-1)*0.145;
            Hgen2=Hgen2+1;
            else
            f2(t-1)=0;
        end
        if s3==1
            E_sup_DG3(t-1)= (((abs(Edx))-(Egen1+Egen2))/1000);
            f3(t-1)= E_sup_DG3(t-1)*0.145;
            Hgen3=Hgen3+1;
            else
            f3(t-1)=0;
        end
        f(t-1)= f1(t-1)+f2(t-1)+f3(t-1);
        Seco2=2.7; %kg/l
        Eco2(t-1)=Seco2*f(t-1);

        soc(t)=soc(t-1)*(1-s_dis_r);
    end
end
end
Eco2=sum(Eco2);
fuel=sum(f);
fuel_cost=fuel*Cfuel_per_l;

Cinit=x1*Cunit_pv+x2*Cunit_wind+x3*Cunit_gen1+x4*Cunit_gen2+x5*Cunit_gen3+x6*
Cunit_battery;

%Replacement cost
N_year_wind=25*365*24; %
N_year_batt=10*365*24;
n_gen=10*365*24;
if Hgen1>n_gen  %to estimate for replacement cost
Crep_gen1=Replacement_cost(Hgen1,n,Cunit_gen1);
else
Crep_gen1=0;
end
if Hgen2>n_gen
Crep_gen2=Replacement_cost(Hgen2,n,Cunit_gen2);
else
Crep_gen2=0;
end
if Hgen3>n_gen
%N_year_gen3=round(Hgen3/n_gen);
Crep_gen3=Replacement_cost(Hgen3,n,Cunit_gen3);
else
Crep_gen3=0;
end
Crep_wind=Replacement_cost(N_year_wind,n,Cunit_wind);
Crep_batt=Replacement_cost(N_year_batt,n,Cunit_battery);
Crep=Crep_wind*x2+Crep_batt*x6+Crep_gen1*x3+Crep_gen2*x4+Crep_gen3*x5;

%Operation and maintenance cost
fo=6;
kd=9;
```

```
Com_pv=0.01*Cunit_pv*x1*((1+fo)/(kd-fo))*(1-((1+fo)/(1+kd))^n); %n=number of
year considered, 1% of intial PV cost is used for its first year op&m cost
Com_wind=0.03*Cunit_wind*x2*((1+fo)/(kd-fo))*(1-((1+fo)/(1+kd))^n); %n=number
of year considered, 3% of intial wind turbine cost is used for its first year
op&m cost
Com_gen1=0.05*Cunit_gen1*x3*((1+fo)/(kd-fo))*(1-((1+fo)/(1+kd))^n); %n=number
of year considered, 5% of intial generator cost is used for its first year
op&m cost
Com_gen2=0.05*Cunit_gen2*x4*((1+fo)/(kd-fo))*(1-((1+fo)/(1+kd))^n); %n=number
of year considered, 5% of intial generator cost is used for its first year
op&m cost
Com_gen3=0.05*Cunit_gen3*x5*((1+fo)/(kd-fo))*(1-((1+fo)/(1+kd))^n); %n=number
of year considered, 5% of intial generator cost is used for its first year
op&m cost
Com_batt=0.03*Cunit_battery*x6*((1+fo)/(kd-fo))*(1-((1+fo)/(1+kd))^n);
%n=number of year considered, 1% of intial battery cost is used for its first
year op&m cost
Cmaint=Com_pv+Com_wind+Com_gen1+Com_gen2+Com_gen3+Com_batt;
T_Dump=sum(Dump);
%life cycle cost
LCC=Cinit+Crep+Cmaint+fuel_cost;

w1=0.5; w2=0.3; w3=0.2;
%if Etotal > El_peak && Etotal < (El_peak*1.20)     %constraints
ECO2=Eco2*0.15; %converting co2 to money using penalty factor
%C_T_Dump=T_Dump* %converting dump energy to money using cost of electricity
(COE)
z=w1*LCC+w2*ECO2+w3*T_Dump;
%else
%obj= inf;
%%% End of the part to be modified -------------------%%%

%%% -------------------------------------------------------%%%
%%% Do not modify the following codes unless you want %%%
%%% to improve its performance etc                      %%%
% -----------------------------------------------------------
% ===Start of the Firefly Algorithm Implementation ======
%         Lb = lower bounds/limits
%         Ub = upper bounds/limits
%   para == optional (to control the Firefly algorithm)
% Outputs: nbest   = the best solution found so far
%          fbest   = the best objective value
%      NumEval = number of evaluations: n*MaxGeneration
% Optional:
% The alpha can be reduced (as to reduce the randomness)
% -----------------------------------------------------------

% Start FA
function [nbest,fbest,fitbest]...
           =ffa_mincon(fhandle,u0, Lb, Ub, para)
% Check input parameters (otherwise set as default values)
if nargin<5, para=[20 500 0.25 0.20 1]; end
if nargin<4, Ub=[]; end
if nargin<3, Lb=[]; end
if nargin<2
disp('Usuage: FA_mincon(@cost,u0,Lb,Ub,para)');
```

```
end

% n=number of fireflies
% MaxGeneration=number of pseudo time steps
% ------------------------------------------------
% alpha=0.25;      % Randomness 0--1 (highly random)
% betamn=0.20;     % minimum value of beta
% gamma=1;         % Absorption coefficient
% ------------------------------------------------
n=para(1);  MaxGeneration=para(2);
alpha=para(3); betamin=para(4); gamma=para(5);

% Total number of function evaluations
NumEval=n*MaxGeneration;

% Check if the upper bound & lower bound are the same size
if length(Lb) ~=length(Ub)
    disp('Simple bounds/limits are improper!');
    return
end

% Calcualte dimension
d=length(u0);

% Initial values of an array
zn=ones(n,1)*10^100;
% ------------------------------------------------
% generating the initial locations of n fireflies
[ns,Lightn]=init_ffa(n,d,Lb,Ub,u0);

% Iterations or pseudo time marching
for k=1:MaxGeneration     %%%%% start iterations

% This line of reducing alpha is optional
 alpha=alpha_new(alpha,MaxGeneration);

% Evaluate new solutions (for all n fireflies)
for i=1:n
   zn(i)=fhandle(ns(i,:));
   Lightn(i)=zn(i);
end

% Ranking fireflies by their light intensity/objectives
[Lightn,Index]=sort(zn);
ns_tmp=ns;
for i=1:n
 ns(i,:)=ns_tmp(Index(i),:);
end

%% Find the current best
nso=ns; Lighto=Lightn;
nbest=ns(1,:); Lightbest=Lightn(1);

% For output only
fbest=Lightbest;
```

```
% Move all fireflies to the better locations
[ns]=ffa_move(n,d,ns,Lightn,nso,Lighto,nbest,...
      Lightbest,alpha,betamin,gamma,Lb,Ub);
% Show Iteration Information
    disp(['It:' num2str(k) ', Cost => ' num2str(fbest)]);
    fitbest(k)=fbest;
end   %%%%% end of iterations

% ----------------------------------------------------
% ----- All the subfunctions are listed here ------------
% The initial locations of n fireflies
function [ns,Lightn]=init_ffa(n,d,Lb,Ub,u0)
  % if there are bounds/limits,
% if length(Lb)>0
%    for i=1:n
%    ns(i,:)=Lb+(Ub-Lb).*rand(1,d);
%    end
% else
%    % generate solutions around the random guess
%    for i=1:n,
%    ns(i,:)=u0+randn(1,d);
%    end
% end
%load position
load Positions
ns=Positions;

% initial value before function evaluations
Lightn=ones(n,1)*10^100;

% Move all fireflies toward brighter ones
function [ns]=ffa_move(n,d,ns,Lightn,nso,Lighto,...
             nbest,Lightbest,alpha,betamin,gamma,Lb,Ub)
% Scaling of the system
scale=abs(Ub-Lb);

% Updating fireflies
for i=1:n
% The attractiveness parameter beta=exp(-gamma*r)
   for j=1:n
      r=sqrt(sum((ns(i,:)-ns(j,:)).^2));
      % Update moves
       if Lightn(i)>Lighto(j), % Brighter and more attractive
   beta0=1; beta=(beta0-betamin)*exp(-gamma*r.^2)+betamin;
   tmpf=alpha.*(rand(1,d)-0.5).*scale;
   ns(i,:)=ns(i,:).*(1-beta)+nso(j,:).*beta+tmpf;
      end
   end % end for j

end % end for i

% Check if the updated solutions/locations are within limits
[ns]=findlimits(n,ns,Lb,Ub);
```

```
% This function is optional, as it is not in the original FA
% The idea to reduce randomness is to increase the convergence,
% however, if you reduce randomness too quickly, then premature
% convergence can occur. So use with care.
function alpha=alpha_new(alpha,NGen)
% alpha_n=alpha_0(1-delta)^NGen=10^(-4);
% alpha_0=0.9
delta=1-(10^(-4)/0.9)^(1/NGen);
alpha=(1-delta)*alpha;

% Make sure the fireflies are within the bounds/limits
function [ns]=findlimits(n,ns,Lb,Ub)
for i=1:n
     % Apply the lower bound
  ns_tmp=ns(i,:);
  I=ns_tmp<Lb;
  ns_tmp(I)=Lb(I);

  % Apply the upper bounds
  J=ns_tmp>Ub;
  ns_tmp(J)=Ub(J);
  % Update this new move
  ns(i,:)=ns_tmp;
end

%% ==== End of Firefly Algorithm implementation ======
```

GPC

```
%% Giza Pyramids Construction (GPC) Algorithm
%programmer: Engr. Convenience
%Date:23-10-2021
%Code version: Improved Version
%Improved in MATLAB R2020a
%
% Paper  : Giza Pyramids Construction: an ancient-inspired metaheuristic
algorithm for optimization
% DOI    : http://dx.doi.org/10.1007/s12065-020-00451-3

clc;
clear;
close all;

%% Problem Definition
tic
CostFunction=@(x) Sphere(x);        % Cost Function
 batt_rated=360;   %battery capacity in AH
       SF=1.5; %safety factor
       rated_pv=385; %watt
       rated_wind=500; %watt
       [~,peak_El]=load_demand;
       u_pv=peak_El*SF/rated_pv;
       u_wind=peak_El*SF/rated_wind;
       u_batt=(battery_capacity(peak_El))/batt_rated;
```

```
        VarMin=[1 1 1 1 1 1];    % Decision Variables Lower Bound
        VarMax=[round(u_pv*SF) round(u_wind*SF) 1 1 1 round(u_batt*SF)];
% Decision Variables Upper Bound

nVar=6;                  % Number of Decision Variables

VarSize=[1 nVar];         % Decision Variables Matrix Size

%% Giza Pyramids Construction (GPC) Parameters

MaxIteration=20;   % Maximum Number of Iterations (Days of work)

nPop=50;             % Number of workers

G = 9.8;             % Gravity
Tetha = 14;          % Angle of Ramp
MuMin = 1;           % Minimum Friction
MuMax = 10;          % Maximum Friction
pSS= 0.5;            % Substitution Probability

%% Initialization
% Empty Stones Structure
stone.Position=[];
stone.Cost=[];
%load position
load Positions
% Initialize Population Array
pop=repmat(stone,nPop,1);

% Initialize Best Solution Ever Found
best_worker.Cost=inf;

% Create Initial Stones
for i=1:nPop
   pop(i).Position=Positions(i,:);
   pop(i).Cost=CostFunction(pop(i).Position);
   if pop(i).Cost<=best_worker.Cost
       best_worker=pop(i);          % as Pharaoh's special agent
   end
end

% Array to Hold Best Cost Values
BestCost=zeros(MaxIteration,1);

%% Giza Pyramids Construction (GPC) Algorithm Main Loop
for it=1:MaxIteration
    newpop=repmat(stone,nPop,1);

    for i=1:nPop
        newpop(i).Cost = inf;

        V0= rand(1,1);                          % Initial Velocity
        Mu= MuMin+(MuMax-MuMin)*rand(1,1);      % Friction
```

```
        d = (V0^2)/((2*G)*(sind(Tetha)+(Mu*cosd(Tetha))));                  %
Stone Destination
        x = (V0^2)/((2*G)*(sind(Tetha)));                                   %
Worker Movement
        epsilon=unifrnd(-((VarMax-VarMin)/2),((VarMax-VarMin)/2),VarSize);  %
Epsilon
        newsol.Position = (pop(i).Position+d).*(x*epsilon);                 %
Position of Stone and Worker
      % newsol.Position = (pop(i).Position+d)+(x*epsilon);                  %
Note: In some cases or some problems use this instead of the previous line to
get better results

        newsol.Position=max(newsol.Position,VarMin);
        newsol.Position=min(newsol.Position,VarMax);

        % Substitution
        z=zeros(size(pop(i).Position));
        k0=randi([1 numel(pop(i).Position)]);
        for k=1:numel(pop(i).Position)
            if k==k0 || rand<=pSS
                z(k)=newsol.Position(k);
            else
                z(k)=pop(i).Position(k);
            end
        end

        newsol.Position=z;
        newsol.Cost=CostFunction(newsol.Position);

        if newsol.Cost <= newpop(i).Cost
           newpop(i) = newsol;
           if newpop(i).Cost<=best_worker.Cost
               best_worker=newpop(i);
           end
        end

    end

    % Merge
    pop=[pop
         newpop];  %#ok

    % Sort
    [~, SortOrder]=sort([pop.Cost]);
    pop=pop(SortOrder);

    % Truncate
    pop=pop(1:nPop);

    % Store Best Cost Ever Found
    BestCost(it)=pop(1).Cost;

    % Show Iteration Information
    disp(['It:' num2str(it) ', Cost => ' num2str(BestCost(it))]);
end
```

```
%% Results
Best_pos=best_worker.Position;
xx=round(Best_pos);
[Cinit,Crep,Cmaint,fuel_cost,LCC,Eco2,T_Dump,Hgen1,Hgen2,Hgen3,Egen,Ewind,EPv
,soc,El]=Results(Best_pos);
toc
fprintf('_____________________________________________\n')
fprintf('----------Simulation Results-----------------\n')
fprintf('PV Modules:           %6d \n',round(Best_pos(1)))
fprintf('Wind Turbine Modules: %6d \n',round(Best_pos(2)))
fprintf('Battery Modules:      %6d \n',round(Best_pos(6)))
fprintf('DG Set1 Module:       %6d \n',round(Best_pos(3)))
fprintf('Hour of operation of DG1:       %6d \n',round(Hgen1))
fprintf('DG Set2 Module:       %6d \n',round(Best_pos(4)))
fprintf('Hour of operation of DG2:       %6d \n',round(Hgen2))
fprintf('DG Set3 Module:       %6d \n',round(Best_pos(5)))
fprintf('Hour of operation of DG3:       %6d \n',round(Hgen3))
fprintf('Initial Capital cost:     %8.2f $ \n',Cinit)
fprintf('Replacement cost:         %8.2f $ \n',Crep)
fprintf('OP and Maintenance cost:  %8.2f $ \n',Cmaint)
fprintf('Fuel cost:                %8.2f $ \n',fuel_cost)
fprintf('Life cycle cost:          %8.2f $ \n',LCC)
fprintf('Total CO2 Emission:            %8.2f kg \n',Eco2)
fprintf('Dump Energy:              %8.2f Watt \n',T_Dump)
fprintf('_____________________________________________\n')


figure;
%plot(BestCost,'LineWidth',2);
semilogy(BestCost,'LineWidth',2);
xlabel('Iteration');
ylabel('Best Cost');
grid on;
figure
%plot hourly output of the hps for 48hrs
TT=1:48;
yyaxis left
plot(TT,EPv(TT),'--g','LineWidth',2)
hold on
plot(TT,Ewind(TT),'-.c','LineWidth',2)
plot(TT,Egen(TT),'--m','LineWidth',2)
stairs(TT,El(TT),'-r','LineWidth',2)
hold off
ylabel('Output Power (Watt)')
xlabel('Duration (Hr)')
yyaxis right
plot(TT,soc(TT),':b','LineWidth',2)
ylabel('State of Charge')
title('System behaviour')
legend('BPv','Wind','3DGs','Eload','SOC')
grid on
grid minor
%plot hourly output of the hps for 10day
figure
T=1:240;
```

```
yyaxis left
plot(T,EPv(T),'--g','LineWidth',2)
hold on
plot(T,Ewind(T),'-.c','LineWidth',2)
plot(T,Egen(T),'--m','LineWidth',2)
stairs(T,El(T),'-r','LineWidth',2)
hold off
ylabel('Output Power (Watt)')
xlabel('Duration (Hr)')
yyaxis right
plot(T,soc(T),':b','LineWidth',2)
ylabel('State of Charge')
title('System behaviour')
legend('BPv','Wind','3DGs','Eload','SOC')
grid on
grid minor
```

Sphere

```
function obj=Sphere(x)
x=round(x);
x1=x(1);
x2=x(2);
x3=x(3);
x4=x(4);
x5=x(5);
x6=x(6);

[El,El_peak]=load_demand;
n=30;
Egen1=0.40*El_peak;
Egen2=0.40*El_peak;
Egen3=0.40*El_peak;
Hgen1=0; Hgen2=0; Hgen3=0;
Eco2=0;
f=0;
Dump=0;
E_sup_DG1=0; E_sup_DG2=0; E_sup_DG3=0;

Cunit_pv=500;
Cunit_wind=500;
Cunit_gen1=0.3*Egen1; %
Cunit_gen2=0.3*Egen2;
Cunit_gen3=0.3*Egen3;
Cunit_battery=300;
Cfuel_per_l=1.5;

eff_inv=0.8;
eff_batt=0.9;
batt_Ah=360;
Vs=24;
s_dis_r=0.01;
CB=batt_Ah*Vs*eff_batt*x6;
soc=0.5*CB;
DoD=0.8;
```

```
soc_min=(1-DoD)*CB;
soc_max=CB;

[wind_speed,solar_irradiance]=speed_irradiance_data;
H=solar_irradiance;
v=wind_speed;

for mm=1:8
    H=[H;H];
    v=[v;v];
end
h=solar_irradiance;
V=wind_speed;
for mn=1:8
    h=[h;h];
    V=[V;V];
end
Hh=[H;h];
vV=[v;V];
%initialize soc
% soc=zeros(1,(365*24*n));
for t=2:365*24*n
Ppv=pvmodule(Hh(t-1));
Ppv=Ppv*1.30;
Pwind=wt_module(vV(t-1)); %loaded wind speed data is accessed here
Eren=Ppv*x1+Pwind*x2;

Edx=Eren-(El(t-1)/eff_inv);
if Edx>0     %i.e if their is excess energy
    if soc(t-1)<soc_max
        %for charging
         soc(t)=soc(t-1)*(1-s_dis_r)+(Eren-(El(t-1)/eff_inv))*eff_batt;
    else
        Dump(t)=abs(Edx);
        soc(t)=soc(t-1);
    end
elseif Edx<0
    if soc(t-1)>soc_min
        %for discharging
        soc(t)=soc(t-1)*(1-s_dis_r)-((El(t-1)/eff_inv)-Eren);
    else
        %Generator
        if abs(Edx)<(x3*Egen1)
            s1=1; s2=0; s3=0;
        elseif abs(Edx)<((x3*Egen1)+(x4*Egen2))

            s1=1; s2=1; s3=0;
        else
            s1=1;
            s2=1;
            s3=1;
        end
        Egen(t-1)=s1*Egen1*x3+s2*Egen2*x4+s3*Egen3*x5;


        if s1==1
```

```
            E_sup_DG1(t-1)= ((abs(Edx))/1000);
            f1(t-1)= E_sup_DG1(t-1)*0.145;
            Hgen1=Hgen1+1;
        else
            f1(t-1)=0;
        end
        if s2==1
            E_sup_DG2(t-1)= (((abs(Edx))-Egen1)/1000);
            f2(t-1)= E_sup_DG2(t-1)*0.145;
            Hgen2=Hgen2+1;
            else
            f2(t-1)=0;
        end
        if s3==1
            E_sup_DG3(t-1)= (((abs(Edx))-(Egen1+Egen2))/1000);
            f3(t-1)= E_sup_DG3(t-1)*0.145;
            Hgen3=Hgen3+1;
            else
            f3(t-1)=0;
        end
        f(t-1)= f1(t-1)+f2(t-1)+f3(t-1);
        Seco2=2.7; %kg/l
        Eco2(t-1)=Seco2*f(t-1);

        soc(t)=soc(t-1)*(1-s_dis_r);
    end
end
end
Eco2=sum(Eco2);
fuel=sum(f);
fuel_cost=fuel*Cfuel_per_l;

Cinit=x1*Cunit_pv+x2*Cunit_wind+x3*Cunit_gen1+x4*Cunit_gen2+x5*Cunit_gen3+x6*
Cunit_battery;

%Replacement cost
N_year_wind=25*365*24; %
N_year_batt=10*365*24;
n_gen=10*365*24;
if Hgen1>n_gen  %to estimate for replacement cost
Crep_gen1=Replacement_cost(Hgen1,n,Cunit_gen1);
else
Crep_gen1=0;
end
if Hgen2>n_gen
Crep_gen2=Replacement_cost(Hgen2,n,Cunit_gen2);
else
Crep_gen2=0;
end
if Hgen3>n_gen
%N_year_gen3=round(Hgen3/n_gen);
Crep_gen3=Replacement_cost(Hgen3,n,Cunit_gen3);
else
Crep_gen3=0;
end
Crep_wind=Replacement_cost(N_year_wind,n,Cunit_wind);
```

```
Crep_batt=Replacement_cost(N_year_batt,n,Cunit_battery);
Crep=Crep_wind*x2+Crep_batt*x6+Crep_gen1*x3+Crep_gen2*x4+Crep_gen3*x5;

%Operation and maintenance cost
fo=6;
kd=9;
Com_pv=0.01*Cunit_pv*x1*((1+fo)/(kd-fo))*(1-((1+fo)/(1+kd))^n); %n=number of
year considered, 1% of intial PV cost is used for its first year op&m cost
Com_wind=0.03*Cunit_wind*x2*((1+fo)/(kd-fo))*(1-((1+fo)/(1+kd))^n); %n=number
of year considered, 3% of intial wind turbine cost is used for its first year
op&m cost
Com_gen1=0.05*Cunit_gen1*x3*((1+fo)/(kd-fo))*(1-((1+fo)/(1+kd))^n); %n=number
of year considered, 5% of intial generator cost is used for its first year
op&m cost
Com_gen2=0.05*Cunit_gen2*x4*((1+fo)/(kd-fo))*(1-((1+fo)/(1+kd))^n); %n=number
of year considered, 5% of intial generator cost is used for its first year
op&m cost
Com_gen3=0.05*Cunit_gen3*x5*((1+fo)/(kd-fo))*(1-((1+fo)/(1+kd))^n); %n=number
of year considered, 5% of intial generator cost is used for its first year
op&m cost
Com_batt=0.03*Cunit_battery*x6*((1+fo)/(kd-fo))*(1-((1+fo)/(1+kd))^n);
%n=number of year considered, 1% of intial battery cost is used for its first
year op&m cost
Cmaint=Com_pv+Com_wind+Com_gen1+Com_gen2+Com_gen3+Com_batt;
T_Dump=sum(Dump);
%life cycle cost
LCC=Cinit+Crep+Cmaint+fuel_cost;

w1=0.5; w2=0.3; w3=0.2;
%if Etotal > El_peak && Etotal < (El_peak*1.20)     %constraints
ECO2=Eco2*0.15; %converting co2 to money using penalty factor
%C_T_Dump=T_Dump* %converting dump energy to money using cost of electricity
(COE)
x=w1*LCC+w2*ECO2+w3*T_Dump;
```

WOA

```
% The Whale Optimization Algorithm
function
[Leader_score,Leader_pos,Convergence_curve]=WOA(SearchAgents_no,Max_iter,lb,u
b,dim,fobj)

% initialize position vector and score for the leader
Leader_pos=zeros(1,dim);
Leader_score=inf; %change this to -inf for maximization problems

%Initialize the positions of search agents
Positions=initialization(SearchAgents_no,dim,ub,lb);

Convergence_curve=zeros(1,Max_iter);

t=0;% Loop counter
```

```
% Main loop
while t<Max_iter
    for i=1:size(Positions,1)

        % Return back the search agents that go beyond the boundaries of the
search space
        Flag4ub=Positions(i,:)>ub;
        Flag4lb=Positions(i,:)<lb;

Positions(i,:)=(Positions(i,:).*(~(Flag4ub+Flag4lb)))+ub.*Flag4ub+lb.*Flag4lb
;
        % Calculate objective function for each search agent
        fitness=fobj(Positions(i,:));

        % Update the leader
        if fitness<Leader_score % Change this to > for maximization problem
            Leader_score=fitness; % Update alpha
            Leader_pos=Positions(i,:);
        end

    end

    a=2-t*((2)/Max_iter); % a decreases linearly fron 2 to 0 in Eq. (2.3)

    % a2 linearly dicreases from -1 to -2 to calculate t in Eq. (3.12)
    a2=-1+t*((-1)/Max_iter);

    % Update the Position of search agents
    for i=1:size(Positions,1)
        r1=rand(); % r1 is a random number in [0,1]
        r2=rand(); % r2 is a random number in [0,1]

        A=2*a*r1-a;  % Eq. (2.3) in the paper
        C=2*r2;      % Eq. (2.4) in the paper


        b=1;               %  parameters in Eq. (2.5)
        l=(a2-1)*rand+1;   %  parameters in Eq. (2.5)

        p = rand();        % p in Eq. (2.6)

        for j=1:size(Positions,2)

            if p<0.5
                if abs(A)>=1
                    rand_leader_index = floor(SearchAgents_no*rand()+1);
                    X_rand = Positions(rand_leader_index, :);
                    D_X_rand=abs(C*X_rand(j)-Positions(i,j)); % Eq. (2.7)
                    Positions(i,j)=X_rand(j)-A*D_X_rand;      % Eq. (2.8)

                elseif abs(A)<1
                    D_Leader=abs(C*Leader_pos(j)-Positions(i,j)); % Eq. (2.1)
                    Positions(i,j)=Leader_pos(j)-A*D_Leader;      % Eq. (2.2)
                end
```

```
            elseif p>=0.5

                distance2Leader=abs(Leader_pos(j)-Positions(i,j));
                % Eq. (2.5)

Positions(i,j)=distance2Leader*exp(b.*l).*cos(l.*2*pi)+Leader_pos(j);

            end

        end
    end
    t=t+1;
    Convergence_curve(t)=Leader_score;
    [t Leader_score]
end


% To run WOA:
[Best_score,Best_pos,WOA_cg_curve]=WOA(SearchAgents_no,Max_iteration,lb,ub,di
m,fobj)
%_____________________________________________

clear all
clc
close all
SearchAgents_no=50; % Number of search agents

Function_name='F1'; % Name of the test function that can be from F1 to F23
(Table 1,2,3 in the paper)

Max_iteration=2; % Maximum numbef of iterations

% Load details of the selected benchmark function
[lb,ub,dim,fobj]=Get_Functions_details(Function_name);

[Best_score,Best_pos,WOA_cg_curve]=WOA(SearchAgents_no,Max_iteration,lb,ub,di
m,fobj);

xx=round(Best_pos);
[Cinit,Crep,Cmaint,fuel_cost,LCC,Eco2,T_Dump,Hgen1,Hgen2,Hgen3,Egen,Ewind,EPv
,soc,El]=Results(Best_pos);
%% Results
fprintf('_____________________________________________\n')
fprintf('----------Simulation Results----------------\n')
fprintf('PV Modules:           %6d \n',round(Best_pos(1)))
fprintf('Wind Turbine Modules: %6d \n',round(Best_pos(2)))
fprintf('Battery Modules:      %6d \n',round(Best_pos(6)))
fprintf('DG Set1 Module:       %6d \n',round(Best_pos(3)))
fprintf('Hour of operation of DG1:       %6d \n',round(Hgen1))
fprintf('DG Set2 Module:       %6d \n',round(Best_pos(4)))
fprintf('Hour of operation of DG2:       %6d \n',round(Hgen2))
fprintf('DG Set3 Module:       %6d \n',round(Best_pos(5)))
fprintf('Hour of operation of DG3:       %6d \n',round(Hgen3))
```

```
fprintf('Initial Capital cost:     %8.2f $ \n',Cinit)
fprintf('Replacement cost:         %8.2f $ \n',Crep)
fprintf('OP and Maintenance cost:  %8.2f $ \n',Cmaint)
fprintf('Fuel cost:                %8.2f $ \n',fuel_cost)
fprintf('Life cycle cost:          %8.2f $ \n',LCC)
fprintf('Total CO2 Emission:            %8.2f kg \n',Eco2)
fprintf('Dump Energy:              %8.2f Watt \n',T_Dump)
fprintf('_____________________________________________\n')

figure
figure('Position',[269   240   660   290])
%Draw objective space
semilogy(WOA_cg_curve,'Color','r')
title('Objective space')
xlabel('Iteration');
ylabel('Best score obtained so far');

axis tight
grid on
box on
legend('WOA')
figure
%plot hourly output of the hps for 48hrs
TT=1:48;
yyaxis left
plot(TT,EPv(TT),'--g','LineWidth',2)
hold on
plot(TT,Ewind(TT),'-.c','LineWidth',2)
plot(TT,Egen(TT),'--m','LineWidth',2)
stairs(TT,El(TT),'-r','LineWidth',2)
hold off
ylabel('Output Power (Watt)')
xlabel('Duration (Hr)')
yyaxis right
plot(TT,soc(TT),':b','LineWidth',2)
ylabel('State of Charge')
title('System behaviour')
legend('BPv','Wind','3DGs','Eload','SOC')
grid on
grid minor
%plot hourly output of the hps for 10day
figure
T=1:240;
yyaxis left
plot(T,EPv(T),'--g','LineWidth',2)
hold on
plot(T,Ewind(T),'-.c','LineWidth',2)
plot(T,Egen(T),'--m','LineWidth',2)
stairs(T,El(T),'-r','LineWidth',2)
hold off
ylabel('Output Power (Watt)')
xlabel('Duration (Hr)')
yyaxis right
plot(T,soc(T),':b','LineWidth',2)
ylabel('State of Charge')
title('System behaviour')
```

```
legend('BPv','Wind','3DGs','Eload','SOC')
grid on
grid minor
display(['The best optimal value of the objective funciton found by WOA is :
', num2str(Best_score)]);
```